ISSN 2542-1565

Vol. 16 2023 No. 03

GEOGRAPHY ENVIRONMENT SUSTAINABILITY

«The journal GEOGRAPHY, ENVIRONMENT, SUSTAINABILITY was founded in 2008 by Russian Geographical Society, the Lomonosov Moscow State University Geography Department, and the Russian Academy of Sciences Institute of Geography. Since that time the journal publishes **4 issues per year**, containing original research papers and reviews. The journal issues are open source and distributed through subscriptions, library exchanges of leading universities, and via the website through the world»

FOUNDERS OF THE JOURNAL: Russian Geographical Society, Faculty of Geography, Lomonosov Moscow State University and Institute of Geography of the Russian Academy of Sciences

The journal is published with financial support of the Russian Geographical Society.

The journal is registered in Federal service on supervision of observance of the legislation in sphere of mass communications and protection of a cultural heritage. The certificate of registration: ПИ № ФС77-67752, 2016, December 21.

PUBLISHER
Russian Geographical Society
Moscow, 109012 Russia
Novaya ploshchad, 10, korp. 2
Phone 8-800-700-18-45
E-mail: press@rgo.ru
www.rgo.ru/en

EDITORIAL OFFICE
Lomonosov Moscow State University
Moscow 119991 Russia
Leninskie Gory, 1,
Faculty of Geography, 1806a
Phone 7-495-9391552
Fax 7-495-9391552
E-mail: ges-journal@geogr.msu.ru
www.ges.rgo.ru

DESIGN
Layout designer: Tereshkin Anton
Moscow, 115088,
26 Simonovsky Val str., bldg. One
Phone: +7 (903) 108-04-44
E-mail: smile.tai@gmail.com

DOI prefix: 10.24057

Format A4 (210x297mm)

"GEOGRAPHY, ENVIRONMENT, SUSTAINABILITY" is the only original English-language journal in the field of geography and environmental sciences published in Russia. It is supposed to be an outlet from the Russian-speaking countries to Europe and an inlet from Europe to the Russian-speaking countries regarding environmental and Earth sciences, geography and sustainability. The main sections of the journal are the theory of geography and ecology, the theory of sustainable development, use of natural resources, natural resources assessment, global and regional changes of environment and climate, social-economical geography, ecological regional planning, sustainable regional development, applied aspects of geography and ecology, geoinformatics and ecological cartography, ecological problems of oil and gas sector, nature conservations, health and environment, and education for sustainable development.

Date of publication: October 10th, 2023.

EDITORIAL BOARD

EDITORIAL OFFICE

CONTENTS

RESEARCH PAPER

SATELLITE IMAGES INTERPRETATION FOR HEALTH STUDIES OF URBAN AREAS

M.Y. Grishchenko[1,2*], N.M. Fazleeva[1], N.V. Shartova[2], Marina G. Titova[2]
[1]Lomonosov Moscow State University, Faculty of Geography, Moscow, 119991, Russia
[2]HSE University, Faculty of Geography and Geoinformatics, Moscow, 109028, Russia
*Corresponding author: m.gri@geogr.msu.ru
Received: January10th, 2023 / Accepted: September 4th, 2023 / Published: October 10th, 2023
https://DOI-10.24057/2071-9388-2023-2704

ABSTRACT. Every year a variety of vector-borne infectious diseases claims the lives of millions of people worldwide. The study of the favorable conditions for their vectors and hosts is a particularly important task for understanding the patterns of the distribution with the focus on the urban environment, characterizing by a high population density and rapid transmission of the diseases. The existing methodology of Local Climate Zones (LCZ), which are areas with homogeneous land surface coverage, structure, and a specific nature of human activity was the first attempt to standardize urban environmental studies and has become an international standard for the analysis of urban morphology. The article provides an algorithm for adapting the methodology of identifying LCZ accounting vegetation and water areas for the tasks of medical geographical zoning and assessment of epidemiological risks and using the geographic information technology. The examples of the outbreaks of vivax malaria in the Moscow region in 1999–2003 and West Nile fever in the Volgograd region in 2010–2011 were used. As a result, a methodology of medical geographical zoning based on the idea of fragmenting the classification of LCZ using the normalized difference water index as indicator of the favorability for vector habitats was developed. The use of the methodology made it possible to reveal that the areas of various LCZs change after outbreaks, which may reflect changes in conditions and an increase in the favorability for vectors. Thus, LCZ can be used as indicators of changes in the natural and man-made environment that can provoke disease outbreaks.

KEYWORDS: satellite image interpretation, local climate zones, medical-geographical zoning, infectious diseases, medical geography, risk analysis, West Nile fever, malaria, geoinformation technologies

CITATION: Grishchenko M.Y., Fazleeva N.M., Shartova N.V., Titova M. G. (2023). Satellite images interpretation for health studies of urban areas. Geography, Environment, Sustainability, 3(16), 6-13
https://DOI-10.24057/2071-9388-2023-2704

Conflict of interests: The authors reported no potential conflict of interest.

INTRODUCTION

Infectious diseases have always played an important role in human health and society. Due to the observed climate change, the analysis of the distribution of vector-borne diseases is becoming increasingly relevant. These are diseases, the causative agents of which are transmitted through various arthropod vectors, thus, are directly dependent on climate conditions. Climate and weather conditions are direct abiotic factors affecting the ability of vectors to acquire, maintain, and transmit a pathogen. Geoinformation technologies (GIS) have greatly expanded the possibilities of medical geography in identifying the geographical factors of diseases, modeling their distribution, and predicting the development of epidemics. However, the distribution of vector-borne diseases outbreaks in urban settings have not been studied well (Eder et al. 2018).

Today, most of the world's population is concentrated in cities, and urban and suburban areas become the main object of study. Despite the great favorability of rural areas for the development of vectors, urban areas are particularly susceptible to outbreaks of vector-borne diseases today (Roehrig 2013; Misslin et al. 2016). Rapid urban growth, migration flows (often uncontrolled) and the formation of specific climate conditions lead to the emergence of vector-borne diseases. The example is the distribution of Dengue fever in American regions in 2019, when densely populated areas of large cities close to water bodies were at most risk (Dengue and severe dengue… 2022). While climate and weather conditions have well-documented effects on infectious diseases, urban environment could significantly enhance the influence.

The study of urban climate resulted in the concept of local climate zones (LCZ) (Stewart and Oke 2012), fundamentally different from each other on a number of parameters. They represent various types of buildings and of natural surface cover. The idea of the LCZ has become the international standard for the study of urban morphology and its impact on urban climate. However, a more thorough elaboration of the vegetation and water bodies in the allocated zones is required for the purposes of medical geography. The focus should be on vegetation cover and water areas which play a particularly important role as a favorable environment for the life cycle of the arthropod vectors.

A number of works that propose the use of LCZ theory to study the distribution of vector-borne diseases in cities have been published. All of them are based on a comprehensive analysis and identification of factors that influence the distribution of vectors. For example, studies on cities in sub-Saharan Africa (Brousse et al. 2019; Brousse et al. 2020) evaluated the possibility of using LCZ to determine the climate characteristics of urban areas and to study the risks of malaria. In (Tourre et al. 2008), the dependence of the normalized difference vegetation index (NDVI) on precipitation, temperature regime and its relation to the epidemiological situation was studied. Brousse et al. 2020 attempted to model the risks of adverse epidemiological conditions with the further possibility of applying such a model to any city in the world.

Thus, outbreaks of vector-borne diseases in cities necessitated clarifying the LCZ to assess the suitability of urban and suburban conditions for vectors. Previously, we conducted medical and geographic studies of two outbreaks of vector-borne diseases (malaria and West Nile fever) in Russia (Mironova et al. 2020; Shartova et al. 2022). During these studies, the problem of accounting the structure of the land cover of urban and suburban areas arose, which would satisfy the necessary requirements in detail and the set of indicators essential for the life cycle of vectors. This article presents a methodology for adapting the LCZ theory in the context of differentiation of vegetation and water areas under the tasks of medical geographical zoning using GIS on the example of temperate cities.

Study areas

The choice of regions for study was based on the sites of West Nile outbreaks in Volgograd region in 2010–2011 and vivax malaria in the Moscow region in 1999–2003 (Mironova et al. 2020; Shartova et al. 2022). The common feature of West Nile fever and malaria is transmission of pathogens to humans through mosquito bites (mainly, the genus Culex for West Nile virus and the genus *Anopheles* for the malaria pathogen *Plasmodium vivax*).

Outbreaks of West Nile fever in Russia are primarily confined to wetlands in the Volga Delta and floodplain areas (Adishcheva et al. 2016). A number of factors contribute to the focus on the Volgograd region. One of the reasons is the presence of a large ornithological node in the north of the region, since the hosts of the West Nile virus in nature are birds of the wetland complex. Another factor is a large number of small lakes, shallow channels, and wetlands in the floodplain of the Volga River, which are favorable for breeding of mosquitos. The warm southern climate also contributes to the life stages of vectors and replication of the virus in mosquitoes (Lvov et al. 2004).

The outbreak of vivax malaria in the Moscow region was largely contributed by the manifestation of urban heat island, which significantly increases the air temperature in the city, which, in turn, affects the intensification of development of the pathogen in mosquitoes (Mironova et al. 2019; Varentsov et al. 2019). The western part of the region was chosen, since in the previous study (Mironova et al. 2020) we found that the spatial distribution of infection was shifted to the west of the Moscow region. Fig. 1 shows the boundaries of the study areas.

Fig. 1. Study areas: western part of Moscow and its suburbs (northern red square); Volgograd and its suburbs (southern red square)

Local climate zones: the main provisions and allocation techniques

Urbanization over the past half century has not only changed the physical environment in cities but has also shaped local climate characteristics and features unique to urban areas. The LCZ system developed by Stewart and Oke (2012) interprets local climate zones as areas with a homogeneous coverage of the earth's surface and a special nature of human activity. The classification includes 17 types, 10 of which are built-up environments, and the remaining seven are "land cover types" (Samsonov et al. 2018).

There are a number of approaches to the allocation of LCZ. All of them use remote sensing data. In this article, the original WUDAPT technique based on pixel classification is used to determine LCZ of the study areas. The main goal of WUDAPT is to collect data on the cities of the world in order to create a database for a systematic study of the urban climate (World Urban Database – wudapt.org).
Within the framework of this study, to obtain LCZ, a set of reference areas was selected for each of the zone types based on visual interpretation of Landsat satellite images. The use of images from a single shooting system ensures the integrity of the study results. The main source were images from the Landsat-5 satellite, obtained using a seven-band scanning radiometer Thematic Mapper (TM). For later dates, images from the Landsat-8 satellite were used. We used the images dated 2010-07-14, 2011-07-08, 2001-07-05, 2020-07-25 for Volgograd and 2000-08-29, 2001-08-02, 1996-08-18, 2011-08-28 for Moscow. The time period was chosen to cover the outbreaks period and periods before and after the outbreaks.

The training sample was compiled based on height of buildings, density of their distribution, and nature of the underlying surface. For each zone a minimum of 10 test sites with a side length of at least 200 meters were taken, which is a WUDAPT recommendation. In total, 16 types of LCZ were clearly identified for each of the study areas.

Then, we performed an automated classification by the maximum likelihood method in ArcGIS10.5 software on the obtained reference sites. A majority filter was applied to the obtained decoding circuits in order to filter out small clusters of pixels creating image information noise. As a result, decoding circuits showing the distribution of LCZ over Volgograd and its surroundings, as well as over the western part of the Moscow region, were obtained.

It is especially important to correctly identify the essential object of research on images which is vegetation cover. Therefore, during the decoding we used multispectral images in four channels of optical range and synthesis in standard pseudocolors (near-infrared, red, and green).

Adapting the methodology of local climate zones to the task of medical geographical zoning

According to the WUDAPT methodology, the LCZs of vegetation are represented by four groups, which are insufficient for medical geographical studies. The principle of dividing all plant communities into dense and lightly wooded landscapes, shrubs, and low vegetation does not allow defining the most favorable areas for the development of mosquitos. This fact prompted a refinement of the classification, which takes into account not only the layering and density of vegetation, but also its moisture characteristics.

When assessing favorable environmental factors for mosquitoes, hydrographic objects also require special attention, since it is in water that the first three stages of their development take place. To estimate the moisture content, we referred to the normalized difference water index (NDWI). There are at least two indexes for which the abbreviation NDWI is used:

The McFeeters Index:

$$NDWI = \frac{\left(X_{NIR} - X_{SWIR}\right)}{\left(X_{NIR} + X_{SWIR}\right)} \quad (1)$$

and the Gao index (Ceccato et al. 2001):

$$NDWI = \frac{\left(X_{green} - X_{NIR}\right)}{\left(X_{green} + X_{NIR}\right)} \quad (2)$$

The indices themselves are fundamentally different from each other, since they refer to different spectral ranges. To classify vegetation, we use the Gao index, which uses the near infrared (NIR) and middle infrared (SWIR) ranges, as it reflects the water content in the leaves of plants. The McFeeters index was used to identify water bodies, based on the green and NIR channels.

To further divide LCZs into subzones, index images were created based on the presented formulas for the study periods, for which a suitable number of index value steps were then identified.

The optimal number of gradations was determined experimentally by gradually increasing the number of steps and a detailed visual analysis of the area. The division into seven gradations was the most suitable for the territory of Volgograd and its environment. For the territory of the Moscow region, the most suitable was the division into six gradations, which reflects all the main trends in the distribution of the index. Fig. 2 shows the resulting index images for study periods.

To select water bodies according to McFeeters index, a raster image with 2 ranges of values below and above 0 was created using raster calculator. This approach makes it possible to identify water bodies by spectral characteristics, not by visual decoding of images. Further,

(a)

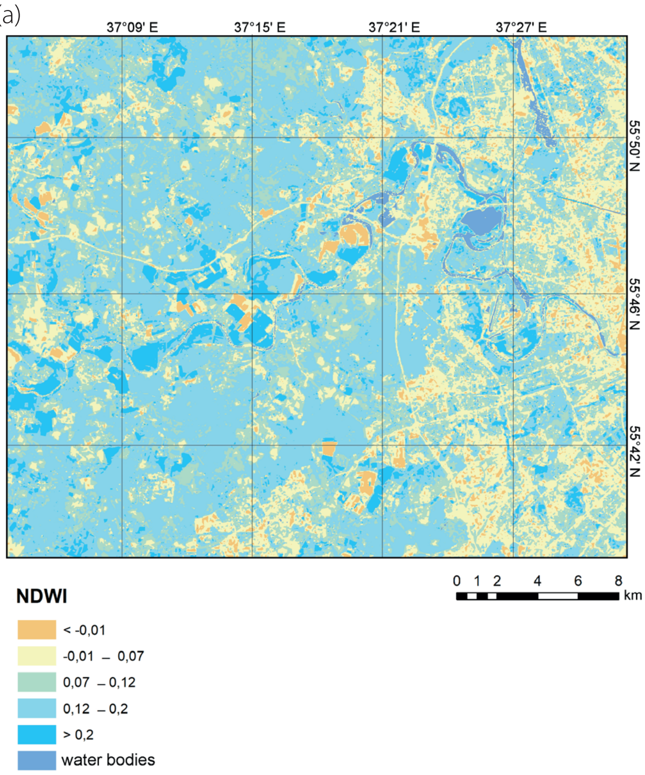

(b)

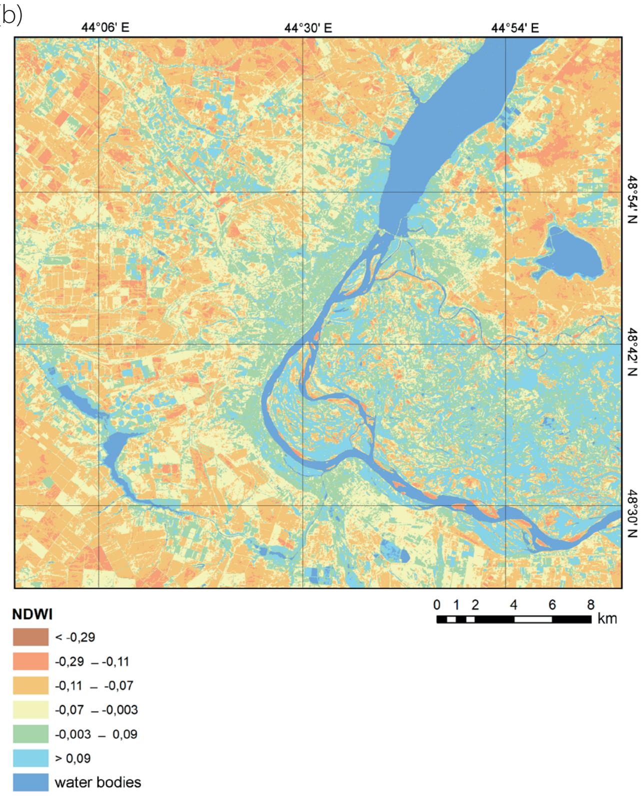

Fig. 2. Study areas index images with selected steps of the Gao NDWI index values: a) the western part of the Moscow region; b) Volgograd and the surrounding area

by spatial sampling based on watercourses flowing out of them, water bodies are divided into effluent and non-drainage ones, as this factor directly affects the creation of conditions for mosquitoes to breed in water bodies.

RESULTS

The resulting index images are the basis for refining the LCZ classification. Integration of LCZ and the results of indices calculation gives us maps of local climate subzones, each of which contains the LCZ type of vegetation cover with an indication of the degree of moisture. A total of six maps of local climate vegetation subzones were made for three-time intervals (outbreak period and periods before and after the outbreak) for each area. Fig. 3 shows maps of local climate subzones of vegetation of the study areas for the period of outbreaks.

All LCZs that are not defined as vegetation are grayed out because they are secondary objects of the study. Gradual darkening of color scales for LCZ vegetation occurs as Gao NDWI index values increase. The main goal of these maps was to reflect as accurately as possible the differentiation of subzones varying in LCZ and Gao NDWI values.

High index values prevailed during outbreak periods for Volgograd and the Moscow region, indicating that vegetation zones are more watered during outbreak periods as compared to the periods before and after them. This result is quite expected and confirms the fact that the moisture content of the vegetation is an indicator of the epidemiological situation. Series of these maps can serve both as intermediate materials for assessing epidemiological risks and as full-fledged materials for studying the nature and changes of vegetation moisture.
In order to study the dynamics of LCZ variability during the study periods, we analyzed the ratio of the obtained zones within the study area for the Volgograd region and the

(a)

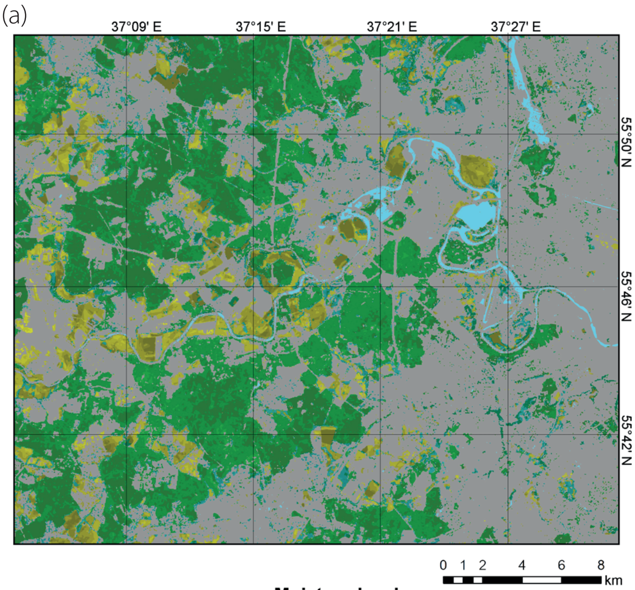

Moisture level

LCZ \ NDWI	Unmoistened	Slightly moistened	Lowly moistened	Moderately moistened	Highly moistened	Overmoistened
	-1 ... -0,18	-0,18 ... -0,06	-0,06 ... 0,03	0,03 ... 0,12	0,12 ... 0,19	0,19 ... 1
Dense trees						
Scattered trees						
Scrub						

Water bodies

Other local climatic zones (LCZ)

(b)

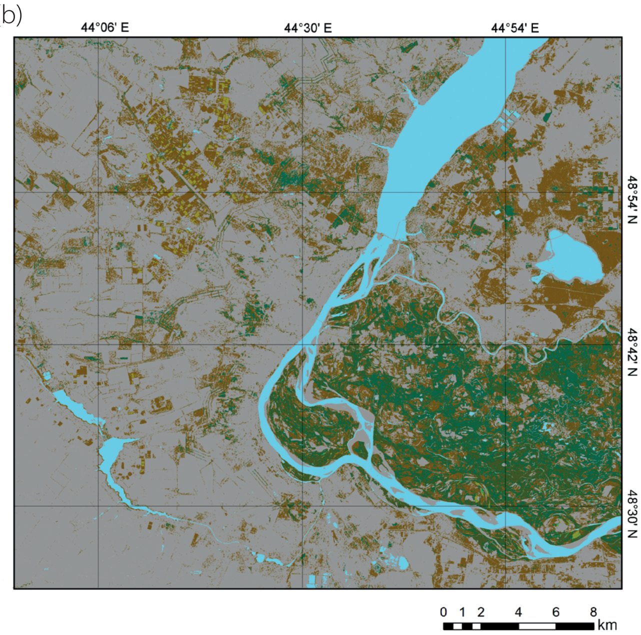

Moisture level

LCZ \ NDWI	Unmoistened	Unmoistened	Slightly moistened	Lowly moistened	Moderately moistened	Highly moistened	Overmoistened
	-0,7 : -0,3	-0,3 : -0,12	-0,12 : -0,08	-0,08 : -0,03	-0,03 : 0,03	0,03 : 0,12	0,12 : 0,42
Dense trees							
Scattered trees							
Scrub							

Water bodies

Other local climatic zones (LCZ)

Fig. 3. Maps of local climate subzones of vegetation during outbreaks of vector-borne diseases: a) the western part of the Moscow region; b) Volgograd and the surrounding area

Moscow region. The results are presented as logarithmic scales and are shown in Fig. 4. The saturation of color corresponds to different years (darker ones are earlier).

The assessment revealed three types of LCZ changes during the study periods. They are the following: steady increase in LCZ area, increase during an outbreak, and decrease during an outbreak. Of greatest interest are the LCZs, the area of which increased during the outbreaks of West Nile fever and vivax malaria. This suggests that an increase of certain types of LCZs areas could have been associated with the outbreaks. The attention must be focused as on potential indicators of the emergence of an unfavorable epidemiological situation.

In LCZ natural surface cover, LCZ A (dense trees) and LCZ B (scattered trees) are the leaders in increasing area during the outbreak in both regions. The increase in LCZ F (bare rock/paved) is due to the construction of asphalt roads. As for water bodies, during the studied periods there is a small, stable increase in their area.

Along with statistical data on infections, maps of local climate sub-zones formed the basis for the assessment of epidemiological risks. The year 2011 for Volgograd and 2001 for Moscow were chosen for the analysis, since according to the initial data set on infections, these years account for the largest number of localizations of possible human infection sites and pathogen detection sites in the nature (see for detail: Mironova et al. 2020; Shartova et al. 2022). First, it calculates percentage of the sites of detected diseases for each LCZ. After that, the number of sites in every local climate subzone is determined. Based on the statistical data obtained, risk matrices were compiled. They form the basis of medical geographical zoning maps for the areas under study. The matrices are presented in the explanation of each map.

The principle of all risk matrices is to determine the level of risk, taking into account the category of probability and severity of consequences (Korolkova 2013). The matrices are built according to the following principle: the parameters under consideration (in our case, these are vegetation LCZs and Gao NDWI steps) are indicated horizontally and vertically in the order of increasing their degree of favorability for vectors depending on the degree of vegetation moistening. Thus, when moving from the beginning of the axes to the upper right corner of the matrix, there is an increase in the degree of favorability. Based on the risk matrices, maps of medical geographical zoning were made. The matrices are presented in the explanation of each map (Fig. 5).

The trend of increasing in favorability of areas for vector-borne transmission can be clearly seen in the matrix for Volgograd. The greatest number of possible human infection sites and virus detection sites in the nature occurred in LCZ D (low plants) and in subzones with Gao NDWI values ranging from 0.12 to 0.42 (with overwatering). When comparing these data, it appears that the areas that correspond to LCZ D and Gao NDWI group 7 at the same time are potentially the most dangerous for the territory of Volgograd. These are the areas in the upper right corner of the matrix. By the same principle, for each subzone a place in the risk matrix is determined. Thus, the position in the matrix and color saturation reflects the level of favorability of vegetation zones based on the degree of moisture for the natural foci activity (the darker, the more favorable).

For the Moscow region the most dangerous are the areas of LCZ A (dense trees) with 3-step Gao NDWI values (low-moisture type). However, test sites with such values do not form large continuous arrays and are practically not visible on the map. The predominant part of suburban areas is covered by forests (LCZ 101) with maximum Gao NDWI values (over-moisture type) and low plants (LCZ 104) with the 3rd stage of boundary index values (low-moisture type). Thus, for the Moscow region, the most dangerous areas are forests of the over- moisture type.

Based on the obtained maps of medical geographical zoning it is possible to identify favorable areas for the development of vectors, as well as the most favorable parts of the inhabited zone in terms of epidemiological conditions. The maps can be used to differentiate the

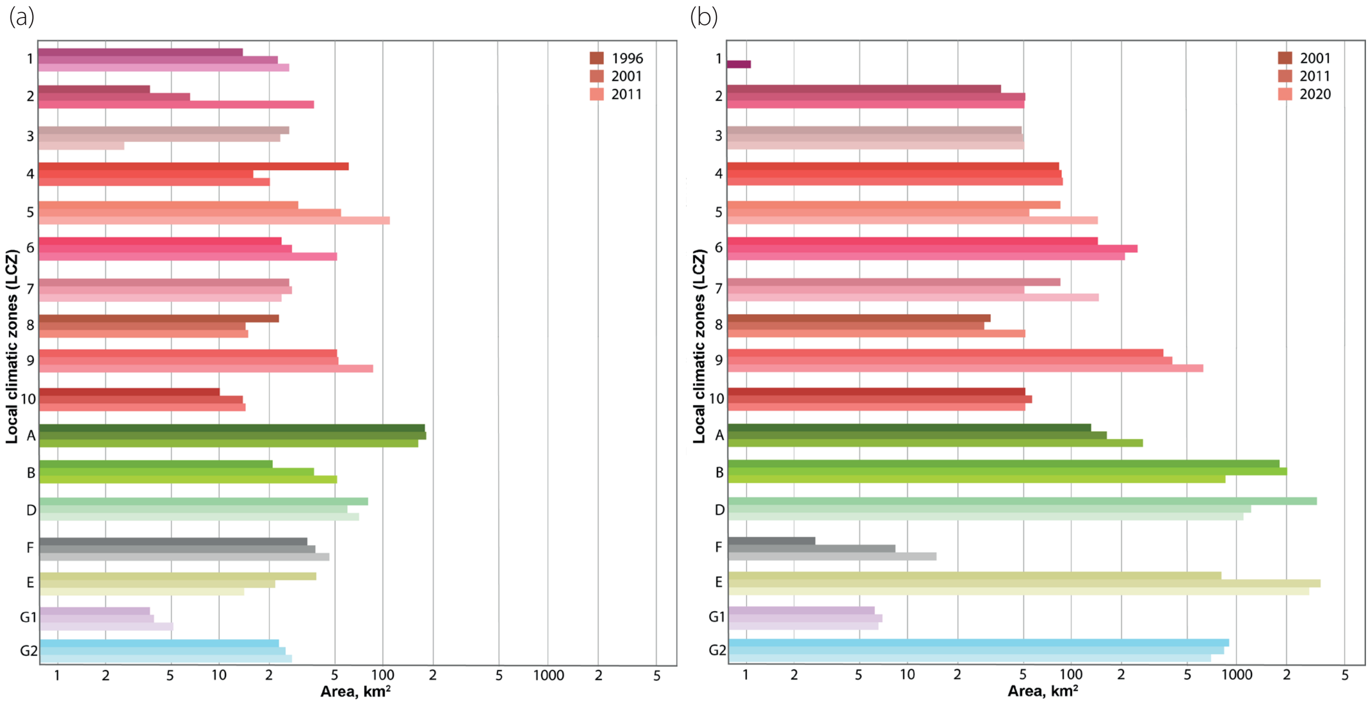

Fig. 4. LCZ types areas ratio for study areas (scale is logarithmic): a) the western part of the Moscow region; b) Volgograd and the surrounding area. Local Climate Zones codes: 1 – compact high-rise, 2 – compact mid-rise, 3 – compact low-rise, 4 – open high-rise, 5 – open mid-rise, 6 – open low-rise, 7 – lightweight low-rise, 8 – large low-rise, 9 – sparsely built, 10 – heavy industry, A – dense trees, B – scattered trees, C – bush, scrub, D – low plants, E – bare rock / paved, F – bare soil / sand, G1 – water (sewage), G2 – water (endorheic)

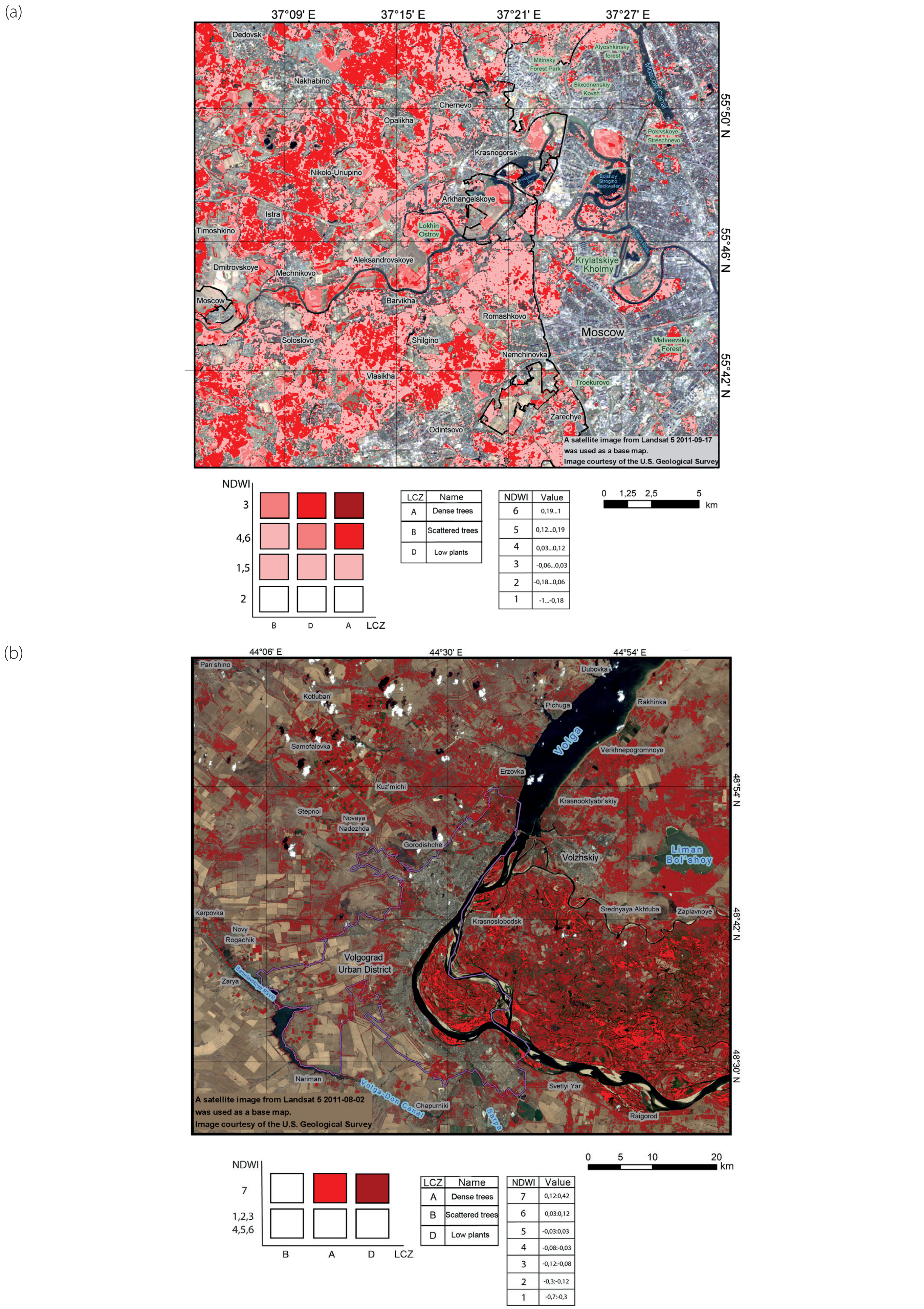

Fig. 5. Maps of medical geographic risks of the study areas: a) the western part of the Moscow region; b) Volgograd and the surrounding area

residential area by medical geographical conditions. On its basis, it is possible to develop a set of protective measures of the study area and to apply such measures (for example, increase the volume of sanitary treatment of water bodies of forest and forest-park zones).

CONCLUSION

The study of local climate zones was a big step in the analysis of the urban climate. It has no less potential for the purposes of medical geography. Despite the various methods used to detail LCZ, the goal of all research is to improve understanding of the mechanism of epidemics and to elaborate the potential of LCZ theory to model epidemiological situations for urban areas. In our study, we developed an improved algorithm for identifying local climate subzones for urban and suburban areas to provide medical geographical zoning and assessment of epidemiological risks of vector-borne diseases. Using the normalized water index (Gao NDWI), it became possible to develop a more detailed classification taking into account the moisture content of the vegetation cover, which can greatly contribute to the identification of the most favorable areas for the development of disease vectors. Based on the numerical values of the index, subzones with different types of moisture, from non-watered to over-watered (six types for the Moscow region and seven types for Volgograd) were identified.

The study revealed changes in the areas of different LCZs before and after outbreak periods, which may reflect changes in conditions and an increase in the degree of favorability for vectors. Thus, LCZs can be used as indicators of changes in the natural and man-made environment that can provoke disease outbreaks.

Maps of epidemiological risks make it possible to assess on which LCZs the preventive measures should be focused.

By increasing the spatial resolution of publicly available satellite imagery, LCZ can be identified with a higher geometric accuracy, which will also increase the information content of the proposed method.

This methodology was developed using the outbreaks of West Nile fever and vivax malaria as examples, but it can be used to analyze the spread of other mosquito-borne diseases as well.

The research was carried out as part of the HSE Basic Research Program in 2022.

REFERENCES

Adishcheva O.S., Malkhazova S.M., Orlov D.S. (2016). Rasprostranenie lihoradki Zapadnogo Nila v Rossii (The spread of West Nile fever in Russia). Vestnik moskovskogo universiteta. Series: Geografia, 5(4), 48-54 (in Russian).

Brousse O., Georganos S., Demuzere M., Dujardin S., Lennert M, Linard C. Can we use local climate zones for predicting malaria prevalence across sub-Saharan African cities? Environmental Reasearch Letters. 2020, 1, 124051.

Brousse O., Georganos S., Demuzere M., Vanhuysseb S., Wouters H. (2019). Using Local Climate Zones in Sub-Saharan Africa to tackle urban health issues. Urban Climate, 27, 227-242.

Brown H.E., Childs J.E., Diuk-Wasser M.A. (2008). Ecologic factors associated with West Nile Virus transmission, northeastern United States. Emerging Infectious Diseases, 14, 1539–1545.

Ceccato P., Flasse S., Tarantola S., Jacquemond S., Gregoire J.M. (2001). Detecting vegetation water content using reflectance in the optical domain. Remote Sensing of Environment, 77, 22–33.

Cornel A.J., Jupp P.G., Blackburn N.K. (1993). Environmental temperature on the vector competence of Culex Univittatus (Diptera: Culicidae) for West Nile Virus. Journal of Medical Entomology, 30, 449–456.

Dengue and severe dengue. World Health Organization. (2022) [online]. Available at: https://www.who.int/ru/news-room/fact-sheets/detail/dengue-and-severe-dengue

Eder M, Cortes F, Teixeira de Siqueira Filha N, Araújo de França GV, Degroote S, Braga C, Ridde V, Turchi Martelli CM. (2018). Scoping review on vector-borne diseases in urban areas: transmission dynamics, vectorial capacity and co-infection. Infect Dis Poverty. Sep 3; 7(1):90. DOI: 10.1186/s40249-018-0475-7.

Kleinman S., Glynn S., Busch M. (2005). The 2003 West Nile virus United States epidemic: the America's Blood Centers experience.

Korolkova E.M. (2013). Risk-management: upravlenie proektnymi riskami (Risk management: project risk management). Uchebnoe posobie dlya studentov ekonomicheskih special'nostej. Tambov: FGBOU VPO TGTU, 160 p. (in Russian).

Lvov D.K., Pisarev V.B., Petrov V.A. (2004). Lihoradka zapadnogo nila po materialam vspyshek v Volgogradskoy oblasti v 1999–2002 (West Nile fever in Volgograd region in 1999-2002). Volgograd., 102 p. (in Russian).

Massaro E, Kondor D, Ratti C. (2019). Assessing the interplay between human mobility and mosquito borne diseases in urban environments. Sci Rep. 2019 Nov 15; 9(1):16911, DOI: 10.1038/s41598-019-53127-z.

Mironova V., Shartova N., Beljaev A., Varentsov M., Grishchenko M. (2019). Effects of Climate Change and Heterogeneity of Local Climates on the Development of Malaria Parasite (Plasmodium vivax) in Moscow Megacity Region. International Journal of Environmental Research and Public Health, 16, 694.

Mironova V.A., Shartova N.V., Beljaev A.E., Varentsov M.I., Korennoy F.I., Grishchenko M.Y. (2020). Re-introduction of vivax malaria in a temperate area (Moscow region, Russia): a geographic investigation. Malaria Journal, 19, 116.

Misslin R., Telle O., Daudé E., Vaguet A., Paul R.E. (2016). Urban climate versus global climate change-what makes the difference for dengue? Ann N Y Acad Sci. Oct; 1382(1), 56-72, DOI: 10.1111/nyas.13084.

Roehrig J.T. (2013). West Nile virus in the United States – a historical perspective. Viruses. Dec 10; 5(12), 3088-108, DOI: 10.3390/v5123088. PMID: 24335779.

Samsonov T.E., Trigub K.S. (2018). Kartografirovanie lokal'nyh klimaticheskih zon Moskvy po kosmicheskim snimkam (Mapping of local climate zones of Moscow city). Geodezija i kartografija, 79(6), 20-31 (in Russian).

Shartova N., Mironova V., Zelikhina S., Korennoy F., Grishchenko M. (2022). Spatial patterns of West Nile virus distribution in the Volgograd region of Russia, a territory with long-existing foci. PLoS Neglected Tropical Diseases, 16(1), No. e0010145.

Stewart I.D., Oke T.R. (2012). Local climate zones for urban temperature studies [online]. Available at : https://www.researchgate.net/publication/258607564_Local_Climate_Zones_for_Urban_Temperature_Studies

Tourre Y., Jarlan L., Lacaux J., Rotela C., Lafaye M. (2008). Spatio-temporal variability of NDVI–precipitation over southernmost South America: possible linkages between climate signals and epidemics. Environment Research Letters, 3, No. 044008.

Varentsov M.I., Grishchenko M.Y., Wouters H. (2019). Simultaneous assessment of the summer urban heat island in Moscow megacity based on in situ observations, thermal satellite images and mesoscale modeling. Geography, Environment, Sustainability., 12(4), 74–95.

World Urban Database – World Urban Database and Access Portal Tools (wudapt.org).

RESEARCH PAPER

ZONING OF DESERT, STEPPE, STEPPE-FOREST AND FOREST ECOSYSTEMS BY CARBON AND NITROGEN ISOTOPE IN MONGOLIA AND WESTERN TRANSBAIKALIA

Anna M. Khubanova[1], Valentin B. Khubanov[1*], Denis A. Miyagashev[2]
[1]Dobretsov Geological Institute of Siberian Branch of Russian Academy of Sciences (GIN SB RAS), 6a, Sakh'yanovoy str., Ulan-Ude, Buryatia, Russia, 670047,
[2]Institute of Mongolian, Buddhist and Tibetan Studies of Siberian Branch of Russian Academy of Sciences (IMBTS SB RAS), 6, Sakh'yanovoy str., Ulan-Ude, Buryatia, Russia, 670047
*Corresponding author: +79246501514, khubanov@mail.ru
Received: January 18th, 2023 / Accepted: September 4th, 2023 / Published: October 10th, 2023
https://DOI-10.24057/2071-9388-2023-2720

ABSTRACT. The Mongolian–Transbaikalian region of the Central Asia is known for its wide range of intracontinental ecosystems from desert through steppe to taiga forest and mountain tundra. Data on the isotopic composition of carbon and nitrogen in the bone and dental tissues of herbivorous animals inhabiting the desert, steppe, and forest–steppe landscapes of Outer Mongolia and Western Transbaikalia are presented. The maximum values of the carbon isotope ratio are observed in animals from the desert (Gobi Desert) and the semi-desert landscapes, median (mean) $\delta^{13}C$ is -17.9‰. The minimum values of $\delta^{13}C$ were obtained by herbivorous animals of the forest-steppe and the forest landscapes (Transbaikalia), which median $\delta^{13}C$ is -23‰. The fauna of the steppes (median $\delta^{13}C$ is -21.7‰) has intermediate values of the carbon isotopic composition. According to the isotope composition of nitrogen, the isotope-geochemical isolation of ecosystems is less pronounced.

KEYWORDS: herbivorous animals, carbon and nitrogen stable isotope, ecosystem zoning, Mongolia, Western Transbaikalia

CITATION: Khubanova A. M., Khubanov V. B., Miyagashev D. A. (2023). Zoning of Desert, Steppe, Steppe-Forest and Forest Ecosystems By Carbon And Nitrogen Isotope in Mongolia And Western Transbaikalia. Geography, Environment, Sustainability, 3(16), 14-31
https://DOI-10.24057/2071-9388-2023-2720

ACKNOWLEDGEMENTS: This work was supported by Russian Science Foundation grant #23-28-01348.
We thank professor Valentin N. Golosov, professor Yaroslav V. Kuzmin and the anonymous reviewer for useful comments that helped to improve the paper.

Conflict of interests: The authors reported no potential conflict of interest.

INTRODUCTION

In biogeographic, paleogeographic and paleontological (zooarchaeological) studies, the stable isotope ($^{13}C/^{12}C$, $^{15}N/^{14}N$) analysis is widely used for reconstruction of diet, landscape and climatic conditions for the growth of plant food resources and animal habitat, including disappeared animals (Bocherens et al. 1991; Fernandez et al. 1991; Fizet et al. 1995; Germonpre and Lbova 1996; Bocherens et al. 1996; Koch 1998; Bocherens 2003; Palmqvist et al. 2003; Barberena et al. 2009; Drucker et al. 2010; Drucker et al. 2011; Di Matteo et al. 2013; Britton et al. 2013; France et al. 2014; Krylovich et al. 2020; Skippington et al. 2021; Kradin et al. 2021; Kuzmin et al. 2021; Kuzmin et al. 2023).

The ratio of carbon isotopes in animals depends on the plants they consume. Plants are divided into three main groups according to the type of photosynthesis: C3-plants, C4-plants and CAM-plants. Plants of temperate and cold natural zones belong to the first type of photosynthesis (C3), they are characterized by an average $\delta^{13}C$ of about -27‰. The second type includes C4 plants, predominantly growing in hot and arid climates, with $\delta^{13}C$ about -13‰. The third group of plants includes cacti and succulents, $\delta^{13}C$ values that are in the range between $\delta^{13}C$ values in plants with C3- and C4-type photosynthesis. In addition, a relatively light isotope composition of carbon is observed in forest vegetation, and a relatively heavy isotopic composition is due to a decrease in the effect of isotope fractionation in the case of growth in open spaces, for example, in the steppe (O'Leary 1988; Bocherens 2003; Svyatko 2016).

The ratios of stable nitrogen isotopes in animals are affected by various physiological (hunger, dehydration, lactation period) and ecological processes (drought, soil salinization, manure) during which $\delta^{15}N$ values are enriched or depleted. For example, when there is a shortage of food and water, the composition of the tissues of herbivores is characterized by enrichment in the heavy isotope of nitrogen; under favorable conditions, on the contrary, the amount of the heavy isotope of nitrogen is relatively reduced. In addition, due to the effects of fractionation, the values of $\delta^{13}C$ and $\delta^{15}N$ in the collagen of the bones of herbivores differ by an increase of 5‰ and 3-5‰, respectively, from the isotopic composition of their food. And further along the food chain, these values increase with each trophic level by 1‰ for $\delta^{13}C$ and by 3-5‰ for

$\delta^{15}N$ (Bocherens 2003; Gorlova et al. 2015; Svyatko 2016; Krajcarz et. al. 2016). Thus, using this method of the ratio of stable isotopes of carbon and nitrogen, it is possible to reconstruct the diet and ecological environment of animals.

The earth sciences widely use the principle of actualism, which is based on the analogy of modern geological processes and settings, including ecosystems, with those that took place in the past. Therefore, for paleogeographic reconstructions with an actualistic approach and the use of stable isotopes, it is necessary to know the ratio of carbon and nitrogen isotopes in modern animals inhabiting various landscape zones with a characteristic food supply.

One example of such studies is the work of H. Bocherens (Bocherens 2003), who compared the isotopic composition of ancient animals with the characteristics of animals from modern biocenoses in order to reconstruct the paleoecosystem of the mammoth steppe based on Upper Pleistocene sites in Eurasia and Alaska. In particular, he carried out isotopic studies of modern vegetation and megafauna in order to quantify the relative contribution of various food resources to the isotopic composition of the bone and dental tissues of animals. What served as the basis for comparing and reconstructing the feeding and living conditions of the following animals in the past: Equus sp., *Rangifer tarandus*, Bos or Bison, Alces sp., *Coelodonta antiquitatis, Mammuthus primigenius*. It should also be noted the work of F. Tahmasebi et al. (Tahmasebi et al. 2018), in which they studied modern and fossil plants and animals to track the dynamics of changes in the nitrogen isotopic composition of flora and fauna in the Yukon Territory, northwestern North America, between the Late Pleistocene and present. N. Fox et al. (Fox et al. 2023) used stable isotope analysis combined with radiocarbon dating for modern and fossil small fauna (squirrels, rabbits) in reconstructions of their ecological niches over the last > 55,000 years.

In the scientific literature for modern animals of Central Asia, there is a lack of such isotope studies (for example, Makarewicz 2017; Makarewicz et al. 2018; Ventressa Miller et al. 2019). Most of the previous work has focused mainly on a specific trophic group or species to analyze their diet. For example, C. Makarewicz and N. Tuross compared the diet between domestic and wild caprines, and M. Burnic Strum et al. investigated the dietary niches between domestic horse (*Equus caballus*) and wild horses (*Equus (ferus) przewalskii and Equus hemionus*) (Makarewicz and Tuross 2006; Burnic Strum et al. 2017). A. Kohzu et al. described food relationships by analyzing the isotopic composition of plants, arthropods, wild and domestic animals, and humans in Central Mongolia (Kohzu et al. 2009). H. Davie et al. studied the isotopic composition of several mammal and plant species from the Ikh Nart Natyre Reserve (Davie et al. 2014). V. Dambaev et al. studied the carbon isotopic composition of vegetation and soils of steppe pastures in Mongolia and Western Transbaikalia (Dambaev et al. 2016.). They also showed that against the backdrop of increasing degradation of pasture ecosystems, the main reason for which is the constant increase in the number of livestock, there is competition between wild and domestic animals for pasture niches.

The insufficiency of isotopic data does not allow one to reliably trace the relationship between variations in the isotopic characteristics of animals and the physiographic zonality of their habitats. At the same time, it should be noted that the region covering Mongolia and Western Transbaikalia is characterized by wide variations in intracontinental landscape settings from deserts-through-steppes to taiga forests and mountain tundra.

The purpose of this study is to compare variations in the isotope characteristics of herbivores with the landscape setting of their habitat. This paper presents the results of a study of carbon and nitrogen isotope composition of bone and dental tissues of livestock (*Bos taurus, Equus ferus caballus,* and *Ovis aries*) pastured in the Outer Mongolia and the Western Transbaikalia, as well as some wild animals (*Capreolus pygargus, Moschus moschiferus*). The sampling of animals done does not reflect the entire species composition of the herbivorous fauna and has a local character from desert, steppe and forest-steppe regions, i.e., does not cover all the diversity of ecosystems. Nevertheless, the data obtained make it possible to get an idea of the possibilities of applying isotope methods for isotope-landscape zoning of the territories of the Central Asia.

ECOSYSTEMS AND MATERIALS

We focused the research on animals grazing on the territory of Mongolia and Western Transbaikalia. This vast region contains various ecosystems stretching as sublatitudinal belts: from deserts through steppes to taiga forests and mountain tundra. The territory division into natural zones (Fig. 1) is based on the landscape (ecosystem) distribution schemes developed by the predecessors (Atlas of Transbaikalia 1967; The Ecological Atlas… 2015; Atlas of ecosystem… 2019; Ecological and Geographical… 2019). The current study covered the following main ecosystems: desert, semi-desert, steppe, forest-steppe, and forest (taiga).

The desert and semi-desert zones occupy about 40% of the Outer Mongolia and represent northern part of the Gobi Desert. The relief combines plains of different heights, low and medium-altitude mountains, as well as desert foothills of bald mountains (Simukov 2007; Petukhov et al. 2018).

The climate is characterized by an average amount of precipitation from 50 to 150 mm with uneven distribution throughout the year with an average annual air temperature of +4 to +8°C in deserts and from 0 to +4°C in the semi-deserts. Summers are dry and warm in the desert, arid and moderately cool in the semi-desert, in both cases with cold winters (Petukhov et al. 2018; Atlas of ecosystems… 2019).

According to botanical and geographic zoning, the desert zone includes various deserts and desert, petrophytic and psammophytic steppes with weakly humus light brown and gray-brown saline soils. These soils are dominated by perennial plants (*Stipa gobica, S. Glareosa*, Allium, *Eurotia ceratoides*), small shrubs (*Anabasis brevifolia, Nanophyton erinaceum, Éphedra*, short Halóxylon, Potaninia, *Artemisia terrae-albae*) are widespread there as well. Such plant species and subspecies as Kalidium, Halóxylon, Reaumuria, Caroxylon *Salsola passerina*, Brachanthemum, Nitraria are widespread on highly saline soils.

The semi-desert zone covers dry and desert steppes dominated by light chestnut soils, as well as brown sandy soils and sands, and often saline soils. The following plant communities mostly grow here: Artemisia - bunchgrass, bunchgrass (Stipa, Cleistogénes, Agropyron) wish Caragána, Stipa–Cleistogénes, Nanophyton, Artemisia, Ajania, Allium, Stipa glareosa. Brown saline soils are planted with communities with bunchgrass (Stipa gobica, S. glareosa), perennial saltworts (Salsola passerine, Reaumuria songarica) and with Stipa – Allium plant communities.

The steppe zone occupies most of northern half of the Outer Mongolia, and is also present in the southern and central parts of the Western Transbaikalia. It covers the

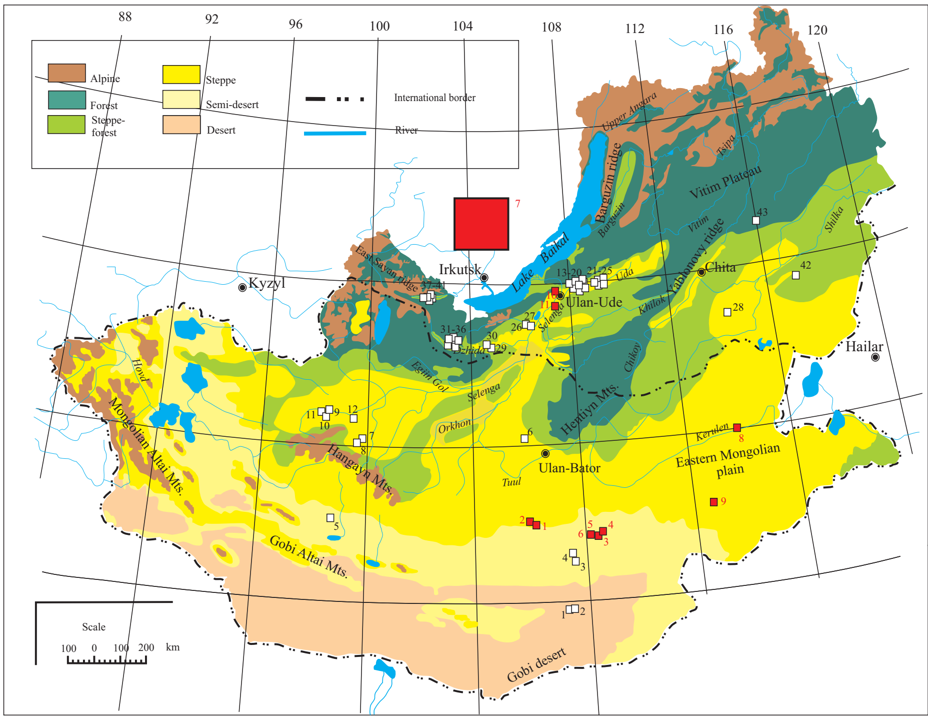

Fig. 1. Landscape zones of Mongolia and Western Transbaikalia (Russian Federation) (by Atlas of Transbaikalia, 1967; The Ecological Atlas…, 2015; Atlas of ecosystems…, 2019; Ecological and Geographical…, 2019) and sampling locations for isotopic analysis. Research sites are presented as squares: white - this study (see Table 1); red - research by other authors: 1 – *Capra sibirica* (Makarewicz, Tuross, 2006), 2 – *Ovis aries* (Makarewicz, Tuross, 2006), 3 – *Bos Taurus*, 4 – *Capra sibirica*, 5 – *Ovis aries*, 6 – *Equus ferus caballus* (Davie et al., 2014); 7 – *Capreolus pygargus* and *Moschus moschiferus* (Weber et al., 2011); 8-11 – plants (Dambaev et al., 2016): Dornod aimag (8), Sukhbaatar aimag (9), Mukhorshibirsky district (10), Ivolginsky district (11)

Khangai Range, the foothills of the Khentei Range, the East Mongolian Plain and the intermountain depressions of the basin of the middle and lower reaches of the Selenga River in the Transbaikalia. The climate is sharply continental, where the average annual air temperature ranges from -2 to +4°C with an average annual precipitation of 150–400 mm. Summers are moderately dry and cool, winters are harsh.

This zone includes moderately dry steppes and meadow steppes. The moderately dry steppes are characterized by dominance of dark chestnut soils, with inclusions of chernozem with the following types of vegetation: forb-bunchgrass and rhizome grass (Stipa, Leymus, Festuca, Carex), shurbs (Caragana) with forb-grass (Festuca ssp.) and Artemisia with shurbs (Caragana, Amygdalus).

The meadow steppes are developed on chernozems, carbonate-free and tundra peaty-gley soils and on sandy soils with forb-grass Filifolium sibiricum, Artemisia and such shrubs, as Armeniaca sibirica, Ribes ssp., Ulmus pumila.

The semi-desert steppe based on sandy loam and rubbly sandy loam soils are of subordinate importance with forb-grass (*Serratula centauroides, Astragalus brevifolius, Cleistogenes squarrosa, Asterothamnus heteropappoides, Vincetoxicum sibiricum)–gropyron criststum–Stipa glareosa, S. krylovii* communities and with shurbs *Eurotia ceratoides, Caragana bungei*. It should be noted that the steppes of Western Transbaikalia mainly occupy low-lying parts of intermountain depressions, which is why pasture lands are relatively limited in area than in the steppes of the Khangai and Khentei highlands. Accordingly, these small pastures may have a higher load from grazing small and large cattle, especially in the case of unsystematic year-round grazing (Boikov et al. 2002). Intensive use of these pastures leads to a change in phytocenoses (plants that are less eaten by livestock become widespread) and destruction of the soil cover (deflation, washout, salinization). In addition, from the increased density of livestock per unit area in the soil, water and plants of these pastures, a relatively increased amount of nitrogen-rich substances is recorded due to the abundance of animal waste. High pressures on rangelands also occur near relatively large settlements.

The forest-steppe zone is common in northern part of the Outer Mongolia and in southern half of the Transbaikalia. It predominantly occupies the foothills and spurs of mountain ranges, where the slopes of the northern exposure are covered with forests, while the southern slopes are represented by a steppe landscape and/or meadows. The Forest zone covers relatively small areas in north of the Outer Mongolia and is widespread in the Transbaikalia. The forest zone is developed along mountain ranges and within the Vitim Plateau.

For the forest-steppe and forest zone of the Transbaikalia, the average annual air temperature is about -2.5 ° C in the forest-steppe and from -2 to -6°C in the forest belts, in the bald mountain belt (on the ridges of the plateau periphery) - from -7 to -11°C, with an average annual precipitation of 400–600 mm in the forest-steppe and up to 800–1200 mm in the mountainous taiga and the bald mountains (Boykov et al. 2002; Osipov 2005; Plyusnin 2015).

Brown-colored, podzolic coarse-skeletal and soddy-carbonate-leached soils predominate in the forested area. The forest cover is represented by: *Pinus sibirica*, Picea, Larix and *Betula rotundifolia* with shurbs (*Rhododendron parvifolium, Vaccinium vitis-idaea, Duschekia fruticosa, Ledum palustre, Calamagrostis lapponica*), Larix with *Betula middendorffii* and *B. exilis*, woodland with Picea and Larix; grassy: *Pedicularis verticillata, Delfinium crassifolium, Carex amgunensis* with moss *Rhytidium rugosum, Geum aleppicum, Crepis praemorsa, Euphorbia jenisseiensis, Crepis praemorsa, Anemone crinita, Saussurea controversa*. The wetlands include peat-bog soils; the vegetation consists of shurbs *Vaccinium uliginosum, Chamaedaphne* *calyculata–Carex meyeriana–Drepanocladus vernicosus, Drepanocladus sendtneri, Meesia triquetra with grass and moss Tomenthypnum nitens, Thuidium abietinum, Rhytidium rugosum, Carex dioica, Carex limosa, Caltha palustris, Equisetum fluviatile, Cicuta virosa, Epilobium palustre*.

The meadow and steppe areas include chernozem, dark chestnut and less often tundra peaty-gley soils. The meadow communities are represented by the following grass: *Leymus secalinus, Poa pratensis, Elytrigia repens, Agrostis mongolica, Bromus secalinus, Sanguisorba officinalis, Medicago falcata with shurbs (Salix microstachya, Hippophae rhamnoides, Ulmus pumila*) and *Populus laurifolia*; with *Carex* and *Calamagrostis*. Forb-grass vegetation dominates in the steppe areas: *Rhinactinidia eremophila, Peucedanum morisonii, Dracocephalum foetidum, Oxytropis oligantha, Saussurea sajanensis, Potentilla fragarioides with Agropyron cristatum and Festuca lenensis; Stipa capillata, Stipa krylovii, Leymus chinensis, Bupleurum scorzonerifolium, Galium verum, Aconogonon angustifolium, Oxytropis filiformis, Astragalus melilotoides*.

The bald mountain zone occupies the watersheds of the Mongolian Altai, Khangai, Eastern Sayan, Barguzin and Northern Transbaikalia ranges. In botanical and geographical terms, these are tundra and light forests with gley and tundra soils. The tundra vegetation is dominated by lichens (*Cladonia alpestris, C. sylvatica, C. rangiferina*), shrubs (*Betula rotundifolia, Rhododendron aureum, Salix glauca, Empetrum sibiricum, Cassiope ericoides*), grass (*Festuca ovina, Carex ensifolia, Pedicularis oederi, Calamagrostis lapponica, Carex globularis, C. ensifolia, Hierochloe alpina*). The woodland vegetation is represented by *Pinus sibirica* and *Larix sibirica–Pinus sibirica –Betula rotundifolia* – shrubs (*Vaccinium vitis-idaea, Vaccinium uliginosum*) – mosses (*Dicranum scoparium, Pleurozium schreberi*) – lichens (*Cladonia turgida, Cladonia uliginosa*) plant communities.

METHODS

Sample collection

In Mongolia, sampling was carried out in the desert (South Gobi aimag), semi-desert (Middle Gobi and Bayankhongor aimags) and steppe (Central, Arkhangai and Dzabkhan aimags) landscape zones. In the Transbaikalia, samples were taken in the steppe (Zaigraevsky, Khorinsky and Selenginsky districts of Buryat Republic of Russia, Aginsky district of Zabaykalsky Krai of Russia), forest-steppe and forest (Dzhidinsky, Zakamensky and Tunkinsky regions of Buryat Republic, Tungokochensky and Baleisky regions of Zabaykalsky Krai) landscape systems (Fig. 1, Table 1).

The sampling was carried out in the central parts of landscape ecosystems (deserts/semi-deserts, forest-steppe/forest steppes) in order to best characterize the isotope composition of animals in their habitat. The geographical location of the sampling points was recorded by the GPS navigator (Table 1). The material was collected from the daylight surface. Samples devoid of muscle and cartilage tissue, and sufficiently preservated as observed by external signs (color, integrity, strength and density of the material, absence of secondary carbonation signs, etc.) were preferred. Basically, dental material was selected, since it turned out to be more accessible, and, in combination with jawbone fragments, it is good for identifying the type of the deceased animal. In addition, bone tissues, unlike dental tissues, are exposed to secondary transformation during fossilization and diagenesis, which to a greater extent affects the poor preservation of the primary isotope composition (Lee-Thorp 2008; Pidoplichko 1952). It should be noted that sampling of the remains of domestic animals in the forest-steppe and forest zones was carried out on open pastures (steppe or meadow) near settlements.

Dental and bone tissues (dentine, bone) of household herbivorous animals (*Bos taurus* (bull), *Bos mutus* (yak), *Equus ferus caballus* (horse), *Ovis aries* (sheep) and wild animals (*Capreolus pygargus* (roe deer), *Moschus moschiferus* (musk deer) were analyzed.

Sample preparation

The weighted amounts of the selected dental (dentin) and bone material for C-N isotope analysis varied from 0.5 to 4 g. The whole selected material was first brush-cleaned, washed in distilled water (ultrasonic bath), and dried in the open air. To calculate the collagen output, each sample was weighed on an Acculab (USA) analytical balance (model ATL- 220d4-I). Then the samples were soaked for 24 h in dichloromethane for degreasing, then dried and processed according to Longin's modified technique (Longin 1971; Arslanov 1987; Nikolaev et al. 2006). The technique included demineralization of the samples for 3–5 days in 0.5 M solution of HCl, until malaxation of the bone tissue, rectification from lipids and humic acids by soaking in 0.125 M solution of NaOH for 20 h, and dissolution of residue in a weak solution of HCl at 100°C for 17 h. The obtained colloid solution was separated into heavy and light fractions by centrifugal separation on an ELMI CM-50 centrifuge (Latvia) at 15000 RPM for 45 min. Then the light fraction (refined collagen) was dried in a drying closet at 70°C until solid residue was obtained. After that, the refined collagen was weighed on an analytical balance and the relative collagen output was calculated ($Y_{coll.}$, wt%) using the formula:

$Y_{coll.} = M_{coll.}/M_{bone.}*100\%$,

$M_{bone.}$ is the mass of the weighed amount of bone or dental tissue and $M_{coll.}$ is the mass of collagen.

Isotope analysis

The isotope analysis of the refined collagen samples was carried out on a Flash EA 1112 element analyzer ("Thermo Finnigan", Germany) in line with a Thermo Finnigan MAT 253 isotope mass-spectrometer at the Analytical Center of Mineralogical, Geochemical and Isotope Studies «Geospektr» of Dobretsov Geological Institute of the Siberian Branch of the Russian Academy of Sciences, Ulan-Ude, Russia. Before the analysis, dry collagen samples were tightly packed into aluminum foil tins and weighed on a Mettler Toledo MX-5 microbalance. The obtained isotope data were conveyed as $\delta^{13}C$ and $\delta^{15}N$ values in per mille (‰):

$\delta^{13}C = [(^{13}C/^{12}Csample/^{13}C/^{12}Cstandard) - 1] \times 1000‰$,

$\delta^{15}N = [(^{15}N/^{14}Nsample/^{15}N/^{14}Nstandard) - 1] \times 1000‰$.

The $\delta^{13}C$ values were calculated regarding the isotopic composition of «Pee Dee Belemnite» (PDB) and $\delta^{15}N$ – of atmospheric air. And the international (USGS 40, IAEA-N-1) and intralaboratory (MCA-7, MCA-8) reference samples were analyzed as control samples. The measurement uncertainty in determining isotope ratios was (1σ) ± 0.2‰ for $\delta^{13}C$ and $\delta^{15}N$.

The percentage content of carbon (C, %) and nitrogen (N, %) was calculated on the basis of the control external standard USGS40 (L-Glutamic acid) in which carbon concentration was 40.82% and nitrogen – 9.52% according to the formulas:

$N_{sample} = S_{Nsample}*N_{stand}/S_{Nstand}*M_{stand}/M_{sample}$

$C_{sample} = S_{Csample}*C_{stand}/S_{Cstand}*M_{stand}/M_{sample}$

where S is a signal of nitrogen (N) or carbon intensity (C) of the sample (sample) or the standard (stand); N –

percentage of nitrogen in the sample (sample) or the standard (stand); C – percentage of carbon in the sample (sample) or the standard (stand); M_{stand} is the mass of the weighed amount of the standard, M_{sample} – the mass of the weighed amount of the sample.

For the assessment of the degree of collagen preservation in the fossil bones, the C/N ratio which is expected to be within the interval from 2.9 to 3.6 was used (DeNiro and Schoeninger 1983; Ambrose 1990; Brown et al. 1988).

Statistical analysis

For statistical comparison of the isotopic compositions of bone and dental tissues of herbivores from different ecosystems, we used the average (median) values calculated using the Bayesian bootstrap method (Rubin 1981). The algorithm is implemented in the environment R (Bååth 2018). It well suited this method for calculating statistical indicators (mean, standard deviation, quantiles, including median) with small samples. In addition, visualization with box plot is convenient for comparing data.

Since the amount of isotope data is small, the non-parametric comparison method of the Mann-Whitney U test was also used. This approach makes it possible to compare two independent small samples and is a nonparametric alternative to the Student's t-test (Mann and Whitney 1947).

RESULTS AND DISCUSSION

In total, the isotope composition of 43 samples was investigated (Table 1). For almost all of them, atomic ratios of carbon to nitrogen (C/Nat) were fixed in the range from 2.9 to 3.6, which indicates a satisfactory preservation of these samples (Ambrose 1990; Svyatko 2016). Samples MNG-05-16, C14(14)-2, C19(14)-1, C15(14)-2, and C10(14) are the exceptions, they are assumed to have their primary isotope composition altered under the influence of secondary processes. These samples were not used in the discussion. The percentages of carbon (C, %) and nitrogen (N, %) are within the range for well-preserved collagen, at least 16.4% and 6.2%, respectively (Ambrose 1990).

Carbone isotope ratio

It is known that carbon and nitrogen isotope composition can provide information on the sources of protein in the diet. The carbon isotope composition of collagen and dentin isolated from bone and dental tissues of herbivorous animals reflects the isotope composition of vegetation and, therefore, the basis of food chains (Nikolaev et al. 2006; Bocherens and Drucker 2003; LI et al. 2009; Ma et al. 2012). Depending on the photosynthesis type, the major part of the plants is divided into C3– and C4–plants. In steppes, boreal forests of the temperate climatic zone and tundra of moderately cold and cold regions, plants with C3-type photosynthesis form the basis of the biomass. On average, these plants are characterized by $\delta^{13}C$ value of about -27‰ (O'Leary 1988; Bocherens 2003; Svyatko 2016) which, however, can widely vary. The reasons for lightweight carbon isotope composition in the vegetation are reduction of illumination under the forest canopy, re-assimilation of CO_2 in a relatively closed space (in a dense forest) and/or depletion of nutrients in the soil. Whereas the relatively heavyweight isotope composition is due to a decrease in the effect of isotope fractionation in the case of growing in open spaces, for example, in steppe, as well as due to water and salt stress. C4 plants grow in hot and warm climates – in tropical humid forests, semi-deserts and deserts, $\delta^{13}C$ values from - 14‰ to - 10‰ are typical for them (O'Leary 1988; Bocherens 2003; Svyatko 2016). The carbon isotope composition for herbivorous animals will be weighted by 5‰ regarding the composition of their plant food (Bocherens 2003; Svyatko 2016).

In **the desert/semi-desert** landscapes, herbivorous animals have the maximum values of carbon isotope ratios (Fig. 2, Table 1). Values $\delta^{13}C$ for desert and semi-desert *Equus ferus caballus* and *Ovis aries* range from -18.8‰ to -15.4‰. The indicators for horses living in semi-deserts are lower and are -18.6‰ and -18.4‰. The isotope values for sheep from semi-deserts are $\delta^{13}C$ = -18.8‰. The obtained values of carbon isotope ratios indicate a diet consisting of plants with C3– and C4–type photosynthesis. The following C4 plants are known in this area: *Cleystogenes squarrosa, Eragrostis minor, Enneapogon borealis, Setaria viridis, Tribulus terrestris,* etc. (Table 2), which have a carbon isotope composition varying from -14.6 to -11.4‰. Plants with C3–type of photosynthesis are characterized by lighter indicators, varying from -29.8 to -24.3‰ (Table 2). Taking into account the correction for isotope fractionation from producers to consumers of the first order, for herbivorous animals with a mixed diet (C3 and C4), δ13C will vary approximately in the range from -21.5 to -7.5‰ (van der Merwe 1992).

The values of dentin carbon isotope ratios of horses inhabiting in the deserts and semi-deserts are within this range, and they are also well compared with the carbon isotope data of horses of the semi-deserts in the Ikh Nart reserve (East Gobi aimag) located in the eastern part of the Gobi Desert ($\delta^{13}C_{hair}$ / $\delta^{13}C_{bone}$ = -18.8±1.1‰ / -16.8±1.1‰) (Davie et al. 2014). It should be noted that in (Davie et al. 2014) the values of carbon and nitrogen isotopes are given for hair samples. Therefore, to correctly compare $\delta^{13}C$ and $\delta^{15}N$ hair keratin and bone collagen for herbivores, the following corrections were used: $\delta^{13}C_{bone} = \delta^{13}C_{hair} + 2.0‰$ and $\delta^{15}N_{bone} = \delta^{15}N_{hair} + 2.1‰$ (Kohzu et al. 2009). Similar values of carbon isotope ratios are observed in horses that lived in the arid landscapes of Southeast Kazakhstan during the Bronze Age ($\delta^{13}C_{bone}$ = -18.9±0.9‰) (Table 3) (Ananyevskaya et al. 2020).

The observed $\delta^{13}C$ of a single individual sheep is within the range of isotope variations of small cattle (*Ovis aries*) (-17.5±0.8‰) from the semi-desert landscape of the Baga Gazryn Chuluu, Middle Gobi Aimak (Makarewicz and Tuross 2006) and the Ikh Nart reserve ($\delta^{13}C_{hair}$ / $\delta^{13}C_{bone}$ = -19.3±1.4‰ / -17.3±1.4‰) (Table 3) (Davie et al. 2014).

In **the steppe** landscapes, herbivorous animals have a relatively light carbon isotope composition compared to the herbivores of arid landscapes. The values of carbon isotope ratios of cows and sheep vary from -22.4‰ to -20.2‰, which indicates the predominance of steppe grass with C3 photosynthesis (possibly xerophytic plants) in their diet growing in open areas with a temperate climate, where C4 plants have a sharply subordinate position (Bocherens 2003).

The carbon isotope compositions of animals of the steppes of Mongolia and Western Transbaikalia are comparable to each other. Values $\delta^{13}C$ in bone and dental collagen of herbivorous animals of the steppe landscapes of Mongolia and Western Transbaikalia vary from -22.1 to -20.0‰ and from -22.9 to -20.4‰, respectively. The carbon isotope composition of horses (-22.9 to -20.0‰) is relatively lightweight, suggesting an extended diet that included grass from meadows and/or forest-steppes. This

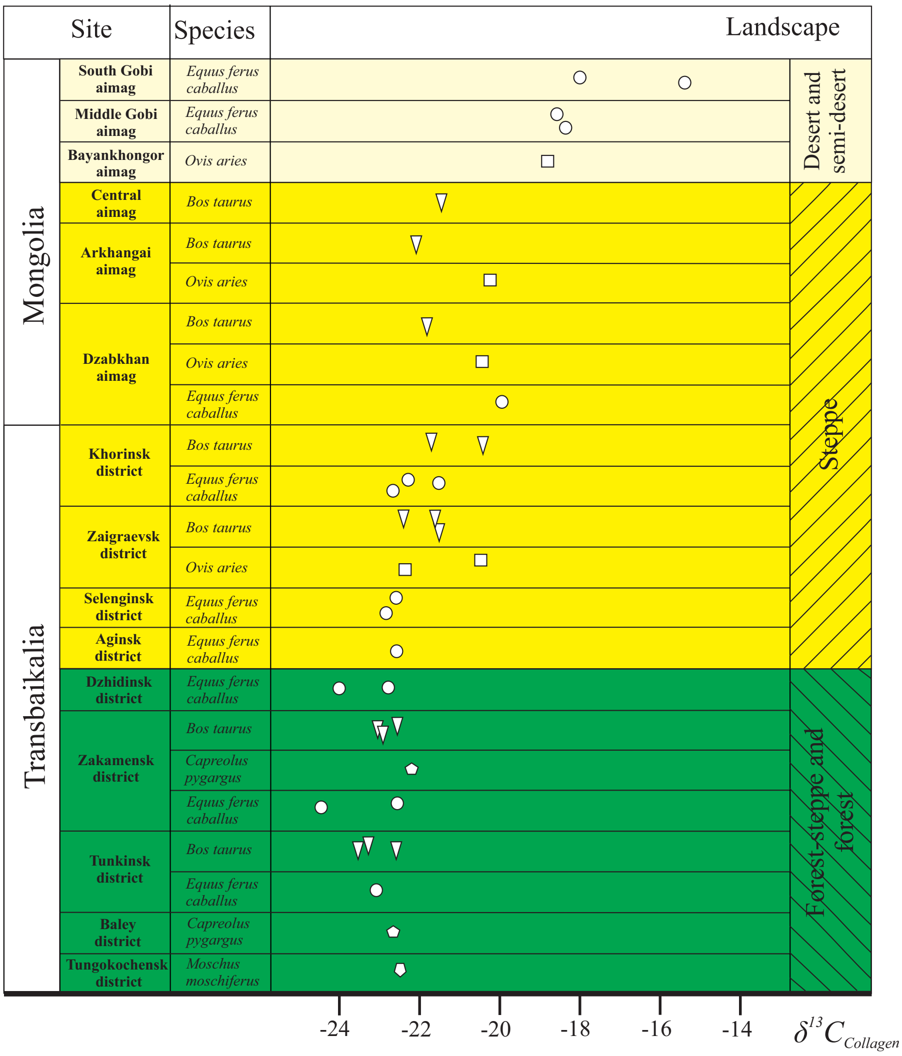

Fig. 2. Carbon isotope composition (δ^{13}C) of collagen from the herbivorous fauna of Mongolia and Western Transbaikalia. Square - *Ovis aries* ; circle - *Equus ferus caballus*; triangle - *Bos taurus*; pentagon - *Capreolus pygargus*; elongated pentagon - *Moschus moschiferus*

Table 2. Mongolian and Transbaikalian forage plants and carbon isotope composition

Latin name	Life form	Abudance			C3/C4 type	δ^{13}C (‰)
		Mongolia		Transbaikalia		
		Desert, Semi-desert	Steppe			
Poaceae						
Agropyron cristatum	Ph	++	+++	+	C3	-27.1
Achnatherum splendens	Ph	++	+	+	C3	-26.9
Cleistogenes squarrosa	Ph	++	++	+	C4	-14.6
Eragrostis minor	Ah		+		C4	-11.6 (for *Eragrostis sp.*)
Eragrostis pilosa	Ah	++	+		C4	-14.1
Enneapogon borealis	Ph	++	+		C4	-13.3
Festuca lenensis	Ph		+	+++	C3	-27±0.17
Festuca sibirica	Ph		+++		C3	-
Koeleria cristata	Ph		+++		C3	-28.8
Leymus chinensis	Ph		+++	+++	C3	-26.4
Poa attenuata	Ph		+		C3	-24.6 (for *P.pratensis*)

Poa botryoides	Ph			+	C3	-
Setaria viridis	Ah	+			C4	-12.3
Stipa krylovii	Ph	+	+++		C3	-25.2
Stipa glareosa	Ph	++	+++		C3	-
Stipa gobica,	Ph	++	++		C3	-
Stipa klemenzii	Ph	+	++		C3	-
Stipa baicalensis	Ph			+	C3	-25.7
Stipa sibirica	Ph		+		C3	-
Carex						
Carex duriuscula	Ph		+++	+++	C3	-27.5 (*Carex spp.*)
Carex pediformis	Ph		+	+	C3	
Fabaceae						
Astragalus adsurgens	Sh			+	C3	-26.5 (for *A. melilotoides*)
Astragalus brevifolius	Sh		++			
Caragana eucophloea	Sh	+	++		C3	-24.3
Caragana microphylla	Sh	+	++		C3	-24.5
Caragana pygmaea	Sh	+	++	+	C3	-
Caragana stenophylla	Sh	+	++		C3	-24.6
Oxytropis oxyphylla	Sh			+	C3	-
Oxytropis myriophylla	Sh			+	C3	-27.5
Forbs						
Allium bidentatum	Ph			+	C3	-25.1
Allium mongolicum	Ph	++			C3	-25
Allium polyrhizum	Ph	++			C3	-25.8
Amblynotus rupestris	Ph			+	C3	-
Arenaria capillaris	Ph	++	+	+	C3	-
Artemisia anethifolia	Bh	+		+	C3	-
Artemisia frigida	Se		+	+++	C3	-28.1
Artemisia commutata	Ph			+	C3	-
Artemisia dracunculus	Ph		+		C3	-26.9
Artemisia scoparia	Bh	+	+++	+	C3	-29.8 to -25.1
Artemisia terrae-albae	Se	++			C3	-
Arctogeron gramineum	Ph			+	C3	-
Aster alpinus	Se		+		C3	-28
Bupleurum scorzonerifolium	Ph		+	+	C3	-
Chamaerhodos erecta	Bh			+	C3	-
Convolvulus ammannii	Ph		+	+	C3	-25
Dasiphora fruticosa	Sh		+		C3	-
Ephedra sinica	Sh	++			C3	-24.4

Euphorbia discolor	Ph		+		C4	-12.1 to -13.5 (for *Euphorbia* sp.)
Filifolium sibiricum	Ph		++		C3	-26.8
Heteropappus altaicus	Ph			+	C3	-26.9
Heteropappus biennis	Bh			+	C3	-
Iris potaninii	Ph		+	++	C3	-26.7 (for *I.lactea*)
Lappula squarrosa	Ph			+	C3	-
Orostachus malacophylla	Bh			+	C3	-25
Polygonum aviculare	Ah		+		C3	-28.7
Potaninia mongolica	Se	++			C3	-26.6
Potentilla acaulis	Ph		+	+	C3	-27.3
Potentilla sericea	Ph			+	C3	-26.14±0.17
Potentilla bifurca	Ph		+	+	C3	-25.6
Ptilotrichum tenuifolium	Se			+	C3	-26.5
Ptilotrichum canescens	Se		+		C3	-
Taraxacum dissectum	Ph			+	C3	-
Taraxacum mongolicum	Ph			+	C3	-26
Thymus baicalensis	Se			+	C3	-29.1 (for *T. serphyllum*)
Thymus gobicus	Se	+	++		C3	
Tribulus terrestris	Se	++	+		C4	-13.4
Salicornia perennans	Se			+	C3	-26.6 (for *S. brachiata*)
Scorzonera austriaca	Ph			+	C3	-25.4
Silene chlorantha	Ph			+	C3	-25.4 (for *S. acaulis*)
Reaumuria soongorica	Sh	++			C3	-24.6
Vincetoxicum sibiricum	Ph		++	+	C3	-
Chenopodioideae						
Anabasis brevifolia	Sh	++	+		C4	-13.3
Bassia dasyphylla	Ah	++	+		C3	-25.1
Chenopodium aristatum	Ah		+	+	C3	-26.1
Eurotia ceratoides	Se	++	++		C3	-28.8
Halogeton glomeratus	Ah	++	+		C4	-14.6
Haloxylon ammodendron	Sh	++			C4	-13.5
Salsola collina	Ah	++	+		C4	-11.4
Salsola passerina	Ah	++			C4	-13.6
Kochia prostrata	Se		+	+	C4	-14
Nanophyton erinaceum	Sh	++			C4	-13.5

«+», «++», «+++» – presence of this plant species in this region in small, medium and larger quantities, respectively.
Ph : Perennial herb; Bh-biennial herb; Ah : Annual herb; Sh : Shrub; Se : Semishrub
C3/C4 type and $\delta^{13}C$ (‰) by (Boikov et al., 2002; Petukhov et al., 2018; Safronova et al., 2018; Danzhalova, Bazha, 2008; Structure and dynamics…, 2018; Urtnasan, Lyubarskiy, 2013; Golovanov et al., 2004; Tsognamsrai, Dugarzhav, 2016; Naidanov, 2009; Yudina et al., 2015; Pyankov et al., 2000; Chen et al., 2007; Codron et al., 2005; Goldman, 2010; Kalapos et al., 1997 ; Khatri et al., 2021; Li et al., 2006; Liu et al., 2004; Liu et al., 2009; Martin, Thorstenson, 1988; Oyungerel et al., 2004; Pearcy, Troughton, 1975; Spasojevic, Weber, 2021; Su et al., 2019; Tanaka-Oda et al., 2018; Wang et al., 2006; Wen, Zhang, 2011; Winter, 1981).

Table 3. Carbon and nitrogen isotope rations for Mongolian, Transbaikalian and Angarian herbivorous animals by other authors

#	Aimag or disrict	Specie	Material	$\delta^{13}C$ (‰)	$\delta^{15}N$ (‰)	Location
Desert/semi-desert (Mongolia)						
1	Middle Gobi[1]	*Capra sibirica*	*Molar*	-19.5±0.7	8.1±1.0	N 46°12´0´´ E 106°0´0´´ ~1450-1750 m high
2	Middle Gobi[1]	*Ovis aries*	*Molar*	-17.5±0.8	11.2±1.1	
3	Dornogobi[2]	*Bos Taurus*	*Hair / bone**	-18.0±1.1 / -16.0±1.1	10.2±0.7 / 12.3±0.7	N 45°25´48´´ E 108°23´24´´ ~1570 m high
4	Dornogobi[2]	*Capra sibirica*	*Hair / bone*	-20.9±0.9 / -18.9±0.9	9.3±0.8 / 11.4±0.8	
5	Dornogobi[2]	*Ovis aries*	*Hair / bone*	-19.3±1.4 / -17.3±1.4	10.6±0.4/12.7±0.4	
6	Dornogobi[2]	*Equus ferus caballus*	*Hair / bone*	-18.8 ±1.1 / -16.8 ±1.1	8.1±0.7 / 10.2±0.7	
Steppe (Mongolia)						
7	Dornod[3]	*Stipa krylovii, Artemisia frigida, Allium teniussum, Potentilla acaulis*	*Plant / bone***	~ -25,43 /~ -20,43	–	N 48°2´24´´ E 114°18´0´´ ~720 m high
8	Sukhbaatar[3]	*Stipa krylovii, Cleistogenes squarrosa, Agropyron cristatum*	*Plant / bone*	~ -25,94 /~ -20,94	–	N 46°24´36´´ E 113°10´12´´ ~1000 m high
Steppe (Transbaikalia)						
9	Mukhorshibirsky[3]	*Stipa krylovii, Artemisia frigida, Carex duriuscula, Potentilla acaulis*	*Plant / bone*	~ -27,16 /~ -22,16	–	N 51°02´50´´ E 107°49´25´´ ~950 m high
10	Ivolginsky[3]	*Stipa krylovii, Artemisia frigida, Potentilla acaulis*	*Plant / bone*	~ -27,57/~ -22,57	–	N 51°44´50´´ E 107°16´45´´ ~550 m high
Forest-steppe/forest (Angara)						
11	Angara[4]	*Capreolus pygargus*	Bone	-21.7±1.3	6.2±2.4	–
12	Angara[4]	*Moschus moschiferus*	Bone	-20.4±0.4	6.2±0.6	–

[1]Makarewicz, Tuross, 2006; [2]Davie et al., 2014; [3]Dambaev et al., 2016; [4]Weber et al., 2011.
* $\delta^{13}C_{bone} = \delta^{13}C_{hair}$ + 2.0‰ and $\delta^{15}N_{bone} = \delta^{15}N_{hair}$ + 2.1‰ (Kohzu et al., 2009).
** $\delta^{13}C_{bone} = \delta^{13}C_{plant}$ + 5.0‰ (Bocherens, 2003; Svyatko, 2016)

may be due to the fact that horses graze far away from human habitation and accordingly seek better pastures, while cows and sheep graze near shepherds' camps, within a kilometer radius, in degraded pastures (Davie 2014). It is also possible that horses chose floodplains, with a tree and shrub canopy, for grazing. In this case, the isotope composition of the grass would be close to that of the forest vegetation.

It should be noted that since carbon isotope ratios in the bone and dental collagen of the first-order consumers are enriched by 5‰ compared to the producers, the $\delta^{13}C$ of the steppe vegetation is expected to be between -28‰ and -25‰. It is these $\delta^{13}C$ values (from -27.6 to -25.4‰) that are observed in the vegetation of the steppes of Mongolia and Transbaikalia (Dambaev et al. 2016) (Table 2).

Horses ($\delta^{13}C$ from -24.5 to -22.5‰) and cattle (from -23.6 to -22.6‰) from **the steppe-forest/forest** landscapes are characterized by relatively lightweight carbon isotope composition. It indicates a decrease in their diet of steppe grass and an increased proportion of forest herbaceous and possibly shrub vegetation. Carbon isotope values of roe deer (-22.7‰; -22.2‰) from the forest-steppe and/or the forest landscape are within the range of variability of modern individuals of the Angara region inhabiting also the forest and forest-steppe biocenoses (from -18.9‰ to -23.8‰) (Weber et al. 2011). In contrast to the roe deer, the Siberian musk deer (-22.6‰) from the Transbaikalia have relatively lightweight carbon isotope values than modern individuals from the Angara region (from -20.9 to -20.3‰). It is possible that the Siberian musk deer from the Angara region inhabited more open area.

For statistical comparison of the carbon isotope composition in animals from different ecosystems, we calculated statistical criteria such as mean, standard deviation, quantiles including medians using Bayesian bootstrap (Table 4). This method works well with small sample sizes. In addition, since the median, in contrast to the mean, is less affected by extreme values, this approach allows us to exclude the influence on the sample of individual animals that had grazing outside a certain ecosystem. The display of quantiles and medians for $\delta^{13}C$ values using box diagrams (Fig. 3) clearly shows the difference in the isotopic composition of carbon in animals of desert/semi-desert, steppe, and forest-steppe/forest landscapes.

The Mann-Whitney U-test (Table 5) also shows the difference in the nutritional conditions of herbivores that had grazing in different ecosystems. In all three cases of comparison of U($\delta^{13}C$)-criterion for pair of independent samples (desert/semi-desert vs Steppe; steppe vs forest-steppe/forest; forest-steppe/forest vs desert/semi-desert) with critical U_{Cr} values we observe that U_{Cr} > U($\delta^{13}C$).

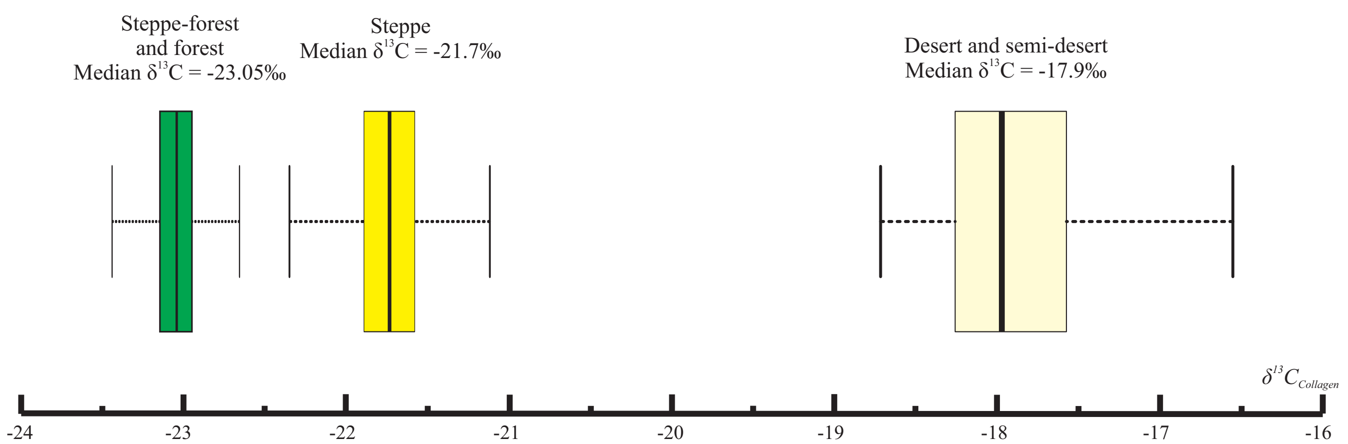

Fig. 3. Box plot (by Bayesian bootstrap method) demonstrating the landscape isolation by carbon isotope composition of the herbivorous fauna in Mongolia and Western Transbaikalia

Table 4. Bayesian bootstrap results*. Herbivore data by landscape.

Landscape (number of samples)	Summary of the posterior (with 95% Highest Density Intervals)				Quantiles				
	Min	Max	Mean	SD	2.5	25	Median	75	97.5
$\delta^{13}C$‰									
Desert/semi-desert (5)	-18.6	-16.8	-17.9	0.5	-18.9	-18.3	-17.9	17.6	-16.6
Steppe (23)	-22.2	-21.3	-21.7	0.2	-22.7	-21.9	-21.7	-21.6	-21.3
Steppe-forest/forest (15)	-23.4	-22.8	-23.1	0.2	-23.4	-23.1	-23.05	-22.9	-22.8
$\delta^{15}N$‰									
Desert/semi-desert (5)	6	7.9	6.9	0.5	6	6.6	6.9	7.3	7.9
Steppe (23)	6.3	7.9	7.1	0.4	6.3	6.8	7.1	7.3	7.9
Steppe-forest/forest (15)	5.5	7.2	6.3	0.4	5.6	6	6.3	6.6	7.2

*Number of posterior draws: 4000

This suggests that the divergence of carbon isotope composition in animals from different landscapes is statistically reliable.

Thus, the values of the carbon isotopic composition are increased in animals of desert landscapes, and the lowest values are in animals of forest-steppe landscapes. This may be because the diet of the herbivorous fauna of deserts and semi-deserts includes C4 and C3 plants. At the same time, C3 plants may have a relatively heavy isotopic composition of carbon because of the openness of the landscape and the prevalence of dry climate. For mammals of the steppe landscape, the diet comprises plants with the C3 type of photosynthesis (mainly herbaceous plants). In the forest-steppe/forest landscapes, the diet of animals contains woody, shrubby, and herbaceous plants with the C3-type of photosynthesis, but with a relatively light carbon isotopic composition. Therefore, forest-steppe/forest animals have the lightest carbon isotopic composition. The results got correlate well with the carbon isotopic composition of modern desert, steppe, and forest herbivores in other regions of the Earth (Bocherens 2003).

Nitrogen isotope ratio

The nitrogen isotopic composition ($\delta^{15}N$) of animals from different landscape zones varies from 4 to 11‰ (Fig. 4, Table 1). This indicator is controlled by the intake of N_2 (and the excretion of nitrogen metabolism products), which depends on the degree of acidity, salinity and depletion of the soils on which vegetation grows, the composition of the plant diet and the trophic level. In addition, nitrogen isotope composition is also sensitive to water and food

Table 5. Mann-Whitney U-test results. Herbivore data by landscape

Landscape (number of samples)	*U_{Cr}	Carbon isotope ratio		Nitrogen isotope ratio	
		**$U(\delta^{13}C)$	Result	$U(\delta^{15}N)$	Result
Desert/semi-desert (5) vs Steppe (23)	24	6	$UCr > U(\delta^{13}C)$ The differences are statistically significant	64.5	$UCr < U(\delta^{15}N)$ The differences are not statistically significant and are random.
Steppe (23) vs Forest-steppe/forest (15)	106	39.7		118	
Forest-steppe/forest (15) vs Desert/semi-desert (5)	14	4		46	

*U_{Cr} – Table Critical Values for the Mann – Whitney U-Test https://real-statistics.com/statistics-tables/mann-whitney-table/
**U – calculated according to (Mann, Whitney, 1947).

stress (Schoeninger and DeNiro 1984; DeNiro and Epstein 1981; Bocherens and Drucker 2003). At each transition to a higher trophic level, the δ15N values of animals change by 2-6‰ (Gorlova et al. 2015; Svyatko 2016; Krajcarz et. al. 2016).

For horses of **the desert/semi-desert** landscapes, the nitrogen isotopic composition obtained from dentin ranges from 5.5 to 8.3‰ (Fig. 4, Table 1). These values are relatively lightweight compared to the ratios of nitrogen isotopes of modern horses from the Ikh Nart Reserve ($\delta^{15}N_{hair}$ / $\delta^{15}N_{bone}$ = 8.1±0.7 / 10.2±0.7‰) (Davie et al. 2014) and Holocene horses ($\delta^{15}N_{bone}$ = 8.5± 2.0‰) from the semi-desert landscapes of Southeast Kazakhstan (Ananyevskaya et al. 2020) (Fig. 5, Tables 1, 3).

The isotope composition of nitrogen in sheep from the semi-desert landscape ($\delta^{15}N$ = 8.4‰) is also lighter relative to the range of isotopic characteristics of sheep (Ovis aries, domestic, provisioned) from the Middle Gobi aimag ($\delta^{15}N$ from 8.6 to 12.9‰, with an average of 11.2±1.1‰) (Makarewicz and Tuross 2006) (Fig. 5, Tables 1, 3).

The relatively lightweight nitrogen isotopic composition in the studied animals, especially Equus ferus caballus, may be due to the fact that these individuals experienced food and water stress to a lesser extent.

Horses from **the steppe** landscapes are characterized by relatively lightweight values of the nitrogen isotope ($\delta^{15}N$ from 5.0 to 7.9‰) compared to animals of the desert and the semi-desert. At the same time, cows ($\delta^{15}N$ from 4.6‰ to 10.0‰) and sheep ($\delta^{15}N$ from 5.2‰ to 11.0‰) show wide variations of $\delta^{15}N$ values (Fig. 4, Table 1).

Perhaps one reason for the high nitrogen isotope value in some cows and sheep is that they grazed near human habitations, where pastures are depleted and soils and waters are enriched with nitrogen waste (Davie 2014). Whereas horses grazed in larger areas and/or away from dwellings, where pastures are less degraded. Other hand, higher values of the nitrogen isotope of sheep may be because they need less water and can do without it for a long time (Burnik Sturm et al. 2017). Also, the heavyweight nitrogen composition in herbivores can be observed when they are fed with mother's milk (Fogel et al. 1989; Bocherens 2003). Usually, in sheep farms, individuals of the first and second years of life, who have not reached full maturity and the change of milk teeth, are slaughtered to obtain meat products (Ulyanov et al. 2011). Therefore, high values of δ15N in dentin can be explained by lactose nutrition and δ15N may be overestimated by 4–5‰, considering the trophic fractionation of isotopes (Jenkins et al. 2001; Svyatko 2016).

Horses of **the forest-steppe/forest** landscapes are characterized by a relatively lightweight nitrogen isotopic composition ($\delta^{15}N$ from 3.6 to 7.1‰). The isotopic composition of nitrogen of cow varies from 5.5 to 7.1‰ (Fig. 4, Table 1).

The ratios of nitrogen isotopes of roe deer and musk deer are increased and vary from 6.0 to 10.0‰. These

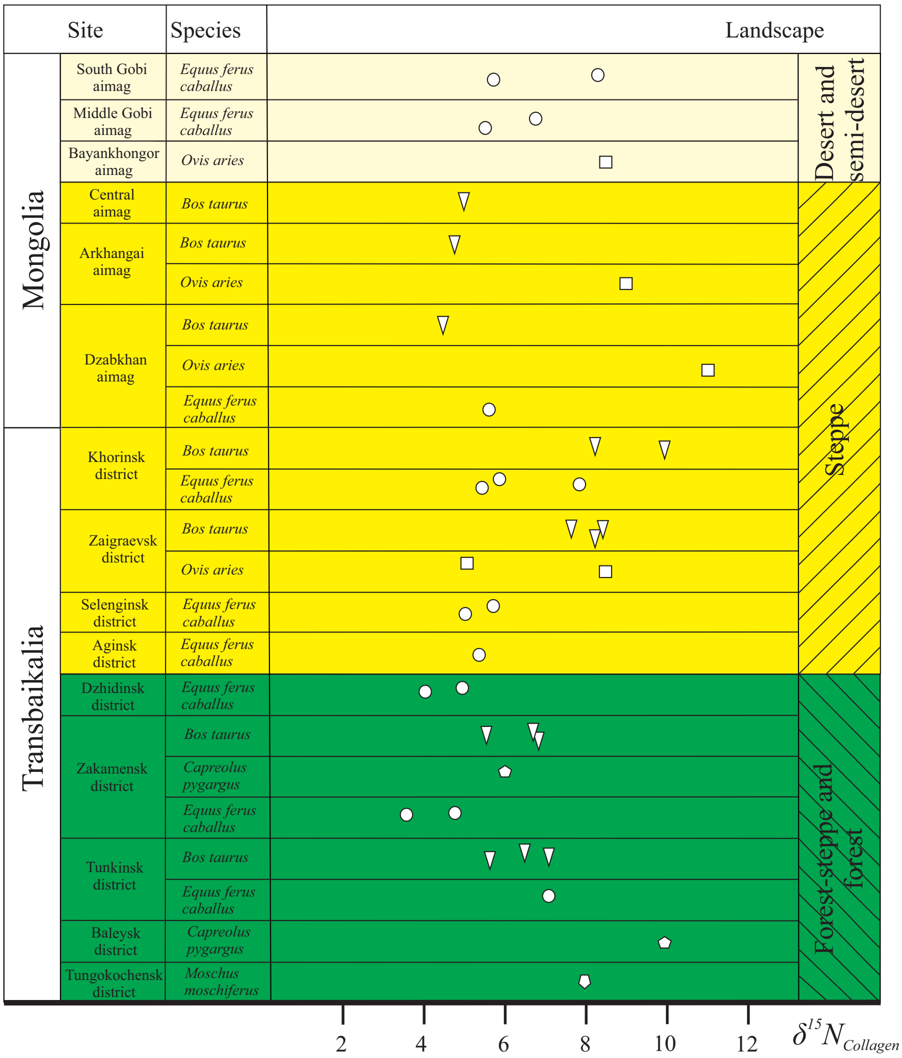

Fig. 4. Nitrogen isotope composition of collagen ($\delta^{15}N$) of the herbivorous fauna of Mongolia and Western Transbaikalia. Square - *Ovis aries*; circle - *Equus ferus caballus*; triangle - *Bos taurus*; pentagon - *Capreolus pygargus*; elongated pentagon - *Moschus moschiferus*

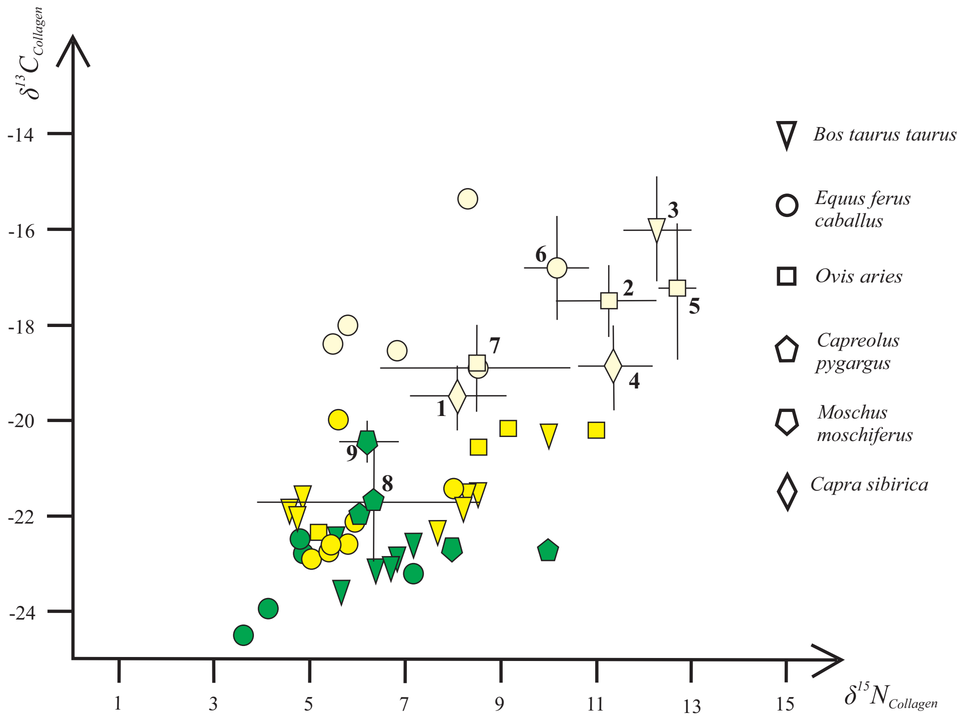

Fig. 5. Carbon ($\delta^{13}C$) and nitrogen ($\delta^{15}N$) isotope composition of collagen of the herbivorous fauna of Mongolia and Western Transbaikalia. Pale yellow marks – desert/semi-desert animals, yellow – steppe, green – steppe-forest/forest. Extra data presented with one standard deviation: Central Asian desert and semi-Desert: 1 – *Capra sibirica* (Makarewicz, Tuross, 2006), 2 – *Ovis aries* (Makarewicz, Tuross, 2006), 3 – *Bos taurus*, 4 – *Capra sibirica*; 5 – *Ovis aries*; 6 – *Equus ferus caballus* (Davie et al., 2014); 7 – *Equus sp*. (Ananyevskaya et al., 2020); Central Asian steppe-forest and forest: 8 – *Capreolus pygargus*, 9 – *Moschus moschiferus* (Weber et al., 2011)

values are in diapason of nitrogen isotope composition of roe deer and musk deer ($\delta^{15}N$ from 2.6 to 10.6‰) from the Angara region, where Forest and Forest-Steppe landscapes dominate (Weber et al. 2011). Probably, such scatter of isotope characteristics is associated with the heterogeneity of the diet and feeding on food with a heavy nitrogen isotope composition, for example, fungi and near-water plants (O'Regan et al. 2016; Khubanova et al. 2017).

The close mean and median values of $\delta^{15}N$ (Table 4, Fig. 6) show the absence of differences in this index between animals from different landscape zones. $U_{Cr} < U(\delta^{15}N)$ according to the Mann-Whitney U-test (Table 5) also shows that differences in the nitrogen isotope composition in animals from desert/semi-desert, steppe, forest-steppe/forest are not statistically significant and are random. Thus, the isotope-geochemical isolation of landscapes in terms of the nitrogen isotopic composition is less pronounced. However, there is some tendency of heavier average isotopic composition of nitrogen of forest-steppe/forest animals (median $\delta^{15}N$ = 6.3‰) relative to steppe and desert/semi-desert ungulates (median $\delta^{15}N$ = 6.9 and 7.1‰) (Table 4). Especially this small difference is expressed in horses from forest-steppe/forest ($\delta^{15}N$ from 3.6 to 7.1‰) to desert and semi-desert horses ($\delta^{15}N$ from 5.5 to 8.3‰) (Table 1).

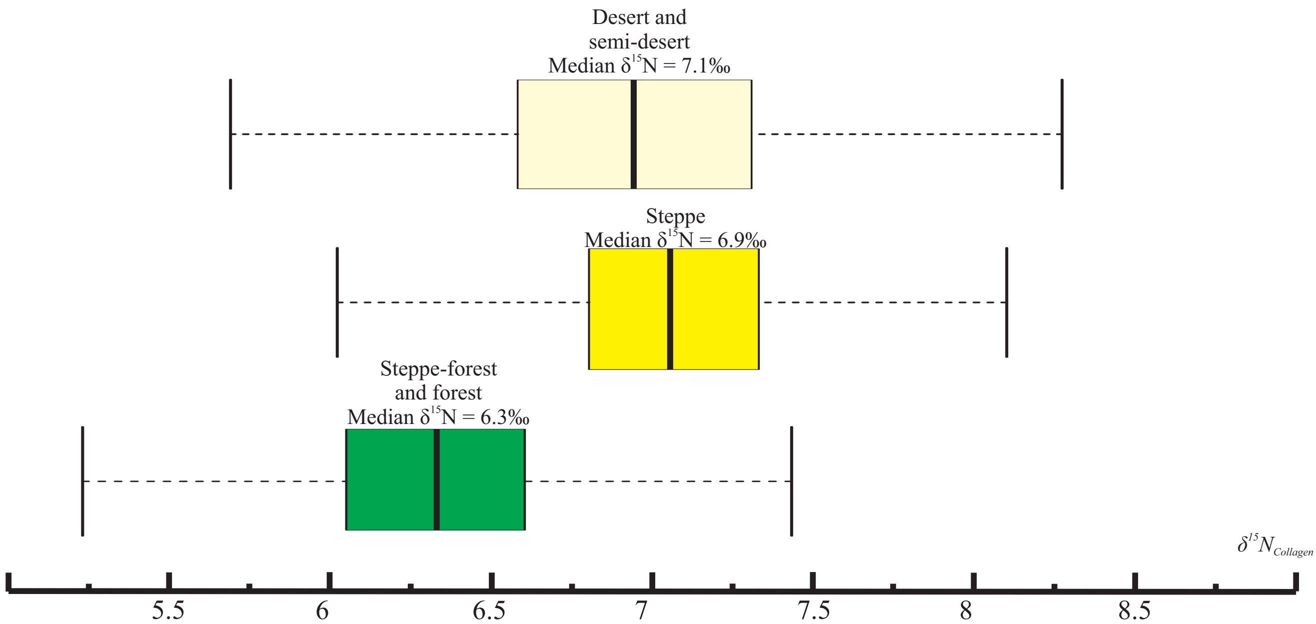

Fig. 6. Box plot (by Bayesian bootstrap method) of nitrogen isotope composition of the herbivorous fauna in Mongolia and Western Transbaikalia

CONCLUSION

In Mongolia and Transbaikalia, there is a wide variety of intracontinental landscape environments (ecological systems). From south to north, they form landscape-climatic zones from the desert and dry steppes through the steppes and meadows to the forest-steppes, taiga and high-mountain tundra. Their difference is due to the difference in average annual and seasonal temperatures, the amount and uniformity of annual distribution of precipitation. In these landscape zones, the species composition of vegetation, including forage vegetation, differs significantly: in warm and arid open landscapes (deserts and dry steppes), C4 plants are widtheely represented along with C3, the latter being strongly enriched in heavy carbon. In steppes, forest-steppes and forests, C3 plants dominate. However, in forest-steppes and forests, grass is under the canopy of woody and shrub vegetation, so it has a slightly lighter carbon isotope composition.

The isotope ratio of carbon in herbivorous animals reflects well the landscape conditions of their habitat. The maximum values of the carbon isotope ratio are observed in animals from the desert (Gobi Desert) and the semi-desert landscapes, median (mean) $\delta^{13}C$ is -17.9‰. The minimum values of $\delta^{13}C$ were obtained in herbivores of the forest-steppe and the forest landscapes (Transbaikalia), median $\delta^{13}C$ is -23‰. The fauna of the steppes (median $\delta^{13}C$ is -21.7‰) has intermediate values of the carbon isotopic composition.

The nitrogen isotope composition indicates that a large proportion of cattle and small cattle grazed in the dry steppe conditions, possibly on pastures with a depleted vegetation cover and a high degree of fertilization. Such conditions are typical near pastoral settlements. An insignificant part of domestic animals, including horses, was characterized by a less weighted nitrogen composition, which indicates more favorable conditions for their nutrition, without water and food stress, and the presence of shrub vegetation in their diet. This suggests that nitrogen isotope composition of animals is largely controlled by water and food sufficiency and is less dependent on the landscape setting.

REFERENCES

Ambrose S.H. (1990). Preparation and characterization of bone and tooth collagen for isotopic analysis. Journal of Archaeological Science, 17, 431–451.

Ananyevskaya E., Akhatov G., Loman V., Dmitriev E., Ermolayeva A., Evdokimov A., Garbaras A., Goryachev A., Kukushkin A., Kukushkin I., Kurmankulov Z., Logvin A., Lukpanova Y., Onggar A., Sakenov S., Sapolaite J., Shevnina I., Usmanova E., Utubayev Z., Varfolomeev V., Voyakin D., Yarygin S., Motuzaitė Matuzeviciute G. (2020). The effect of animal herding practices on the diversity of human stable isotope values in north central Asia. Journal of Archaeological Science: Reports, 34, 102615. DOI: 10.1016/j.jasrep.2020.102615.

Arslanov Kh A. (1987). Radiocarbon: Geochemistry and Geochronology. Leningrad, USSR: Publishing House of Leningrad University (in Russian).

Atlas of Transbaikalia. (1967). (Buryat Autonomous Soviet Socialist Republic and the Chita Region). Sochava V B (eds.) Moscow–Irkutsk: Izd-vo GUGK,. 176 p. (in Russian).

Atlas of ecosystems of Mongolia. (2019). Gunin P.D., Sandar M. (eds.) Ulaanbaatar. ADMON Print.. 264 p.

Bååth R. (2023). Bayesboot: An Implementation of Rubin's (1981) Bayesian Bootstrap. R package version 0.2.2, DOI: //CRAN.R-project.org/package=bayesboot.

Barberena R., Zangrando A.F., Gil A.F., Martínez G.A., Politis G.G., Borrero L.A., Neme G.A. (2009). Guanaco (Lama guanicoe) isotopic ecology in southern South America: spatial and temporal tendencies, and archaeological implications. Journal of Archaeological Science, 36(12), 2666–2675, DOI: 10.1016/j.jas.2009.08.003.

Bocherens H., Fizet M., Mariotti A., Lange-Badre B., Vandermeersch B., Borel J.P., Bellon G. (1991). Isotopic biogeochemistry (13C, 15N) of fossil vertebrate collagen: application to the study of a past food web including Neandertal man. Journal of Human Evolution, 20, 481- 492, DOI: 10.1016/0047-2484(91)90021-M.

Bocherens H., Pacaud G., Lazarev A. P., Mariotti A. (1996). Stable isotope abundances (13C, 15N) in collagen and soft tissues from Pleistocene mammals from Yakutia. Implications for the palaeobiology of the Mammoth Steppe. Palaeogeography, Palaeoclimatology, Palaeoecology, 126, 31-44, DOI: 10.1016/S0031-0182(96)00068-5.

Bocherens H. (2003). Isotopic biogeochemistry and the paleoecology of the mammoth steppe fauna. In: J.W.F. Reumer, J. De Vos, D. Mol ed., Advances in mammoth research. Proceedings of the Second Mammoth International Conference. Rotterdam, DEINSEA, 9, 57–76.

Bocherens H., Drucker D. (2003). Trophic level isotopic enrichment of carbon and nitrogen in bone collagen: case studies from recent and ancient terrestrial ecosystems. International Journal of Osteoarchaeology, 13(1/2), 46-53, DOI: 10.1002/oa.662.

Bocherens H., Drucker D.G., Madelaine S. (2014). Evidence for a 15N positive excursion in terrestrial foodwebs at the Middle to Upper Palaeolithic transition in south-western France: Implications for early modern human palaeodiet and palaeoenvironment. Journal of Human Evolution, 69, 31-43, DOI: 10.1016/j.jhevol.2013.12.015.

Boldanov T.A., Mukhin G.D. (2019). Ecological Adaptation of Agricultural Land Use Under the Climate Change in the Republic of Buryatia. Arid Ecosystems, 9(1), 7-14, DOI: 10.24411/1993-3916-2019-00040.

Boykov T.G., Kharitonov Yu. D., Rupyshev Yu. A. (2002). The Steppes of Zabaikalye: Productivity, forage value, rational management and conservation. Ulan-Ude: BCS SB RAS (in Russian).

Britton K., Knecht R., Nehlich O., Hillerdal C., Davis R.S., Richards M.P. (2013). Maritime adaptations and dietary variation in prehistoric Western Alaska: Stable isotope analysis of permafrost-preserved human hair. American journal of physical anthropology, 151(3), 448-461, DOI: 10.1002/ajpa.22284.

Brown T.A., Nelson D.E., Vogel J.S., Southon J.R. (1988). Improved collagen extraction method by modified Longin method. Radiocarbon, 30(2), 171-177, DOI: 10.1017/S0033822200044118.

Burnik Šturm M., Ganbaatar O., Voigt C. C., Kaczensky P. (2017). Sequential stable isotope analysis reveals differences in dietary history of three sympatric equid species in the Mongolian Gobi. Journal of Applied Ecology, 54(4), 1110-1119, DOI: 10.1111/1365- 2664.12825.

Chen S., Bai Y., Lin G., Huang J., Han X. (2007). Isotopic carbon composition and related characters of dominant species along an environmental gradient in Inner Mongolia, China. Journal of Arid Environments, 71(1), 12-28, DOI: 10.1016/j.jaridenv.2007.02.006.

Codron D., Codron J., Lee-Thorp J.A., Sponheimer M., de Ruiter D.D. (2005). Animal diets in the Waterberg based on stable isotopic composition of faeces. South African Journal of Wildlife Research, 35(1), 43–52, DOI: 10.5167/uzh-25362.

Dambaev V.B., Banzaraktsaeva T.G., Buyantueva L.B., Namsaraev B.B., Zyakun A.M. (2016). Carbon isotope variations of vegetation and soils in steppe pastures of Inner Asia. Geography and Natural Resources, 2, 118-124 (in Russian).

Davie H., Murdoch J.D., Lini A., Ankhbayar L., Batdorj S. (2014). Carbon and nitrogen stable isotope values for plants and mammals in a semi-desert region of Mongolia. Mongolian Journal of Biological Sciences, 12(1-2), 33-43, DOI: 10.22353/mjbs.2014.12.04.

Danzhalova E.V., Bazha S.N. (2008). Transformation of the main types of steppe ecosystems of Central Mongolia under the influence of grazing. The bulletin of KSAU, 2, 98-104.

DeNiro M.J., Epstein S. (1981). Influence of diet on the distribution of nitrogen isotopes in animals. Geochimica et cosmochimica acta, 45(3), 341-351, DOI: 10.1016/0016-7037(78)90199-0.

DeNiro M.J., Schoeninger M.J. (1983). Stable Carbon and Nitrogen Isotope Ratios of Bone Collagen: Variations within Individuals, Between Sexes, and Within Populations Raised on Monotonous Diet. Journal of Archaeological Science, 10(3): 199-203, DOI: 10.1016/0305-4403(83)90002-X.

Di Matteo A., Kuznetsova T.V., Nikolaev V.I., Spasskaya N.N., Jakumin P. (2013). Isotope studies of fossil bones of Pleistocene Yakut horses. Ice and Snow, 53(2), 93-101, DOI: 10.15356/2076-6734-2013-2-93-101.

Drucker D.G., Hobson K. A., Ouellet J.-P., Courtois R. (2010). Influence of forage preferences and habitat use on 13C and 15N abundance in wild caribou (Rangifer tarandus caribou) and moose (Alces alces) from Canada. Isotopes in Environmental and Health Studies, 46 (1), 107-121, DOI: 10.1080/10256010903388410.

Drucker D.G., Bridault A, Cupillard C., Hujic A., Bocherens H. (2011). Evolution of habitat and environment of red deer (Cervus elaphus) during the Late-glacial and early Holocene in eastern France (French Jura and the western Alps) using multi-isotope analysis ($\delta^{13}C$, $\delta^{15}N$, $\delta^{18}O$, $\delta^{34}S$) of archaeological remains. Quaternary International, 245(2), 268-278, DOI: 10.1016/j.quaint.2011.07.019.

Ecological and Geographical Atlas-monograph «Selenga – Baikal». (2019). N.S. Kasimov, ed., Lomonosov Moscow State University Publ. (in Russian).

Fernandez J., Markgraf V., Panarello H.O., Albero M., Angio1ini F.E., Valencio S., Arriaga M. (1991). Late Pleistocene/Early Holocene environments and climates, fauna, and human occupation in the Argentine Altiplano. Geoarchaeology: An International Journal, 6(3), 251-272. DOI: 10.1002/gea.3340060303.

Fizet M., Mariotti A. M., Bocherens H., Lange-Badre B., Vandermeersch B., Borel J.P., Bellon G. (1995). Effect of diet, physiology and climate on carbon and nitrogen stable isotopes of collagen in a late Pleistocene anthropic palaeoecosystem: Marillac, Charente, France). Journal of Archaeological Science, 22: 67-79, DOI: 10.1016/S0305-4403(95)80163-4.

Fogel M.L., Tuross N., Owsley D.W. (1989). Nitrogen isotope tracers of human lactation in modern and archaeological populations. Annual report of the director, geophysical laboratory. Carnegie Inst. Wash. 89, 111-117.

Fox N.S., Southon J.R., Howard C.M., Takeuchi G.T., and Potze S. and Farrell A.B., Lindsey E.L., Blois J. L. (2023). Millennial-scale drivers of small mammal isotopic niche dynamics in Southern California. Palaeogeography, Palaeoclimatology, Palaeoecology, 612, 111378, DOI: 10.1016/j.palaeo.2022.111378.

France C.A.M., Owsley D.W., Hayek L.C. (2014). Stable isotope indicators of provenance and demographics in 18th and 19th century North Americans. Journal of Archaeological Science, 42, 356-366, DOI: 10.1016/j.jas.2013.10.037.

Germonpre M., Lbova L. (1996). Mammalian Remains from the Upper Palaeolithic Site of Kamenka, Buryatia (Siberia). Journal of Archaeological Science, 23, 35-57, DOI: 10.1006/jasc.1996.0004.

Goldman R. (2010). Spatial Variation of Stable Carbon and Nitrogen Isotope Ratios and C:N of Perennial Plant Species in the Steppe Grassland of Northern Mongolia. Master of Environmental Studies Capstone Projects [online]. 38. Available at: https://repository.upenn.edu/mes_capstones/38.

Golovanov D.L., Kazantseva T.I., Yamnova I.A. (2004). Natural and anthropogenic degradation processes of the soil cover of the desert steppes of Mongolia (on the example of somon Bulgan). Arid ecosystems, 10, 24-25.

Gorlova E.N., Krylovich O.A., Tiunov A.V., Khasanov B.F., Vasyukov D.D., Savinetskiy A.B. (2015). Stable-isotope analysis as a method of taxonomical identification of archaeozoological material. Archaeology, Ethnology and Anthropology of Eurasia, 43(1): 110–121, DOI: 10.17746 / 1563-0102.2015.43.1.110–121 (in Russian).

Jenkins S.G., Partridge S.T., Stephenson T.R., Farley S.D., Robbins C.T. (2001). Nitrogen and carbon isotope fractionation between mothers, neonates, and nursing offspring. Oecologia, 129, 336-341, DOI: 10.1007/ s004420100755.

Kalapos T., Baloghne-Nyakas A., Csontos P. (1997). Occurrense and ecological characteristiks of C4 dicot and Cyperaceae species in the Hungarian flora. Photosynthetica, 33 (2), 227–240, DOI: 10.1023/A:1022112329990.

Khatri P.K., Larcher R., Camin F., Ziller L., Tonon A., Nardin T., Bontempo L. (2021). Stable Isotope Ratios of Herbs and Spices Commonly Used as Herbal Infusions in the Italian Market. ACS Omeg, 6, 11925–11934, DOI: 10.1021/acsomega.1c00274.

Khubanova A.M., Khubanov V.B., Novoseltseva V.M., Sokolova N.B., Klementyev A.M., Posokhov V.F. (2017). Features of the composition of carbon and nitrogen isotopes in teeth collagen of Equus ferus and Alces americanus from archaeological location Ust-Keul I (Northern Angara region). The Bulletin of Irkutsk State University. Series "Geoarchaeology. Ethnology. Anthropology", 21, 33–59.

Koch P.L., Hoppe K.A., Webb S.D. (1998). The isotopic ecology of late Pleistocene mammals in North America: Part 1. Florida. Chemical Geology, 152(1-2), 119-138, DOI: 10.1016/S0009-2541(98)00101-6.

Kohzu A., Iwata T., Kato M., Nishikawa J., Wada E., Amartuvshin N.,

Namkhaidorj B., Fujita N. (2009). Food webs in Mongolian grasslands: The analysis of 13C and 15N natural abundances. Isotopes in Environmental and Health Studies, 45(3), 208-219, DOI: 10.1080/10256010902871887.

Kradin N.N., Khubanova A.M., Bazarov B.A., Miyagashev D.A., Khubanov V.B., Konovalov P.B., Klementiev A.M., Posokhov V.F., Ventresca Miller A.R. (2021) Iron age societies of Western Transbaikalia: Reconstruction of diet and lifeways. Journal of Archaeological Science: Reports, 38, 102973, DOI: 10.1016/j.jasrep.2021.102973.

Krajcarz M., Pacher M., Krajcarz M.T., Laughlan L., Rabeder G., Sabol M., Wojtal P., Bocherens H. (2016). Isotopic variability of cave bears ($d^{15}N$, $d^{13}C$) across Europe during MIS3. Quaternary Science Reviews, 131, 51-72, DOI: 10.1016/j.quascirev.2015.10.028.

Krylovich O.A., Boeskorov G.G., Shchelchkova M.V., Savinetsky A.B. (2020). Trophic position of pleistocene and modern brown bears (Ursus arctos) of Yakutia based on stable isotope analyses. Biology Bulletin, 47, 1013-1021, DOI: 10.31857/S0044513420050074.

Kuzmin Y.V., Bondarev A.A., Kosintsev P.A., Zazovskaya, E.P. (2021). The Paleolithic diet of Siberia and Eastern Europe: evidence based on stable isotopes ($\delta^{13}C$ and $\delta^{15}N$) in hominin and animal bone collagen. Archaeological and Anthropological Sciences, 13, 1-12, DOI: 10.1007/s12520-021-01439-5; WoS: 000702780200001.

Kuzmin, Y.V., Shpansky, A.V. (2023).The Late Pleistocene megafauna of the Chulym River basin, southeastern West Siberian Plain: chronology and stable isotope composition. Journal of Quaternary Science, 38, 1, 2–7, DOI:10.1002/jqs.3470.

Lee-Thorp J. A. (2008). On isotopes and old bones. Archaeometry, 50(6), 925-950, DOI:10.1111/j.1475-4754.2008.00441.x.

Li M. C., Liu H. Y., Yi X. F., Li L. X. (2006). Characterization of photosynthetic pathway of plant species growing in the eastern Tibetan plateau using stable carbon isotope composition. Photosynthetica, 44(1), 102-108, DOI: 10.1007/s11099-005-0164-1.

Li M.C., Zhu J.J., Li L.X. (2009). Occurrence and altitudinal pattern of C4 plants on Qinghai Plateau, Qinghai province, China. Photosynthetica, 47(2), 298-303, DOI:10.1007/s11099-009-0046-z.

Liu X. Q., Wang R. Z., Li Y. Z. (2004). Photosynthetic pathway types in rangeland plant species from Inner Mongolia, North China. Photosynthetica, 42, 339–344, DOI: 10.1023/B:PHOT.0000046150.74045.46.

Liu X.Z., Wang G.A., Li J.Z., Wang Q. (2009). Nitrogen isotope composition characteristics of modern plants and their variations along an altitudinal gradient in Dongling Mountain in Beijing. Science in China Series D-Earth Sciences, 53(1), 128-140, DOI: 10.1007/s11430-009-0175-z.

Longin R. (1971). New method of collagen extraction for radiocarbon dating. Nature, 230, 241–242, DOI: 10.1038/230241a0.

Ma J. Y., Sun W., Liu X. N., Chen F. H. (2012). Variation in the Stable Carbon and Nitrogen Isotope Composition of Plants and Soil along a Precipitation Gradient in Northern China. PLoS ONE, 7(12), e51894, DOI: 10.1371/journal.pone.0051894.

Makarewicz C., Tuross N. (2006). Foddering by Mongolian pastoralists is recorded in the stable carbon (d13C) and nitrogen (d15N) isotopes of caprine dentinal collagen. Journal of Archaeological Science, 33(6), 862-870, DOI: 10.1016/j.jas.2005.10.016.

Makarewicz C. (2017). Winter is coming: seasonality of ancient pastoral nomadic practices revealed in the carbon ($\delta^{13}C$) and nitrogen ($\delta^{15}N$) isotopic record of Xiongnu caprines Archaeological and Anthropological Sciences, 9, 405-418, DOI: 10.1007/s12520-015-0289-5.

Makarewicz C., Winter-Schuh C., Byerly H., Houle J.-L. (2018). Isotopic evidence for ceremonial provisioning of Late Bronze age khirigsuurs with horses from diverse geographic locales. Quaternary International 476 (20): 70–81, DOI: 10.1016/j.quaint.2018.02.030.

Mann H.B., Whitney D.R. (1947). On a test of whether one of two random variables is stochastically larger than the other. Annals of Mathematical Statistics, 18, 50-60. DOI: 10.1214/aoms/1177730491.

Martin B, Thorstenson Y.R. (1988). Stable Carbon Isotope Composition (δ13C), Water Use Efficiency, and Biomass Productivity of Lycopersicon esculentum, Lycopersicon pennellii, and the F1 Hybrid. Plant Physiol, 88, 213–217, DOI: 10.1104/pp.88.1.213.

Naidanov B.B. (2009). The saline habitat flora of Southwestern Transbaikalia: feed assessment. The Bulletin of KSAU, 11(38), 39-43.

Nikolaev V.I., Ryskov Ya. G., Yakumin P. (2006). Stable isotope investigation of bone remains from archaeological excavations (methodological aspects). Stable isotopes in palaeoecological studies. Moscow, Institute of Geography RAS Publ. (in Russian).

O'Leary M.H. (1988). Carbon isotopes in photosynthesis. Bioscience, 38(5), 328-336, DOI: 10.2307/1310735.

Osipov K.I. (2005). Flora of the Vitim Plateau (Northern Transbaikal region). Ulan-Ude: BSC SB RAS (In Russian).

O'Regan H.J., Lamb A.L., Wilkinson D.M. (2016). The missing mushrooms: searching for fungi in ancient human dietary analysis. Journal of Archaeological Science, 75, 139-143, DOI: 10.1016/j.jas.2016.09.009.

Oyungerel S., Tsendeekhuu T., Tserenkhand G. (2004). A Study to Detect CAM Plants in Mongolia. Mongolian Journal of Biological Sciences, 2(1), 29-37, DOI: 10.22353/mjbs.2004.02.04.

Palmqvist P., Grocke D.R., Arribas A., Farina R.A. (2003). Palaeoecological reconstruction of a lower Pleistocene large mammal community using biogeochemical (δ13C, δ15N, δ18O, Sr:Zn) and ecomorphological approaches. Paleobiology, 29(2), 205-229, DOI: 10.1666/0094-8373(2003)029<0205:PROALP>2.0.CO;2.

Pearcy R.W., Troughton J. (1975). C4 photosynthesis in tree form Euphorbia species from Hawaiian rainforest sites. Plant Physiology, 55(6), 1054-1056, DOI: 10.1104/pp.55.6.1054.

Petukhov I.A., Bazha S.N., Danzhalova E.V., Drobyshev Yu.I., Syrtypova S.-Kh.D., Bogdanov E.A., Enkh-Amgalan S., Gunin P.D. (2018). Long-term Dynamics of Pasture Ecosystem Conditions in the Ecotone Zone of Dry and Desert Steppes of Central Mongolia (Middle Gobi Aimag). Ecosystems: Ecology and Dynamics, 2(2), 5-39 (in Russian).

Pidoplichko I.G. (1952). A New Determination Method for Geological Age of Fossil Bones of the Quaternary System), Kiev: Akad. Nauk USSR. (In Russian).

Pyankov V.I., Gunin P.D., Tsoog S., Black C.C. (2000). C4 plants in the vegetation of Mongolia: their natural occurrence and geographical distribution in relation to climate. Oecologia, 123, 15–31, DOI: 10.1007/s004420050985.

Rubin D.B. (1981). The bayesian bootstrap. The Annals of Statistics, 9 (1), 130–134.

Safronova I. N., Karimova T. Y., Zhargalsaikhan L. (2018). Current state assessment of the vegetation cover in the Khentei Aimag of Mongolia. Arid ecosystems, 24(1/74), 68-78.

Simukov A.D. (2007). Publications about Mongolia and for Mongolia. Edited by Yuki Konagaya, Sanjaasüren Bayaraa, and Ichinkhorloo Lkhagvasüren. Osaka: National Museum of Ethnology, 1 (in Russian).

Skippington J., Manne T., Veth P. (2021). Isotopic Indications of Late Pleistocene and Holocene Paleoenvironmental Changes at Boodie Cave Archaeological Site, Barrow Island, Western Australia. Molecules, 26 (9), 2582, DOI: 10.3390/molecules26092582.

Spasojevic M.J., Weber S. (2021). Variation in δ13C and δ15N within and among plant species in the alpine tundra. Arctic, Antarctic, and Alpine Research, 53(1), 340-351, DOI: 10.1080/15230430.2021.2000567.

Svyatko S.V. (2016). Stable Isotope Analysis: Outline of Methodology and a Review of Studies in Siberia and the Eurasian Steppe. Archaeology, Ethnology and Anthropology of Eurasia, 44(2), 47–55, DOI: 10.17746/1563-0110.2016.44.2.047-055.

Structure and Dynamics of the Steppe Ecosystems of Eastern Mongolia (by an example of the Tumentsogt Station). (2018). Moscow: Tovarishchestvo Nauchnykh Izdaniy KMK (in Russian).

Su Y., Chen L., Li Y., Meng W., Zhu Z., Uan C., Wang S., Zhu L. (2019). Relationship between Growth Characteristics and Stable Carbon Isotope of Artemisia scoparia in a Desert Steppe. Acta Agrestia Sinica, 27(4), 859-866, DOI: 10.11733/j.issn.1007-0435.2019.04.009.

Tahmasebi F., Longstaffe F.J., Zazula G. (2018). Nitrogen isotopes suggest a change in nitrogen dynamics between the Late Pleistocene and modern time in Yukon, Canada. PLoS ONE 13 (2), e0192713, DOI: 10.1371/journal. pone.0192713.

Tanaka-Oda A., Endo I., Ohte N., Eer D., Yamanaka N., Hirobe M., ... and Yoshikawa K. (2018). A water acquisition strategy may regulate the biomass and distribution of winter forage species in cold Asian rangeland. Ecosphere, 9(12), e02511, DOI: 10.1002/ecs2.2511.

The Ecological Atlas of the Baikal Basin. In: Plyusnin V M (eds.). Irkutsk: Sochava institute of geography press, 2015.

Tsogmansrai D., Dugarzhav Ch. (2016). The effectiveness of some restoration methods of degraded pastures of the desert-steppe zone of Mongolia. Arid ecosystems, 22(3-68), 56-62.

Ulyanov A.N., Kulikova A.Y., Grigoryeva O.G. (2011). Actual problems of modern sheep breeding in Russia. Sheep, goats, wool business, 3, 54-60.

Urtnasan M., Lyubarskiy E.L. (2013). Pasture digression in the steppes of central Mongolia (on the example of Somon Batsumbar of the central aimag of Mongolia). Scientific notes of Kazan University: series "Natural science", 155(1), 258-170.

Van der Merwe N. J. (1992). Light stable isotopes and the reconstruction of prehistoric diets. In: Pollard A M (eds.). New Developments in Archaeological Science. Proceedings of the British Academy 77, Oxford University Press, Oxford, UK, 247-264.

Ventresca Miller A.R., Bragina T.M., Abil Y.A., Rulyova M.M., Makarewicz C.A. (2019). Pasture usage by ancient pastoralists in the northern Kazakh steppe informed by carbon and nitrogen isoscapes of contemporary floral biomes. Archaeological and Anthropological Sciences, 11, 2151-2166. DOI: 10.1007/s12520-018-0660-4.

Wang G., Han J., Zhou L., Xiong X., Tan M., Wu Z., Peng J. (2006). Carbon isotope ratios of C 4 plants in loess areas of North China. Science in China: Series D Earth Science, 49(1), 97-102, DOI: 10.1007/s11430-004-5238-6.

Weber A.W., White D., Bazaliiskii V.I., Goriunova O.I., Saveliev N.A., Katzenberg M.A. (2011). Hunter–gatherer Foraging Ranges, Migrations, and Travel in the Middle Holocene Baikal Region of Siberia: Insights from Carbon and Nitrogen Stable Isotope Signatures. Journal of Anthropological Archaeology, 30(4), 523–548, DOI: 10.1016/j.jaa.2011.06.006.

Wen Z., Zhang M. (2011). Anatomical types of leaves and assimilating shoots and carbon 13C/12C isotope fractionation in Chinese representatives of Salsoleae s.l. (Chenopodiaceae). Flora, 206, 720–730, DOI: 10.1016/j.flora.2010.11.015.

Winter K. (1981). C4 Plants of High Biomass in Arid Regions of Asia -Occurrence of C4 Photosynthesis in Chenopodiaceae and Polygonaceae from the Middle East and USSR. Oecologia (Berl), 48,100-106, DOI: 10.1007/BF00346994.

Xu Y, He J, Cheng W, Xing X., Li L. (2010). Natural 15N abundance in soils and plants in relation to N cycling in a rangeland in Inner Mongolia. J. Plant Ecol., 3, 201–207, DOI: 10.1093/jpe/rtq023.

Yudina P.L., Ivanova L.A., Ronzhina D.A., Ivanov L.A. (2015). Intraspecific variation of leaf mesostructure indices of steppe plants in Western Transbaikalia. Problems of botany in Southern Siberia and Mongolia: materials of the XIV international scientific and practical conference. Barnaul: ASU. 466-469.

APPENDIX

Table 1. Bone and teeth collagen stable carbon and nitrogen isotope data of herbivorous animals of this study

#	Aimag or District	Sample	Specie	Bone/ Tooth	δ13C, ‰	δ15N, ‰	C,%	N,%	Yield (%)*	C/ N$_{at}$**	Location
Desert and semi-desert (Mongolia)											
1	South Gobi	MNG-03-17	Equus ferus caballus	Molar	-15.4	8.3	40.2	15.1	4.2	3.1	N 43°56´43.6´´ E 107°25´36.9´´ ~1200 m high
2	South Gobi	MNG-04-17	Equus ferus caballus	Molar	-18.1	5.8	30.7	11.3	5.9	3.2	N 43°54´14´´ E 107°19´19´´ ~1400 m high
3	Middle Gobi	MNG-01-17	Equus ferus caballus	Molar	-18.6	6.8	32.9	12.4	5.6	3.1	N 45°43´15.8´´ E 106°18´31.8´´ ~1500 m high
4	Middle Gobi	MNG-02-17	Equus ferus caballus	Molar	-18.4	5.5	41.1	16	5.4	3	N 45°19´45.9´´ E 106°32´14.4´´ ~1400 m high
5	Bayankhongor	MNG-03-18	Ovis aries	Molar	-18.8	8.4	29.9	10.8	11.2	3.2	N 46°14´46.02´´ E 98°49´26.49´´ ~1950 m high
Steppe (Mongolia)											
6	Central	MNG-07-16	Bos taurus	Molar	-21.6	4.9	38.6	14	10	3.2	N 48°17´48.5´´ E 106°13´12.6´´ ~1100 m high
7	Arkhangai	MNG-01-16	Bos taurus	Molar	-22.1	4.8	19.4	7.4	1.9	3.1	N 48°15´23´´ E 99°53´12´´ ~2400 m high
8	Arkhangai	MNG-02-16	Ovis aries	Molar	-20.2	9.1	29.2	11.7	11.4	2.9	
9	Dzabkhan	MNG-03-16	Bos taurus	Molar	-21.9	4.6	16.4	6.2	0.5	3.1	N 48°44´08´´ E 98°04´28´´ ~1800 m high
10	Dzabkhan	MNG-04-16	Ovis aries	Molar	-20.4	11	44.6	16.9	11.8	3.1	
11	Dzabkhan	MNG-05-16	Ovis aries	Bone	-20.3	10.3	41.4	18.6	2	2.6	
12	Dzabkhan	MNG-06-16	Equus ferus caballus	Molar	-20	5.6	45.2	17.2	7.7	3.1	N 48°40´56.1´´ E 98°51´06.4´´ ~1700 m high
Steppe (Transbaikalia)											
13	Zaigraevsky	C14(14)-1	Ovis aries	Molar	-20.6	8.5	40.5	14.6	2.4	3.2	N 51°54´18.4´´ E 107°49´38.8´´ ~ 800 m high
14	Zaigraevsky	C14(14)-2	Ovis aries	Molar	-20.8	7.8	37.3	16.2	1	2.7	
15	Zaigraevsky	C19(14)-1	Ovis aries	Molar	-22.3	5.9	35.3	10.8	0.9	3.8	N 52°12´35´´ E 108°36´53´´ ~ 1000 m high
16	Zaigraevsky	C19(14)-1(2)	Ovis aries	Bone	-22.4	5.2	39	14.5	3.3	3.1	
17	Zaigraevsky	C15(14)-1	Bos taurus	Molar	-21.6	8.5	39.5	15.5	2.1	3	N 51°58´43´´ E 108°01´02´´ 820 m high
18	Zaigraevsky	C15(14)-2	Bos taurus	Molar	-25.1	7.1	25.1	11	1.5	2.7	
19	Zaigraevsky	C16(14)	Bos taurus	Molar	-21.6	8.2	33.3	13.1	6.2	3	N 52°01´53´´ E 108°23´59´´ ~ 950 m high
20	Zaigraevsky	C18(14)	Bos taurus	Molar	-22.4	7.7	34	12.9	3.6	3.1	N 52°06´ 40´´ E 108°34´ 25´´ ~ 1200 m high
21	Khorinsky	C10(15)	Bos taurus	Molar	-20.4	10	47.5	15.4	12.2	3.6	N 52°15´59.2´´ E 108°46´56.7´´ ~ 1150 m high

22	Khorinsky	C22(14)	Bos taurus	Molar	-21.8	8.2	38.5	15.5	5.3	2.9	N 52°16´53´´ E 108°52´18´´ ~ 1300 m high
23	Khorinsky	C5(15)	Equus ferus caballus	Molar	-21.5	7.9	40.3	13.1	8	3.6	N 52°09´58´´ E 108°36´56´´ ~ 1000 m high
24	Khorinsky	C21(14)-1	Equus ferus caballus	Molar	-22.2	5.9	26	9.4	4.6	3.2	N 52°20´0.7´´ E 108°43´44.7´´ ~ 1200 m high
25	Khorinsky	C21(14)-2	Equus ferus caballus	Molar	-22.7	5.4	27.4	9.5	3.9	3.4	
26	Selenginsky	C3(13)	Equus ferus caballus	Molar	-22.9	5	40	15.8	10.4	3	N 50°55´02´´ E 106° 14´08´´ ~ 600 m high
27	Selenginsky	C6(13)	Equus ferus caballus	Molar	-22.6	5.8	46.4	15.2	9.2	3.6	
28	Aginsky	C24(13)	Equus ferus caballus	Molar	-22.6	5.4	39.1	12.6	5.4	3.6	N 51°6´40.1´´ E 114°37´51.9´´ ~ 700 m high
Steppe-forest and forest (Transbaikalia)											
29	Dzhidinsky	C12(13)	Equus ferus caballus	Molar	-24	4.1	39.5	14.6	8	3.2	N 50°36´27´´ E 104°35´35´´ ~ 900 m high
30	Dzhidinsky	C13(13)	Equus ferus caballus	Molar	-22.8	4.9	46,1	15.6	6.3	3.4	
31	Zakamensky	C7(13)	Bos taurus	Molar	-22.6	5.5	40.9	13.8	3.7	3.5	N 50°30´46´´ E 102°55´21´´ ~ 1200 m high
32	Zakamensky	C4(14)	Bos taurus	Molar	-23.1	6.7	45.8	14.9	6.2	3.6	N 50°49´46´´ E 102°47´15´´ ~ 1250 m high
33	Zakamensky	C2(15)	Bos taurus	Molar	-22.9	6.8	33.71	12.14	2.4	3.2	N 50°19´14.7´´ E 103°31´13.9´´ ~ 1250 m high
34	Zakamensky	C1(15)	Equus ferus caballus	Molar	-24.5	3.6	48.6	15.1	4.6	3.6	
35	Zakamensky	C1(14)	Equus ferus caballus	Molar	-22.5	4.8	44	16	7.1	3.2	N 50°28´39´´ E 104°17´13´´ 900 m high
36	Zakamensky	C2(14)	Capreolus pygargus	Molar	-22.2	6	38.7	15.6	5	2.9	
37	Tunkinsky	C7(14)	Bos taurus	Molar	-23.2	6.4	33.85	12.17	4.4	3.2	N 51°47´15´´ E 103°00´41´´ ~ 800 m high
38	Tunkinsky	C10(14)	Bos taurus	Molar	-23.4	8.5	8.3	4.7	0.6	2.1	N 51°40´32´´ E 102°00´41´´ ~ 750 m high
39	Tunkinsky	C11(14)	Bos taurus	Molar	-22.6	7.1	41.2	14.1	4.6	3.4	N 51°40´04´´ E 102°17´06´´ ~ 750 m high
40	Tunkinsky	C13(14)	Bos taurus	Bone	-23.6	5.7	47.2	15.2	2.3	3.6	N 51°41´38´´ E 101° 40´38´´ ~ 1050 m high
41	Tunkinsky	C9(14)	Equus ferus caballus	Molar	-23.1	7.1	37.1	14	5.3	3.1	N 51°52´43´´ E 102°23´34´´ ~ 750 m high
42	Baleysky	C20(15)	Capreolus pygargus	Molar	-22.7	10	42.4	15.9	5.7	3.1	N 51°38´41.6´´ E 117°5´58.8´´ ~ 700 m high
43	Tungokochensky	C4(15)	Moschus moschiferus	Molar	-22.6	8	39.61	15.67	4.8	2.9	N 53°38´118´´ E 114°1´51.9´´ ~ 900 m high

* Collagen yields are calculated as relative part of collagen as a percentage of the weight of the original bone sample.
** C/N_{at} = (%C/%N) x (14/12), atomic ratio.

RESEARCH PAPER

ECOLOGICAL ASSESSMENT OF THE ROLE OF MANGROVE TREES IN CARBON SEQUESTRATION AND BIODIVERSITY IN KARIMUNJAWA NATIONAL PARK INDONESIA

M. Arief Rahman Halim[1*], Tri Retnaningsih Soeprobowati[1,2], Hadiyanto Hadiyanto[1,3]
[1]Doctoral Program of Environmental Science, School of Postgraduate Studies, Universitas Diponegoro, Jl. Imam Bardjo SH No.5, 50241, Semarang, Indonesia
[2]Center of Paleolimnology (CPalim), Jl. Imam Bardjo SH No.5, 50241, Semarang, Indonesia
[3]Center of Biomass and Renewable Energy (CBIORE), Jl. Prof. Soedarto, 50275, Semarang, Indonesia
*Corresponding author: m.ariefrahmanha@gmail.com
Received: september 9th, 2022 / Accepted: September 4th, 2023 / Published: October 10th, 2023
https://DOI-10.24057/2071-9388-2022-2565

ABSTRACT. Mangrove ecosystem has an important role in reducing carbon in the environment. There has been massive conversion of mangrove area into ponds and buildings in the current period. Therefore, the species diversity and carbon sequestration capacity of the mangrove ecosystem must be evaluated to monitor its function. This research aims to evaluate the species diversity and the sequestered carbon in the mangrove ecosystem of Karimunjawa National Park (KNP), Indonesia. The species analysis in the 3 research sites, 9 transects, and 27 plots (10 m × 10 m) that was obtained using the quadrat sampling method. Allometric equations, Shannon–Wiener, and evenness indices were used to estimate the standing biomass and carbon, species diversity, and distribution, respectively. The sediment samples were obtained at a depth of 100 cm and divided into three depths, namely, 0–33, 34–67, and 68–100 cm. The carbon content of mangrove sediments was analyzed in the laboratory using the Walkley–Black method. The results revealed that mangroves in the KNP have moderate diversity and even distribution. The estimated carbon in the mangrove stand was 146.22 t C ha^{-1} and the estimated carbon stock in the sediment was around 360.61 t C ha^{-1}. Although the mangrove ecosystem in Karimunjawa National Park is still in a stable condition, it is necessary to monitor its changes due to the anthropogenic activities.

KEYWORDS: Mangrove ecosystem, Emission reduction, Carbon Sequestration, Biodiversity, Vulnerable

CITATION: Halim M.A.R., Soeprobowati T.R., Hadiyanto H. (2023). Ecological Assessment of The Role of Mangrove Trees In Carbon Sequestration and Biodiversity In Karimunjawa National Park Indonesia. Geography, Environment, Sustainability, 3(16), 32-42
https://DOI-10.24057/2071-9388-2022-2565

ACKNOWLEDGEMENTS: The authors would like to thank the Karimunjawa National Park Office and the coastal communities of Karimunjawa District for their assistance during data collection. This research was carried out with the support of Research Grant for Disertation (Penelitian Disertasi Doktor) from the Ministry of Research and Technology of the Republic of Indonesia/ BRIN [Project Number 187-49/UN7.6.1/PP/2021].

Conflict of interests: The authors reported no potential conflict of interest.

INTRODUCTION

Mangroves are currently recognized as crucial ecosystems that support the reproduction of fish and crabs as well as abrasion barriers against tsunamis. Mangroves are increasingly recognised as significant ecosystems that support the reproduction of aquatic life and can resist damage from extreme weather events. Mangroves also become carbon dioxide sinks that are more effective than peatlands or rainforests (Taillardat et al. 2018). The mangrove ecosystem is one of the most important ecosystems in the effort to maintain the stability of flora–fauna diversity and mitigate global warming, namely, as the best carbon storage compared with all other forest types on earth. Overexploitation for a variety of reasons, including commercial forestry, fuelwood, charcoal, and conversion to other land-uses, primarily aquaculture ponds, has been cited as a cause of mangrove losses (Kusmana 2015; Murdiyarso et al. 2015; Malik et al. 2017). Mangrove forests have a major role as carbon sinks and stores, which range from 4 gigatons C/year to 112 gigatons C/year (Cameron et al. 2019). Thus, efforts to sequester carbon in Indonesia are an important way to curb climate change and save living species from extinction (Roy et al. 2013). Indonesia is one of the countries that has the largest mangrove forest in the world, which can absorb more carbon than tropical forests or peatlands (Malik et al. 2015). Indonesia has 3.63 million hectares of mangrove ecosystems, which is 20.37 % of the world's total. The largest mangrove ecosystem is on the island of Papua, which is 1.63 million hectares. Sumatera is next with 892,835 hectares, and Kalimantan is third with 630,913 hectares (KKP 2021). Karimunjawa National Park (KNP), which is situated in Jepara Regency, Central Java, serves as a symbol of the sustainability of the region's ecosystem. As a conservation area that has very potential natural resources and high diversity, the mangrove ecosystem in Karimunjawa consists of Karimunjawa Island, Sintok, Mengawakan, Big Krakal, Small Krakal, Big Cemara, Small Cemara, Merican, and Kemujan. The largest mangrove forests are on Karimunjawa Island and Kemujan Island with an area of 396.90 ha. Karimunjawa was designated a national park on February 29, 1988 by the Ministry of Forestry, it is divided into nine zones, namely, core, jungle, marine protection, land use, marine tourism utilization, marine cultivation, religious cultural and historical, rehabilitation, and traditional fishing zones.

Karimunjawa is home to coral reefs, mangroves, coastal forests, and nearly 400 species of marine fauna, including 242 species of ornamental fish. The white-breasted sea eagle, hawksbill turtles, and green turtles are a few of the unusual animals that call this place home. Plants that characterize the KNP are dewadaru (*Crystocalyx macrophyla*), which are found in lowland rain forests (BTNKJ 2020). KNP consists of small islands in the middle of the Java Sea. Small islands generally have properties that are very vulnerable to environmental changes and pressures (Utami et al. 2017). Based on the natural resources and the fragile nature of the island, the existence of the KNP really needs to be maintained and protected. However, not all residents are aware of mangrove forests' role, particularly on tiny islands. Mangroves play an important role in protecting the island from eroding waves and ocean currents. Mangrove forests are systematically degraded due to human activities (Basu and Cetzal 2018). On Karimunjawa Island and Kemujan Island, there has been a massive conversion of mangroves to agricultural land and plantations. A total of 82.37 ha has been lost during the period 1992 – 2018 (Latifah et al. 2018). Mangrove forest functions are converted to achieve the decreased ability to absorb carbon in the atmosphere and the decomposition of stored carbon through the decomposition process into the atmosphere (Ha et al. 2014). The role of the mangrove ecosystem as an absorber and a reservoir for CO_2 turns into a contributor to CO_2 emissions. These circumstances exacerbate global climate change (Datta et al. 2012). Mangrove mud substrates have a high potential for carbon storage. Other studies related to the potential for mangrove carbon storage in other Southeast Asian countries, namely: in Banacon Island, Philippines, 145.6 t C ha^{-1} (Camacho et al. 2011), Panabo Philippines, 37.18 t C ha^{-1} (Alimbon and Manseguiao 2021), in Johor Park Malaysia of 50.68 t C ha^{-1}, the Kelantan delta Malaysia 99.13 t C ha^{-1} (Rozainah et al. 2018) and the carbon content of mangrove sediments in the Palawan Philippine forest area of 173.75 t C ha^{-1} (Abino et al. 2014) while the total C soil in Johor Park was 384.57 t C ha^{-1} and the Kelantan delta was 413.33 t C ha^{-1} (Rozainah et al. 2018). Therefore, the estimation of carbon storage in tree parts and mangrove mud substrate can be used as a basic reference in assessing the ecological benefits of mangroves in the form of environmental service commodities (Carugati et al. 2018). Sustainable management of mangrove forests is suitable for stabilizing air quality because carbon will be absorbed and stored in the mangrove ecosystem (Li et al. 2010). This study aimed to assess the species diversity and evenness and to estimate the carbon stored in both stands and sediments of mangroves ecosystem in Karimunjawa National Park, as a basis for sustainable management of mangrove ecosystem.

MATERIALS AND METHODS

Study Area

This research was conducted in the mangrove ecosystem of Karimunjawa National Park which is geographically located at 5°49´9´´S 110°27´32´´E. Karimunjawa National Park is an archipelago in the Java Sea which is included in Jepara Regency, Central Java (Fig. 1). It has a land area of ± 1,500 ha and waters of ± 110,000 ha (BTNKJ 2020). Sampling was done performed in the mangrove area of Karimunjawa Island (Station 1), Kemujan Island (Station 2), and Menjangan Besar Island (Station 3). Based on the presence and health of respective mangrove ecosystems, the sampling sites were chosen. In locations where sampling and selection of various mangrove conditions are not difficult. Because location 1 is in the national park area. Location 2 is near settlements, plantations, and location 3 is on an uninhabited island.

Data Collection

Nondestructive sampling was carried out in August 2021. This study sample consisted of 3 stations, 9 transects, and 27 plots (10 m × 10 m), with a distance of 10–20 m between plots. The species of mangrove trees in the sample plots were identified, and their diameter at breast height (DBH) was also measured (Komiyama et al. 2008). A minimum height of 1.3 metres from the ground is required for the tree to enter the DBH measurement. Then the diameter is measured using a roll meter. Fig. 2 shows details and images from several mangrove roots with height differences.

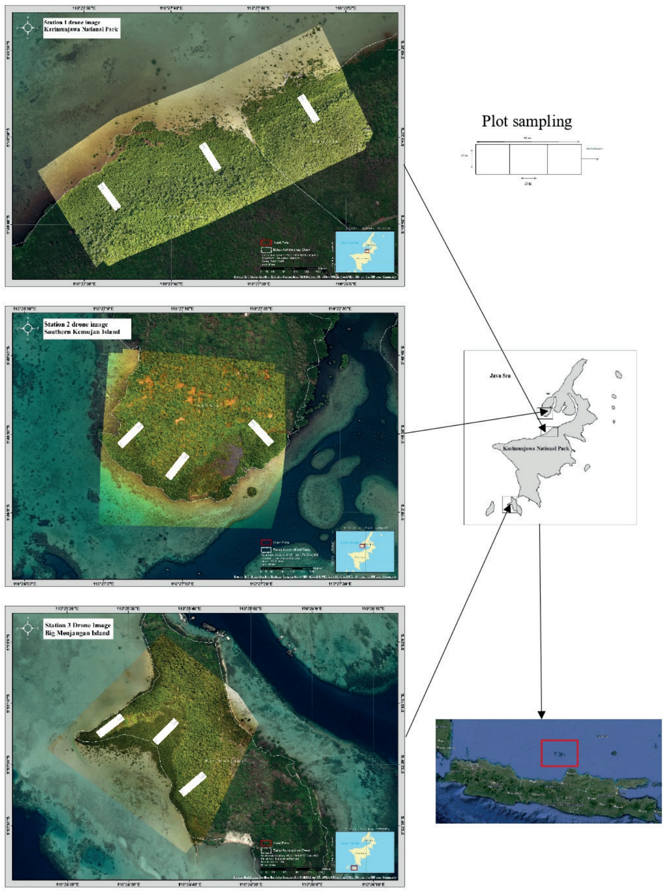

Fig. 1. Maps of (a) Karimunjawa National Park Area, Jepara Regency, Central Java, (b) Karimunjawa Island, (c) Kemujan Island, and (d) Menjangan Besar Island

Meanwhile, the data on the height of mangrove trees were obtained from the height of the observer's eye from the ground and the results of measurement of the distance of the observer from the tree and angle of inclination between the eye of the observer and the treetop (Weyerhaeuser and Tennigkeit 2000). The measurement of mangrove tree stand height was carried out in each plot. The tree category included a diameter of more than 10 cm, and a tree height of more than 2 m (Hadiyanto et al. 2021). Mangrove sediment samples were obtained from three stations using a hand corer type sediment core with a length of 100 cm. The core sediments were divided into three depths, namely, 0–33, 34–67, and 68–100 cm. The level of sediment depth affected the amount of carbon content.

Data Analysis

To obtain the importance value index (IVI) of each species, determined the sum of relative density, relative frequency, and relative dominance. Then, the Shannon–Wiener equation was used to find the value of the diversity index (H') of a species:

$$N' = -\sum_{i=1}^{S} Piln\,(Pi) \tag{1}$$

H' = Shannon diversity, s = number of species, and pi = abundance.

Species diversity is a characteristic that can be used to express community structure. It can also be used to measure community stability, which refers to the ability of a community to maintain itself stable despite disturbances to its components (Fachrul 2007). The range of values of the diversity index scale according to the Magguran (2004) is as follows: H'<1 = low diversity; 1<H'<3 = medium diversity; H'>3 = high diversity.

The value of species evenness index can describe the stability of a community. The evenness index value (E) ranges from 0–1. The smaller or closer to zero value of E, the more uneven the distribution of species in the community, which is dominated by certain species. Conversely, the greater or closer to one value of E, the more evenly spread of species in the community (Sholiqin et al. 2021). The equation for the evenness index is as follows:

$$E = N'/LogS \tag{2}$$

E = species evenness, and H' = Shannon diversity (the log of the number of species).

Calculation of biomass was done using allometric formulas. The allometric equation used is based on the reference from the Forestry Research and Development Agency No.P.01/VIII-P3KR/2012 using the approach to the availability of a tree biomass allometric model, which is appropriate for the type/forest ecosystem where the object is located but not the specific location of the object.

After the biomass had been determined, it was then multiplied by 0.47 to determine the carbon content, which was then converted into a unit area (ton ha^{-1}) (IPCC 2006). The conversion of carbon stock to total CO_2 absorption can use the relative atomic mass ratio C which can be formulated as follows: CO_2 equivalent = C x 3.67 (Azzahra et al. 2020). The carbon content of mangrove sediments was analyzed in the laboratory using the Walkley–Black method (ton ha^{-1}) (Walkley and Black 1934). Then, the sediment layer samples were analyzed to obtain the sediment grain–size data. The results of sediment size analysis laboratory were used to determine each size class based on the Wenworth scale. In addition, the grain size of the resulting sediment was used to determine the types of sediment in the study area based on the sheppard triangle (Shepard 1954).

RESULTS

Mangrove Diversity in Karimunjawa National Park

Species composition, number of trees, average DBH and average tree height of the Karimunjawa National Park mangrove ecosystem are shown in Table 2. Each research station comprised mangrove species including *Rhizophora apiculata, Rhizophora mucronata, Ceriops tagal, Rhizophora*

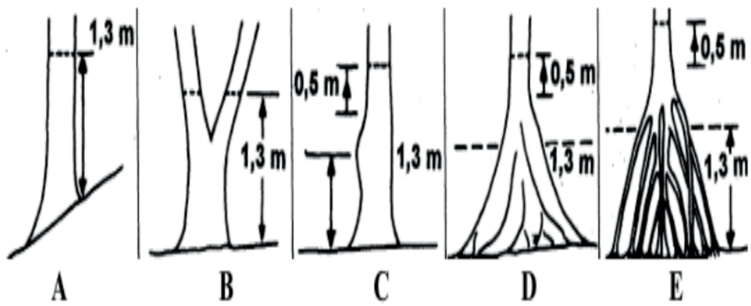

Fig. 2. How to measure DBH based on root state

Fig. 1. Allometric Equation

Species	Allometric
Rhizophora stylosa	B = 0.097 (DBH)$^{2.68}$
Rhizophora apiculata	B = 0.043(DBH)$^{2.63}$
Rhizophora mucronata	B = 0.128(DBH)$^{2.60}$
Xylocarpus molucensis	B = 0.1832(DBH)$^{2.21}$
Sonneratia caseolaris	B = 0.825(DBH)^{2,2}
Cerriops tagal	B = 0.168* ρ*(DBH)$^{2.47}$

B=Biomass; DBH=Diameter Breast High; ρ=density *stylosa* and *Xylocarpus moluccensis*. The distribution was even because these species are natural mangrove species in the KNP.

The results of the analysis of the relative density of mangroves in Karimunjawa National Park (Table 3) showed that Station I had the highest and lowest relative density values. *R. apiculata* had the highest value of 43.42%, whereas *X. moluccensis* had the lowest value (2.91%). The high relative density of *R. apiculata* was due to its high adaptability, which allows to develop well. According to the information in Table 3 the diversity index (H') ranged from 1.47 to 1.62. Referring to the work of Odum (1996), the diversity of mangrove species in the study area was in the moderate category at all stations. The diversity index value can be used to determine the level of stability of a community towards the environment (Odum 1996). Thus, the mangrove ecosystem in Karimunjawa National Park is stable and has a moderate diversity. The value of diversity in a community depends on the numbers of species and individuals in the community. The species diversity of a community is high if the community is composed of many species, and no species dominates (Rahmila and Halim 2018). Conversely, a community has a low species diversity if the community is composed of a few species, and a dominant species persists (Canty et al. 2022). The relationship between Biomass-Carbon, DBH, and Density is presented in the regression analysis (Fig 3).

Fig. 2. Composition of Mangrove Species in Karimunjawa National Park

Station	Species	Mean DBH	Mean Height
1	*Rhizophora apiculata*	22.26	9.40
	Rhizophora mucronata	22.46	7.70
	Ceriops tagal	22.84	6.10
	Rhizophora stylosa	13.83	6.80
	Sonneratia caseolaris	13.36	6.50
	Xylocarpus moluccensis	14.9	7.10
	Value	18.27	7.26
2	*Rhizophora apiculata*	15	8.20
	Rhizophora mucronata	14.64	6.00
	Ceriops tagal	10.23	6.40
	Rhizophora stylosa	14	6.60
	Xylocarpus moluccensis	11.87	6.80
	Sonneratia caseolaris	15.53	5.50
	Value	13.54	6.58
3	*Rhizophora apiculata*	15.25	7.70
	Rhizophora mucronata	15.1	7.20
	Ceriops tagal	10.79	7.25
	Rhizophora stylosa	15.35	7.00
	Xylocarpus moluccensis	11.22	6.60
	Value	13.54	7.15

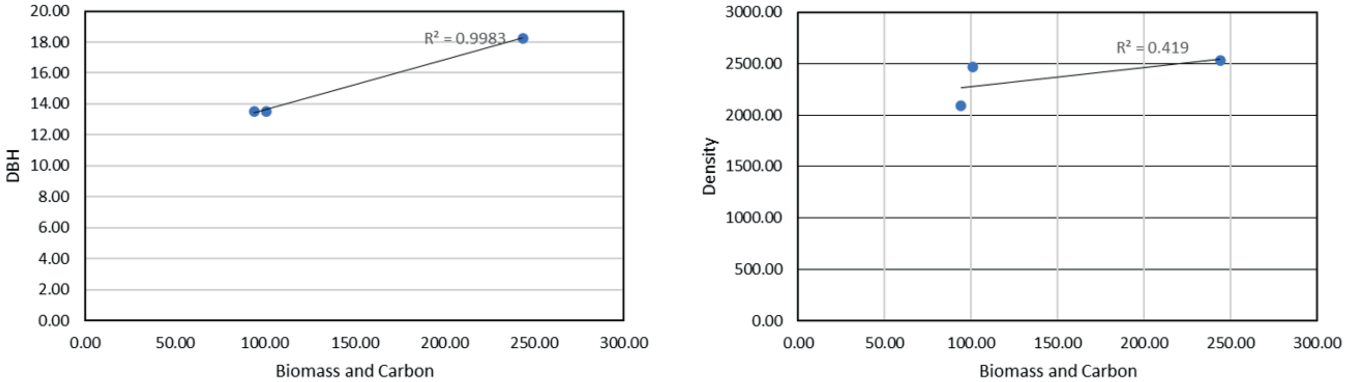

Fig. 3. Regression analysis of the relationship between Biomass-Carbon, DBH, and Density

Fig. 3. Value of IVI, Diversity Index, and Evenness Index

No	Species	Important Value Index (%)			IUCN
		Station 1	Station 2	Station 3	
1	*Rhizophora apiculata*	113.25	69.05	74.01	LC
2	*Rhizophora mucronata*	55.69	61.43	67.67	LC
3	*Ceriops tagal*	44.21	49.05	57.25	LC
4	*Rhizophora stylosa*	52.80	47.13	58.48	LC
5	*Sonneratia caseolaris*	18.20	35.33	-	LC
6	*Xylocarpus moluccensis*	15.82	38.00	42.59	LC
Σ Species		6	6	5	
Diversity index H’		1.47	1.62	1.54	
Evenness Index E		0.82	0.90	0.95	

Sediment Characteristics

According to Fig. 4, silt sediment accounted for an average of 58% of the different types of sediment detected at the three research sites. At a depth of 0–100 cm, the sediment had a texture like that of sandy mud with some clay. *Rhizophora sp*, given their robust roots and efficient sand traps, can thrive in sandy loam textures (Komiyama et al. 2005). Mangroves have a sandy loam substrate because the location of the mangrove ecosystem is not extremely close to the beach, which has high currents or waves. According to Indah et al. (2010), the root forms of *Rhizophora sp.*, namely, anchoring, and tight, also cause formation. This substrate formation is strongly influenced by the presence of currents in tidal and ebb conditions which carry the particles deposited at low tide.

Currents and depth are Oceanographic factors that affect sediment distribution (Wickramasinghe et al. 2009). Waters that have relatively calm currents and shallow water depths between 16 and 20 cm have similar types of sediments distributed in the mangrove ecosystem (Santen et al. 2007). This condition is due to the anchored and tight root forms of *Rhizophora sp.*, which also causes substrate formation (Ortega-Pacheco et al. 2018). These roots allow the excellent capturing process of dust particles in *Rhizophora sp* (Morton 2016). When a backflow exists, the dust particles are blocked by the roots. This condition shows the sediment characteristics that are suitable for the growth of mangroves in the Karimunjawa National Park, which is dominated by *Rhizophora sp.*

Biomass, C-Stock stand, and C-Stock Soil

Table 4 shows the stand biomass yield, stand carbon content, and sediment carbon content. Station 1 has the highest above ground biomass and C-Stock among other stations. The community structure of *R. apiculata* which is spread in all stations and dominates each transect influences the amount of carbon content.

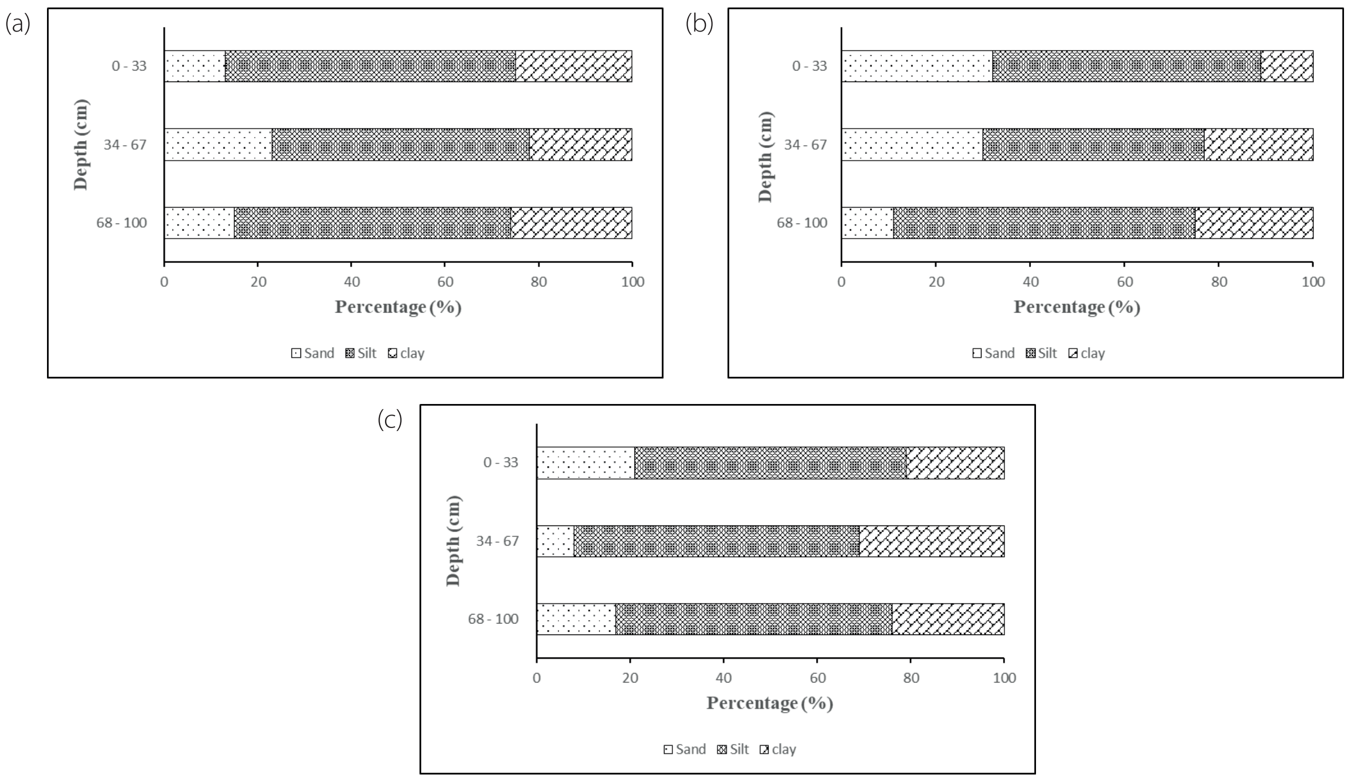

Fig. 4. Type and amount of sediment percentage based on depth. (a) Station 1, (b) Station 2, (c) Station 3

Table 4. Value of Biomass, C-Stock, and Average C-Stock

	Transect	Above-ground Biomass (t ha $^{-1}$)	C-Stock (t C ha $^{-1}$)	Average C-Stock (t C ha $^{-1}$)
St 1	1	638.79	300.23	243.73
	2	427.8	201.07	
	3	489.13	229.89	
St 2	4	240.29	112.93	94.01
	5	177.75	83.54	
	6	182.04	85.56	
St 3	7	244.27	114.80	100.92
	8	193.37	90.88	
	9	206.58	97.09	

The total individual, density value and DBH of *R. apiculata* at Station I showed that this community affected the carbon content at Station I was higher than at other stations. At Station 2, the density of mangrove trees has the lowest value compared to other stations. The dominant mangrove species at stations 2 and 3 is *R. Apiculata* and these two stations have the same average DBH value, which is 13.54 m. The level of diversity at all stations is still in the range of 1<H<3. Which means the level of diversity is included in the medium category. Even though in the case at Station 2 there was land conversion, the damage did not reduce the diversity of mangroves at Station 2. However, with density values, number of individuals in plot plots, and small DBH values compared to stations 1 and 3, the biomass content and carbon stock at Station 2 were the lowest (94.01 t C ha^{-1}). The value of the regression analysis between biomass-carbon and DBH shows 0.998. This demonstrates a directly proportional relationship. While the relationship between biomass-carbon and density shows a relationship that tends to be weak, the value is 0.419 (Fig. 5). The number of vegetation and diameter size indicate the amount of biomass and carbon stored (Datta et al. 2010). In addition, Station 1 is in the National Park area, allowing for natural mangrove conditions and optimal carbon absorption. This case is different from that at Station 2. The condition of mangroves located on the southern coast of Kemujan Island has been damaged considerably. This is presumably because there are residents around the mangrove area which caused the conversion of mangrove land to agricultural land.

Organic carbon in sediments is one of the constituents of organic compounds in waters. Organic carbon is a priority for soil improvement and for carbon storage. The ability to store carbon is higher than the mangrove tree itself. A high potential for emissions was observed due to the disruption of large carbon stores (Burdige 2007). The measurements of carbon content at the three stations based on depth yielded different results for carbon storage (Fig. 5). The carbon storage was measured vertically with three different depths.

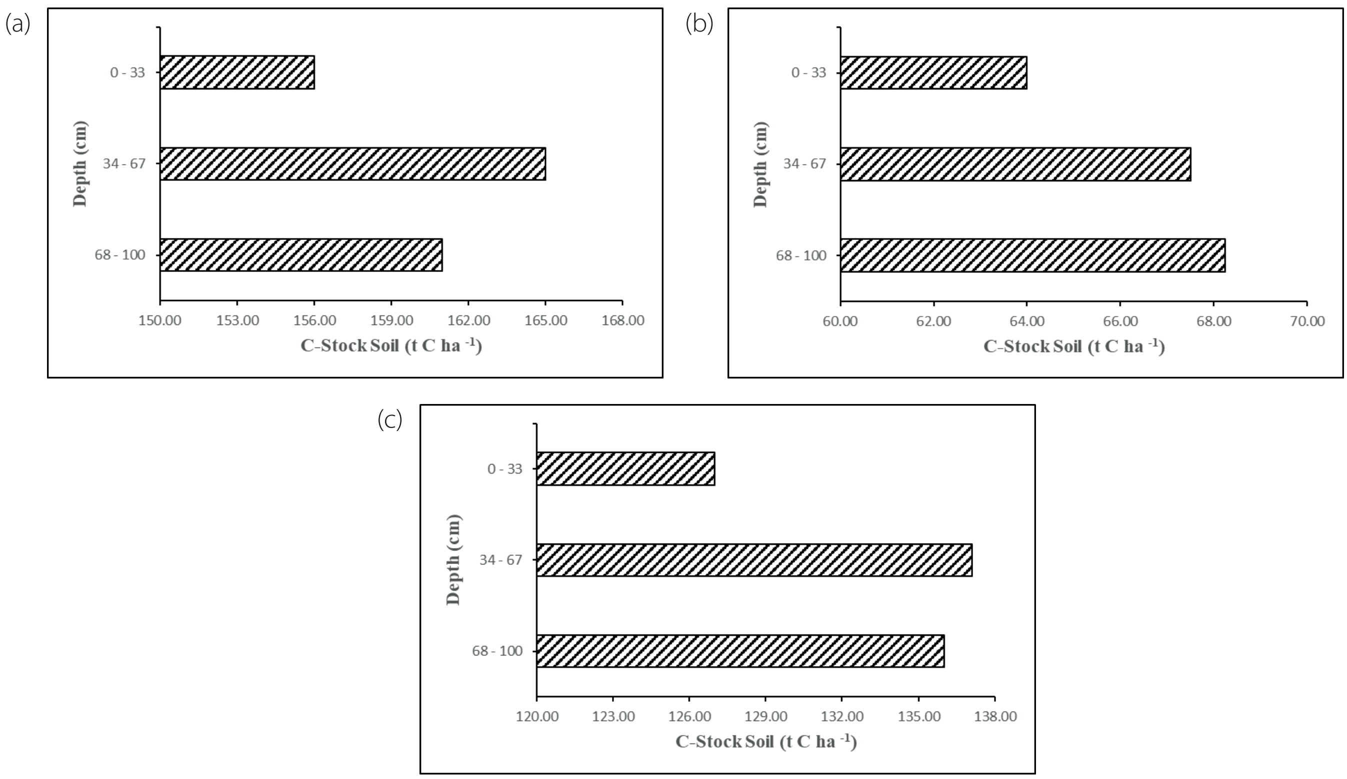

Fig. 5. Comparison of total soil C-stock values based on depth at all stations. (a) Station 1, (b) Station 2, (c) Station 3

Discussion

The order of the total number of trees from the most to the least was as follows: Station 1 (228 trees) > Station 3 (222 trees) > and Station 2 (188 trees). *R. apiculata* dominated the highest number of trees in all research locations. According to Wetlands International, this species grows in silty, smooth, deep soil and is flooded during normal tides (Andradi-Brown et al. 2013). It prefers tidal waters that have a strong permanent influence of freshwater input (Utami et al. 2021). *R. apiculata* has a dominance level that reaches 90% of the vegetation that grows in a location. This finding is in accordance with the substrate conditions in the mangrove ecosystem of Karimunjawa National Park, where many *R. apiculata* species grow and develop because of their very suitable habitat. Fig. 2 displays the type and magnitude of the substrate percentage at each station.

Importance Value Index (IVI) is calculated based on the number obtained to determine the level of species dominance in a plant community (Pollisco and Simorangkir 2013). From the results of calculations that have been carried out at the three observation stations, the difference in the index values among mangrove species was evident. *R. apiculata* found at Station I had the highest IVI of 113.25% while *X. moluccensis* of the same station had the lowest IVI of 15.82%. The IVI shows the range of indices that describe the community structure and distribution pattern of mangroves (Owuor et al. 2019). The difference in the IVI of mangrove vegetation is due to competition between each species for nutrients and sunlight at the study site. In addition, other factors that cause differences in mangrove vegetation density are the type of sediment and tides (Sarker et al. 2019). Gnanappazham and Selvam (2011) argued that the dominant species in a plant community will have a high IVI. Raymond et al. (2010) added that species with a high IVI have a high cumulative value of mastery and excellent control over their habitat. These species will be superior in utilizing resources or more adaptable to the environment. Furthermore, the difference in the IVI illustrates that the influence of a species in the mangrove community is different. This condition is influenced by a high species density value, resulting in a high IVI. According to Odum (1993), the influence of a population on communities and ecosystems not only depends on the species of the organizations involved but also on the number or density of the population. Sandy mud substrate conditions and water conditions, which are always inundated, were strongly suspected to affect the survival of *R. apiculata* (Rahim et al. 2017). The low relative density of *X. moluccensis* was thought to be due to the inaccessibility of the sampling plot. Sampling did not reach the land area. Thus, only a few tree samples were detected in the plot. This species prefers aquatic habitats that with low salinity and is often found on riverbanks (Dasgupta et al. 2010).

Frequency is one of the parameters that can show the distribution pattern of vegetation types in an ecosystem (Ha et al. 2012). Species frequency also describes the probability of species that can grow and be found in a location. The frequency of mangrove species is influenced by the number of plots where the species is found. Finding mangrove species is more likely to occur when there are more plots (Sidik et al. 2018). The results of the analysis of the relative frequency of mangroves that have been carried out in the mangrove ecosystem of Karimunjawa National Park at the highest tree level are at Station 3, which is the same for all species at 20%. The species found were *R. apiculata, R. mucronata, C. tagal, R. stylosa,* and *X. moluccensis*. Meanwhile, the lowest relative frequency at the tree level was that of *S. caseolaris* (11.76 %) at Station 2. The large number of *R. apiculata* was due to the condition of the sediment substrate at the study site in the form of sandy silt, which can support mangrove growth, allowing this type of mangrove to survive and develop well. The silt substrate that is spread in almost all stations contained a huge amount of organic matter when compared with the type of sediment in sand form, which only contains minerals (Sarathchandra et al. 2018). Furthermore, the typical life cycle of Rhizophora with seeds that can germinate when they are still on the parent plant is very supportive of the wide distribution process of this species in the mangrove ecosystem (Thatoi et al. 2012).

R. apiculata at Station I had the highest relative dominance of 51.08 % due to its root system that is well-adapted in obtaining more nutrients when compared with other species. Meanwhile, *X. moluccensis* of the same station had the lowest relative dominance at 1.13 % due to its uneven distribution and the level of habitat suitability. The substrate type in the Karimunjawa mangrove ecosystem is mostly silt-sand type, whereas *X. moluccensis* prefers a harder substrate. The mangrove vegetation found showed varying zonings at each station. These mangroves do not fully form zoning based on their tolerance to salinity and periods of inundation, as suggested by many mangrove experts. In this study, mangroves grow from the edge of the sea to the mainland. The part near the sea is dominated by *R. apiculata*, which is very dominant along the coastlines of Karimunjawa Island, Kemujan Island, and Menjangan Besar Island. *S. caseolaris, C. tagal, R. stylosa* and *R. mucronata* were also found in the zone after *R. apiculata. Meanwhile, X. moluccensis* belongs to a minor mangrove group that is far from the coast and prefers aquatic habitats that are not too salty (Jugale et al. 2009).

Based on the description above, differences existed in the mangrove zoning at each research station, especially for the rear zoning. The front zoning tends to be uniform and is dominated by *Rhizophora sp*. There are different findings regarding the presence of *Avicennia Marina* in KNP. According to the research of Ulyah et al. (2022), there are *Avicennia Marina* species in all research locations (Menjangan Besar Island and Kemujan Island), while according to Susilo (2017), the existence of Avicennia Marina is not in the research location. It is suspected that this difference is caused by the size of the study area and the different sampling locations. Zoning that occurs in mangrove forests is influenced by several factors, including the frequency of inundation, salinity, dominance of plant species, tidal water movements and the openness of the mangrove forest location to wind and waves, as well as the distance of plants from the shoreline (Bunt 1996). According to (Odum 1972) the structure of the mangrove ecosystem in KNP is the estuary type of mangrove formation. In this type of the influence of sea water is as strong as the influence of river water. Estuary mangroves are characterized by the presence of *Rhizophora sp. At the edge of the groove, followed by a mixed commu*nity of Rhizophora – Bruguiera and ending with a pure community of *Nypa sp*. This is what makes *Avicennia sp* species not found in this study. Because the sampling location is in the estuary area, while *Avicennia sp* species enters the coastal mangrove. According to the conservation status of the International Union for Conservation of Nature (IUCN) Red List, all mangrove species found in the study in Karimunjawa National Park are classified as least concern (LC). Although it is still classified as low risk, in the next few years, the number of species may be threatened along by the increase in anthropogenic activities in Karimunjawa National Park. Conservation efforts still need to be carried out. Furthermore, the evenness index value at each research station ranged from 0.82 to 0.95. This shows that the species found at each research station tend to have uniformity, meaning that no species dominates a station. If the value of the evenness index is small, then the species uniformity in the community is lacking, meaning that the number of individuals for each species is not the same, so there is a tendency to be dominated by certain species (Zhila et al. 2014). On the other hand, the higher the uniformity index value, the higher the distribution pattern in the community and no species is dominant.

Distribution patterns in clusters are generally found in nature, due to the need for the same environmental factors (Syahid et al. 2020). Several reasons explain why plants show a clumped distribution (Mangora 2011). Most of the mangrove seeds/fruits are not consumed by animals. Thus, the ripe fruit will fall near the parent tree and grow into an adult tree. According to Santos et al. (2014), the formation of a clustered distribution pattern is related to the pattern or way of eating because certain areas have abundant food sources. In addition, external reproduction factors and substrate characteristics that are suitable for mangrove growth are one of the factors for the formation of a group distribution pattern. At stations 1 – 3, the carbon content increased with the increase in depth. The high organic matter in the surface layer (0 cm) was due to the high litter production from each station, where the mangrove density also affected the level of organic matter content. This result is in accordance with the opinion of Oliver et al. (2012), who stated that the decomposition process of litter (leaves/branches/twigs) only occurs on the soil surface, whereas at a depth of more than 20 cm, the effect of this process is not significant (Moriizumi et al. 2010). The condition of the sustainability of subsurface carbon stocks is still poorly understood, but evidence from this study shows that land clearing, drainage, and/or conversion to ponds/agriculture, in addition to having an impact on vegetation biomass, significantly reduces the carbon content of mangrove soils (Duan and Kaushal 2013).

The highest carbon storage on average was at a depth of 34–67 cm, with values ranging from 67.5 t C ha^{-1} to 165 t C ha^{-1}. The lowest value was found in the upper layer (0–33 cm) at Station 2 with a value of 64 t C ha^{-1}. This condition was thought to be the surface layer being heavily affected by currents, waves, and tides, which cause the organic content, including carbon, to be carried along with the movement of water (Halim et al. 2018). The layer beneath reveals solid forms that have been held together over years by sedimentation. In theory, from the sedimentation process, a biogeochemical process occurs which causes the carbon content at the bottom to increase with increasing depth. But in this study, at stations 1 and 3 the carbon content only increased after a depth of 33 cm leading to a depth of 67 cm. After a depth of 67 to 100 cm the carbon content decreases. Only Station 2 has an increase in carbon content with increasing depth. One reason for this is that it is suspected that the sample at a depth of 68 - 100 cm contains sand type sediments. At Station 3 the sand content increased after a depth of 67 cm. Whereas at station 1 it is slightly different, because the sand content at a depth of 68 - 100 cm is less than at a depth of 34 - 67 cm. At Station 1 at a depth of 34 - 67 the sediment conditions are very dark black, while at a depth of 68 - 100 cm the sediment is not as dense as at a depth of 34 - 67 cm. According to Ati et al. (2014), the proportion of the particle size of sand, silt and clay affects the permeability, fertility, and salinity of the soil. The presence of nutrients is also influenced by the composition of the sediment. Sediments that contain a lot of silt are generally richer in organic matter than sandy sediments. Sari et al. (2017) in their research located in West Kalimantan where sediment research was carried out based on a depth range of 0-5 cm, 5-10 cm, 10-20 cm and 20-30 cm. where at a depth of 0-5 cm it has a carbon stock value of 1705.27 t C ha^{-1} and has increased to 8899.62 t C ha^{-1} at a depth of 10-20 cm, but at a depth of 20-30 it has decreased by 6745.22 t C ha^{-1}. The soil organic carbon content in the 0-5 cm layer is in an active weathering process and often changes. According to (Lorenz and Lal 2005) soil organic carbon reserves in the top layer often experience rapid decomposition by increased microbial activity near the soil surface and fluctuations in soil temperature. Soil organic carbon stocks in the lower layers are protected in soil aggregates and have a low decomposition rate. The total average value of C-Stock stands and C-Stock soil at all observation stations was 438.66 t C ha^{-1} and 1081.85 t C ha^{-1}, respectively. This value is equivalent to the absorption of CO_2 from the atmosphere of 1,609.88 t C ha^{-1} and 3,970.38 t C ha^{-1}. Efforts to increase the contribution of emission reduction in KNP can be achieved by conducting emission reduction interventions. One form of intervention that can be done is to reduce emissions due to changes in mangrove land by rehabilitating or planting mangroves that can increase carbon sequestration and storage. In addition, conservation of mangrove ecosystems is also to prevent increased emissions in the land-based sector. This effort can be considered in the mitigation actions of Central Java Province.

The biogeochemical cycle is the transfer of organic and inorganic elements/compounds (Alongi 2020). The biogeochemical cycle maintains life on earth. The total average value for the estimated carbon of mangrove stands was 146.22 t C ha^{-1}, and for the estimated carbon stock in sediments, the value was around 360.61 t C ha^{-1}. The estimated carbon of mangrove stands in Karimunjawa National Park is lower than the carbon content in the coastal village of Botoc, Philippines (Abino et al. 2013). On a national scale, the carbon content in the mangrove sediments of Karimunjawa National Park is higher than that of mangrove forests in Mangunharjo (Hadiyanto et al. 2021), Baturapa (Marbun et al. 2020), the northern part of the mangrove ecosystem of Bunaken National Park (Verisandria et al. 2018), and Jembrana Bali (Mahasani et al. 2015). According to Komiyama et al. (2008), in a study of mangrove forest biomass in various countries that was carried out for several years, variations in biomass estimates not only depended on species but also on ecological conditions and geographical locations. Based on research by Latifah et al. (2018), there has been deforestation of 82.37 ha of mangroves in Karimunjawa during the period 1992 - 2017. That means that there has been a decrease in mangroves by 0.3 ha per year. Meanwhile in this study, the value of the carbon content of the stands was 146.22 t C ha^{-1} or a CO_2 equivalent of 1609.88 t CO_2 ha^{-1}. So, we can assume that if the reduction in area in the research of Latifah et al. (2018) is combined with our carbon research, the result is that the mangrove ecosystem in Karimunjawa loses an average of 48.74 t C ha^{-1} of carbon stock each year or a CO_2 equivalent absorption of 536.62 t CO_2 ha^{-1} due to anthropogenic activities. The Karimunjawa mangrove habitat has a reasonably high-density value, which means that the potential for litter fall is also to be very significant. Carbon content is influenced by the number and density of trees, tree species, and environmental factors, including sunlight, water content, temperature, and soil fertility, which affect the rate of photosynthesis (Alongi 2002).

CONCLUSIONS

Karimunjawa National Park has a stable mangrove ecosystem and sufficient species diversity. The condition of the mangrove ecosystem, which was still good at the time of sampling in August 2021, requires special attention in sustainable management. The potential for carbon sequestration is high in stands (146.22 t C ha^{-1}) and sediments (360.61 t C ha^{-1}). The main factors that influence this potential are the density of species and diameter of mangrove trunks. Deforestation of mangrove land causes the release of carbon in the atmosphere. It is suspected that there has been a loss of mangrove carbon stocks in Karimunjawa with an average of 48.74 t C ha^{-1}/year or CO_2 equivalent absorption of 536.62 t CO_2 ha^{-1}/year.

REFERENCES

Abino A.C., Castillo J.A.A., Lumbres R.I.C., Kim S.Y., Jang M.N., Lee Y.J. (2013). Assessment of Plant Diversity, Biomass and Carbon Sequestration Potential of Natural Mangrove Forest in Samar, Philippines. Korea: Korea Forest Recreation Society Academic Presentation Material Book.

Abino A.C., Castillo J.A.A., Lee Y.J. (2014). Species Diversity, Biomass, and Carbon Stock Assessments of a Natural Mangrove Forest in Palawan, Philippines. Pak. J. Bot, 46(6), 1955-1962.

Alimbon J.A., Manseguiao M.R.S. (2021). Species composition, stand characteristics, aboveground biomass, and carbon stock of mangroves in Panabo Mangrove Park, Philippines. Biodiversitas. 22(6), 3130-3137, DOI: 10.13057/biodiv/d220615.

Alongi D.M. (2020). Global significance of mangrove blue carbon in climate change mitigation. Sci, 2(3), 67, 1-15, DOI: 10.3390/sci2030067.

Alongi D.M. (2002). Present state and future of the world's mangrove forests. Environ Conserv, 29(3), 331–349, DOI: 10.1017/s0376892902000231.

Andradi-Brown D.A., Howe C., Mace G.M., Knight A.T. (2013). Do mangrove forest restoration or rehabilitation activities return biodiversity to pre-impact levels? Environmental Evidence, 2(1), 20, 1-8, DOI: 10.1186/2047-2382-2-20.

Andrianto F., Bintaro A., Yuwono S.B. (2015). Produksi dan laju dekomposisi serasah mangrove (Rhizophora sp) di Desa Durian dan Desa Batu Menyan Kecamatan Padang Cermin. Sylva Lestari, 4(2), 9–20.

Azzahraa F.S., Suryantia S., Febrianto S. (2020). Estimasi Serapan Karbon Pada Hutan Mangrove Desa Bedono, Demak, Jawa Tengah. Journal of Fisheries and Marine Research, 4(2), 308–315.

Basu S.K., Cetzal-Ix W. (2018). Traditional honey collectors in the Sunderbans region and their impact on the local mangrove ecosystem and biodiversity: a case study with reference to human–animal conflict. Biodiversity, 1–7, DOI: 10.1080/14888386.2018.1508365.

BTNKJ. (2020). Statistics in Karimunjawa National Park figures. Indonesia: Karimunjawa National Park Hall, Ministry of Environment and Forestry.

Bunt J.S. (1996). Mangrove Zonation: An Examination of Data from Seventeen Riverine Estuaries in Tropical Australia. Annals of Botany, 78(3), 333-341, DOI: 10.1006/anbo.1996.0128.

Burdige D.J. (2007). Preservation of Organic Matter in Marine Sediments: Controls, Mechanisms, and an Imbalance in Sediment Organic Carbon Budgets? Chem Rev, 107(2), 467-485, DOI: 10.1021/cr050347q.

Camacho L.D., Dixon T., Gevaña., Antonio P., Carandang., Sofronio C.C., Edwin A., Combalicer., Lucrecio L.R., Youn Y.C. (2011). Tree biomass and carbon stock of a community-managed mangrove forest in Bohol, Philippines. Forest Science and Technology 7(4), 161-167, DOI: 10.1080/21580103.2011.621377.

Cameron C., Lindsay B.H., Daniel A.F., Ben B. (2019). High greenhouse gas emissions mitigation benefits from mangrove rehabilitation in Sulawesi, Indonesia. Ecosystem Services, 40, 1-9, DOI: 10.1016/j.ecoser.2019.101035.

Canty S.W.J., Kennedy J.P., Fox G. (2022). Mangrove diversity is more than fringe deep. Sci Rep 12, 1695, DOI: 10.1038/s41598-022-05847-y.

Carugati L., Gatto B., Rastelli E., Lo M.M., Coral C., Greco S., Danovaro R. (2018). Impact of mangrove forests degradation on biodiversity and ecosystem functioning. Scientific Reports, 8(1), 1-11, DOI: 10.1038/s41598-018-31683-0.

Dasgupta N., Nandy P., Tiwari C., Sauren D. (2010). Salinity-imposed changes of some isozymes and total leaf protein expression in five mangroves from two different habitats. Journal of Plant Interactions, 5(3), 211-221, DOI: 10.1080/17429140903438076.

Datta D., Guha R.N., Chattopadhyay. (2010). Application of criteria and indicators in community based sustainable mangrove management in the Sunderbans, India. Ocean and Coastal Management, 53(8), 468-477, DOI: 10.1016/j.ocecoaman.2010.06.007.

Datta D., Chattopadhyay R.N., Guha P. (2012). Community based mangrove management: A review on status and sustainability. Journal of Environmental Management, 107, 84-95, DOI: 10.1016/j.jenvman.2012.04.013.

Duan S.W and Kaushal S.S. (2013). Warming increases carbon and nutrient fluxes from sediments in streams across land use. Biogeosciences, 10(2), 1193–1207, DOI: 10.5194/bg-10-1193-2013.

Fachrul M.F. (2007). Metode Sampling Bioekologi. Buku. Bumi Aksara. Jakarta. 198 p.

Gnanappazham L., Selvam V. (2011). The dynamics in the distribution of mangrove forests in Pichavaram, South India – perception by user community and remote sensing. Geocarto International, 26(6), 475–490, DOI: 10.1080/10106049.2011.591943.

Hadiyanto, Halim M.A.R., Muhammad F., Soeprobowati T.R., Sularto. (2021). Potential for Environmental Services Based on the Estimation of Reserved Carbon in the Mangunharjo Mangrove Ecosystem. Polish Journal of Environmental Studies, 30(4), 3545-3552, DOI: 10.15244/pjoes/126374.

Halim M.A.R., Rahmila Y.I., Muhammad F., Safitri Y. (2018). The Effect on Mangrove Density with Sediment Rate in Coastal Pasar Banggi of Rembang Regency. E3S Web of Conferences, 73, 04020, DOI: 10.1051/e3sconf/20187304020.

Ha T.T.T., Han V.D., Simon R.B. (2012). Mangrove conservation or shrimp farmer's livelihood? The devolution of forest management and benefit sharing in the Mekong Delta, Vietnam. Ocean and Coastal Management, 69, 185-193, DOI: 10.1016/j.ocecoaman.2012.07.034.

Ha T.T.P., Han V.D., Leontine V. (2014). Impacts of changes in mangrove forest management practices on forest accessibility and livelihood: A case study in mangrove-shrimp farming system in Ca Mau Province, Mekong Delta, Vietnam. Land Use Policy, 36, 89-101, DOI: 10.1016/j.landusepol.2013.07.002.

Huxham M., Lucy E., James K., Fridah M., Hassan A., Tabitha M., Fiona N., Robert A.B. (2015). Applying Climate Compatible Development and economic valuation to coastal management: A case study of Kenya's mangrove forests. Journal of Environmental Management, 157, 168-181, DOI: 10.1016/j.jenvman.2015.04.018.

Indah R.A., Jabarsyah, Laga A. (2010). Differences in Substrate and Distribution of Mangrove Types (Case Study: Mangrove Forest in Tarakan City). Jurnal Harpodon Borneo, 3(1), 1-19.

IPCC (Intergovermental Panel on Climate Change). (2006). IPCC Guidelines for National Greenhouse Gas Inventories, Agriculture, Forestry and Other Land Use. Keith Paustian, N. H. Ravindranath, Andre van Amstel, Michael Gytarsky, Werner A. Kurz, Stephen Ogle, Gary Richards, and Zoltan Somogyi: The Institute for Global Enviromental Strategies (IGES).

IUCN. (2022). The IUCN Red List of Threatened Species, [online] IUCN. Available at: http://www.iucnredlist.org/ [Accessed 10 April 2022].

Jugale S.B., Bhosale L.J., Kad T.D., Nadaf A.B. (2009). Genetic diversity assessment in intra- and inter-populations of Xylocarpus granatum Koen.: a critically endangered and narrowly distributed species of Maharashtra. Current Science, 97(5), 695-701.

Komiyama A., Ong J.E., Poungparn S. (2008). Allometry, biomass and productivity of mangrove forests: a review. Aquat Bot, 89, 128–137, DOI: 10.1016/j.aquabot.2007.12.006.

Komiyama A., Poungparn S., Kato S. (2005). Common allometric equations for estimating the tree weight of mangroves. J Trop Ecol, 21(4), 471–477, DOI: 10.1017/s0266467405002476.

Latifah N., Febrianto S., Endrawati H., Zainuri M. (2018). Pemetaan Klasifikasi Dan Analisa Perubahan Ekosistem Mangrove Menggunakan Citra Satelit Multi Temporal di Karimunjawa, Jepara, Indonesia. Jurnal Kelautan Tropis, 21(2), 97-102, DOI: 10.14710/jkt.v21i2.%202977.

Li J., Liao Q., Li M., Zhang J., Tam NF, Xu R. (2010). Community Structure and Biodiversity of Soil Ciliates at Dongzhaigang Mangrove Forest in Hainan Island, China. Applied and Environmental Soil Science, 1–8, DOI: 10.1155/2010/103819.

Lorenz K and Lal R. (2005). The Depth Distribution Of Soil Organic Carbon In Relation to Land Use And Management And The Potential Of Carbon Sequestration in Subsoil Horizons. Advance in Agronomy, 88, 35-66.

Magurran A.E. (2004). Measuring Biological Diversity. United Kingdom: Blackwell Sciene Ltd.

Mahasani G., Nuryani W., Wayan K. (2015). Estimated Percentage of Organic Carbon in Ex-Pond Mangrove Forests, Perancak, Jembrana, Bali. Journal of Marine and Aquatic Sciences, 1, 14-18.

Malik A., Fensholt R., Mertz O. (2015). Mangrove exploitation effects on biodiversity and ecosystem services. Biodiversity and Conservation, 24(14), 3543–3557, DOI: 10.1007/s10531-015-1015-4.

Mangora M.M. (2011). Poverty and institutional management stand-off: a restoration and conservation dilemma for mangrove forests of Tanzania. Wetlands Ecol Manage, 19(6), 533-543, DOI: 10.1007/s11273-011-9234-2.

Marbun A., Rumengan A.P., Schaduw J.N.W., Paruntu C., Angmalisang P.A., Manoppo V.E.N. (2020). Analysis of Carbon Stock in Mangrove Sediments in Baturapa Village, Lolak District, Bolaang Mongondow Regency. Jurnal Pesisir dan Laut Tropis, 8, 20-30.

Moriizumi Y., Naohiro M., Hiroki H. (2010). Simplified life cycle sustainability assessment of mangrove management: a case of plantation on wastelands in Thailand. Journal of Cleaner Production, 18(16), 1629-1638, DOI: 10.1016/j.jclepro.2010.07.017.

Morton B. (2016). Hong Kong's mangrove biodiversity and its conservation within the context of a southern Chinese megalopolis. A review and a proposal for Lai Chi Wo to be designated as a World Heritage Site. Regional Studies in Marine Science, 8, 382–399, DOI: 10.1016/j.rsma.2016.05.001.

Odum E.P. (1993). Dasar-dasar Ekologi, 1st ed. Yogyakarta: Gadjah Mada University Press.

Odum E.P. (1996). Dasar-dasar Ekologi, 3rd ed. Yogyakarta: Gajah Mada University Press.

Oliver T.S.N., Kerrylee R., Chris J.C., Colin D.W. (2012). Measuring, mapping and modelling: an integrated approach to the management of mangrove and saltmarsh in the Minnamurra River estuary, southeast Australia. Wetlands Ecol Manage, 20(4), 353-371, DOI: 10.1007/s11273-012-9258-2.

Ortega-Pacheco D., Mendoza-Jimenez M.J., Herrera P. (2018). Mangrove Conservation Policies in the Gulf of Guayaquil. Handbook of Climate Change and Biodiversity, 25–43, DOI: 10.1007/978-3-319-98681-4_2.

Owuor M.A., Mulwa R., Otieno P., Icely J., Newton A. (2019). Valuing mangrove biodiversity and ecosystem services: A deliberative choice experiment in Mida Creek, Kenya. Ecosystem Services, 40, 1-12, DOI: 10.1016/j.ecoser.2019.101040.

Pollisco F., Simorangkir D. (2013). The economics of ecosystems and biodiversity, REDD+ and climate change in mangrove ecosystems of Southeast Asia. International Journal of Rural Law and Policy, (1), 1–6, DOI: 10.5130/ijrlp.i1.2013.3350.

Rahim S., Baderan D.W.K., Hamidun M.S. (2017). The density, composition, and mangrove forest habitat in coastal areas of Torosiaje Jaya Village, Gorontalo, Indonesia. International Journal of Bonorowo Wetlands, 7(1), 38 – 42. DOI: 10.13057/bonorowo/w070108.

Rahmila Y.I., Halim M.A.R. (2018). Mangrove forest development determined for ecotourism in Mangunharjo Village Semarang. E3S Web of Conferences, 73, 04010, DOI: 10.1051/e3sconf/20187304010.

Raymond G., Harahap N., Soenarno. (2010). Community Based Mangrove Forest Management in Gending District, Probolinggo. Agritek, 18(2), 185-200.

Roy A.K.D., Khorshed A., Jeff G. (2013). Community perceptions of state forest ownership and management: A case study of the Sundarbans Mangrove Forest in Bangladesh. Journal of Environmental Management, 117, 141-149, DOI: 10.1016/j.jenvman.2012.12.004.

Rozainah M.Z., Nazri M.N., Sofawi A.B., Hemati Z., Juliana W.A. (2018). Estimation of carbon pool in soil, above and below ground vegetation at different types of mangrove forests in Peninsular Malaysia. Marine Pollution Bulletin, 137, 237-245, DOI: 10.1016/j.marpolbul.2018.10.023.

Santen P.V., Augustinus P.G.E.F., Janssen-Stelder B.M., Quartel S., Tri N.H. (2007). Sedimentation in an estuarine mangrove system. Journal of Asian Earth Sciences, 29(4), 566-575, DOI: 10.1016/j.jseaes.2006.05.011.

Santos L.C.M., Humberto R.M., Yara S.N., Marília C.L., Marisa D.B., Nico K., Farid D.G. (2014). Anthropogenic activities on mangrove areas (São Francisco River Estuary, Brazil Northeast): A GIS-based analysis of CBERS and SPOT images to aid in local management. Ocean & Coastal Management, 89, 39-50, DOI: 10.1016/j.ocecoaman.2013.12.010.

Sarathchandra C., Kambach S., Ariyarathna S., Xu J., Harrison R., Wickramasinghe S. (2018). Significance of Mangrove Biodiversity Conservation in Fishery Production and Living Conditions of Coastal Communities in Sri Lanka. Diversity, 10(2), 21-12, DOI: 10.3390/d10020020.

Sari T., Rafdinal., Linda R. (2017). Hubungan Kerapatan Tanah, Karbon Organik Tanah dan Cadangan Karbon Organik Tanah Di Kawasan Agroforestri Tembawang Nanga Pemubuh Sekadau Hulu Kalimantan Barat. Protobiont, 6(3), 263-269. DOI: 10.26418/protobiont.v6i3.22492.

Sarker S.K., Reeve R., Paul N.K., Matthiopoulos J. (2019). Modelling spatial biodiversity in the world's largest mangrove ecosystem-The Bangladesh Sundarbans: A baseline for conservation. Diversity and Distributions, 1-14, DOI: 10.1111/ddi.12887.

Shepard F.P. (1954). Nomenclature Based on Sand-Silt-Clay Ratio. Jour. Sed. Pet., 24:151-158.

Sholiqin M., Pramadaningtyas P.S., Solikah I., Febriyanti I., Pambudi D.M., Mahartika S.B., Umam A.F., Liza N., Setyawan A.D. (2021). Analysis of the diversity and evenness of mangrove ecosystems in the Pacitan Coast, East Java, Indonesia. International Journal of Bonorowo Wetlands, 11(2), 84-94, DOI: 10.13057/bonorowo/w110205.

Sidik F., Bambang S., Haruni K., Muhammad Z.M. (2018). Mangrove conservation for climate change mitigation in Indonesia. Wiley Interdisciplinary Reviews: Climate Change, 9(5), 1-9, DOI: 10.1002/wcc.529.

Syahid L.N., Sakti A.D., Virtriana R., Wikantika K., Windupranata W., Tsuyuki S., Caraka R.E., Pribadi R. (2020). Determining Optimal Location for Mangrove Planting Using Remote Sensing and Climate Model Projection in Southeast Asia. RemoteSensing, 12(22), 3734, DOI: 10.3390/rs12223734.

Taillardat P., Daniel A.F., Massimo L. (2018). Mangrove blue carbon strategies for climate change mitigation are most effective at the national scale. Biology Letters, 14(10), 1-6, DOI: 10.1098/rsbl.2018.0251.

Thatoi H., Behera B.C., Mishra R.R., Dutta S.K. (2012). Biodiversity and biotechnological potential of microorganisms from mangrove ecosystems: a review. Annals of Microbiology, 63(1), 1–19, DOI: 10.1007/s13213-012-0442-7.

Utami W., Wibowo Y.A., Hadi A.H., Permadi F.B. (2021). The impact of mangrove damage on tidal flooding in the subdistrict of Tugu, Semarang, Central Java. Journal of Degraded and Mining Lands Management, 9(1), 3093-3105, DOI: 10.15243/jdmlm.2021.091.3093.

Verisandria R.J., Schaduw J.N.W., Sondak C.F.A., Ompi M., Rumengan A., Rangan J. (2018). Estimation of Carbon Potential in Mangrove Ecosystem Sediments in the Northern Coast of Bunaken National Park. Jurnal Pesisir dan Laut Tropis, 1, 81-97.

Walkley, A. and Black I.A. (1934). An examination of the Degtjareff Method for Determining Soil Organic Matter, and a proposed Modification of the Chromic Acid Titration Method. Soil Science, 37(1): 29-38.

Wan-Talaat W.I.A., Tahir N.M., Husain M.L. (2012). The Existing Legislative, Administrative and Policy Framework for the Mangrove Biodiversity Management and Conservation in Malaysia. Journal of Politics and Law, 5(1), 1-9, DOI: 10.5539/jpl.v5n1p180.

Weyerhaeuser H., Tennigkeit T. (2000). Forest inventory and monitoring manual. Chaiang Mai: HBS-ICRAF-CMU.

Wickramasinghea S., Maurizio B., Sarath W.K., Roland C., Alfredo J.A., Oleg V.S. (2009). Multi-functional pollution mitigation in a rehabilitated mangrove conservation area. Ecological Engineering, 35(5), 898-907, DOI: 10.1016/j.ecoleng.2008.12.021.

Zhila H., Mahmood H., Rozainah M.Z. (2014). Biodiversity and biomass of a natural and degraded mangrove forest of Peninsular Malaysia. Environmental Earth Sciences, 71(11), 4629–4635, DOI: 10.1007/s12665-013-2853-6.

RESEARCH PAPER

DISTRIBUTION OF POISONOUS PLANTS IN BIOMES OF THE SOUTHERN FAR EAST OF RUSSIA

Tatiana V. Dikareva*[1], Vadim Yu. Rumyantsev[1], Mikhail S. Soldatov[1], Wang Li (LI Wang)[2], Svetlana M. Malkhazova[1]
[1]M.V. Lomonosov Moscow State University, Faculty of Geography
Russia, 119992, Moscow, Leninskie Gory, 1
[2]Key Laboratory of Land Surface Pattern and Simulation, Institute of Geographical Sciences and Natural Resources Research, Chinese Academy of Sciences, Beijing 100101, Chinan
***Corresponding author:** tvdikareva@yandex.ru
Received: June 8th, 2023 / Accepted: September 4th, 2023 / Published: October 10th, 2023
https://DOI-10.24057/2071-9388-2023-2928

ABSTRACT. Poisonous plants are a collective group of plants of various systematic categories that contain phytotoxins that pose a potential danger to humans and animals. A number of publications both in Russia and abroad are devoted to the problem of patterns of distribution of plants hazardous to human health in connection with environmental factors. This work is a continuation of research into the spread of plants dangerous to humans in Russia. The aim of this work is ecological and geographical analysis of poisonous plants distribution in biomes of the Far East in Russia. Resulted from the research work on the territory of the far-eastern biomes of Russia we revealed 87 the most toxic vascular plant species that belong to 21 plant families. Some of the most poisonous plants of the Russian flora are plants of the genus *Aconitum*, of the family (Ranunculaceae). About 70 species of this genus grow in Russia, of which 40 are found only in the Far East, since this territory is considered the center of botanical diversity of the genus in question. The cartographical analysis showed that the highest number of poisonous plant species could be found in the south-east regions – in Primorye, the basin of Ussuri river, in the lower and middle course of the river Amur. Based on a map of Russian biomes, optimal habitats for poisonous plants were identified. Maximum number of *Aconitum* species, as the most poisonous genus of Russian flora, is in the mountain biomes and in the plain forest-steppe biomes in the Amur basin. The types of ecosystems with the maximum abundance and diversity of poisonous plants have been identified. The species richness distribution shows the concentration of poisonous plant species in small mountain biomes and in arid-like biomes. Correlation analysis of relationships between the number of plant species and climatic factors revealed the significant closeness of the correlation with the average annual air temperature (0,66). Maximum correlation closeness appeared to be between number of poisonous plant species per 10 000 km^2 and total number of vascular plants per 10 000 km^2 (0,81).

KEYWORDS: poisonous plants, regional biomes, climatic factors, cartographical and correlation analysis

CITATION: Dikareva T. V., Rumyantsev V. Yu., Soldatov M. S., Wang Li (LI Wang), Malkhazova S. M. (2023). Distribution Of Poisonous Plants In Biomes Of The Southern Far East Of Russia. Geography, Environment, Sustainability, 3(16), 43-51
https://DOI-10.24057/2071-9388-2023-2928

ACKNOWLEDGEMENTS: The methodological part of the work was supported by the Russian Science Foundation project No. 21-47-00016 «New and re-emerging natural infectious diseases in China and Russia: spatial-temporal analysis and assessment of transboundary risks».

The thematic part of the study was carried out within the framework of the Development Program of the Interdisciplinary Scientific and Educational School of Moscow State University named after M.V. Lomonosov «The future of the planet and global environmental changes».

Conflict of interests: The authors reported no potential conflict of interest.

INTRODUCTION

Poisonous plants are a combined group of plant species of various systematic categories which contain phytotoxins potentially dangerous for people and animals. The poisonous properties od plants formed in the process of evolution and are the significant mechanist in struggle for existence. According to the degree of toxicity, plants are divided into unconditionally poisonous and conditionally poisonous. The last ones are toxic only in certain seasons or in some habitats. The seasonality of the content of toxic substances is determined by the peculiarities of the functioning of various plant organs during year cycle: above-ground parts of the plant are most toxic during the flowering period; in underground organs, the amount of toxins increases during the winter dormancy; the majority of fruits in plants are highly toxic when ripe.

About four hundred poisonous plant species grow on the territory of Russia with various degree of toxicity. The systematic study of these plants began in the 1930s of XX century (Krechetovich 1931) and was devoted to the analysis of the biochemical and botanical characteristics of poisonous plants. Later, numerous reference books and monographs on poisonous plants of the USSR and Russia appeared in the domestic literature (Gusinin 1962; Dudar 1971; Luferov 1995; Zoricov 2005), in which the poisonous plants are considered as important source of biologically active substances included into many medications. Studies of poisonous plants were also carried out in order to prevent and treat poisoning.

Numerous works of foreign authors are devoted to distribution, danger and use of poisoning plants (Unschuld 1985; Blake et al. 2007; Banasik and Stedeford 2014; San Andres Larrea et al. 2014; Bradberry and Vale 2016). In recent years many Chinese authors work in nearby territories studying poisoning plants and their possible use (Li et al. 2016; Zhang et al. 2021; Liu et al. 2022; Yahn and Chen 2022; Zhou et al. 2022).

A number of publications of the authors are devoted to the problem of the patterns of distribution of plants dangerous to human health in connection with some factors of their habitat (Dikareva and Rumyantsev 2015; Dikareva et al. 2017; 2018; 2022).

This work is a continuation of research on the distribution of plants dangerous to humans in Russia. Its purpose is to analyze the distribution of poisonous plants in the south of the Far East region in connection with environmental factors. The authors are aware that, for example, the Trans-Baikal Territory is not the Far East at all. However, the use of more strict wording would greatly complicate both the text and the title of the article. The tasks of the work included compiling a list of the most poisonous plants in the study area, conducting a statistical analysis of the relationships between the number of poisonous plant species in regional biomes and climatic indicators, and constructing appropriate thematic maps.

MATERIALS AND METHODS

This research work is based on the map "Biomes of Russia" (Ogureeva et al. 2018; 2020). 19 biomes with subbiomes of the Russian Far East are included into analysis (Fig. 1). The study area includes the territories of the Trans-Baikal, Khabarovsk and Primorsky Territories, the Amur Region and the Jewish Autonomous Region.

Of the approximately four hundred species of poisonous plants known in Russia according to the literature, 87 species were selected for analysis, which are common in the Far East and are definitely poisonous.All selected species are toxic to humans and contain large doses of toxic substances (alkaloids, saponins, flavonoids, bergapten, isobergapten, isopimpinelin, xanthotoxin, psoralen, etc.) (Orlov et al. 1990; Donchenko et al. 2009; Konovalova and Shevireva 2011, etc.)

One of the most poisonous plants of Russian flora are plants of the genus *Aconitum* (hereinafter referred to as aconites) from Ranunculaceae family (Avdeev and Ananiev 2010). All organs of all species of the genus contain alkaloids, primarily aconitine. About 70 species of this genus grow in Russia, 40 of which are found only in the Far East, since this territory is considered to be the center of botanical diversity of the genus under consideration (Luferov 1995). The 40 most toxic species of the genus were selected, for which the authors considered it interesting to compare their distribution with the distribution of other poisonous plants.

Data on the areals of poisonous species are obtained from the guides of higher vascular plants (Gubanov et al. 1995; Vascular…1996; Flora…1987-2003; and others), as well as from atlases (Atlas…1983; Agroecological…2015; Medical-geographical atlas…2019).

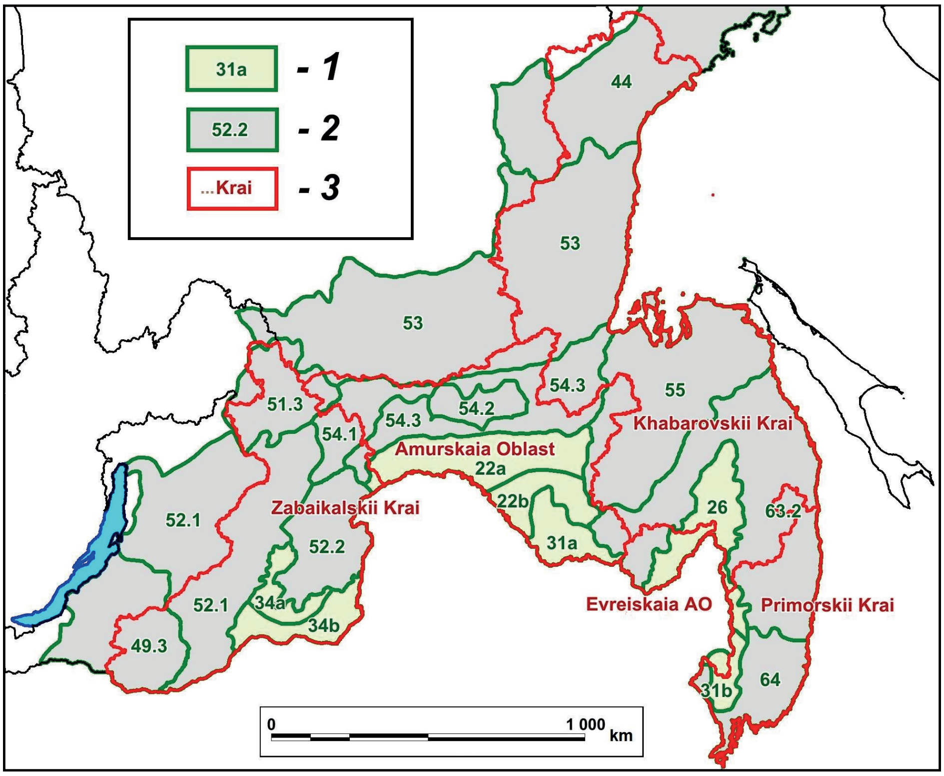

Fig. 1. Biomes (numeric designations) and subbiomes (letter designations) (source: Ogureeva et al. 2018; 2020) included in the analysis

1– Lowland:22 - Amuro-Zeiskii (a – southern taiga, b – subtaiga); 26 - Amuro-Ussuriiskii subtaiga; 31 - Zee-Bureinskii forest-steppe (a–Priamurskii oak forest-steppe, b–Prikhankaiskii pine-oak forest-steppe); 34 - Daurskii steppe (a - northern strip of forb-tussock-grass steppes, b - southern strip of forb-tussock-grass steppes).

2 – Mountain: 44 – Severookhotskii; 49 - Sayano-Yuzhnozabaikal'skii (49.3 - Buryatskii); 51 - Kodaro-Kalarskii (51.3 - Kodaro-Kalarskii); 52–Yuzhnozabaikal'skii (52.1–Vitimskii, 52.2 -Shilkinskii); 53 - Aldano-Maiskii; 54 - Yankan-Dzhagdinskii (54.1–Verkhnegilyuiskii, 54.2 - Tukuringra-Dzhagdinskii. 54.3 - Verkhnezeiskii); 55 – Yuzhnookhotskii; 63 - Sakhalino-Sikhote-Alin'skii (63.2 - Srednesikhote-Alin'skii); 64 - Sikhote-Alin'skii southern.

3– Subjects of the Russian Federation, limiting the study area.

The presence of a particular species of a poisonous plant in a biome was determined by the presence of at least a small part of its areal within a given unit (regional biome or subbiome). For each of the biomes, the total number of species of vascular plants was determined (taken directly from the map "Biomes of Russia" (Ogureeva et al. 2018; 2020) as well as number of species of poisonous plants (total, without *Aconitum* species and only *Aconitum* species). Next, the relative species richness of each regional division (biome or subbiome) was calculated, i.e., number of species per 10,000 km^2 for all species, poisonous species, poisonous species without *Aconitum* species and for *Aconitum* species. The materials are organized into a computer database linked to a digital base map in the MapInfo GIS (Fig. 1). On this basis, a series of maps of the distribution of all plant species and poisonous plants in the studied biomes was compiled.

The analysis included two climatic indicators – the average annual air temperature and the average annual precipitation. The relevant data was taken directly from the "Biomes of Russia" map (Ogureeva et al. 2018; 2020). If there was more than one value of this indicator for a biome (or subbiome), they were averaged. Working hypotheses were considered: 1) the number of poisonous plants depends on the total number of vascular plant species in a particular biome or subbiome; 2) the number of species of poisonous plants in a biome (subbiome) is directly related to climatic factors; 3) relative species richness (species per 10,000 km^2) of poisonous plants in a biome is related to the species richness of all vascular plant species in the biome (subbiome).To verify them, the Pearson pair correlation coefficients of the relationship between the number of plant species and environmental parameters were calculated in the STATISTIKA program for the traits listed below. The initial data for the corresponding calculations are presented in Table 1.

RESULTS AND DISCUSSION

The study area mainly refers to the Amur River basin, but also includes territories that do not belong to it. These are the eastern slopes of the Sikhote-Alin in the Primorsky region and the eastern slopes of the Dzhugdzhur Ridge in the north of the Khabarovsk region.

The territory of the region is mostly mountainous. Absolute heights are at 1000-2500 m above sea level. The appearance of the modern relief is determined by a combination of the sublatitudinal and submeridional location of the main mountain ranges, which form characteristic climatic barriers that prevent the penetration of oceanic monsoons far to the west. Therefore, the highest precipitation rates were noted in the coastal part of the region. The peculiarity of the nature of

Table 1. Characteristics of biomes and subbiomes included in the analysis

Biomes and subbiomes*	Square km^2	Average annual air temperature, C	Annual precipitation, mm	Total number of vascular plant species		Number of species of poisonous plants					
						all poisonous plants		aconites		without aconites	
				total	per 10000 km^2	total	per 10000 km^2	total	per 10000 km^2	total	per 10000 km^2
22a	90712	-3,97	421	1260	138,5	41	4,51	9	0,99	32	3,52
22b	38371	-3,6	540	1260	331,6	35	9,21	7	1,84	28	7,37
26	65743	1,5	645	1020	154,5	37	5,61	6	0,91	31	4,7
31	19234	2,7	625	800	421,1	35	18,42	9	4,74	26	13,68
31a	35063	-0,96	505	1000	285,7	46	13,14	11	3,14	35	10,0
34a	24187	-2,2	324	665	277,1	33	13,75	8	3,33	25	10,42
34b	39866	-3,2	300	657	164,3	23	5,75	8	2,0	15	3,75
44	410351	-3,3	536	1200	29,3	25	0,61	5	0,12	20	0,49
49.3	124568	0	342	1000	80,0	40	3,2	13	1,04	27	2,16
51.3	76393	-7,7	341	820	107,9	30	3,95	11	1,45	19	2,5
52.1	275599	-2,6	345	1550	56,2	33	1,2	12	0,43	21	0,76
52.2	83489	-5,4	427	1550	186,7	25	3,01	7	0,84	18	2,17
53	474314	-7,7	561	1100	23,2	18	0,38	7	0,15	11	0,23
54.1	52291	-4,7	579	1050	201,9	14	2,69	4	0,77	10	1,92
54.2	30149	-4,7	579	1050	350,0	18	6,0	5	1,67	13	4,33
54.3	120399	-4,7	579	1050	87,5	25	2,08	8	0,67	17	1,42
55	221424	-5,4	709	1130	51,1	34	1,54	7	0,32	27	1,22
63.2	272710	2,3	813	2000	73,3	43	1,58	12	0,44	31	1,14
64	63496	4,3	832	2535	402,4	43	6,83	11	1,75	32	5,08

* Indices – see Fig. 1.

the region is also determined by the fact that the territory has a characteristic mountain-valley relief structure, which provides a variety of natural conditions for the formation of vegetation cover.

Most of the biomes (and subbiomes) of the study region belong to the taiga hypoarctic type. They are located in the west and north of the study area. In the mountains, there is a vertical zonality of vegetation, in which the taiga belt, composed mainly of larch and, less often, spruce and fir forests, is replaced higher by subalpine stone-birch crooked forests and creeping forests. On many ridges in the upper bald belt, lichen groups are common, related to similar groups of plain tundra.

The biomes of Primorye are located at the junction of four geobotanical regions (Manchurian, Okhotsk, East Siberian and Daurian). In Primorye, on the plains and lower slopes of the mountains, there are specific broad-leaved and coniferous-broad-leaved forests. The presence of heat-loving relict tertiary plants belonging to the so-called "Manchurian flora" is a characteristic feature not only of Primorye, but of the entire Amur basin.

On the Zeya-Bureya plain, located in the middle reaches of the Amur, as well as on the Khanka-Ussuri lowland of the Ussuri river basin, forest-steppes are widespread. This is due to the fact that these plains are delimited from the sea air masses by the Bureinsky and Sikhote-Alinsky ridges, as a result of which conditions are created for the formation of a more continental climate, which contributes to the development of the forest-steppe.

With distance to the west from the sea coast, the continentality of the climate increases, which largely influences the formation in Transbaikalia, on the plains surrounded by mountain ranges, of peculiar steppe communities belonging to the Daurian steppe biome.

The species of poisonous plants included in the analysis belong to 21 families. The largest number of species belongs to the Ranunculaceae family – 44 species including 40 species of *Aconitum* genus. Equisetaceae and Melanthiaceae families include 6 species of poisonous plants each. Solanaceae family – 4 species, Apiaceae – 3 species, Rutaceae – 2 species of poisonous plants. The remaining families (15) include one species of poisonous plants each. Table 2 lists poisonous plants that are found in more than 50% of the biomes and subbiomes included in the analysis.

Table 2. Species of poisonous plants found in more than 50%considered biomes and subbiomes

№	Poisonous species	Biomes number	
		number	% of total
1	*Andromeda polifolia* L.	18	95
2	*Equisetum arvénse* L.	17	89
3	*Ranunculus sceleratus* L.	17	89
4	*Equisetum sylvaticum* L.	16	84
5	*Equisetum pratense* Ehrh.	16	84
6	*Actaea erythrocarpa* (Fisch.) Freyn	16	84
7	*Erýsimum cheiranthoídes* L.	16	84
8	*Polygonatum humile* Fisch. Ex Maxim.	15	79
9	*Equisetum fluviatile* L.	14	74
10	*Equisetum palustre* L.	14	74
11	*Ledumpalustre* L.	14	74
12	*Calla palūstris* L.	14	74
13	*Polygonatum odoratum* (Mill.) Druce.	14	74
14	*Convallaria keiskei* Mio.	14	74
15	*Aconitum sczukinii* Turcz	13	68
16	*Cicúta virósa* L.	12	63
17	*Huperzia selago* (L.) Bernh. ex Schrank & Mart.	12	63
18	*Menispermum dauricum* DC.	11	58
19	*Dictamnus dasycarpus* Tursz,	11	58
20	*Heracleum sosnowskyi* Manden.	11	58
21	*Aconitum ranunculoides* Tursz ex Ledeb	11	58
22	*Cánnabis satíva* L.	11	58
23	*Veratrum lobelianum* Bernh.	10	53
24	*Aconitum macrorhynchum* Tursz ex Ledeb.	10	53

Only 24 of the 87 dangerous plant species are commonly found in biomes and subbiomes. Some species of this group have wide ranges and are distributed mainly in disturbed communities – for example, *Equisetum pretense* L. and *E. arvénse* L., *Ranunculus sceleratus* L., *Cánnabis sativa* L., *Erýsimum cheiranthoídes* L., *Heracleum sosnowskyi* Manden. The specificity of the region reflects a significant number of aquatic and semi-aquatic plants. They are *Equisetum fluviatile* L. and *E. palustre* L., *Cicúta virósa* L., *Calla palūstris* L. and *Ledum palustre* L. The remaining species are predominantly forest plants.

Although aconites make up almost half of the total list of poisonous plants in the region, only three species are found in more than 50% of biomes and subbiomes. They are *Aconitum sczukinii* Turcz, A. *macrorhynchum* Tursz ex Ledeb. And *A. ranunculoides* Tursz ex Ledeb, usually confined to numerous river valleys. The remaining species of the genus are limited in distribution, which is generally characteristic of endemic relict plants.

To conduct a correlation analysis, the following factors were taken as factors that can affect the number of poisonous plant species in a biome or subbiome: 1) average annual air temperature, C°; 2) annual amount of precipitation, mm; 3) total number of vascular plant species in a biome or subbiome; 4) number of vascular plant species per 10,000 km^2 (relative species richness). We consider the number of plant species, both poisonous and all vascular (absolute and per 10,000 km^2), to be features that probably depend on these factors. Thus, factors 3 and 4 are both features.

The results are presented in Table 3. In the column "factors", 3 and 4 – correspond to the total number of poisonous species (87) and the number of species of poisonous plants without species of the genus Aconite (47), because they act here as "factors". And the column of indicators is the number of species in each biome (sub biome).

An analysis of the relationship between plant species, including poisonous ones, and climatic indicators showed a significant closeness of the relationship between the number of poisonous species without aconites, the total number of poisonous species in biomes and the average annual air temperature – the correlation coefficient is 0.66. However, for aconites, this figure turned out to be quite low – only 0.40. A relatively high correlation coefficient was obtained for the relationship between the total number of vascular plant species and the annual amount of precipitation (0.59). But the tightness of the relationship between the number of poisonous species and the annual amount of precipitation turned out to be minimal (0.02-0.26). Thus, no clear links between the number of species in the territory and climatic factors have been identified.

The maximum tightness of the relationship (0.79-0.81) was found between the number of poisonous species per 10,000 km^2 and the total number of vascular plant species per 10,000 km^2. At the same time, the tightness of the relationship between the total number of vascular plant species and the number of poisonous species is only (0.31-0.36). The distribution of relative species richness demonstrates the concentration of poisonous species in small mountain biomes – Sikhote-Alin, Yankano-Dzhagda and in arid biomes – Daursky steppe, Amur-Zeya forest-steppe. This is explained by the fact that a small mountain biome with a dissected topography, elevation changes, microclimate regimes, soils objectively demonstrate a higher diversity of species, and also confirms the hypothesis that higher temperatures contribute to the concentration of poisonous plant species.

Analysis of the data given in Table 2 and in Fig. 2 clearly showed that the largest number of vascular plant species includes the southern Sikhote-Alin biome (64), located in the south of Primorsky Krai, as well as the middle Sikhote-Alin biome (63.2), also located in favorable climatic conditions. The second place in terms of the number of species is occupied by the taiga hypoarctic biomes – Vitimsky and Shilkinsky (52.1, 52.2), located in Transbaikalia, in the southwest of the study region. The smallest number of species is naturally noted for biomes experiencing a moisture deficit – the Daurian steppe biome (34) and the Zee-Bureya forest-steppe biome (31).

A different picture is observed when calculating species richness per 10,000 km^2. Relatively small biomes have the highest relative species richness: steppe (34), forest-steppe (31), subtaiga (22b), mountain subbiomes of the Yankano-Dzhagda biome (54.1, 54.2), as well as the southern Sikhote-Alin nemoral biome (64). In the latter, the number of species and relative species richness are the highest among others in the region. Large taiga biomes – Severo-Okhotsk (44), Aldan-Mai (53), South-Okhotsk (55) biomes, having average indicators for the total number of species, are characterized by the lowest relative species richness.

Table 3. Pearson pair correlation coefficients (n = 19)

Features (number of plant species)	Factors			
	1	2	3	4
All species of vascular plants	0,43	**0,59**	---	---
Number of species of vascular plants per 10 000 km^2	0,44	0,20	---	---
All species of poisonous plants – total 87	**0,66**	0,19	0,36	---
All species of poisonous plants – per 10 000 km^2	0,44	0,05	---	**0,81**
Poisonous species without aconites – total 47	**0,66**	0,26	0,33	---
Poisonous species without aconites – per 10 000 km^2	0,45	0,02	---	**0,81**
Poisonous species of aconites – total 40	0,41	-0,13	0,31	---
Poisonous species of aconites – per 10 000 km^2	0,40	0,12	---	**0,79**
All correlations are significant at $p < 0.05$. Cases with closeness of connection more than **0.50** were marked bold.				

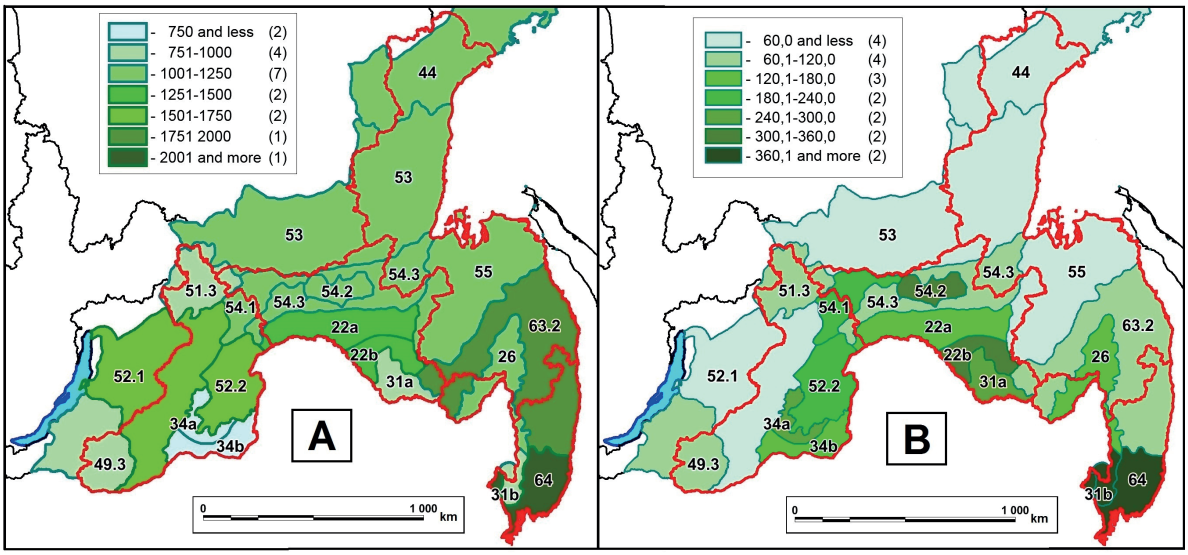

Fig. 2. Total number of vascular plant species

A – total number of vascular plant species in a biome (subbiome);

B – number of vascular plant species per 10,000 km^2 (relative species richness). Here and below: in parentheses, the number of map sections (biomes and subbiomes) in a given gradation.

The map (Fig. 3) reflects the distribution of all poisonous plants (including aconites) in the biomes and subbiomes of the study region.

The largest number of poisonous species was noted in the Amur and Ussuri basins (31, 22, 26) and in the east of the region, in the biomes of Primorye (64, 63.2). A relatively high number of species of poisonous plants is observed in the western mountain-taiga biomes of Transbaikalia: Buryat (49.3), South-Zabaikal (52.1), and steppe Daur (34a). A low abundance of poisonous species was found in the mountain biomes directly adjacent to the Amur (54.3) or its large first-order tributaries, the Zeya and Bureya (54.3), as well as in the Severo-Okhotsk biome (44), located in the north of the study region. An extremely low number of species is typical for small mountain biomes (54.1, 54.2) and for the large Aldan-Maya biome (53).

The distribution of relative species richness is determined by the size of biomes or subbiomes, that is why it is especially high in small territorial units. These are mainly subbiomes of arid appearance – Daursky steppe (34a), Amur-Zeya forest-steppe (31). The average relative species richness of poisonous plants was noted in the Daurian steppe (34b), the southern Sikhote-Alin biome of mixed forests (64), and the Amur-Ussuri subtaiga biome (26). The mountain taiga biomes Buryatsky (49.3), Vitimsky (52.2), Kodaro-Kolarsky (51.3), subbiomes of the Yankano-Dzhigda biome (54.1, 54.2) are characterized by low relative species richness. The remaining biomes are characterized by extremely low relative species richness.

The map (Fig. 4) reflects the distribution of poisonous plants in the biomes of the region, excluding aconites, which are considered separately below.

The distribution of relative species richness of poisonous plants (Fig. 4A) shows that the largest number of species of poisonous plants is observed in the east of the region, in the biomes of Primorsky Krai (63.3, 64), as well as on the plains, in biomes immediately adjacent to the channels of the Amur and Ussuri (26), including forest-steppe biomes (22a, 31a). The average abundance of poisonous plants was noted in the western and southwestern mountain taiga biomes (49.3, 52, 51.3), as well as in the Daurian steppe biome (34). The smallest abundance is observed in the large mountain Aldan-Maya biome (53), as well as in the small mountain subbiomes of the Yankano-Dzhagda biome (54).

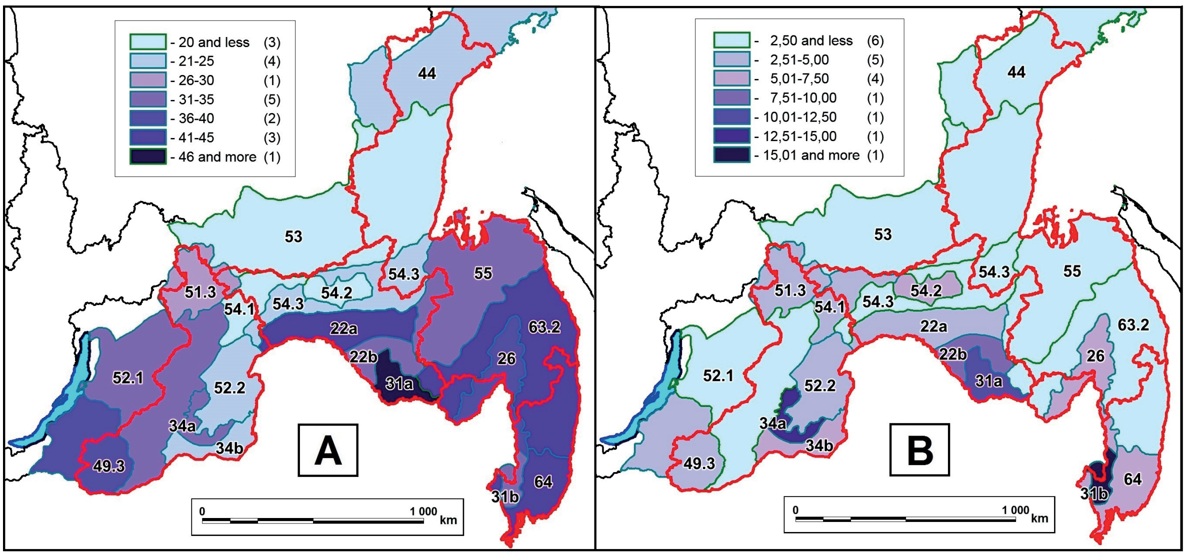

Fig. 3. Total number of poisonous plant species (including aconites)

A – total number of species of poisonous plants in the biome (subbiome);

B – number of poisonous plant species per 10,000 km^2 (relative species richness)

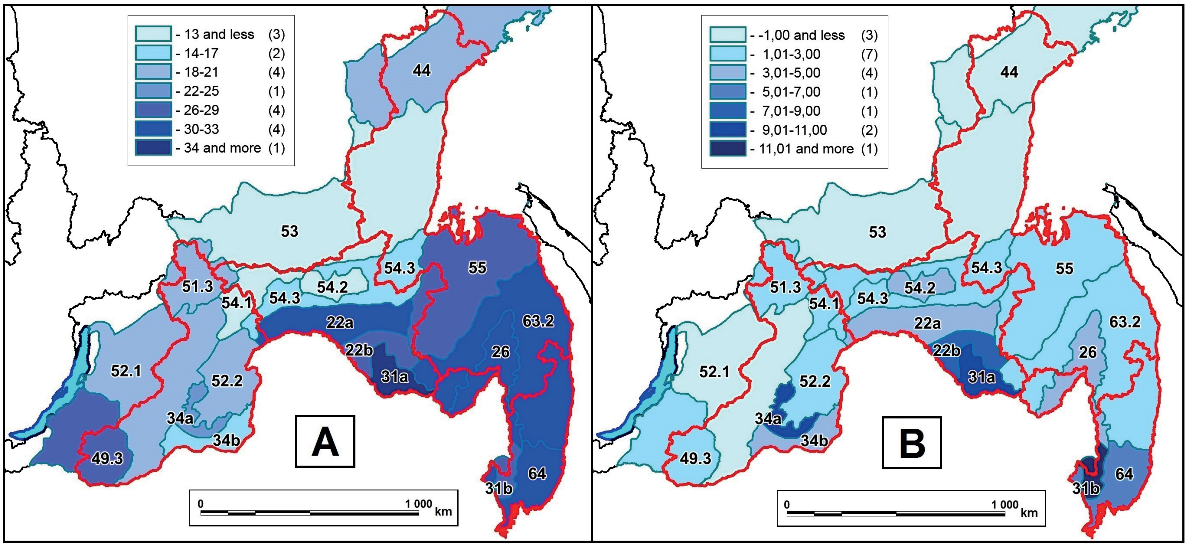

Fig. 4. Number of species of poisonous plants without aconites

A – total number of species of poisonous plants without aconites in the biome (subbiome);
B – number of poisonous plant species without aconites per 10,000 km^2 (relative species richness)

The relative species richness of poisonous plants is distributed somewhat differently (Fig. 4B). Relatively high species richness or density of species was noted in the biomes of Primorye and the Amur Region. At the same time, the highest relative species richness is characteristic of biomes with small areas: Daurian steppe (34), Zee-Bureya forest-steppe (31), and nemoral forest southern Sikhote-Alin (64).

The distribution of the number of species of the genus *Aconite* (Fig. 5A) shows that their greatest number was recorded in the mountain-taiga Buryatsky (49.3), South-Zabaikalsky (52.1), Kodar-Kolarsky (51.3) and in the forest biomes of Primorye (63.2, 64). A significant number of aconite species have been identified in forest-steppe biomes (31). In most of the biomes of the region, with the exception of small mountain-taiga subbiomes (54.1, 54.2), the number of *Aconite* species is average.

The distribution of relative species richness of *Aconites* in the biomes of the region (Fig. 5B) is characterized by the fact that the highest density of species was noted in small subbiomes – Zee-Bureya (31), Daursky (34a). A relatively high density was found in the southern Sikhote-Alin biome (64), small mountain subbiomes of the Yankano-Dzhagda biome (54). In general, a relatively noticeable species richness is characteristic of subbiomes directly adjacent to the channels of the rivers Amur, Zeya, Bureya, Ussuri.

Thus, the largest number of all vascular plants includes the Sikhote-Alin biomes (63.2 and 64) – 2000–2535 species, respectively. The Transbaikalian biome contains somewhat fewer species (52.1, 52.2) – 1550 species. A relatively high number of species includes the Amur-Zeya southern taiga biome (22) – 1260 species. The smallest number of species among other biomes was noted in the Daursky steppe (34) – 657 species.

The largest number of poisonous plants is characteristic of the Amur forest-steppe subbiome (31a). Slightly fewer species were recorded in the biomes of Primorye (63.2, 64), as well as in the Amur-Zeya southern taiga (22a). The smallest number of poisonous plants is characteristic of the Upper Gilyui subbiome (54.1), located on the watershed of two large river basins, the Lena and Amur.

It should be noted that the highest average annual air temperature and total precipitation are characteristic of the biomes of Primorye (63.2, 64). In this case, this generally corresponds to the number of plant species, including poisonous ones. However, this pattern is weakly observed

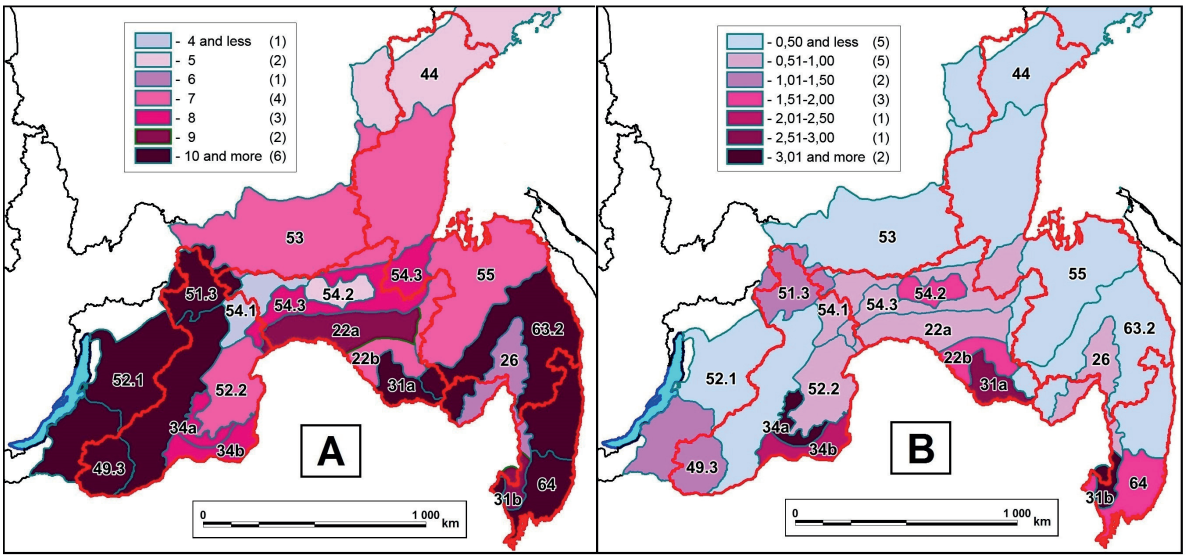

Fig. 5. The number of species of poisonous plants –*Aconite* genus

A – total number of species of poisonous aconites in the biome (subbiome);
B – number of poisonous aconite species per 10,000 km^2 (relative species richness)

for other biomes. For example, the low abundance of all species in the Daurian steppe biome corresponds to a low amount of precipitation, but does not correlate with the average annual air temperature.

CONCLUSION

The list of poisonous plants of the Far East region includes 87 plant species belonging to 21 families. The largest number of species belongs to the Ranunculaceae family – a total of 44 species. Of these, 40 species are plants of *Aconitum* genus – the most poisonous species in Russian flora.

The largest number of species of all plants includes the southern Sikhote-Alin biome, located in the south of Primorsky Krai, and the middle Sikhote-Alin biome, also located in favorable hydrothermal conditions. Relatively small biomes have the highest species richness – steppe (Daurian steppe), forest-steppe (Zeya-Bureinsky forest-steppe, Amur-Zeya subtaiga), mountain subbiomes of the Yankano-Dzhagda biome, as well as the southern Sikhote-Alin nemoral biome.

The largest number of poisonous species was noted in the east of the region – in the biomes of Primorye, in the Ussuri basin, in the lower and middle Amur. The relative species richness of poisonous species is higher in arid subbiomes – Daurian steppe, Amur-Zeya forest-steppe. The distribution of the species richness of poisonous plants without aconites shows that their greatest number is observed in the east of the region, in the biomes of Primorsky Krai (Middle Sikhote-Alin and Sikhote-Alin southern), as well as on the plains, in biomes immediately adjacent to the channel of the Amur and Ussuri (Amur -Ussuri subtaiga), including forest-steppe biomes (Amur-Zeya subtaiga and Zee-Bureinsky forest-steppe Amur oak forest-steppe). Their relative species richness is distributed somewhat differently. In general, the trend continues; relatively high species richness was noted in the biomes of Primorye and the Amur Region.

An analysis of the distribution of the number of aconite species shows that it is maximum in the mountain forest biomes of Primorye (Middle Sikhote-Alin and Sikhote-Alin southern), as well as on the plains of the Amur valley in forest-steppe biomes (Zeya-Bureinsky forest-steppe). The distribution of relative species richness of *Aconites* in the biomes of the region is characterized by a maximum in small subbiomes – Daursky, Zee-Bureinsky.Highrichness was found in the southern Sikhote-Alin biome, in small mountain subbiomes of the Yankano-Dzhagda biome. Relatively high species richness is typical for subbiomes directly adjacent to the channel of the rivers Amur, Zeya, Bureya, Ussuri.

An analysis of the relationship between plant species, including poisonous ones, and climatic indicators revealed a significant closeness of the relationship between the number of poisonous species without aconites, the total number of poisonous species in biomes and the average annual air temperature – the correlation coefficient is 0.66, however, the closeness of the relationship between the number of poisonous species and the annual amount of precipitation was minimal (0.02-0.26). The closeness of the relationship (0.79-0.81) between the number of poisonous species per 10,000 km^2 and the total number of vascular plants per 10,000 km^2 is maximum. At the same time, the tightness of the relationship between the total number of vascular plant species and the number of poisonous species is only (0.31-0.36). All correlations are significant at $p < 0.05$. Thus, "hypothesis 3" was most confirmed, and "hypothesis 2" (see "Materials and methods") was partially confirmed.

The patterns of distribution of plant species dangerous to human health and their relationship with environmental factors are practically not studied. This work represents only one of the initial approaches to understanding these patterns. In the future, the authors plan to conduct a similar analysis for allergenic plants.

REFERENCES

Avdeev A.I. Anan'ev V.K. (2010). Features of poisoning by a poisonous plant aconite // Selected issues of forensic medical examination, Khabarovsk, 11, 51-54 (in Russian).

Agroecological atlas of Russia and neighboring countries [online]. Available at: http://www.agroatlas.ru/ [Accessed 21 Apr. 2023].

Atlas of habitats and resources of medicinal plants of the USSR. (1983), Moscow: GUGK, 340 p. (in Russian).

Banasik M., Stedeford T. (2014). Plants, Poisonous (Humans) // Encyclopedia of Toxicology, 970-978.

Blake Froberg M.D., Danyal Ibrahim M.D., Brent Furbee M.D.R. (2007). Plant Poisoning, Emergency // Medicine Clinics of North America, (25), 375-433.

Bradberry S., Vale A. (2016). Plants // Medicine, 44(2), 113-115.

Dikareva T.V., Rumyantsev V.Yu. (2015). Cartographic analysis of the distribution of allergen plants in Russia // Bulletin of Moscow University. Series 5: Geography, 6, 34-40 (in Russian).

Dikareva T.V., Malkhazova S.M., Rumyantsev V.Yu., Soldatov M.S. (2017). Ecological and geographical analysis of the distribution of poisonous plants in Russia // Bulletin of Moscow University. Series 5: Geography, 4, 29-37 (in Russian).

Dikareva T.V., Malkhazova S.M., Rumyantsev V.Yu., Soldatov M.S. (2018). Effect of Arid Conditions on the Distribution of Poisonous Plants in the Regional Biomes of Russia // Arid ecosystems, 8(1), 64-72, DOI: 10.1134/S2079096118010031.

Dikareva T.V., Rumyantsev V.Y., Soldatov M.S., Malkhazova S.M. (2022). Plants Hazardous to Human Health in Arid and Semiarid Biomes of Russia // Arid Ecosystems, 12(1), 68-77, DOI: 10.1134/S2079096122010048.

Donchenko A.S., Kashevarov N.I., Zvereva G.K., Shkil' N.I., Bogolyubova E.V., Shkurina M.N., Chupakhina N.V. (2009). Poisonous and harmful plants of Siberia, Irkutsk: IITs TsNSKhB SO Rossel'khozakademii, 224 p. (in Russian).

Dudar' A.K. (1971). Poisonous and harmful plants of meadows, hayfields and pastures, Moscow: Rossel'khozizdat, 108 p.

Gubanov I.A., Kiseleva K.V., Novikov V.S., Tikhomirov V.N. (1995). Key to vascular plants of the center of European Russia. The second edition augmented and revised, Moscow: Argus, 560 p. (in Russian).

Gusynin I.A. (1962). Toxicology of poisonous plants, Moscow: Publishing House of Agricultural Literature, Magazines and Posters, 197 p. (in Russian).

Konovalova T.Yu., Shevyreva V.A. (2011). Poisonous Plants: Key Atlas, Moscow: ZAO «Fiton+», 112 p. (in Russian).

Flora of Siberia. In 14 volumes. (1987-2003), Novosibirsk: Nauka.

Krechetovich L.M. (1931). Poisonous plants, their benefits and harms. M.-L.: Sel'khozgiz, 317 p. (in Russian).

Li Xiaohua, Liang Tongjun, Chen Bohong, Bao Haiou (2016). Study on the characteristics and application of poisonous and medicinal plant resources in Lushan Mountain // Ecological Science, 35(6), 164-170, DOI: 10.14108/j.cnki.1008-8873.2016.06.023.

Liu Lihong, Bai Guodong, Tai Feng, Zhang Nan, Gao Xinlei, Li Nan, Zhang Li, Qin Lijin. (2022). Survey and analysis of wild poisonous vascular plants in Chifeng City // Journal of Northern Agriculture, 50(6), 105-112, DOI: 10.12190/j.issn.2096-1197.2022.06.14.

Luferov A.N. (1995). Genus 16. Aconitum L [Rod 16. Borets - Aconitum L.] // Vascular plants of the Soviet Far East, SPb.: Nauka, 7, 43-68 (in Russian).

Medical-geographical atlas of Russia «Healing springs and plants». (2019). Red. S.M. Malkhazova, M.: Geograficheskii fakul'tet MGU, 304 p. (in Russian).

Ogureeva G.N., Leonova N.B., Emel'yanova L.G., Buldakova E.V., Kadetov N.G., Arkhipova M.V., Miklyaeva I.M., Bocharnikov M.V., Dudov S.V., Ignatova E.A., Ignatov M.S., Muchnik E.E., Urbanavichyus G.P., RumyantsevV.Yu., Leont'eva O.A., Romanov A.A., Gubanov M.N., Kotova T.V., Konstantinov P.I. (2018). Biomes of Russia. Map M. 1:7500000. 2nd edition, revised and enlarged. Moscow: WWF , 8 p. (in Russian).

Ogureeva G.N., Leonova N.B., Miklyaeva I.M., Bocharnikov M.V., Fedosov V.E., Muchnik E.E., Urbanavichyus G.P., Emel'yanova L.G., Khlyap L.A., RumyantsevV.Yu., Kuzikov I.V., Lipka O.N., Arkhipova M.V., Buldakova E.V., Kadetov N.G. (2020). Biodiversity of biomes in Russia. Plains biomes, Pod red. G.N. Ogureevoi, Moscow: FGBU «IGKE», 623 p. (in Russian).

Orlov B.N., Gelashvili D.B., Ibragimov A.K. (1990). Poisonous animals and plants of the USSR. Reference manual for university students on special. «Biology», M.: Vyssh. shk., 272 p. (in Russian).

Parshina E.A. (1995). Poisonous plants of the Far East. Tutorial. Khabarovsk: Publishing House of the Khabarovsk State Medical Institute, 36 p. (in Russian).

San Andres Larrea M.I., San Andres Larrea M.D. Rodrigues Fernandes C. (2014). Plants, Poisonous (Animals) // Encyclopedia of Toxicology, 960-969.

Unschuld Paul U. (1985). Medicine in China. A History of Ideas., University of California Press, LTD, London, England, 423 p.

Vascular plants of the Soviet Far East. In 8 volumes. (1996). Otv. red. S.S. Kharkevich, SPb.: Nauka (in Russian).

Yahn Li-dan, Chen Ying-qiang. (2022). Investigation on Wild Poisonous Plant Resources in Taijiang County, Guizhou Province // Journal of Temperate Forestry Research, 5(4), DOI: 10.3969 /j. issn. 2096-4900. 2022. 04.006.

Zeinalova S.Z. (2022). Poisons: around and inside. A guide to the most dangerous substances on the planet, Moscow: Eksmo, 304 p. (in Russian).

Zhang Fan-jing, Zhou Wen, Yan Jing-ru, Chen Jia-bei, Chen Gong-xi. (2021). Wild Poisonous Plant Resources in Wugongshan Region, China // Subtropical Plant Science, 50(4), 290-300, DOI: 10.3969/j.issn.1009-7791.2021.04.008.

Zhou Jianfen, Zhong Xiaohua, Zhou Jie, Shu Xiazhu. (2022). Toxic Plant Resources and Their Utilization in Huizhou City // Inner Mongolia Forestry Investigation and Design, 45(2), 79-82, DOI: 1006-6993 (2022) 02-0079-04.

Zorikov P.S. (2005). Poisonous plants of the forest: textbook. Otv. red. V.D. Chernyshev, Vladivostok: Dal'nauka, 119 p. (in Russian).

RESEARCH PAPER

HOW PROTECTED AREAS ARE TRANSFORMING WITHIN MEGAPOLIS: AN ADVANCED SPATIOTEMPORAL LEGISLATIVE MODEL

Vitaly A. Kryukov[1], Elena I.Golubeva[1]
[1]Lomonosov Moscow State University, Faculty of Geography, Leninskiye Gory 1, 119234, Moscow, Russia
***Corresponding author:** vit.kryukov@gmail.com
Received: October 6th, 2022 / Accepted: September 4th, 2023 / Published: October 10th, 2023
https://DOI-10.24057/2071-9388-2022-2614

ABSTRACT. Compared to pristine ecosystems, urban protected areas (PAs) are exposed to intensified pressure and deterioration due to rapid population growth and entangled stakeholders' interests. At the same time, these valuable ecosystems provide cities with ecosystem services, including cultural ones, and enhance the quality of life. Spatial analysis of PAs' transformations in the context of the multidisciplinary approach contributes to the detection and safeguarding of vulnerable ecosystems. The study object is the protected areas of Moscow megapolis (within boundaries until 2012), whereas the study subject is the spatial and temporal PA's transformations established by legislative acts. The research question is to devise a model of transformations designated by law within urban PAs and affecting their borders, land use, and rate of ecosystem deterioration. To achieve the research question, three goals were set: to gather spatial data on PAs' transformations within Moscow designated by legislative acts; to design a comprehensive and exhaustive classification of PAs' transformations established by legislative acts; to model spatial and temporal trends in transformations of Moscow PAs (1985-2022), according to the classification devised. The 3-compound framework for the analysis of legislative transformations (downgrading, downsizing, degazettment of protected areas) was coupled by content analysis of transformation events, GIS mapping, and spatial analysis of urban vegetation through NDVI (normalized difference vegetation index) estimations and raster computations in QGIS and GDAL software. The originality of our study derives from: the analysis of the 4th transformations' compound (design failures of new PAs); spatial comparison with positive transformations, strengthening nature conservation; uncovering detailed subtypes and levels of transformations; applying this approach to the local scale of megapolis. Our study is based on: 1985-2022 legislative acts with text and map representations of PAs' borders, zones and land-use designated by regional government and national ministries; national and Moscow open-access spatial data hubs; Moscow online news; 2001-2021 Landsat imageries and Global Forest Change data on Moscow region. Adverse transformations affected a larger area than positive ones (53.8% of a total PA area compared to 22.6%). Positive transformations contributed by PAs' design (49.5%) mostly, while adverse ones – by easing of restrictions on land use (60.3%) and failures in the design of new PAs (22.8%). Adverse transformations are mainly reflected in the downsizing of zones with the strictest prohibitions on land use (-68% on average) and a low share of designed PAs (54%) through the period 1985-2022. Woodland plantations dramatically expanded (+86.5%), replacing semi-natural urban forests (2005-2021). Hence, PA's ability to supply ecosystem services has been considerably diminished. In regard to Moscow, considerable adverse trends in nature protection were revealed, generally hidden from the public. The analyzed typology of Moscow PAs' transformations is quite conventional and may be improved through comparisons with other megapolises abundant in natural heritage to advance the model devised and elicit threats to nature conservation.

KEYWORDS: adverse and positive transformations of protected areas; PADDD (protected area downgrading, downsizing, degazettement); Moscow protected areas; nature conservation; urban planning; environmental legislation

CITATION: Kryukov V. A., Golubeva E. I. (2023). How Protected Areas Are Transforming Within Megapolis: An Advanced Spatiotemporal Legislative Model. Geography, Environment, Sustainability, 3(16), 52-63
https://DOI-10.24057/2071-9388-2022-2614

ACKNOWLEDGEMENTS: This research was performed according to the Development program of the Interdisciplinary Scientific and Educational School of M.V. Lomonosov Moscow State University «Future Planet and Global Environmental Change» and the State program of the Department of Environmental Management «Sustainable development of territorial nature management systems».

Conflict of interests: The authors reported no potential conflict of interest.

INTRODUCTION

Urban protected areas (PAs) are transformed specific natural and cultural spaces, heavily affected by population growth, increasing recreational pressure, habitat fragmentation and entangled interests of the state, regional, city institutions, dwellers, third-party land-users, academic community (Leroux and Kerr 2013, Trzyna et al. 2014). Moreover, urban dwellers contribute about 55% of the total world population now, and about 68% is expected by 2050 (United Nations 2019). Despite all efforts to retain urban ecosystems, the amount of green infrastructure per capita of the largest European cities has significantly (e.g., more than 12% in Rome and Paris) declined in recent years (Aurambout and Vallecillo 2016). Hence, our study's relevance is substantiated by the contribution of spatial analysis of PAs' transformations to the safeguarding of vulnerable ecosystems.

Many PAs transformed by human impact may be considered highly valued cultural landscapes (Berkes and Folke 1998; Ban et al. 2013; Sarmiento-Mateos et al. 2019). Although urban PAs have a rather low ecosystem value due to the high deterioration, they should be considered the most valuable parts of urban green infrastructure. These spaces provide not only supporting, provisioning, and regulating ecosystem services, but also cultural ones (MEA 2005; Haines-Young, Potschin 2018), e.g., enhancing the comfort of life, recreation, landscape aesthetics, spiritual values, sense of place, cultural identity, etc. (MEA 2005; Daniel et al. 2012; Baro et al. 2014).

To date, plenty of multidisciplinary case studies related to urban planning and protected areas concurrently are known (Elmqvist et al., 2013; Trzyna et al. 2014; Tenk 2016; Girault 2017; Ioja et al. 2018; Mahmoud and Morello 2021; Gan 2021 et al.), while classic environmental surveys do not comprehensively cover the management issues of nature conservation in cities. For the time being, the task of linking social sciences with nature conservation still exists due to contradictions within academia, between policies and locals, urban planners and biologists (Vaccaro et al. 2013).
PAs' adverse transformations enacted by law may be divided into downgrading, downsizing, and degazettment (PADDD), widespread in areas of intensive land use (Mascia and Pailler 2011; Golden Kroner et al. 2019), including urban areas. PADDD ramifications have yet to be explored. Now, the PADDD number is increasing worldwide: 64% of them have been enacted between 2008 and 2018. Moreover, PADDD have been dramatically striking marine PAs (Albrecht et al. 2021) and UNESCO World Heritage iconic PAs (Siyu et al. 2019). However, not every PADDD should be considered an adverse one – e.g., Buffalo National Park in Alberta, Canada, and some others were abolished due to strong bison growth and accomplishing park aims (Lothian 2010).

Most urban PAs' studies are dedicated to one of the PADDD compounds – mostly downgradings and less often downsizings. However, any delays in PAs' design and failures in establishing new PAs can drastically reduce ecosystem value due to the rapid deterioration of urban ecosystems, e.g., deforestation within Kuskovo park for highway construction (TEEB-Russia 2021). Moreover, slow PAs' designation hits non-urban PAs as well and arouses adverse transformations of ecosystems combined with habitat deterioration (Stepanitsky and Kreyndlin 2004). Therefore, the incorporation of the fourth PA4D component is justified by human pressure on landscapes, outpacing complicated procedures of establishing new PAs and appropriate regulations on land use.

The study object – is the PAs of Moscow megapolis within boundaries until 2012, whereas the study subject – is the spatial and temporal PA's transformations established by legislative acts. According to the city borderline until 2012, Moscow had one of the largest urban PAs' networks in the world – 17.8% of the total area (139 PAs)[1].

To address issues in urban PAs' transformations, the following research question has been set up: to devise a model of transformations designated by law within urban PAs and affecting their borders, land use, and rate of ecosystem deterioration. To achieve this question, three goals were set:

- to gather spatial data on PAs' transformations within Moscow designated by legislative acts;
- to design a comprehensive and exhaustive classification of PAs' transformations established by legislative acts;
- to model spatial and temporal trends in transformations of Moscow PAs (1985-2022), according to the classification devised.

MATERIALS AND METHODS

The main sources of data on transformations are law acts followed by functional zoning, mostly of 2020, known as "Polozhenija" (Regulations) of PAs, designated by Moscow authority and the Ministry of Natural Resources and Environment (fig. 1). These data have been retrieved mainly from two open-access online hubs aggregating spatial data, text descriptions and illustrations: IAIS OGD (Information System Ensuring Spatial Planning) focused on Moscow and national Russia Protected Areas database[2]. Moreover, advanced descriptions of some legislative acts with appendices have been obtained from the Bulletin of Moscow[3].

Most of the PAs' borders have been changed by these Regulations. Moreover, a system of nature conservation restrictions on land use (prohibited and allowed human activities) has been established. The Regulations are supplied by maps and text representations, including coordinates of borders and zones, but sometimes coordinates are not disclosed.

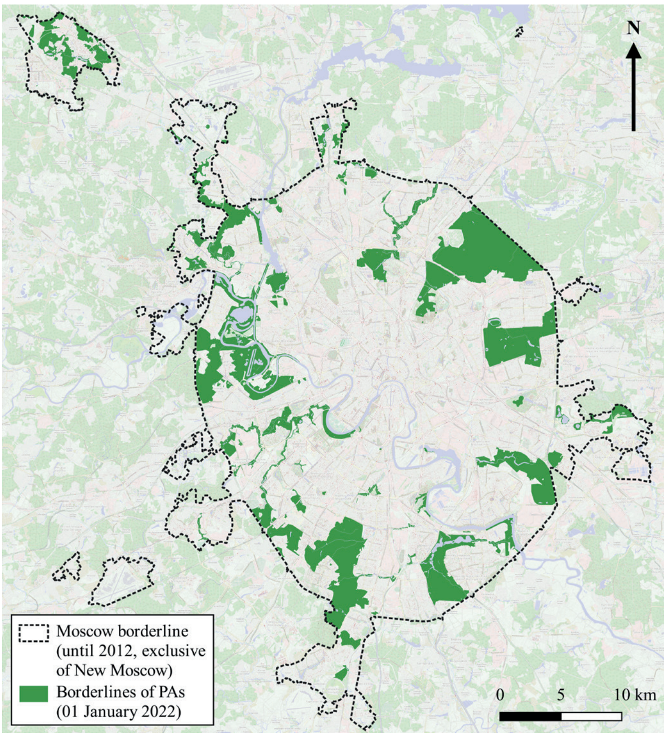

Fig. 1. Protected areas of Moscow (*IAIS OGD database and OpenStreetMap*[4])

[1]IAIS OGD (Information System Ensuring Spatial Planning on a GIS Server). Available at: https://isogd.mos.ru/isogd-portal [Accessed 10 Jan., 2022]
[2]Russia Protected Areas. Available at: http://oopt.aari.ru/ [Accessed 10 Feb., 2022]
[3]The Bulletin of Moscow (law acts of Moscow city). Available at: https://vestnikmoscow.mos.ru/ [Accessed 5 Jun., 2022]
[4]OpenStreetMap. [online] Available at: https://www.openstreetmap.org/ [Accessed 10 Feb., 2022]

Speaking about categories of Moscow PAs, nature monuments (NMs) are the most popular category due to mild prohibitions, small sizes, and management ease. These PAs may be located в within other larger PAs (inland nature monuments) or outside them (separated ones). However, more than 60% of the total PAs' area is occupied by 11 nature and historic parks – large (1075.5 ha on average) green areas combining semi-natural ecosystems and highly transformed cultural landscapes. Besides these, 28 so-called nature reserves under mild prohibitions, two eco-parks and 5 botanical gardens are included in the PAs' network. Thus, the categories of Moscow PAs have no direct relation to the IUCN categories (Lausche, 2011), except the national park and nature monuments.

Moscow gained its unified comprehensive system of PAs' zoning in 2020. Before that, some large PAs had had own zoning complicated by multiple variations of the zone's names. These variations were established by planning projects of the Moscow government and transformed later during forest inventory works carried out in 2010-2013. One notable exception is Elk Island National Park (NP) zoned 5 times: 1979, 1988, 2002, 2010, 2012. At the same time, land use restrictions within historical and cultural zones are designated by heritage law acts, special development blueprints and management plans in each PA specifically.

Previous environmental impact assessments or ecosystem services' assessments of the largest Moscow PAs were carried out in the Bitcevsky forest (Semenyuk and Bodrov 2019), Moskvoretsky park (Kolbowsky et al. 2015), Elk Island NP (Lelkova, Pakina, 2020), Sparrow Hills reserve (Samsonova et al. 2013), etc. A significant number of surveys are dedicated to vegetation and its ecosystem services, including cultural ones (Rysin 2012; Kiseleva et al. 2019; Reitz et al. 2021; Semenyuk et al. 2021 et al.). Few issues of Moscow's environmental policy resulting from spatial planning peculiarities have been examined over the last years (Kolbowsky et al. 2015; Mukhin et al. 2015; Frolova and Batarin 2015; Kryukov 2021 et al.), but there is no complex review.

Implementation of the 3-compound PADDD framework into the study focused on urban ecosystems requires a multidisciplinary approach. This approach has been applied for the analysis of legislative transformations through the following steps of mixed qualitative and quantitative procedures:

1. retrieval of actual spatial data on PAs established by law;
2. content analysis of transformation events within PAs;
3. devising a typology of PAs' transformations;
4. dynamic GIS mapping of transformation events;
5. retrieval of spatial data on urban vegetation;
6. raster computations of urban vegetation distribution;
7. spatial analysis of historical transformations within PAs.

Downsizing and upsizing information has been obtained from IAIS OGD – to gain the latest versions of borders, The Protected Areas of Russia and Bulletin of Moscow – to collect older borders in the vector format.

Data on degazettment events and ad hoc design of PAs have been collected through the Russia Protected Areas database, online news, and comparing the current PAs' network with the planned one. The plan of the PAs' network of 2005 from the Bulletin of Moscow and the last versions of borders from IAIS OGD have been extracted to obtain information about the design of protected areas.

Upgrading and downgrading transformations have been assessed based on 12 large Moscow PAs represented about 59% of the total Pas' actual area with at least one zoning earlier, before the 2020 version.

Secondly, all data retrieved have undergone content analysis which is common in qualitative and quantitative legal and policy studies (Paloniemi et al., 2012; Slapin and Proksch 2014; Hall and Steiner 2020) to reveal the exact areas affected by all types of adverse and positive transformations.

As the next, 3^{d} step, all PAs' transformations have been divided into two broad categories: adverse (PA4D) and positive (PA4P) on biodiversity protection. PA4D in Moscow are expressed in different forms which require more meticulous examination than the classic 3-type PADDD structure (Fig. 2). The fourth extra type has been identified in the typology of transformations – design of PAs planned earlier. Some components of the PA4P model are similar to PA4D, but the numerous distinctions between them have been revealed (see Appendix A).

The results of transformed areas extraction and QGIS spatial vector overlays (Longley et al., 2005; Ahlqvist 2008) have been combined with our advanced PA4D-PA4P typology through QGIS mapping (4th step).

Afterwards, the actual vegetation distribution and dynamics within PAs have been revealed through NDVI (normalized difference vegetation index) computations of Landsat 7 (2001) and Landsat 8 (2021) and images which are considered to be a reliable source for analysis of green infrastructure (Vogelmann et al. 2001; Claverie et al. 2015). Deforestation of reserved PAs, but not designed yet, has been assessed on the basis of Global Forest Change[5] data with a spatial resolution of 30 meters. QGIS and GDAL software have been used to carry out these procedures (raster calibration, clipping, elimination of null and invalid values, cleaning of raster grids corrupted by cloudiness, calculation, zonal statistics extraction, overlay with PAs' borders in vector format).

Finally, a statistical comparison of borders, zones, restrictions on land use, and vegetation has been carried out through QGIS tools of spatial analysis. Speaking about the analysis of upgrading and downgrading, two versions of 2020 and 2002-2010 have been compared through QGIS overlay spatial analysis to assess the extent of positive and adverse transformations. Since there are no open-access vector data on zones' borders of 2002-2010, digitized raster grayscale images based on the Bulletin of Moscow have been used. The cadastral borders[6] and the latest borders of zones, partly overlapping with the former ones, have been added to increase the accuracy of raster images.

Therefore, the originality of our study derives from: the implementation of the 4th transformations compound (design failures of new PAs); spatial comparison with positive transformations, strengthening nature conservation; uncovering detailed subtypes and levels of transformations; and applying this framework to the local study scale of megapolis.

RESULTS

As it was mentioned, adverse and positive transformations have been divided into 4 main types (Fig. 2). Transformation mapping has revealed a wide range of changes in sizes and regulations on land use, features of planned PAs and degazettment cases (Fig. 3).

Adverse transformations (PA4D)

1. Downgrading

1.1. Full downgrading is a transformation of PA's status at the general level to another with milder restrictions. No PAs in Moscow exposed to these transformations are known yet. Such transformations may be related to the governing level (national/

[5]Global Forest Change. Available at: https://glad.earthengine.app/view/global-forest-change [Accessed 12 Feb., 2022]
[6]Public Cadastral map. Available at: https://pkk.rosreestr.ru/#/search [Accessed 10 Feb., 2022]

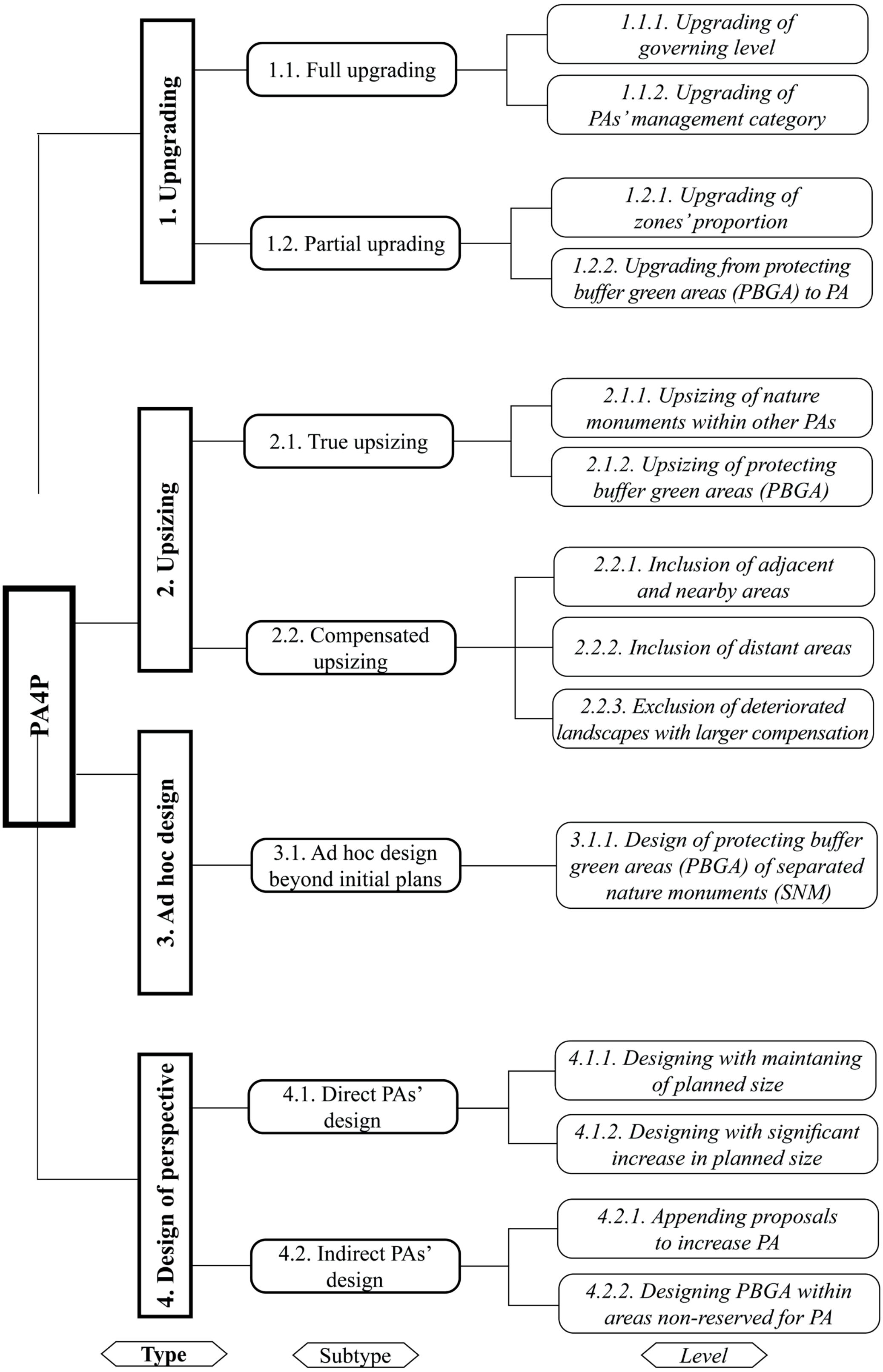

Fig. 2. Advanced PA4D model. Devised by the authors

regional/municipal) (1.1.1) or PA's category, e.g., downgrading from nature reserve to eco-park (1.1.2).

1.2. Partial downgrading has been divided into 3 levels.

1.2.1. Downgrading of zones' proportion comprises a decline in zones with strong restrictions on human activities ("cores") and an increase in zones with less strong restrictions.

To date, 9 types of zones have been established, attending to different restriction levels on land use activities (Tables 1-2).

Besides those, some activities are banned within all zones by default, e.g., tree cutting in the birds' nesting season, planting of introduced species, extraction of birch sap and resin etc. Land use restrictions within historical and cultural zones are defined by other documents protecting heritage objects – legal acts and special development plans.

Zones' names given are deciphered as follows: WS – wildlife sanctuaries, PL – protected landscapes, E – excursion and education zones, R – recreation zones, HC – historical and cultural zones, RC – recreation centres, S - sport zones, AE – administrative and economic zones, TP – third-party land-users. Subtypes of recreation zones (R1-R4) have been revealed through content analysis, as zones with the same name can differ in regulations on land use.

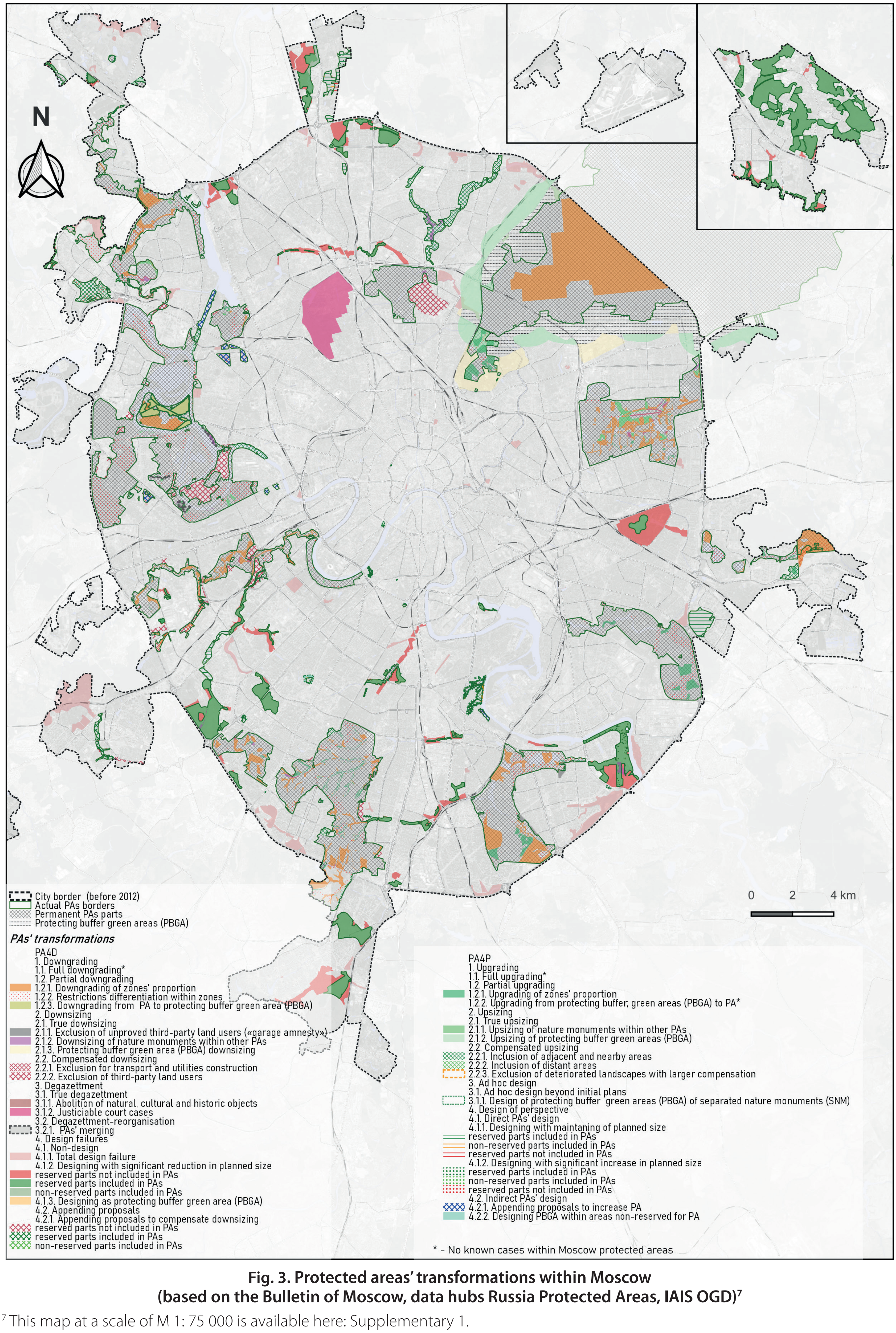

Fig. 3. Protected areas' transformations within Moscow (based on the Bulletin of Moscow, data hubs Russia Protected Areas, IAIS OGD)[7]

[7] This map at a scale of M 1: 75 000 is available here: Supplementary 1.

Table 4. Zones and restrictions on land use within Moscow PAs (The Bulletin of Moscow; data hub Russia Protected Areas, IAIS OGD). Prohibited land use activities are coloured red, and permitted ones are coloured green. The activities' numbers are transcribed in Table 2

Types of land use activities	Number of land use activities	Zones										
		WS	PL	E	R				RC	S	AE	TP
					R1	R2	R3	R4				
Relief and water bodies	1											
	2											
	3											
	4											
	5											
	6											
	7											
	8											
Vegetation and animals	1											
	2											
	3											
	4											
	5											
	6											
	7											
	8											
	9											
	10											
	11											
Social infrastructure	1											
	2											
	3											
	4											
	5											
	6											
	7											
	8											
	9											
	10											
	11											
	12											
	13											
	14											
	15											
	16											
	17											
	18											
	19											

Table 2. Land use activities within Moscow protected areas (The Bulletin of Moscow; data hub Russia Protected Areas). ***Activities' numbers are given in Table 1***

Relief and water bodies	Vegetation and animals	Social infrastructure
1. Any activities transforming natural relief followed by changes in absolute height 2. Any activities transforming natural relief followed by changes of absolute height more than 0,5 m 3. Draining of waterlogged spaces 4. Slope reinforcements based on artificial material 5. Any activities could lead to significant hydrogeological, soil transformations, erosion and landslides without using technical arrangements to decrease environmental impact 6. Springs captured using natural substances 7. Springs captured using natural-like substances 8. Springs captured using artificial substances	1. Designing of flowerbeds 2. Designing of flowerbeds with no linkages with culture and historical landscape 3. Elimination of fallen leaves 4. Elimination of organic debris, except fallen leaves 5. Raking fallen leaves and other organic debris and putting it around trees and shrubs 6. Irrigation of trees, shrubs groups and meadows 7. Trees and shrubs whitewashing 8. Cutting lower tree branches, except dangerous for people and transport vehicles; crowns pruning 9. Planting in non-forested areas after trees/shrubs elimination due to abnormal weather conditions or deadwood cuttings 10. Use of organic fertilizers 11. Use of mineral fertilizers	1. Building of mobile non-permanent constructions 2. Maintenance and reconstruction of current walkways 3. Maintenance and reconstruction of current roads and utilities, except outdoor lighting 4. Maintenance and reconstruction of current permanent buildings and constructions 5. Designing of permanent buildings and constructions 6. Designing of motor roads and utilities, except outdoor lighting 7. Construction of pedestrian walkways covered with waterproof artificial surfaces 8. Construction of pedestrian walkways covered with permeable surfaces made of natural substances 9. Maintenance, reconstruction and deploying of children's and sport playgrounds 10. Maintenance, reconstruction and deployment of street furniture (benches, fountains, sculptures, garbage bins, etc.) 11. Artificial lighting 12. Artificial lighting at nighttime in wildlife habitats 13. Deploying of mobile retail objects 14. Designing of cycling routes 15. Designing of inline skating routes 16. Designing of information areas 17. Designing of beachfront recreation spaces 18. Organization of picnic spaces 19. Dog walking

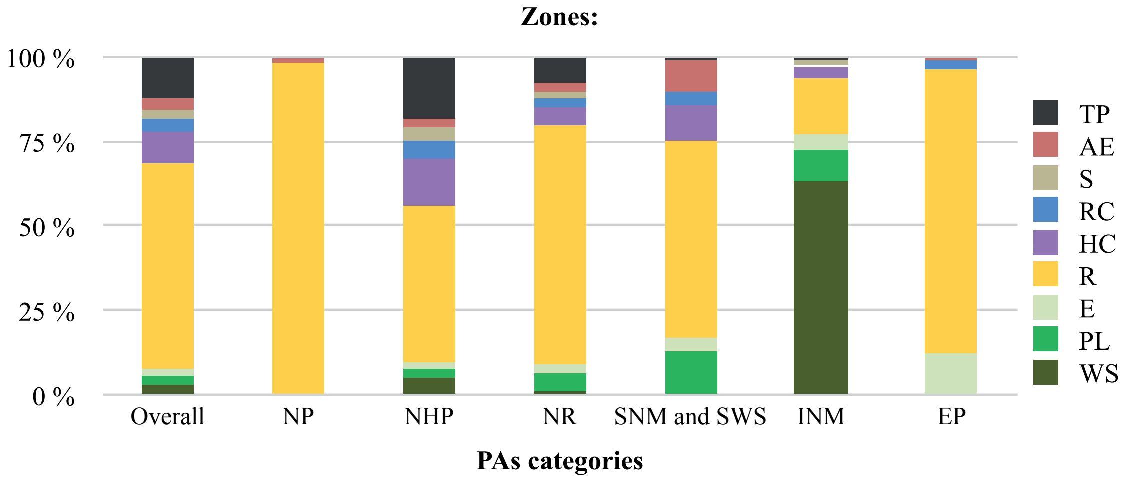

Fig. 4. Zones within Moscow PAs of different categories (for abbreviations of zones see Table 1). ***Estimated by the authors through the Bulletin of Moscow and Russia Protected Areas. *Botanical gardens are not included (zoning is almost absent)***

Wildlife sanctuaries, protected landscapes, excursion and education zones being under the strictest prohibitions are not widespread (7.8% of the total area), while recreation zones are the most common (60.5%) (Fig. 4).

The analysis of zones' dynamics within 12 large PAs has been focused on the PA "cores" – the sum of WS+PL+E zones of the strongest restrictions. There is no clear relation between PAs' categories and their cores' dynamics (Fig. 5).

The most excessive reductions took place in Elk Island National Park (Kryukov and Golubeva 2022) and Silver Pinewood nature monument.

1.2.2. Restriction's differentiation derives from the differences in prohibitions on land use within recreation zones. As an illustration, about 29% of the total recreation zones area in Moscow have no restrictions on maintenance and construction of utilities and motor roads, crowns pruning, use of mineral fertilizers, retail objects deploying etc., i.e., are under mild restrictions.

It is the most complicated way of downgrading that is difficult for laymen to reveal.

1.2.3. A sole case of downgrading from PA to protecting buffer green areas (PBGA) has been found within Silver Pinewood nature monument.

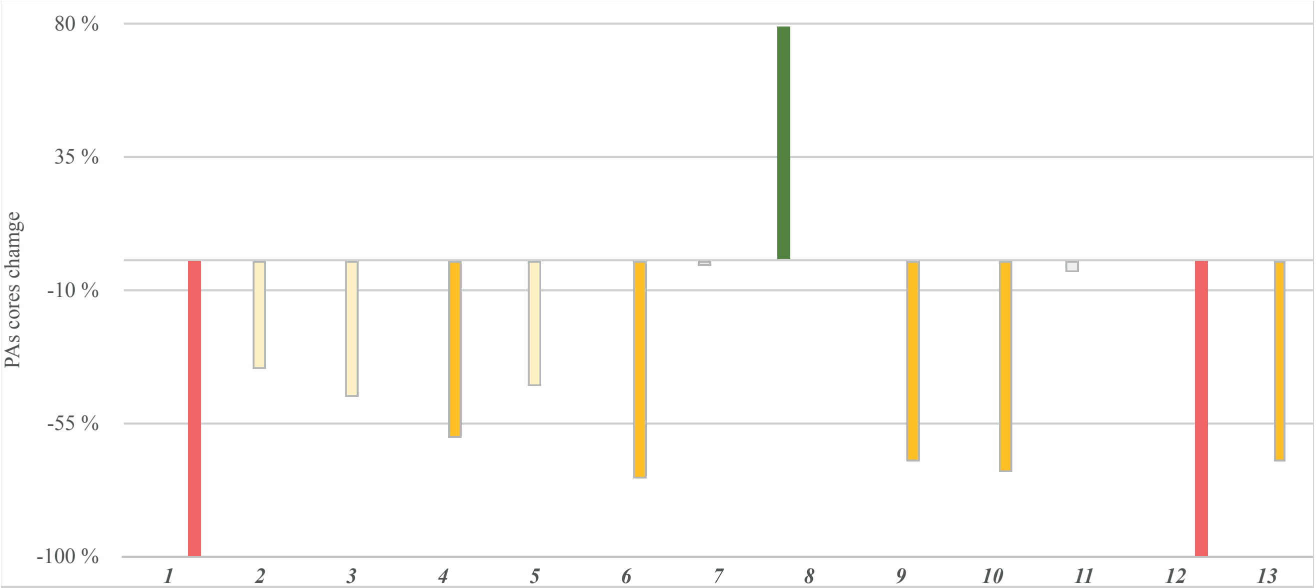

Fig. 5. PAs' cores change, % of the total sum (*1 – Elk Island national park; 2-8 – nature and historic parks: 2 – Bitcevsky forest, 3 – Izmaylovo, 4 – Tsaritsyno, 5 – Tushinsky, 6 – Kosinsky, 7 – Pokrovskoe-Streshnevo, 8 – Sokolniky; 9-11 – nature reserves: 9 – Setun valley, 10 – Tyoply Stan, 11 – Skhodnya valley in Kurkino; 12 – Silver Pinewood nature monument; 13 – overall value). Estimated by the authors using the Bulletin of Moscow and IAIS OGD data hub*

2. Downsizing

2.1. True downsizing is rare because of the legislative ban without offsetting. However, 11 PAs lost their parts occupied by garages in 2016 (about 0.5% of the total PA area at that moment) – "garage amnesty" (2.1.1). Such transformations allowed additional construction there, which may lead to an increase in human pressure on ecosystems. Borders of some inland nature monuments within large PAs have been transformed in 2020 *(2.1.2)*.

Only one downsizing case of protecting buffer zone *(2.1.3)* is known – around Elk Island National Park in 2022, despite the conservation ability of these zones.

2.2. Compensated downsizing occurs through all PAs' categories and is caused by transport and utility development *(2.2.1)* or the elimination of third-party land users *(2.2.2)*. There are no formal indications of adverse transformation, but compensation areas may have less strict restrictions than excluded areas.

3. Degazettment

3.1. True degazettment is the abolition of PA, established by the main entity of executive authority or by a court decision:

3.1.1. The elm in the square of Povarskaya street was cut down in 2013 because of an alarm condition, Dutch elm disease infestation, and the threat of fall on city dwellers[8];

3.1.2. Petrovsko-Razumovsky reserve lost its status in 2010 due to violations in design by regional authorities in the federally administered area[9].

3.2. Degazettment-reorganisation is related to the merging of two or more PAs *(3.2.1)*. Only nature monuments, mostly located within larger PAs and often overlapped, are exposed to this subtype (less than 0.4 % of the total transformations' area).

4. Design failures

Only 38 out of 112 PAs proposed in 2005, besides inland nature monuments and wildlife sanctuaries within other PAs, have been designed by 01.05.2022 – about 46% of the total proposed area. All cases fall into two subtypes.

4.1. Non-design. A lot of proposed PAs (65) have not yet been designed, occupying about 46% of the total reserved area. There is no information about their legal state and therefore these PAs are referred to as *totally failed (4.1.1)*.

The share of barren areas is quite large (5.9%) in these proposed PAs. Moreover, the significant increase in barren areas (+40.4% of 2001 value) and cultural landscapes occupied by woodland plantations (+86.5%) is revealed. Fragile grasslands have also dramatically declined within included PAs' parts (-38.3%) due to replacement by contemporary parks and secondary succession.

Deforestation of proposed, but not designed areas (2000-2020) affects little space, i.e., about 1.1% of the total area. However, 9 large PAs have a deforestation rate of more than 2%, especially one swamp with high biodiversity (7.1%) and the slope of the Moscow River valley (23%).

The most remarkable illustration of the *4.1.2 level (designing with significant reduction in proposed area)* is Kuskovo park, covering only about 12% of the initially proposed area.

4.2. Appending proposals. 9 of the proposed PAs were not established as separate but were appended to other, larger PAs. As a result, about 54% of the overall reserved area gained PA status. These transformations have taken place to compensate for exclusions from larger PAs.

Positive transformations (PA4P)

Some components of the PA4P model are similar to PA4D, but the numerous distinctions between them have been revealed (see Appendix A).

1. Upgrading and 2. Upsizing

Like full downgrading, ***full upgrading actions (1.1)*** are unknown in Moscow. ***Partial upgradings (1.2)*** are less spread than partial downgradings as opposed to partial upsizing-downsizing pair.

Cases of upgrading from the protecting buffer zone to a protected area (1.2.2) are unknown.

Two subtypes of upsizing are defined: ***true (2.1)*** and ***compensated (2.2),*** which makes up almost all upsizings (99.6%), while 2.1 is represented by upsizing two inland and one separated nature monuments (*2.1.1*) only. Upsizings of protecting buffer green areas are unknown (*2.1.2*).

Compensated upsizings are divided into inclusions of adjacent and nearby areas (*2.2.1*) or inclusions of distant areas (*2.2.2*). Such differentiation seems to be

[8]Available at: https://ria.ru/20130221/924143646.html [Accessed 5 Jun., 2022].
[9]Available at: http://sudbiblioteka.ru/vs/text_big3/verhsud_big_44789.htm [Accessed 5 Jun., 2022].

the most evident in assessing ecosystem value because the remoteness of green patches is strongly related to biodiversity loss (Benedict and McMahon 2006). Distant (more than 100 meters from PAs' borders or separated by large highways or railroads) upsizings are more common (75% of total area), which pinpoints issues in the effectiveness of nature protection.

The exclusion of highly deteriorated and transformed landscapes (*2.2.3*) within nature monuments has been carried out with a following increase in protected areas. Formal borderlines established earlier (e.g., the Moscow River floodplain has been designated as a rectangle with rounded edges) have been fixed by these changes in legislative acts.

3. Ad hoc design

The establishment of protecting buffer green areas around separated nature monuments in 2020 is considered to be the only case of such transformation (*3.1.1*), but not significant (about 0.2% of the total PAs' area). Other PAs' design cases not established by official plans are unknown.

4. Design of perspective

Multiple cases of ***direct PAs' design (4.1)*** are known in Moscow. However, many proposed parts may be finally placed beyond PA. It could be justified by an elaboration of development plans or detailing of biodiversity studies. Only 5.6 % of reserved PAs have maintained (5%) or increased (0.6%), while the others have decreased (48.8%) or failed (45.6%).

4.2. Indirect PAs' design – the establishment of the proposed area as other PA's part (appending). Moscow PAs' appendings have been entirely designated to compensate excluding parts within the current PA which a planned PA adjoined. Any appending aimed at the true PAs' expansion is unknown.

The high share of non-designed PAs reveals a disparity between the eco-positive strategy of the Moscow government and the actual state of proposed PAs: green areas with almost no prohibitions were mostly overused by recreation activities and various third-party stakeholders and consequently deteriorated.

Therefore, the essential results of our study are as follows:

•Adverse transformations affected a larger area than positive ones (53.8% of a total PA area compared to 22.6%).

•Adverse and positive transformations of PAs contributed by various components unevenly (Fig. 6). Positive transformations contributed by PAs' design (49.5%) mostly, while adverse ones – by easing of restrictions on land use (60.3%) and failures in the design of new PAs (22.8%) (Fig. 6). Adverse transformations are reflected mostly in downsizing of zones with the strictest prohibitions on land use (-68% on average), low share of designed PAs (54%), decrease in proposed PAs' area (up to 88%) through the period 2005-2022.

•Adverse vegetation transformations (2005-2021) affected areas where planned PAs have been failed. Semi-natural urban forests have been partially replaced by woodland plantations (+86.5%). Fragile grasslands declined considerably (-38.3%) within areas included in PAs. Barren areas increased within lands reserved for PAs' design (+40.4% of 2001 value).

DISCUSSION

It is proposed to expand the PADDD framework based on the multi-step qualitative and quantitative approach, including analysis of new PAs' design and its failures. Compared to worldwide statistics, the most common PADDD type is downgrading, making up 90% of the total transformations' number (Golden Kroner et al. 2019). There are multiple causes of downgrading dominance in Moscow as well:

• Direct law bans on downsizing without compensation (total PA's areas must not lower);

• Direct law bans on PAs' degazettment except for the vanishing of basic natural, cultural or historical objects;

• Active engagement of locals in continuous recreation, leading to a high interest in the sustainable condition of PAs. More complicated downgrading actions are much more difficult to reveal in law acts than degazettment or downsizing. Thus, government entities prefer this type of PA4D in case of some planned construction of transport, engineering, leisure, and sport facilities due to the shortage of free space.

As our study is the first implementation and advancement of this framework in megapolis, a few limitations should be clarified.

Some subtypes and levels are strongly related to the management system of the city analyzed: PAs' categories, number of zones, presence of inland nature monuments embedded into other larger PAs, existence of protecting buffer green areas but applied to separated nature monuments only, set of zones etc. Some of these features may be not elicited in other cities.

Detailed typology of urban ecosystems with subtypes delimitated by dominating tree species, succession stages, moisture gradients, levels of recreational pressure etc. or

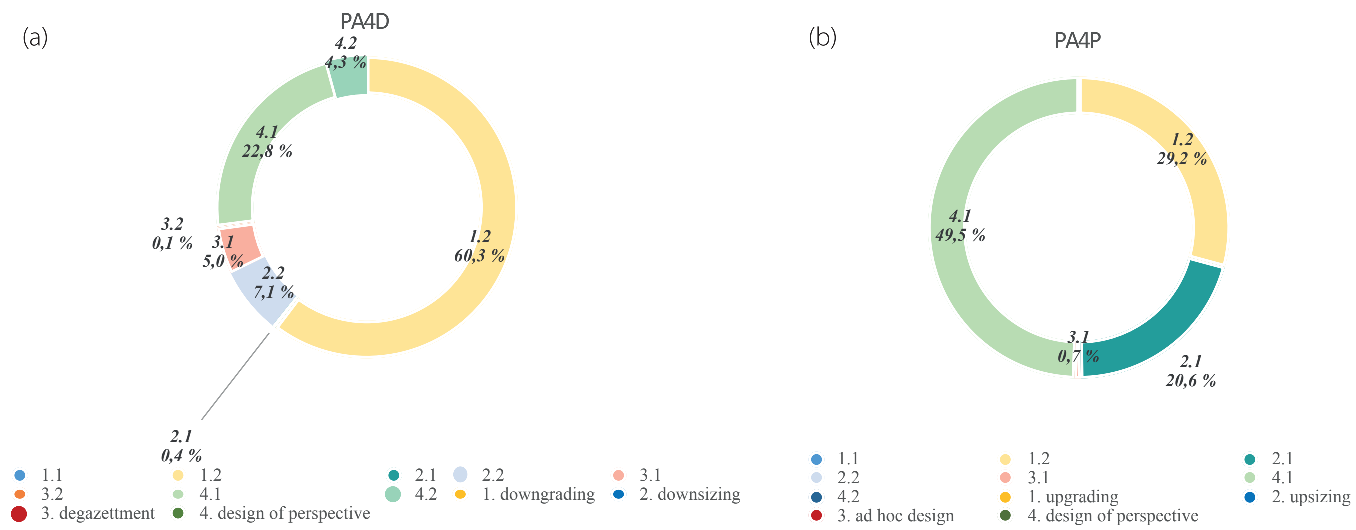

Fig. 6. PA4D (a) and PA4P (b) ratios.
Estimated by the authors on the basis of the Bulletin of Moscow, data hubs IAIS OGD and Russia Protected Areas

exhaustive land use maps have not been implemented as no unified and actual typology has been devised and applied to all study objects. At the same time, any spatial data following such typology may be harnessed for advanced analysis of transformations in other cities, e.g., covered by Urban Atlas 2018[10] or Saint-Petersburg (Khramtsov et al. 2016).

Moreover, not all transformations were mapped accurately as PAs' borders and zones are given sometimes as text descriptions or figures instead of coordinates in legislative acts, especially in older legislative acts. Another assumption regarding downgrading is that zones and zonal differences in restrictions on land use have not been articulated in acts of the 1990s and early 2000s, except Elk Island National Park.

Moscow has no open-access data about planned PAs' gestation (just proposed/scientific research was conducted/final establishment procedures etc.), but a model of PA's transformations should be advanced by it if possible.

It is important to mention that the 30-m spatial resolution of Landsat satellite imageries might be not sufficient to reveal small transformations of land cover within included or excluded areas that may be represented by narrow strings, e.g., overlapping cadastral parcels. At the same time, Sentinel-2 imageries with a spatial resolution of 10 m (bands B2, B3, B4, B8)[11] could not be used in studies covering lengthy periods as these sensors were launched in 2015 only. We assume that local field observations of these target areas would be more efficient and accurate to reveal actual land cover that may be quite dynamic.

The exact volume of transformations within protected areas of New Moscow adjoined to the city after 2012 has not been estimated. Instead of designing PAs new "specially protected green areas", covering more than 40% of converted space, have been established followed by less strict prohibitions and a high share of natural and semi-natural ecosystems, disturbed to a lesser extent than PAs which are closer to the city centre. To date, it is possible to downsize such areas in compliance with legal acts (TEEB-Russia 2021). PAs designed before 2012 are under ambiguous status currently – they have not been either degazetted or listed in official documentation anymore. This fact implies considerable limitations to a continuation of PAs' transformations analysis within actual Moscow boundaries.

Overall, it is necessary to note that the analyzed typology of Moscow PAs' transformations is quite conventional and may be improved through comparisons with other megapolises abundant in natural heritage.

CONCLUSIONS

The multidisciplinary approach, combining various methods from the fields of nature conservation, GIS, urban planning and environmental law, has been used to assess grave challenges for protected areas in megapolis. The outcomes of our study should develop an ecological awareness about the future of nature in cities as urban liveability may be considerably compromised by reducing of large green cores and corridors in the context of ecosystem services, global climate change, biodiversity decline, physical health and even mental crisis of urban dwellers (Peen et al., 2010).

By now, the biotopes' ability to supply ecosystem services is dramatically reducing, even though positive transformations have been also revealed. Regarding the planning of nature conservation, reserves for new PAs are extremely limited. Since 2005 a lot of severely transformed landscapes of a rather low biodiversity have been declared as protected areas. Such actions might be considered restoration of vegetation and water bodies, but the experience of recent years is rather questionable. The laying of new walkways accompanied by severe environmental disturbances as well as the construction of sport and entertainment facilities on the ruderal grasslands have become a core of so-called "land improvement" (TEEB-Russia 2021).

The typology of PAs' transformations devised is considered to be quite dynamic in future (as an illustration, cases of upgrading from the protecting buffer zone to a protected area are possible in future as the first protecting zones of nature monuments were established in 2020 only).

This study may be advanced by the following surveys:

•spatial comparison of our results with more detailed land cover dynamics, including data from forest inventories;

•implementation of PA4D-PA4P model into analysis of protected areas in New Moscow and other cities, covering marine areas as well;

•conjunction of legislative transformation analysis with field observations of urban ecosystems to reveal local trends;

•implementation of typology units (especially derived from downsizing) to management analysis of national parks beyond urban areas, as national parks commonly tend to be maintained through spatial zoning and a diverse set of restrictions on land use;

•economic evaluation of ecosystems' losses in the framework of ecosystem services;

•design of tradeoff model that should be applied in any cases of legislative transformations within protected areas.

All PAs' peculiarities mentioned above may be reflected in all cities of emerging and developed countries managed by state-led systems of spatial planning. Because of the greater disadvantages of emerging countries in environmental policy and the late design of PAs' networks, exploring the fourth component of PA4D seems to be more significant there. Moreover, current global and regional economic challenges will likely jeopardize PAs' design. Subsequently, our study may be continued provided that data on PAs of other cities are available. Besides that, such surveys may be focused on protected areas in cities not only with state-led systems of spatial planning, but market-led and conformative ones (Berisha et al. 2021; Bulkeley et al. 2021) as well to elicit differences and develop new ways to safeguard natural heritage.

[10]Copernicus programme. Urban Atlas 2018. Available at: https://land.copernicus.eu/local/urban-atlas/urban-atlas-2018

[11]European Space Agency. Sentinel Online. Available at: https://sentinels.copernicus.eu/web/sentinel/user-guides/sentinel-2-msi/resolutions/spatial

[12]Moscow government. The law act of №17 17.04.2013. The amendment to article 14 of law act of Moscow government №48 26.09.2001 "About specially protected natural areas of Moscow" (in Russian). [online] Available at: https://docs.cntd.ru/document/537934140?marker [Accessed 29 June, 2022].

REFERENCES

Albrecht R., Cook C.N., Andrews O., Roberts K.E., Taylor M.F.J., Mascia M.B. and Golden Kroner R.E. (2021). Protected area downgrading, downsizing, and degazettement (PADDD) in marine protected areas. Marine Policy, 129, 104437, DOI: 10.1016/j.marpol.2021.104437.

Ahlqvist O. (2008). Extending post-classification change detection using semantic similarity metrics to overcome class heterogeneity: A study of 1992 and 2001 U.S. National Land Cover Database changes. Remote Sensing of Environment, 112, 3, 1226-1241. DOI: 10.1016/j.rse.2007.08.012.

Aurambout J.P. and Vallecillo S. (2016). UDP - green Infrastructure per capita, 2010 - 2050 (JRC LUISA Reference Scenario 2016). [online] Available at: http://data.europa.eu/89h/jrc-luisa-udp-greenpercap-reference-2016 [Accessed 5 June, 2022].

Ban N.C., Mills M., Tam J., Hicks C.C., Klain S., Stoeckl N., Bottrill M.C. et al. (2013). A social-ecological approach to conservation planning: embedding social considerations. Frontiers in Ecology and Environment, 11, 194–202, DOI:10.1890/110205.

Benedict M.A. and McMahon E.T. (2006). Green infrastructure: linking landscapes and communities. Washington, DC: Island Press.

Berisha E., Cotella G., Janin Rivolin U. and Solly A. (2021). Spatial governance and planning systems in the public control of spatial development: a European typology. European Planning Studies, 29, 181–200, DOI: 10.1080/09654313.2020.1726295.

Berkes F. and Folke C. (1998). Linking social and ecological systems: management practices and social mechanisms for building resilience. Cambridge, UK: Cambridge University Press.

Bulkeley H., Kok M. and Xie L. (2021). Policy brief: realising the urban opportunity: cities and post-2020 biodiversity governance. Hague: PBL Publishers. Available at: https://oppla.eu/sites/default/files/uploads/realising-urban-opportunitycities-and-post-2020-biodiversity-governance.pdf [Accessed 12 May, 2022].

Claveri M., Vermote E.F., Franch B., Masek J.G. (2015). Evaluation of the Landsat-5 TM and Landsat-7 ETM+ surface reflectance products. Remote Sensing of Environment, 169, 390-403, DOI: 10.1016/j.rse.2015.08.030.

Daniel T.C., Muhar A., Arnberger A., Aznar O., Boyd J.W., Chan K.M.A., Costanza R. et al. (2012). Contributions of cultural services to the ecosystem services agenda. PNAS 109(23): 8812-8819, DOI: 10.1073/pnas.1114773109.

EEA. (2011). Green infrastructure and territorial cohesion: The concept of green infrastructure and its integration into policies using monitoring systems. Technical report. Luxembourg: Publications Office of the EU. Available at: https://www.eea.europa.eu/publications/green-infrastructure-and-territorial-cohesion [Accessed 12 Jan., 2022].

Elmqvist T., Fragkias M., Goodness J. et al. (eds.). Urbanization, Biodiversity and Ecosystem Services: Challenges and Opportunities. A Global Assessment. (2013). Cham: Springer, DOI: 10.1007/978-94-007-7088-1.

Frolova V.A. and Batarin A.A. (2015). Specialties of using large green areas within the metropolis. Research results of the Izmailovo park in Moscow. Forestry Bulletin, 5, 42-50 (in Russian with English summary).

Gan J. (2021). Urban Biodiversity and Built Environment: Case Study of Shanghai. Cham: Springer Nature B.V., DOI: 10.1007/978-981-16-0949-7.

Girault C. (2017). Between naturalness and urbanity, how are protected areas integrated into cities? The case of Helsinki (Finland). Urban nature, 16, DOI: 10.4000/articulo.3270/.

Golden Kroner R.E., Qin S., Cook C.N., Krithivasan R., Pack S.M., Bonilla O.D., Cort-Kansinally K.A. et al. (2019). The uncertain future of protected lands and waters. Science, 364(6443), 881-886, DOI: 10.1126/science.aau5525.

Haines-Young R. and Potschin M.B. (2018). Common international classification of ecosystem services (CICES) v5.1 and guidance on the application of the revised structure. [online] Available at: https://cices.eu/content/uploads/sites/8/2018/01/Guidance-V51-01012018.pdf [Accessed 12 May, 2022].

Hall D.M., Steiner R. Policy content analysis: Qualitative method for analyzing sub-national insect pollinator legislation. MethodsX, 7, 100787, DOI: 10.1016/j.mex.2020.100787.

Ioja C., Osaci-Costache G., Breuste J., Hossu C., Gradinaru S., Onose D.A., Nita M. and Skokanova H. (2018). Integrating urban blue and green areas based on historical evidence. Urban Forestry & Urban Greening, 34, 217-225, DOI: 10.1016/j.ufug.2018.07.001.

Khramtsov V.N., Kovaleva T.V., Natsvaladze N.J. et al. (2016). The Atlas of specially protected natural areas. Saint-Petersburg: Directorate of Saint-Petersburg's protected areas.

Kiseleva V.V., Korotkov S.A., Stonozhenko L.V. and Naidenova E.V. (2019). Structure and regeneration of spruce forests as affected by forest management practices in the Moscow region. In: The International Jubilee Scientific and Practical Conference «Innovative directions of development of the forestry complex". IOP Conference Series: Earth and Environmental Science, 226, 012-042, DOI: 10.1088/1755-1315/226/1/012042.

Kolbowsky E.Y., Klimanova O.A., Arshinova M.A. and Margolina I.L. (2015). Landscape management within the Moscow city protected areas. In: Luc., M., Somorowska, U., and Szmańda J. (eds). Landscape Analysis and Planning, 257-269, DOI: 10.1007/978-3-319-13527-4_15. Cham: Springer.

Kryukov V.A. (2021). Environmental, social and economic potentials of urban protected areas: case study of Moscow, Russia. In: Advanced Technologies for Sustainable Development of Urban Green Infrastructure. SSC 2020 Conference, 218-229, DOI: 10.1007/978-3-030-75285-9_21. Cham: Springer.

Kryukov V.A., Golubeva E.I. (2022). Elk Island (Losinyi Ostrov) national park: transformation of regulations in urban environment. Vestnik of Saint Petersburg University. Earth Sciences, 67(1), 181–198, DOI: 10.21638/spbu07.2022.110 (in Russian with English summary).

Langemeyer J., Baró F., Roebeling P., Gómez-Baggethun E. (2015). Contrasting values of cultural ecosystem services in urban areas: The case of park Montjuïc in Barcelona. Ecosystem Services, 12, 178-186, DOI: 10.1016/j.ecoser.2014.11.016.

Lausche B. (2011). Guidelines for protected areas legislation. Gland, Switzerland: IUCN. [online] Available at: https://portals.iucn.org/library/efiles/documents/eplp-081.pdf [Accessed 29 June, 2022].

Lelkova A. and Pakina A. (2020). Assessment of the "Elk Island" national park's ecosystem functions. Ecosystems: ecology and dynamics, 4(3), 180–192, DOI: 10.24411/2542-2006-2020-10068.

Leroux S.J. and Kerr J.T. (2013). Land development in and around protected areas at the wilderness frontier. Conservation Biology, 27(1), 166-176, DOI: 10.1111/j.1523-1739.2012.01953.x.

Longley P. A., Goodchild M. F., Maguire D. J. and Rhind D. W. Geographic Information Systems and Science. 2nd ed. New York: Wiley; 2005.

Lothian W.F. (2010). A history of Canada's national parks. Parks Canada 4. [online] Available at: http://parkscanadahistory.com/publications/history/lothian/eng/vol4/chap7.htm [Accessed 4 Apr., 2022].

Mahmoud I. and Morello E. (2021). Co-creation pathway for urban nature-based solutions: testing a shared-governance approach in three cities and nine action labs. In: Smart and Sustainable Planning for Cities and Regions. SSPCR 2019. Green Energy and Technology. Cham: Springer, 259-276, DOI: 10.1007/978-3-030-57764-3_17.

Mascia M.B. and Pailler S. (2011). Protected area downgrading, downsizing, and degazettement (PADDD) and its conservation implications. Conservation Letter, 4(1), 9–20, DOI: 10.1111/j.1755-263x.2010.00147.x.

Millennium Ecosystem Assessment. (2005). Ecosystems and human well-being: synthesis. Washington, DC: Island Press.

Mukhin G.D., Leonova N.B., Margolina I.L. and Pakina A.A. (2015). Development of the Moscow city's network of protected areas: the current trends. Regional environmental issues, 6, 67-71 (in Russian with English summary).

Paloniemi R., Apostolopoulou E., Primmer E., Grodzinska-Jurcak M., Henle K., Ring I., Kettunen M., Tzanopoulos J., Potts S., van den Hove S., Marty P., McConville A. and Simila J. (2012). Biodiversity conservation across scales: lessons from a science–policy dialogue. Nature Conservation, 2, 7-19, DOI: 10.3897/natureconservation.2.3144

Peen J., Schoevers R. A., Beekman A. T., and Dekker J. (2010). The current status of Urban-rural differences in psychiatric disorders. Acta Psychiatrica Scandinavica, 121(2), 84–93. DOI: 10.1111/j.1600-0447.2009.01438.x.

Qin S., Golden Kroner R.E., Cook C., Tesfaw A.T., Braybrook R., Rodriguez C.M., Poelking C. and Mascia M.B. (2019). Protected area downgrading, downsizing, and degazettement as a threat to iconic protected areas. Conservation Biology, 33(6), 1275-1285, DOI: 10.1111/cobi.13365.

Reitz O., Yaroslavtsev A., Meshalkina J., Vasenev I., Vasenev V., Valentini R. and Leuchner M. (2021). Carbon dioxide fluxes of an urban forest in Moscow. In: Advanced Technologies for Sustainable Development of Urban Green Infrastructure. SSC 2020 Conference. Cham: Springer, 40-50, DOI: 10.1007/978-3-030-75285-9_5.

Rysin L.P. (2012). Forests of Moscow oblast (in Russian). Moscow: KMK.

Samsonova S.Y., Belutina V.S., Baraboshkina T.A., Samarin E.N. and Ogorodnikova E.N. (2013). Eco-geomorphologic analysis in substantiation of environmental management in urban conservation areas (case study of "Sparrow Hills" park, Moscow, Russia). RUDN Journal of Ecology and Life Safety, 2, 93-97 (in Russian with English summary).

Sarmiento-Mateos P., Arnaiz-Schmitz C., Herrero-Jáuregui C., Pineda D.F. and Schmitz M.F. (2019). Designing protected areas for social-ecological sustainability: effectiveness of management guidelines for preserving cultural landscapes. Sustainability, 11, 2871, DOI: 10.3390/su11102871.

Semenyuk O., Telesnina V., Bogatyrev L. and Benediktova A. (2021). Structural and functional organization of forest litters as indicators of biological cycling intensity in urban forest stands (an example of Moscow). Eurasian Soil Science, 54, 738-749, DOI: 10.1134/S1064229321050173.

Semenyuk O.V., Bodrov K.S., Stoma G.V. and Yakovlev S.A. (2019). Estimating the ecosystem services' value of the Bitzevsky forest natural park. Moscow University Soil Science Bulletin, 74, 111–117, DOI: 10.3103/S014768741903007.

Slapin J.B., and Proksch S.-O. (2014). Words as Data: Content Analysis in Legislative Studies', in Martin S., Saalfeld T., and Kaare W. Strøm (eds), The Oxford Handbook of Legislative Studies ; Oxford Academic, DOI: 10.1093/oxfordhb/9780199653010.013.0033.

Stepanitsky V.B., Kreyndlin M.L. (2004). National nature reserves and national parks of Russia: threats, failures, missing opportunities. Moscow, Greenpeace Russia.

TEEB-Russia. Issue 3. (2021). Green infrastructure and ecosystem services of the largest Russian cities (in Russian). [online] Available at: http://teeb.biodiversity.ru/publications/Ecosystem-Services-Russia_V3_web.pdf [Accessed 5 Jun., 2022].

Tenk A. (2016). Destination management of protected areas in Budapest. Current Issues of Tourism Research, 5(1), 41-58.

Trzyna T., Edmiston J.T., Hyman G., McNeely J.A., Menezes P.C., Myrdal B., Phillips A. et al. (2014). IUCN. Urban protected areas. Profiles and best practice guidelines. [online] Available at: https://www.iucn.org/content/urban-protected-areas-profiles-and-best-practice-guidelines [Accessed 10 Feb., 2022].

United Nations, Department of Economic and Social Affairs, Population Division. (2019). World Urbanization Prospects: The 2018 Revision (ST/ESA/SER.A/420). New York: United Nations. [online] Available at: https://www.un.org/development/desa/publications/2018-revision-of-world-urbanization-prospects.html#:~:text=Projections%20show%20that%20urbanization%2C%20the,and%20Africa%2C%20according%20to%20a [Accessed 10 Feb., 2022]

Vaccaro I., Beltran O. and Paquet P.A. (2013). Political ecology of conservation: some theoretical genealogies. Journal of Political Ecology, 20(1), 255-272, DOI: 10.2458/v20i1.21748.

Vogelmann J.E, Helder D., Morfitt R., Choate M.J., Merchant J.W., Bulley H. (2001). Effects of Landsat 5 Thematic Mapper and Landsat 7 Enhanced Thematic Mapper plus radiometric and geometric calibrations and corrections on landscape characterization. Remote Sensing of Environment, 78(1–2), 55-70, DOI: 10.1016/S0034-4257(01)00249-8.

RESEARCH PAPER

SPATIAL DISTRIBUTION OF WATER QUALITY IN WELANG, GEMBONG AND REJOSO RIVERS, PASURUAN, EAST JAVA, INDONESIA

Arief Darmawan[1*], Endang Yuli Herawati[1], Arina Maksurotin Filhiyam[2], Evitta Sherin Arinda[2], Zalfa Salsabila Wijanarko[2]
[1]Lecturer of Dept. Aquatic Resource Management, Faculty of Fisheries and Marine Science, Univ. Brawijaya, Malang, Indonesia
[2]Student of Dept. Aquatic Resource Management, Faculty of Fisheries and Marine Science, Univ. Brawijaya, Malang, Indonesia
*Corresponding author: ariefdarma@ub.ac.id
Received: April 3st, 2022 / Accepted: September 4th, 2023 / Published: October 10th, 2023
https://DOI-10.24057/2071-9388-2022-2365

ABSTRACT. A river is a naturally formed freshwater stream that traverses land and eventually flows into a lake, sea, or another body of water. River provides fresh water for human activities such as irrigation for their paddy fields, aquaculture, industrial purposes, and many other purposes. At the same time, there exists an inherent disparity in the demand, availability, and quality of river water, often giving rise to significant challenges and issues. Environmental experts, commonly use a multivariate statistical method such as Principal Component Analysis (PCA), Storage and Retrieval (STORET), and cluster analysis for water quality analysis. However, those methods are numerical and limited in spatial visualization. Inverse Distance Weighting (IDW) interpolation, Voronoi, and Kriging were applied to obtain the spatial representation of water quality distribution Welang, Gembong, and Rejoso rivers in Pasuruan as study. The objectives are to locate on a map any river segments that experienced poor water quality throughout the observation period. We successively combined STORET with those spatial interpolation. The result shows that IDW interpolation, Voronoi, and Kriging can visualize and map river segments that had poor water quality during the observation time. However, due to the limited input data, the interpolation results exhibit variability. For instance, at a measured location with a STORET value of -28, IDW yielded -28, Voronoi -28, and Kriging -27. Beyond the measurement points, each interpolation method began to produce less accurate values. This study involves interpolating dynamic objects with limited measurements data in narrow channels, which differs from interpolating elevation in broader area, in terms of the accuracy of representation or visualization obtained from this spatial analysis still remain unresolved in this study.

KEYWORDS: interpolation, STORET, water quality, Pasuruan.

CITATION: Darmawan A., Herawati E. Y., Filhiyam A. M., Arinda E. S., Wijanarko Z. S. (2023). Spatial Distribution Of Water Quality In Welang, Gembong And Rejoso Rivers, Pasuruan, East Java, Indonesia. Geography, Environment, Sustainability, 3(16), 64-74
https://DOI-10.24057/2071-9388-2022-2365

ACKNOWLEDGEMENTS: The authors would like to appreciate to University of Brawijaya for the research funding (Professor and Doctor Research Grant Program: DIPA-023.17.2.677512/2021) and supporting team: Rahmi Valina.

Conflict of interests: The authors reported no potential conflict of interest.

INTRODUCTION

A river is a natural flow of freshwater that crosses land and goes into a sea, an ocean, a lake, etc. River has ecological functions such as habitat, conduit, filter, barrier, source, and sink (Wang and Pan 2011). On the other hand, rivers provide freshwater for human activities such as irrigation for their paddy fields, aquaculture, industrial purposes, etc. The demand, availability, and quality of river water are significant concerns. As the water quality of three rivers, Welang, Gembong, and Rejoso, in Pasuruan City and Pasuruan Regency, East Java, Indonesia (Figure 1) is deteriorating. They are crossing dense settlements, industrial clusters, and agricultural areas and end up in the Madura Strait. A previous study by Misnawati (2013) revealed that land use changes in the upper stream of the Welang River caused erosion, and the other problem was flooding (Arifin 2021).

The Welang River is located in a distinct watershed from the Gembong and Rejoso Rivers. Welang River is in the Welang watershed while Gembong and Rejoso Rivers are in the Rejoso watershed. The boundary of those two watersheds is adjacent and both have upstream in Bromo Mountain at the southern region of its watershed. The middle stream and the downstream Gembong River cross the City of Pasuruan with a high-density settlement and industrial area than the Welang and Rejoso rivers. As a result, theoretically, those three rivers will have different statuses and conditions.

Water quality analysis commonly uses multivariate statistical methods such as Principal Component Analysis (PCA) or cluster analysis as research by Ustaoğlu and Tepe

(2019), Muangthong and Shrestha (2015), Boyacioglu and Boyacioglu (2008). On the other hand, in Indonesia, there is a method called STORET (Storage and Retrieval), the United States Environmental Protection Agency (US EPA) based to determine the overall pollution rate implemented in a water quality study conducted by Sugiyarto et al. (2018), Yoviandianto et al. (2019), Aidi et al. (2021) and Mudjiardjo et al. (2021). This method is for general water quality assessment rather than for fishery purposes, and it lacks spatial visualization to show the areas of the river with a water quality concern. Therefore, this study is focused on spatial analysis to reflect water quality distribution in the Welang, Gembong, and Rejoso rivers. The aim is to identify areas of the river with water quality issues during the observation period and visualize them on the map.

MATERIALS AND METHODS

This study made use of a time series water quality dataset derived from three measurements taken at three different places along the Welang, Gembong, and Rejoso rivers (Figure 1). Meanwhile, the common factors to estimate pollution levels according to Tomar (1999) are temperature, color, BOD, suspended solid (TSS), pH, ammonia, phosphorus, and heavy metals. For this research, the dataset consists of physical and chemical variables of water such as temperature, pH, turbidity, DO, BOD, etc. STORET method works by comparing the water quality properties with the standard and giving them a certain score. The scoring calculation of the STORET method is represented in Table 1 and Table 2 which is from the Decree of the Indonesian Minister of the Environment Number 115 of 2003 concerning Guidelines for Determining the Status of Air Quality Status. For water quality standards, this study uses the Indonesian Government Regulation Number 22 of 2021 concerning the Implementation of Environmental Protection and Management.

According to Table 1, the STORET scoring required 3 components, maximum, minimum, and average. As a consequence, the data must be in series where at least obtained from three different measurements. In this research, the measurements were conducted in each river on 10 March 2021, 10 April 2021, and 29 April 2021 in the morning. The average time of measurements was between 08:00 am to 10:00 am and started from Station 1, Station 2, and Station 3 in sequence. Each river has three measurement stations as represented in Figure 1. We measured 12 water quality parameters in each river, those were temperature: TSS, turbidity, pH, DO, COD, nitrate, orthophosphate, Total Organic Matters (TOM), alkalinity, Cadmium, total nitrate, and total phosphate. To produce the visualization, spatial analysis used river network shapefiles received from the Indonesian Bureau of Geospatial (BIG) at a scale of 1: 25.000. Similar to Oke et al. (2013), the IDW (Inverse Distance Weighted) method in ArcGIS used in the mapping of water properties as obtained from the survey and laboratory analysis. IDW is also commonly used to predict the parameter in the field of hydrology science as research conducted by Rostami et al. (2019) and Yang et al. (2020). As continued, a raster data (grid) of water quality parameters resulted. As a comparison, we did interpolation with Voronoi and Kriging.

IDW takes on that the value at an unsampled location is a distance-weighted average of values sampled points within a defined neighbourhood surrounding the unsampled points (Tan and Xu 2014). Meanwhile, Kriging assumes that the weights are not only based on the distance between the measured points but also on the overall spatial arrangement of the measured points (Tan and Xu 2014). Kriging is a stochastic method similar to IDW (Wu and Hung 2016), and raster-based, so we are interested to compare it. On the other hand, Voronoi is vector based, and it is constructed from a series of polygons formed around the location of a sample point (ESRI 2016). It seems that Voronoi attempts to calculate a value based on the data points that are already known in an area. Moreover, the location of measurements in the field in this study is also very limited. It can be seen from Fig. 1, there were only 9 measurement locations spread over three rivers. Each measurement location or station in a river channel is also quite far apart. Theoretically, this is certainly less acceptable. However, a comparison of these three methods will be interesting to see.

In the step of processing, the river networks shapefile which was in polylines format converted to polygon by the buffering process. The reason was to make it able to clip the interpolated raster data resulting from the IDW, Voronoi, and Kriging method (interpolation) and as a representation of river boundary or boundary line of the river that separates with other land use. The boundary lines are virtual lines on the left and right river as a set of boundaries for river protection. According to Article No 9b, Government of Republic Indonesia Regulation Number 38 the Year 2011, river where at least 15 m (fifteen meters) from the edge left and right of the riverbed along the river channel, in case the river depth is more than 3 m (three meters) up to 20 m (twenty meters). Only the overlayed cells or grids with

Table 1. STORET Scoring for water quality assessment (source: Government of Republic Indonesia (2003))

Number of parameters	Value	Physical	Chemical	Biological
<10	Maximum Minimum Average	-1 -1 -3	-2 -2 -6	-3 -3 -9
>=10	Maximum Minimum Average	-2 -2 -6	-4 -4 -12	-6 -6 -18

Table 2. Water quality classification according to STORET Method (source: Government of Republic Indonesia (2003))

Class	Total Score	Name
A	0	Meet the water quality standard
B	-1 to -10	Lightly polluted
C	-11 to -30	Moderately polluted
D	>= -30	Highly polluted

the river networks remained the process and are used to depict the water quality variables of those rivers. The process was repeated to obtain spatial data for each water quality variable as well. The procedure for mapping water quality parameters is basically as seen in Fig. 2 for IDW and Kriging because both are in raster formats. In the meantime, Voronoi followed the same processes but in vector format.

For the spatial analysis, water quality grid data as the output of the process in Fig. 2 were vectorized to obtain vector data format. Finally, we dissolved it according to the water quality attributes to produce the final shapefile and layout it as a map displaying the spatial distribution of water quality. A detail of the spatial data processing is represented in Fig. 2.

RESULTS

The time series data collected from the Welang, Gembong, and Rejoso rivers were analyzed according to the STORET method. Table 3 provides an example of STORET scoring calculation based on water quality parameter measurements at Station 1 of the Welang River. Overall, the result of water quality was calculated with the STORET method for the Welang, Gembong, and Rejoso rivers represented in Table 4.

From Table 4, it clearly can be seen that water quality in both three rivers are at moderate to high pollution status. The only exception was the Welang River, which had moderate pollution at measuring Stations 1 and 2, but severe pollution at Station 3. It was discovered that two

Fig. 1.Research location in Pasuruan

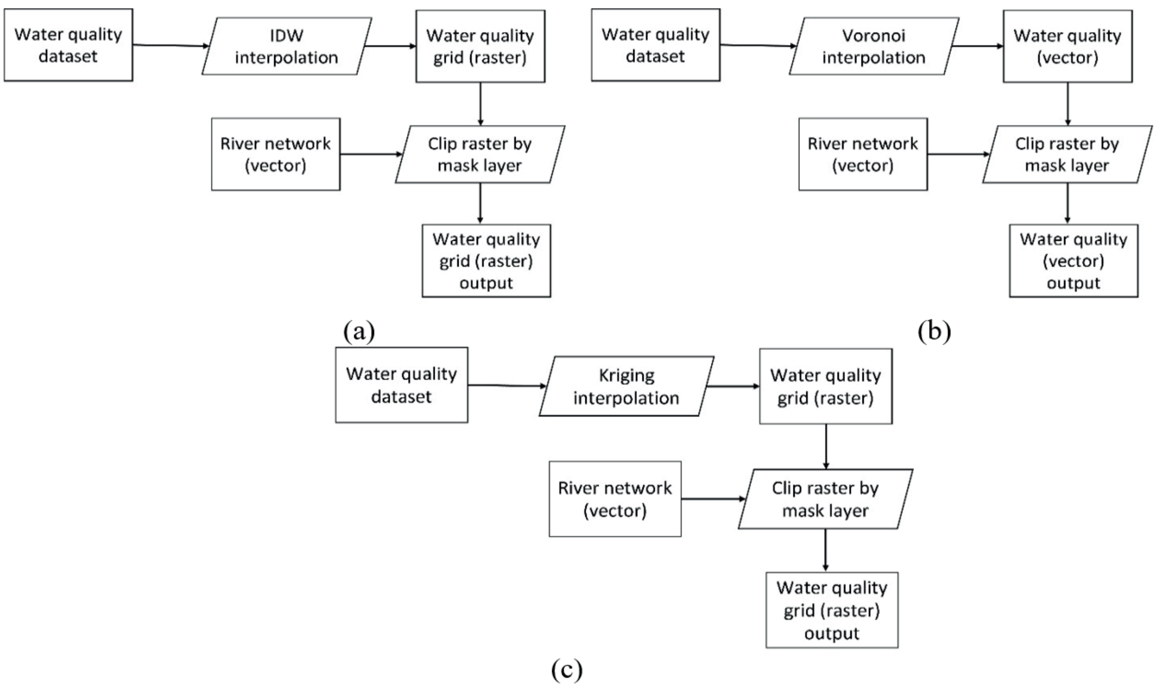

Fig. 2. Spatial data processing, (a) IDW, (b) Voronoi, and (c) Kriging Interpolation

parameters (TSS and alkalinity) caused pollution status to moderate at Station 1 by observing the calculation of the STORET score as shown in Table 3. TSS and alkalinity were above the water quality standard that was used for the analysis respectively. With the same principles, the calculation of the score was also conducted for the rest stations. When comparing the three rivers, the Gembong and Rejoso rivers were in worse condition than the Welang. For the Gembong River, it is understandable due to the river crossing city with a high density of settlements and industrial area where we found cadmium (Cd), Total P, pH, and temperature in each station that more than water quality standard.

Meanwhile, the Rejoso River although at the same water quality as the Gembong River had a bit different cause factor. In the Rejoso River total organic matter (TOM) was above the standard except for cadmium, Total P, pH, and temperature. According to TOM, water contains dissolved, suspended (particulate), and colloidal organic matter, implying that the Rejoso River was higher in this matter than the Welang and Gembong rivers. Meanwhile, Fig. 3 represents a visualization of water quality distribution based on STORET analysis for the Welang, Gembong, and Rejoso Rivers as well. The mapping procedure to obtain Fig. 3 was explained earlier in Fig. 2.

According to Fig. 3, it can be explained why TOM of the Rejoso River was high. It was high because the Rejoso River ran through the agricultural area. Furthermore, sediments spread through the end of the Rejoso River that linked with Madura Strait, and it was not in the same condition as the end of the Gembong River. We believe that part of the upper stream of the Rejoso River had faced degradation.

Table 3. Example of STORET Method calculation

Parameters		Units	Water quality standard	Station 1 - Welang River Calculation						Total Score
				Minimum	Score	Maximum	Score	Average	Score	
Physical	Temperature	°C	28-30	27.80	0	30.00	0	28.65	0	0
	TSS	mg/L	100	55.00	0	160.30	-2	132.3	-6	-8
	Turbidity	cm	200	8.90	0	35.00	0	15.58	0	0
Chemical	pH		6-9	7.68	0	8.60	0	8.05	0	0
	DO	mg/L	3	5.60	0	6.86	0	6.07	0	0
	COD	mg/L	40	16.60	0	21.70	0	19.65	0	0
	Nitrate	mg/L	20	0.28	0	0.94	0	0.76	0	0
	Orthophosphate	mg/L	1	0.100	0	0.147	0	0.123	0	0
	TOM	mg/L	30	8.01	0	21.50	0	11.46	0	0
	Alkalinity	mg/L	75	116.20	-4	244.00	-4	148.28	-12	-20
	Cd	mg/L	0.01	0.00	0	0.00	0	0.00	0	0
	Total N	mg/L	25	0.80	0	1.50	0	1.15	0	0
	Total P	mg/L	1	0.44	0	0.66	0	0.56	0	0
Total Score										-28

Table 4. STORET result of the Welang, Gembong and Rejoso rivers

Location	Station (ST)	Total Score	Pollution Status
Welang River	1	-28	Moderate
	2	-26	Moderate
	3	-46	High
Gembong River	1	-48	High
	2	-68	High
	3	-62	High
Rejoso River	1	-60	High
	2	-62	High
	3	-60	High

Fig. 3. Water Quality Distribution: Welang, Gembong, and Rejoso Rivers - STORET Method, visualized with IDW Interpolation in GIS

Fig. 4. Water Quality Distribution: Welang, Gembong, and Rejoso Rivers - STORET Method, visualized with Voronoi Interpolation in GIS

Fig. 5. WWater Quality Distribution: Welang, Gembong, and Rejoso Rivers - STORET Method, visualized with Kriging Interpolation in GIS

DISCUSSION

The IDW interpolation in this study is enabled to help in the visualization of the water quality variation as seen in Fig. 3. It was similar to Oke et al. (2013) that used the same method for the visualization of water parameters along the river course. But, due to limited measurement stations, the result from this study did not reach the detail of Oke et al. (2013). Meanwhile, Voronoi is not commonly to be applied for flowing water. Most researchers such as Dakowicz and Gold (2007) used Voronoi for terrain modeling, Daoud (2020) used Voronoi for surface groundwater modeling, Skamarock et al. (2012) – for the atmospheric model, and Hoffman et al. (2018) use Voronoi grids for earth system modeling. However, as shown in Fig. 4, the Voronoi diagram produced a good visualization of water quality variation. Similarly, Kriging interpolation is commonly used for terrain modeling or surface modeling, and this research also gives a good visualization as IDW and Voronoi (see Fig. 5). In general, those methods are spatial interpolation processes that use a set of point data to create surface data (Longley et al. 2005). With a limited number of stations to collect data for each river, the visualization of water quality (WQ) distribution will inevitably encounter challenges.

As we continue, there was an unexpected finding while studying the water quality (WQ) distribution that was visualized by those three various interpolation methods. In IDW interpolation, there were two water quality change borders. The first was a bit distance from Station 3, perhaps only separated approximately 0.5 Km, and the second was about 4 Km south of Station 1. Meanwhile, Voronoi interpolation resulted in an almost similar WQ change border at the southern site. But, on the north side which is close to Station 3, it was not the same. WQ change visually appears in the middle of Station 2 and Station 3. It was approximately 1.5 Km from Station 2 and 1,3 from Station 3 respectively. Then, the result from Kriging interpolation shows almost similar to IDW interpolation at the WQ change border near Station 3 and different at the south of Station 1. The WQ change border was approximately 2.5 Km distance from Station 1. Overall, with IDW interpolation, Voronoi had nearly the same WQ change border at the southern of Station 1. But, IDW interpolation and Kriging interpolation had similar WQ change border nearly the same at Station 3.

Furthermore, even if the distance between Station 1, Station 2, and Station 3 for the Welang River was not similar to the distance of stations on the Gembong and Rejoso rivers, the process can be completed through ArcGIS. Meanwhile, when looking back to the total score resulting from the STORET calculation for the Welang River, those scores scattered between -26 to -68 respectively. As an example, in the Welang River STORET score of 3 stations was -28, -26, and -46. The score at Station 1 and Station 2 was in the same range, but the score at Station 3 was far away. However, closer examination of the mapping result revealed a unique representation, as shown in Fig. 3, Fig. 4, and Fig. 5. There was a variation in the water quality change border as seen in Fig. 6. We did not examine the Gembong and Rejoso rivers in detail because the conditions were the same, all extremely polluted and depicted with the same visualization in Fig. 3, Fig. 4, and Fig. 5 from all interpolation methods.

From the GIS procedure, there are two main steps as the key to accurate visualization with GIS spatial analysis. The first is the number of points that represent the measurement station of water quality parameters at each river and the distance between those points as well. The second is the gap or distance between each point that represents locations of measurement water quality parameters itself. It occurred because, during the interpolation stage, IDW interpolation took into account the distance between points in the prediction. The IDW interpolation is fast, simple, and able to work on scattered data (Gentile et al. 2012). All of the points that filled in with the STORET score for this research only took a few seconds to complete in the interpolation process.

From a perspective of achieving smooth and clear visualization, the Voronoi result is indeed highly effective for representing the distribution of water quality due to its vector format. In contrast, IDW interpolation and Kriging methods are raster-based, meaning they operate on a grid-like structure, which can result in a different representation style compared to the Voronoi approach. In terms of the accuracy of the visualization resulting from the GIS analysis that has been conducted, we admit that still unable to address it due to limitations. As we are aware that water in the river flows away and it is dynamic from time to time, and it has just given the challenge to conduct real-time ground truth of the GIS analysis result as well. As an example, when observing in detail Fig. 7, the water quality change border that resulted from IDW interpolation, Voronoi and Kriging were not the same. IDW interpolation and Kriging interpolation WQ change border in the middle of land use ponds and aquaculture. Although it was looking the same, both were in different distance WQ change border if measured from Station 3. Meanwhile, Voronoi's result shows that WQ change the border located before the ponds and aquaculture areas.

Furthermore, readers may conclude from Fig. 7 that the transition of WQ in the midst of ponds and aquaculture is the accumulation of prior water flow, and it was growing worse over there based on IDW interpolation and Kriging interpolation. On the other hand, the change in WQ before entering the ponds and aquaculture region as a result of the Voronoi interpolation result may lead to a better understanding of how land use influences water quality. Misinterpretation risks arise if the dynamics of moving water features are not thoroughly comprehended. This is because, logically, water quality would typically not undergo significant changes simply upon entering a different land use, as illustrated in Fig 7-part Voronoi. As a result, the outcomes obtained from IDW interpolation and Kriging interpolation were found to be more logically consistent when compared to the Voronoi method, although it's worth considering that these differences might have arisen due to possible coincidental factors.

For a further detailed comparison between the three interpolation methods that are used for STORET visualization, we conduct detailed observation through the values. We randomly made points along the river channel to check the STORET values after the interpolation process. Fig. 8 shows the position of those points respectively. Meanwhile, Fig. 9 shows the plot of the value on the graph. We marked with box position numbers 5, 6, 8, 10, 11, 12, 14, 15, and 16 because those were locations where field measurements were conducted. Thus, STORET values from

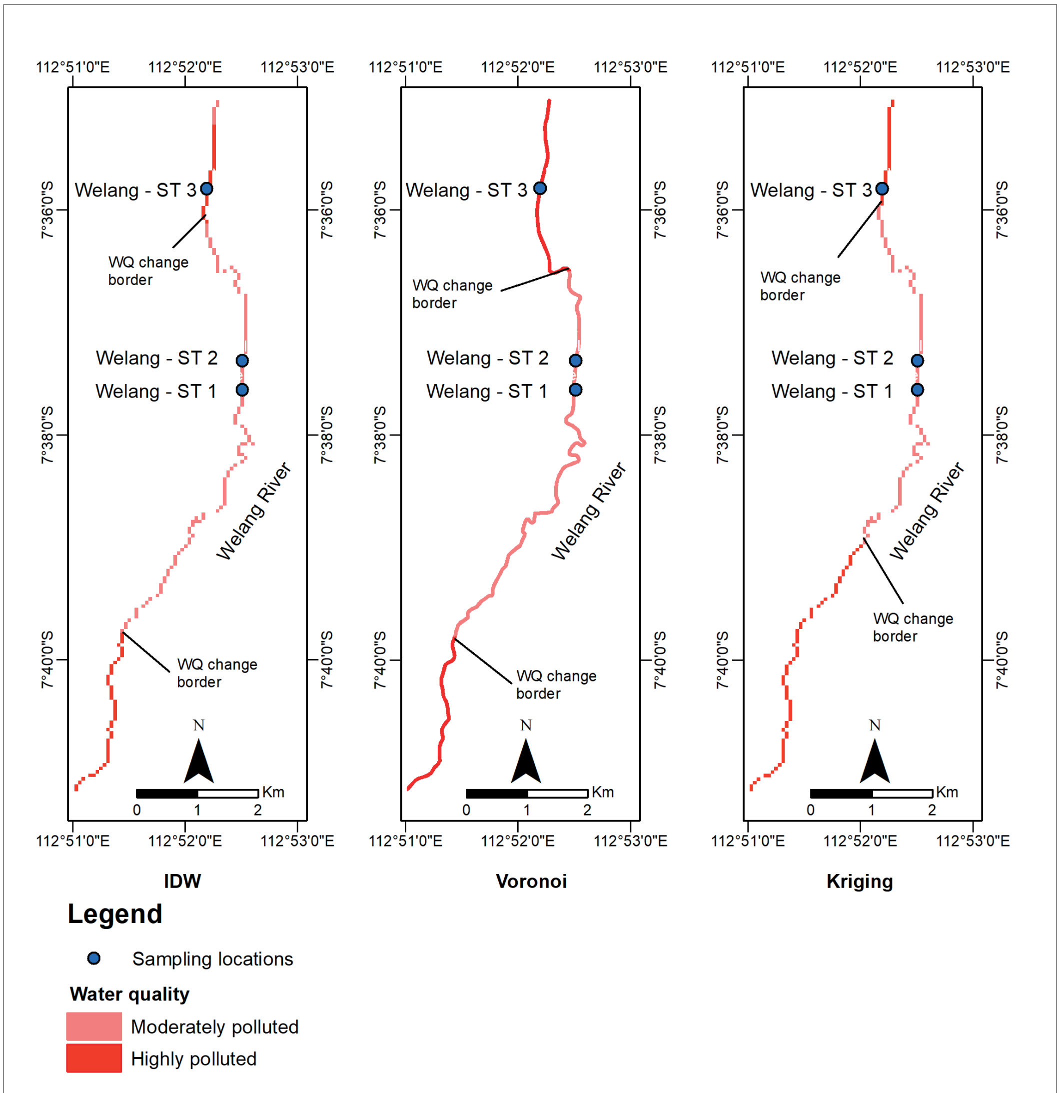

Fig. 6. omparison of water quality distribution in the Welang Rivers according to STORET method and visualized using IDW, Voronoi, and Kriging interpolation in GIS

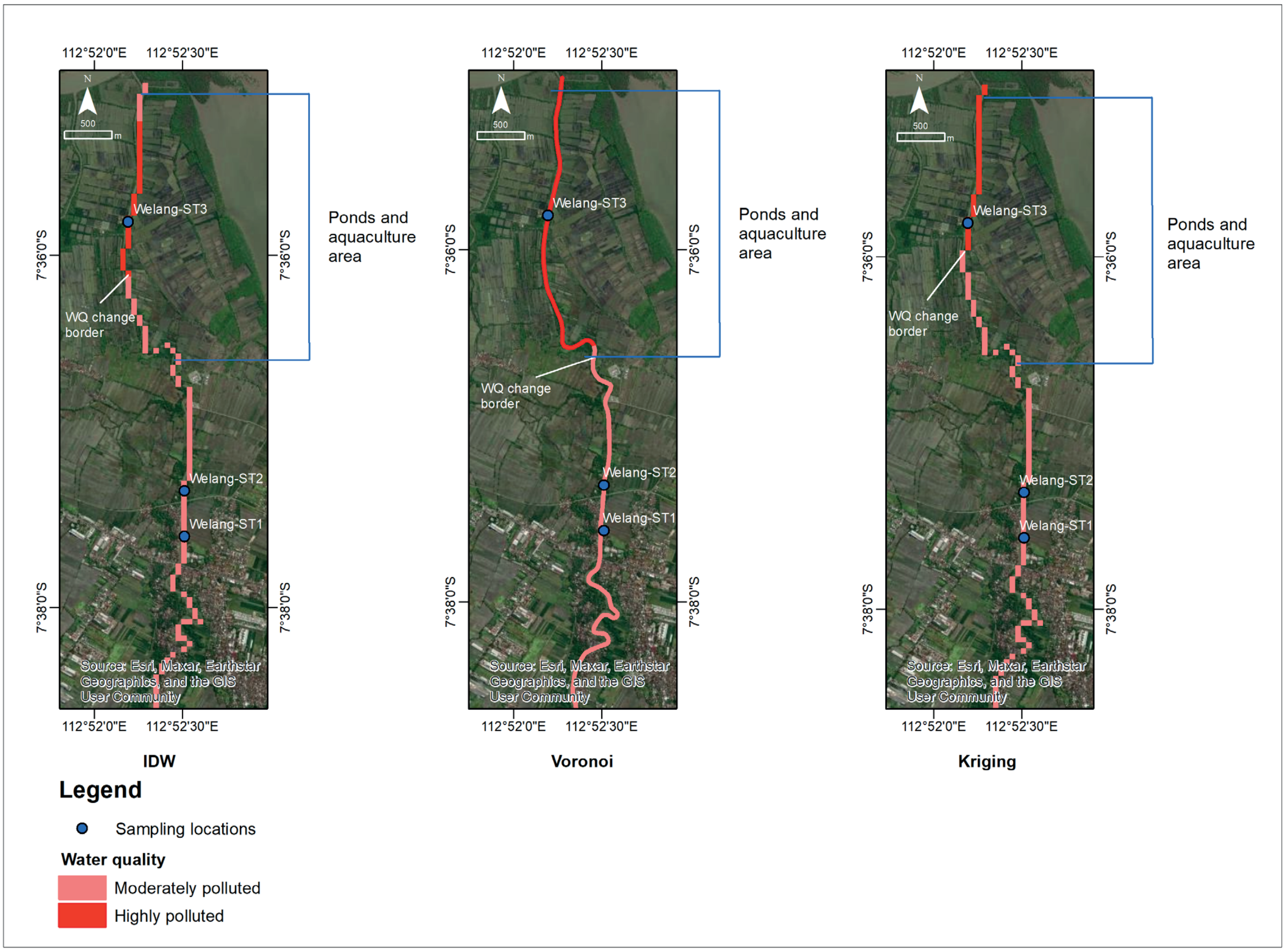

Fig. 7. Comparison of water quality transition border in the Welang rivers according to STORET method and visualized using IDW, Voronoi, and Kriging interpolation in GIS

those positions were results of calculation-based according to field measurement data and the others resulted from interpolation as well. As continue, Fig. 9 explains that the value resulted from three interpolation methods getting worse when it far from the field measurement positions. It means that a small number of samples or limited field measurements are not viable for those interpolation methods to gain accurate value. For example, at position 5, the STORET value = -28, IDW = -28, Voronoi = -28, Kriging = -27.79. Meanwhile, at position 4, IDW = -34, Voronoi = -28, Kriging = -38. When it outside the field measurement location, the interpolation gives contrast value. We admit that a limited number of field measurements that became the basis for the interpolation might be dangerous, gave inaccurate results, and produce the wrong visualization of the water quality distribution on the map. In the future, it is necessary to set more samples as a basis for interpolation in accordance to avoid imprecise results. We also admit that the appropriate distance between field measurement locations must be considered in order to be more representative.

Above all, interpolation is related to finding a set of discreet data based on measured data (Steffensen 2006) and it is based on the principle of spatial dependence (Childs 2004). This study involves interpolating dynamic objects in narrow channels, which differs from interpolating broader field elevation data with limited measurements. Consequently, there is a heightened potential for interpolation errors. Moreover, the study of water quality especially in lotic ecosystems such as a river that have two main zones, (1) rapids, and (2) pools (Reinbold 2018), will be more accurate if use bio-indicator such as micro-invertebrates that live in the bottom of waters such as research by B.T. Hart et al. (2001), Rizo-Patrón et al. (2013), Young et al. (2014) or with periphytons such as Kurteshi et al. (2008), Lili et al. (2010), Montuelle et al. (2010) rather than only rely on physical, chemical, and biological water properties. Thus, a combination of those approaches and GIS will be more accurate in representing the spatial distribution of water quality in the river.

Last but not least, despite this limitation, from the perspective of aquatic resource management, the spatial distribution of water quality represented on the map will be invaluable in supporting action planning to reduce river pollution. Utilizing methods such as STORET, PCA, Pollution Index, bio-indicators, or others would yield only numerical and descriptive information. However, incorporating GIS analysis as an additional step to visualize the results obtained from the previous methods elevates the information representation to the next level and enhances comprehension, particularly for individuals who tend to prefer visualized information over numerical data

CONCLUSIONS

The water quality study in the Welang, Gembong, and Rejoso rivers can be conducted properly, and the conclusions were as follows:

(1) The GIS for spatial analysis to represent water quality can help in the identification of river parts or river segments that face water quality problems during the period of observation and represent it on the map. Boundaries between different water quality conditions can be estimated and identified clearly through visualization. It

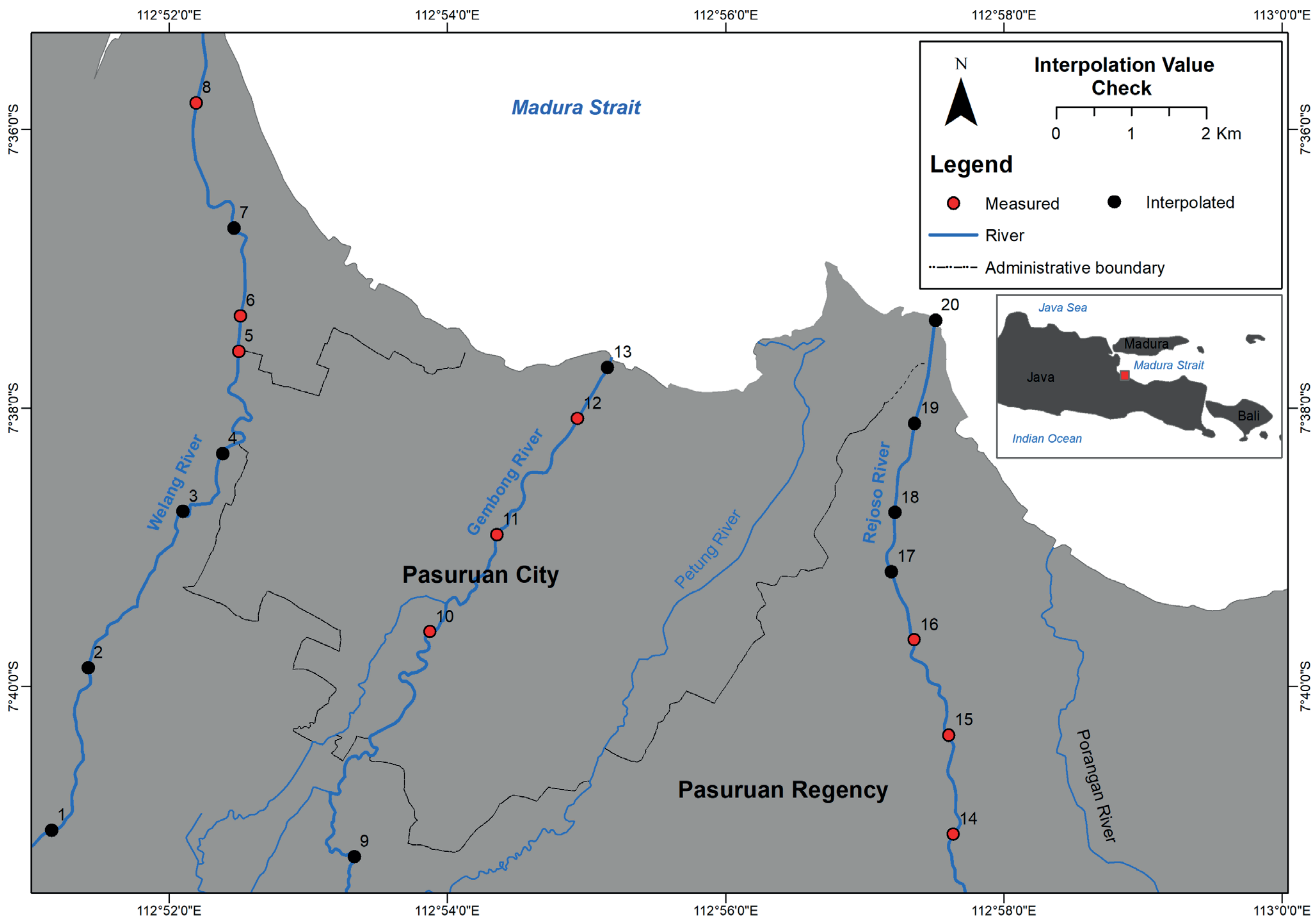

Fig. 8. Interpolation value check positions

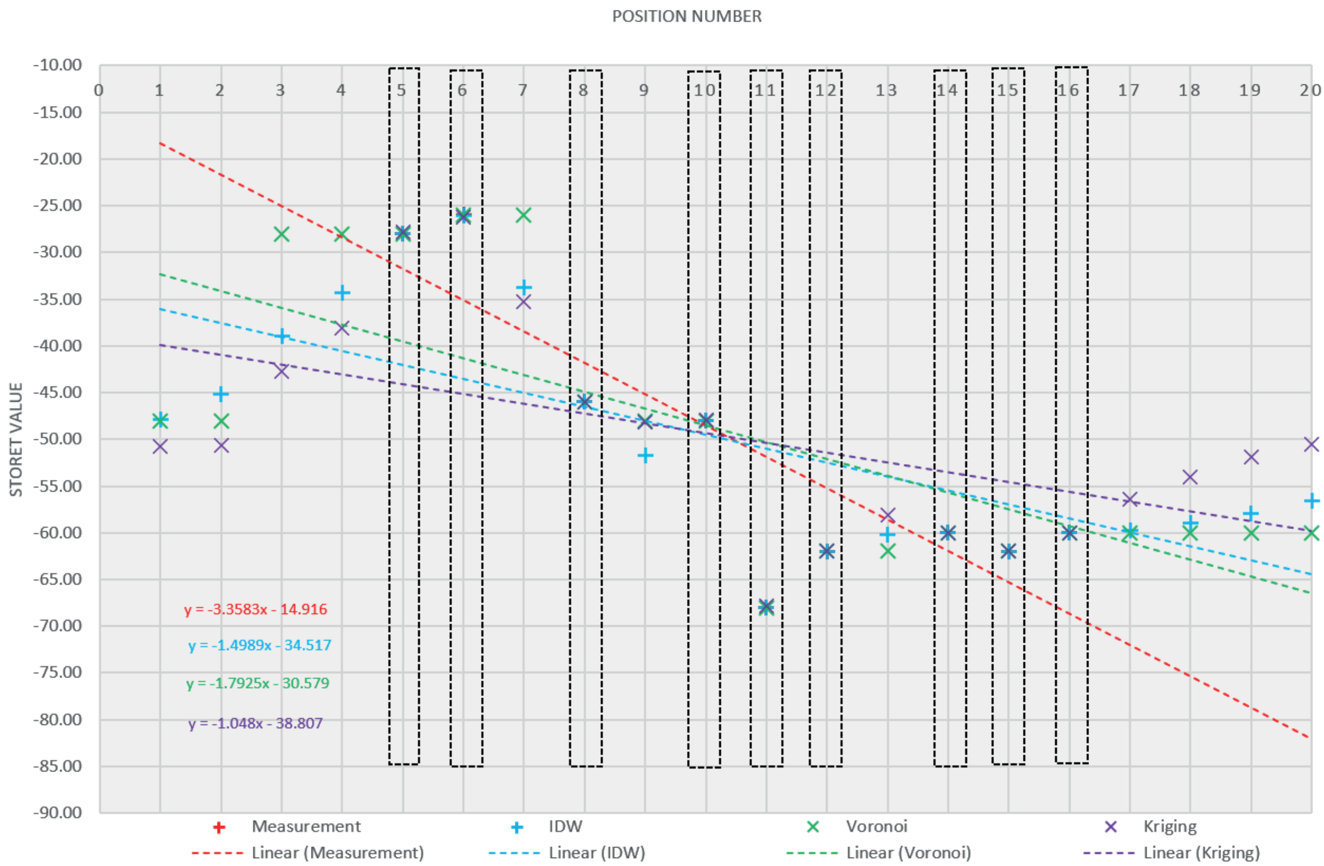

Fig. 9. Interpolation value plot

will be beneficial to support the activity of aquatic resource management, pollution reduction, or river management in general.

(2) The Small number of samples or limited field measurements are not viable for those interpolation methods to gain accurate value. The use of limited field measurements as the basis for interpolation may have adverse effects since it leads to inaccurate conclusions and the incorrect visualization of the water quality distribution on the map.

(3) Despite the several advantages, questions arise concerning the accuracy of representation or visualization derived from spatial analysis. Additionally, there is a significant challenge in conducting real-time ground truth verification of GIS analysis results. Further research is essential to address these concerns and provide a comprehensive answer.

REFERENCES

Aidi B., Pangestu B.A., Setioningrum R.N.K., Azizah R. (2021). Water Pollution Assessment in Madiun River Using STORET Method. Journal Ilmiah Pendidikan Lingkungan Dan Pembangunan, 22(01), 26 – 42, DOI: 10.21009/PLPB.221.03.

Arifin M. (2021). 'Three rivers overflow in Pasuruan, hundred people settlements submersed', Detik, 28 February 2021, in Bahasa [online]. Available at: https://news.detik.com/berita-jawa-timur/d-5474867/tiga-sungai-meluap-di-pasuruan-ratusan-rumah-warga-terendam-banjir [Accessed 7 Oct. 2021].

Boyacioglu Hülya and Boyacioglu Hayal. (2008). Water pollution sources assessment by multivariate statistical methods in the Tahtali Basin, Turkey. Environmental Geology, 54, 275-282, DOI: 10.1007/s00254-007-0815-6.

Buditama G., Damayanti A., and Pin T.G. (2017). Identifying Distribution of Chlorophyll-a Concentration Using Landsat 8 OLI on Marine Waters Area of Cirebon. IOP Conf. Series: Earth and Environmental Science, 98, 012-040, DOI: 10.1088/1755-1315-98-1-012040.

Childs C. (2004). Interpolating Surfaces in ArcGIS Spatial Analyst. ArcUser Juli-September 2004. [online]. ESRI. Available at: https://community.esri.com/ccqpr47374/attachments/ccqpr47374/arcgis-spatial-analyst-questions/2376/1/interpolating.pdf.

Dakowicz M. and Gold C. (2007). Finite Difference Runoff Modelling Using «Voronoi Buckets,» 6th International Conference on Computer Information Systems and Industrial Management Applications (CISIM'07), 121-124, DOI: 10.1109/CISIM.2007.30.

Daoud M.G.M. (2020). Integrated Hydrological Model to Study Surface-Groundwater Interaction in Hard Rock Systems Using Unstructured Grid Approach, The Sardon Catchment, Spain. Thesis. Faculty of Geo-Information Science and Earth Observation of the University of Twente.

Environmental Systems Research Institute (ESRI). (2016). ArcMap 10.5 ArcGIS desktop help. ESRI: Redlands, CA.

Fikret Ustaoğlu, Yalçin Tepe. (2019). Water quality and sediment contamination assessment of Pazarsuyu Stream, Turkey using multivariate statistical methods and pollution indicators, International Soil and Water Conservation Research, 7(1), 47-56, DOI: 10.1016/j.iswcr.2018.09.001.

Government of Republic Indonesia. (2003). Decree of the Indonesian Minister of the Environment Number 115 the Year 2003 concerning Guidelines for Determining the Status of Air Quality Status. Ministry of Environment the Republic of Indonesia. Jakarta.

Government of Republic Indonesia. (2011). Government of Republic Indonesia Regulation Number 38 the Year 2011 concerning River. Ministry the Republic of Indonesia Year 2011 Number 74. State Secretariat. Jakarta.

Government of Republic Indonesia. (2021). Government Regulation Number 22 the Year 2021 concerning the Implementation of Environmental Protection and Management. State Gazette of the Republic of Indonesia Year 2021 Number 32. State Secretariat. Jakarta.

Hoffman M.J., Perego M., Price S.F., Lipscomb W.H., Zhang T., Jacobsen D., Tezaur I., Salinger A.G., Tuminaro R., and Bertagna L. (2018). MPAS-Albany Land Ice (MALI): a variable-resolution ice sheet model for Earth system modeling using Voronoi grids, Geosci. Model Dev., 11, 3747–3780, DOI: 10.5194/gmd-11-3747-2018.

Hart B.T., Davies P.E., Humphrey C.L., Norris R.N., Sudaryanti S., Trihadiningrum Y. (2001). Application of the Australian river bioassessment system (AUSRIVAS) in the Brantas River, East Java, Indonesia, Journal of Environmental Management, 62(1), 93-100, DOI: 10.1006/jema.2001.0424.

Kurteshi K., Vehapi I., Gecaj A., and Millaku F. (2008). Periphyton Bioindicators in the Sitnica River (Kosovo). ANNALES. Ser.hist.nat, 18 (2), 265-270.

Li Li, Binghui Zheng, Lusan Liu. (2010). Biomonitoring and Bioindicators Used for River Ecosystems: Definitions, Approaches, and Trends. Procedia Environmental Sciences, 2, 1510-1524, DOI: 10.1016/j.proenv.2010.10.164.

Longley P.A., Goodchild M.F., Maguire D.J., and Rhind D.W. (2005). Geographic information systems and sciences, 2nd Ed. John Wiley & Sons Ltd: West Sussex, UK.

Montuelle B., Dorigo U., Bérard A., Volat B., Bouchez A., Tlili A., Gouy V. and Pesce S. (2010). The periphyton as a multimeric bioindicator for assessing the impact of land use on rivers: An overview of the Ardières-Morcille experimental watershed (France). Hydrobiologia, 657, 123-141, DOI: 10.1007/s10750-010-0105-2.

Muangthong S., Shrestha S. (2015). Assessment of surface water quality using multivariate statistical techniques: a case study of the Nampong River and Songkhram River, Thailand. Environ Monit Assess, 187, 548, DOI: 10.1007/s10661-015-4774-1.

Mudjiardjo A.S.U, Moersidik S.S., Damarjanti L. (2021). Analysis of Water Pollution using the STORET method in the Upper Citarum Watershed. IOP Conf. Series Earth Environ. Sci, 716, 012012, DOI: 10.1088/1755-1315/716/1/012012.

Oke A.O., Sangodoyin A.Y., Ogedengbe K., Omodele T. (2013). Distance Weighted Interpolation in Ogun-Osun River Basin, Nigeria. Landscape and Environment 7, 2, 48-62.

Reinbold J. (2018). Lentic and Lotic Ecosystems [online]. Sciencing.com. Available at: https://sciencing.com/lentic-lotic-ecosystems-7355077.html. [Accessed 13 March 2022].

Rizo-Patrón F., Kumar A., McCoy Colton M., Springer M. and Trama F. (2013). Macroinvertebrate communities as bioindicators of water quality in conventional and organic irrigated rice fields in Guanacaste, Costa Rica. Ecological Indicators, 29, 68–78, DOI: 10.1016/j.ecolind.2012.12.013.

Skamarock W.C., Klemp J.B., Duda M.G., Fowler L.D., Park S.-H., and Ringler T.D. (2012). A multiscale non-hydrostatic atmospheric model using centroidal Voronoi tessellations and C-grid staggering. Monthly Weather Review, 140(9), 3090– 3105.

Sugiyarto M., Hariono B., Destarianto P. and Nuruddin M. (2018). Determination of Water Quality Status at Sampean Watershed Bondowoso Residence Using Stored Method. J. Phys. Conf. Ser, 953, 012126, DOI: 10.1088/1742-6596/953/1/012126.

Steffensen J.F. (2006). Interpolation (Second ed.). Mineola, N.Y. ISBN 978-0-486-15483-1. OCLC.

Tan Q., and Xu X. (2014). Comparative analysis of spatial interpolation methods: an experimental study. Sensors and Transducers, 165(2), 155.

Wu Y. and Hung M. (2016). Comparison of Spatial Interpolation Techniques Using Visualization and Quantitative Assessment. In (Ed.), Applications of Spatial Statistics. Intech Open. DOI: 10.5772/65996.

Yang W., Zhao Y., Wang D., Wu H., Lin A., He Li. (2020). Using Principal Components Analysis and IDW Interpolation to Determine Spatial and Temporal Changes of Surface Water Quality of Xin'anjiang River in Huangshan, China. International Journal of Environmental Research and Public Health, 17, 2942, DOI: 10.3390/ijerph1708294.

Yoviandianto I.A., Darmawan A., Mahmudi M. (2019). Mapping of Water Quality Distribution for Supporting Aquatic Resource Management with Geographic Information System, Case in Brantas River, Bumiaji Sub-district. JFMR (Journal of Fisheries and Marine Research), 3(3), 373-381, DOI: 10.21776/ub.jfmr.2019.003.03.13.

Young Shuh-Sen, Hsi-Nan Y., Da-Ji H., Su-Miao L., Yueh-Han H., Chung-Ting C., and Jin-Wei L. (2014). Using Benthic Macroinvertebrate and Fish Communities as Bioindicators of the Tanshui River Basin Around the Greater Taipei Area – Multivariate Analysis of Spatial Variation Related to Levels of Water Pollution. International Journal of Environmental Research and Public Health 11, 7, 7116-7143, DOI: 10.3390/ijerph110707116.

RESEARCH PAPER

THERMAL REGIME OF PERMAFROST ON THE WESTERN YAMAL UNDER CLIMATE WARMING

Kirill A. Nikitin[1], Nataliya G. Belova[1*], Alexander A. Vasiliev[2]
[1]Lomonosov Moscow State University, 119991 Moscow, Russia
[2]Earth's Cryosphere Institute, Tyumen Scientific Center SB RAS, 625026 Tyumen, Russia
***Corresponding author:** nataliya-belova@yandex.ru
Received: March 24th, 2023 / Accepted: September 4th, 2023 / Published: October 10th, 2023
https://DOI-10.24057/2071-9388-2023-2810

ABSTRACT. Climate change observed in the Arctic affects all components of the natural environment, including the state of permafrost. The purpose of this study is to quantify the response of permafrost in various landscapes to changing climatic parameters. The results of long-term field observations (1978-2021) of the thermal regime of permafrost on the Western Yamal are presented. Along with the increase in mean annual air temperatures, the mean annual ground temperature over the past 43 years has increased by 1.5-2.2°C. The maximum increase of permafrost temperature values is observed on flat and polygonal tundra, the minimum increase is typical for flooded lake basins. A decrease in the annual permafrost temperature amplitude was revealed. That is caused by a rapid increase in the air temperature of the cold period, an increase in the snow thickness and an increase in soil moisture in the active layer. The shrinking in ground temperature amplitude at a depth of 5 m is 0.5-3.6°C. A trend of reducing depth of zero annual amplitude from 12-18 m (1980) to 13-16 m (2021) has been revealed.

KEYWORDS: permafrost, permafrost thermal regime, climate warming, depth of zero annual amplitude, monitoring, Western Yamal

CITATION: Nikitin K. A., Belova N. G., Vasiliev A. A. (2023). Thermal Regime Of Permafrost On The Western Yamal Under Climate Warming. Geography, Environment, Sustainability, 3(16), 75-82
https://DOI-10.24057/2071-9388-2023-2810

ACKNOWLEDGEMENTS: The work was supported by the Russian Science Foundation project 22-27-00181.

Conflict of interests: The authors reported no potential conflict of interest.

INTRODUCTION

Assessment of the permafrost state under conditions of climate change is a priority problem in recent decades in permafrost science (Romanovsky et al., 2010; AMAP, 2011, 2021; Stocker et al., 2013; Biskaborn et al., 2019; Noetzli et al., 2021; Streletskiy et al., 2021). The cryosphere and, in particular, permafrost, influence the planetary water and carbon cycles, the evolution of the Arctic and subarctic ecosystems, the stability of the Arctic infrastructure, etc.

It has been established that the response of the permafrost to climate change differs in time and space in the regions of the permafrost zone (Brown et al., 2000; Romanovsky, 2006; Khrustalev et al., 2008; Vasiliev et al., 2011; Streletskiy et al., 2015; Sergeev et al., 2016; Vasilchuk et al., 2017; Kaverin et al., 2017; Farquharson et al., 2019; Kotov, Khilimonyuk, 2021; Tregubov et al., 2021). Over the past 50 years, the temperature of permafrost has increased, as well as the active layer thickness (ALT); there has been a decrease in the area and thickness of permafrost near its southern boundary (Pavlov et al., 2007; Moskalenko, 2009; Drozdov et al., 2010; Dubrovin, Kritsuk, 2011; Konstantinov et al., 2014; Vasilchuk et al., 2015a,b; Biskaborn et al., 2019; Vasiliev et al., 2020). Thus, in the western part of the Russian Arctic the long-term monitoring of the thermal state of permafrost indicated permafrost temperature increase rates from 0.01 to 0.06–0.07°C/year across cryogenic landscapes (Malkova et al., 2022). At Marre-Sale area at Westen Yamal the previous studies indicated the highest rate of permafrost temperature increase in the western Russian Arctic since the 1970s with temperatures at the depth of zero annual amplitude increasing 0.06°C/year (Vasiliev et al., 2020).

No general patterns of frozen ground changes across the entire permafrost zone have been identified. In this regard, studies based on long-term observational data obtained by a single method in different regions and types of permafrost are of great importance.

The aim of the work is to reveal the changes in thermal regime of permafrost in a changing climate on the key site of Western Yamal. The results made it possible to assess the change in the thermal state of the permafrost over the past 50 years and to identify general patterns and quantitative indicators of the temperature regime for Western Yamal, which can be used for a general understanding of the processes of transformation of the permafrost.

MATERIALS AND METHODS

Study area

The study area is located on the coast of the Kara Sea near the Marre-Sale weather station (Fig. 1). The Marre-Sale research station is located in bioclimatic subzone D of a typical tundra (Walker et al., 2005; Oblogov et al., 2020) within the third marine terrace with altitudes of 15-30 m above sea level. The marine terrace is dissected by a system of water tracks, gullies and lake basins. The northern part of the research area is limited by the floodplain of the local river with absolute elevations of 0.5-3.0 m. The landscape structure of the study area is representative of the entire range of typical Yamal tundra. Lakes occupy about 12% of the territory. A comparison of data on vegetation cover dynamics over several years shows a relatively stable state of vegetation. Most species are characterized by irregularly cyclic changes in their occurrence associated with climate (Anthropogenic changes…, 2006). Although recent studies reveal NDVI changes in the Arctic since the 1980s (Walker et al., 2012; Berner et al., 2020; Jespersen et al., 2023), these changes are spatially heterogeneous and can include not only an increase but also a decrease of NDVI. In the study area, the type of vegetation cover has not changed significantly during ground temperature monitoring.

The geological profile is represented by two complexes of Late Quaternary deposits (Streletskaya et al., 2021). The upper complex is composed of continental (alluvial, lacustrine) sands and sandy loams on average 10 m thick, the lower complex is marine and shallow marine saline clays and loams with rare sand interlayers, and its visible thickness is about 20 m.

The territory belongs to the area of continuous permafrost distribution. Permafrost of the third marine terrace has a two-layer structure. The upper layer down to the depth of 90 m (Kanevskiy et al., 2005) is represented by hard frozen ground, the lower permafrost layer contains no ice due to the high salinity of the sediments. The hard-frozen rocks contain ice inclusions, lenses and interlayers of visible ice. The average annual ground temperature at a depth of zero annual amplitudes varies from -2.5 to -7.5°C depending on the location. The depth of seasonal thawing varies from 0.4 to 2.2 m depending on the type of landscape.

The thickness of the hard frozen strata on the floodplain is about 40 m. Geophysical studies have shown the presence of a closed talik up to 10 m deep under the Marre-Yakha River. The outlines of the talik repeat the relief of the channel (Melnikov et al., 2010).

Within the plains in the permafrost zone, there is a strong correspondence between the average annual temperature of frozen ground, the ALT, and the type of landscape (Landscapes of the permafrost zone ..., 1983). Each landscape is characterized by specific morphology, ground composition, moisture regime of the active layer, type of tundra soils, vegetation, temperature regime of permafrost and depth of seasonal thawing. Therefore, permafrost in dominant landscapes was chosen as the object of geocryological monitoring. To characterize landscapes, a simplified classification (von Fisher et al., 2010) was used. Landscapes and observation sites (boreholes) IDs are given in Table 1.

Western Yamal is located in the subarctic zone, a moderately cold humid Atlantic province of the Western Arctic climatic region, characterized by a harsh climate. Analysis of climate change for the period 1970-2020 was made on the basis of meteorological data from the open database of the All-Russian Research Institute of Hydrometeorological Information – the World Data Center[1] and the archive of observations of the Marre-Sale weather station.

Climate warming has been observed since the beginning of the 1970s (Fig. 2). Compared with 1961-1990, the mean annual air temperature (MAAT) has increased by 5.9°C, the mean annual temperature amplitude has decreased by 5.2°C. Its decrease depends on the rapid increase in the average winter temperature by 7.3°C. The mean summer air temperature is characterized by a less pronounced warming of 4.1°C. The greatest amount of precipitation falls

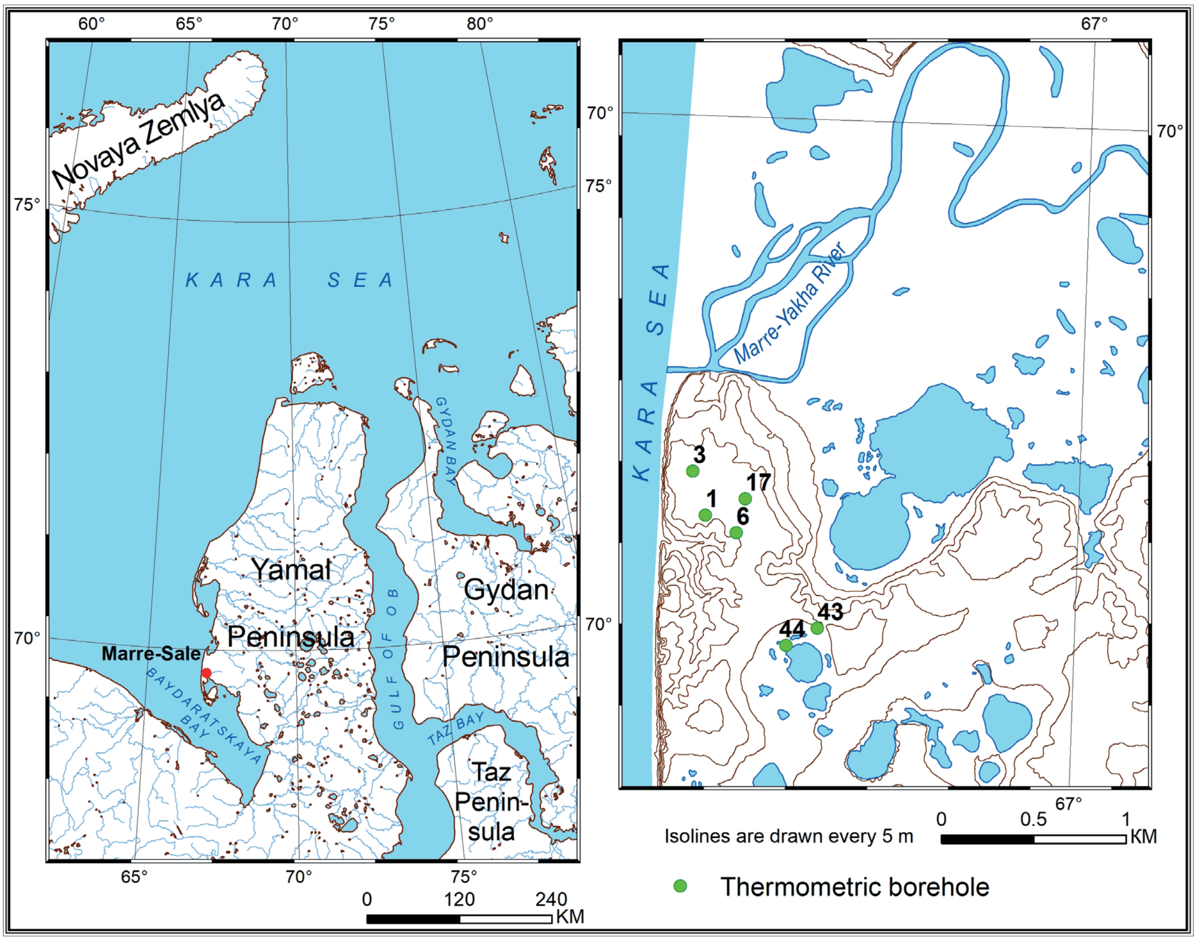

Fig. 1. Location of the study area and observation boreholes

[1]http://meteo.ru/data/, accessed 14.11.2021

Table 1. Conditions for the permafrost temperature regime monitoring within one geomorphological level (III^rd marine terrace)

Landscape	Monitoring site ID (borehole)
Dry landscapes	
Sand fields (6)*	43
Well-drained flat tundra (24)	6
Moist landscapes	
Wet tundra (7)	1
Wet landscapes	
Polygonal saturated tundra (17)	3
Water tracks and gullies (3)	Not observed
Flooded landscapes	
Lake basins (20)	44
Peatlands (4)	17

*The proportion of landscapes is given in parentheses, in % of the total area (Landscapes of permafrost …, 1983).

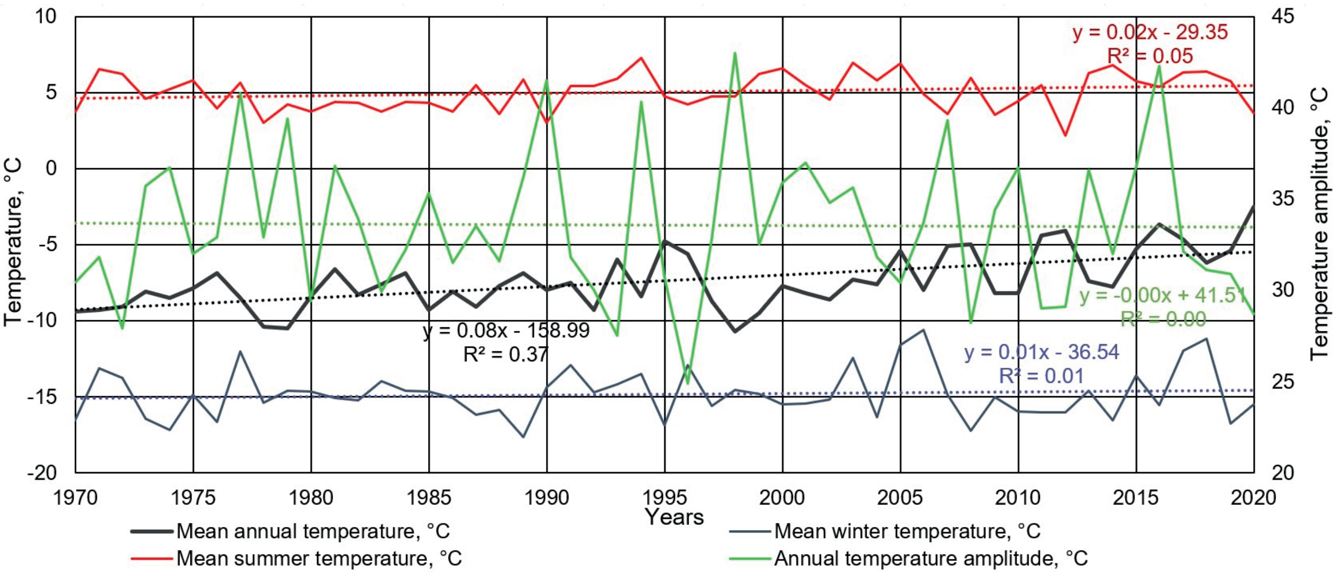

Fig. 2. Changes in the main meteorological parameters in Western Yamal (1970-2020). Dotted lines show linear trends

in the summer-autumn transitional period, mainly in August-September. Since 1970, total precipitation value has increased by 105 mm from 297 mm standard amount of annual precipitation (averaged over 1961–1990). For all months (except December), the average monthly temperature increase was observed during the specified period.

The maximum snow depth per season (the highest value of 3 snow stakes) had been increased from 16 to 49 cm from 1970 to 2020. Snow density ranges from 0.22 g/cm^3 in autumn to 0.45 g/cm^3 in spring, with an average per season of 0.32 g/cm^3. Table 2 summarizes the results of our observations of snow distribution over landscapes in comparison with the data on the weather station site. Observations were carried out from 1984 to 1992 every 10 days, starting from the day a stable snow cover was established to the day the snow cover began to break – the end of April. For each measurement, the ratio of snow depth on a particular landscape to one at the weather station site was found. Then, for each landscape, we calculated the average ratio for the entire time of snow accumulation. Observations of the spatial distribution of snow cover showed that each landscape type is characterized by a more or less stable ratio of snow height in dominant landscapes compared with the weather station site – the individual coefficient of snow accumulation (Table 2).

Table 2. Snow accumulation coefficient in monitoring sites

	Site ID (borehole)					
	1	3	6	17	43	44
Snow accumulation coefficient (ratio of snow depth near borehole to snow height at the weather station)	1.0	0.86	1.03	0.87	0.86	1.32

Methods

The study of the permafrost temperature regime at the geocryological research station was carried out in specially equipped boreholes with a depth of 10 m. The boreholes were drilled in 1978, drilling was accompanied by a detailed description and sampling of the core. The boreholes are protected by a casing pipe within the mean annual ALT, additionally buried in the frozen ground at 1 m depth. The upper part of the pipe, protruding 0.2 m above the day surface, is filled with heat-insulating materials (peat or foam insulation). The inlet of the pipe is tightly closed with a lid that prevents precipitation and condensate from entering the well.

At the time of drilling, the moisture content (ice content) of permafrost and active layer was determined. Since 2016, the sampling and determination of moisture/ice content of the active layer and the upper permafrost horizon has been carried out annually at the end of the warm season by drilling other boreholes at a certain site.

In 1978-1990 temperature measurements were carried out by the Russian Institute of Hydrogeology and Engineering Geology every ten days, and after 1990 once a year at the end of the warm period using soil thermometers (Pavlov, 1997). Thermometers were installed at depths of 0.5; 1 m and further every meter. Measurement accuracy was ±0.1°C. Since 1996, measurements in wells have been carried out by the Earth's Cryosphere Institute, Tyumen Scientific Center SB RAS. In 2006, four-channel data loggers HOBO U12-008 with thermistor sensors with a measurement accuracy of ±0.2°C were installed. The sensors are installed at depths of 0.02; 2; 3; 5 and 10 (12) m. Readings at a depth of 0.02 m correspond to the temperature under vegetation. In the well ID 1, additional loggers were installed at the depths of 4; 6 and 8 m. Temperature measurement is made every 6 hours.

RESULTS

Mean annual permafrost temperature

The mean annual temperature of the permafrost, determined at the level of zero annual amplitude, increased in all observed landscapes from 1978 to 2021 (Fig. 3).

Two groups of landscapes can be distinguished according to the mean annual permafrost temperature values. The first group includes "cold" landscapes of flat and polygonal tundra, confined to positive landforms. Here, the average annual temperatures in 1978-79 were -5.8…-7.4°C, and by 2021 they reached -3.7…-5.2°C. The "warm" landscapes of the second group with comparatively high mean annual permafrost temperatures include wet or flooded landscapes of lake basins and water tracks; river floodplain also belongs to this landscape group. The average annual temperatures had been increasing there from -4.2°C in 1978 to up to -2.7…-3.6°C in 1996-2002. Such a stable difference in temperatures of the two groups is explained by increased snow accumulation in negative landforms. The lowest temperatures are characteristic of polygonal and well-drained flat tundra (boreholes 3 and 6, respectively), and the highest temperatures are characteristic of lake basins (borehole 44). During 1978-2021 the average temperature increase in the landscapes of the first group was approximately 2.2°C, and in the second group – 1.5°C.

Following the change in air temperature, the change in the mean annual temperature of the permafrost was uneven over time. Positive deviations from the linear trend were observed in 1985 and 1996, and negative deviations in 1989 and 2001. Since 2007, the temperature has risen evenly in all observed landscapes.

Thus, under conditions of climate warming, landscapes of a typical tundra have a different response to warming, expressed in the mean annual temperature of the permafrost.

Annual temperature amplitude at 5 m depth

The shifting of permafrost thermal regime is not limited to an increase in the mean annual temperature. To study the effect of climate warming on permafrost thermal regime, the change in the annual temperature amplitude at the depth of 5 m was considered. The depth of 5 m is not special and was chosen for analysis because surface effects are already insignificant here, but all the features of the formation of the temperature amplitude are well reflected. As an example, Figure 4 shows the temporal changes of the permafrost temperature at a depth of 5 m in borehole

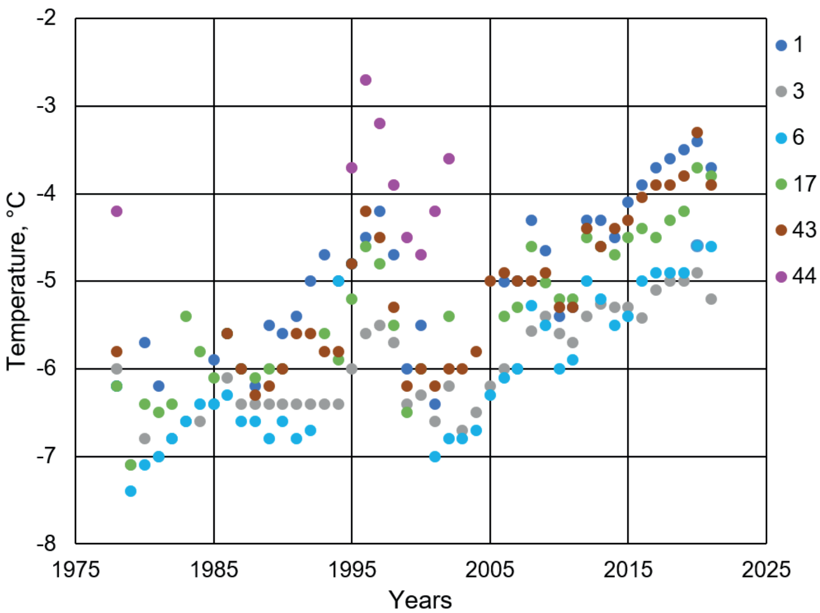

Fig. 3. Changes in the mean annual temperature of permafrost in dominant landscapes. The legend contains the site ID (borehole)

1, located in the wet tundra landscape. The situation is similar in all the studied landscapes.

Figure 5 shows the change in the amplitude of permafrost temperature fluctuations at the depth of 5 m over time. There is a clear downward trend in the amplitude of annual fluctuations in time for all the landscapes. The almost synchronous reduction occurs mainly due to the increase in winter temperatures, which has accelerated since the beginning of the century. The strongest reduction in the amplitude occurred in dry landscapes; in moistened and wet areas the reduction was less pronounced.

In addition to air temperature, the amplitude of annual permafrost temperature fluctuations is most affected by the height of the snow cover and the humidity (ice content) of the soils of the active layer due to the extra energy necessary to phase transitions of water in the active layer.

The relationship between the values of the annual temperature amplitude at the depth of 5 m and the maximum snow depth was studied, taking into account the conversion factors. As at the key site the snow depth increases with climate warming (Oblogov et al., 2020), the amplitude of permafrost temperature fluctuations rapidly decreases (Fig. 6). This trend is most pronounced within wet tundra, and least pronounced within dry tundra and sand fields. With a power-law approximation, the radius of correlation between the amplitudes and snow depth for drained tundra is $R^2 = 0.37$.

Soil moisture measurements in active layer were carried out in 1978 during boreholes drilling and in 2016-2021. This made it possible to estimate the change in the weighted average water content in the active layer of various landscapes over time. In the water tracks, with an increase in permafrost temperature by an average of 1.5°C, the moisture content of the active layer remained unchanged, close to full water saturation. In the rest of the landscapes, characterized by a more pronounced increase in the mean annual permafrost temperature, the average weight humidity changed from 20-23% (1978) to 24-27% (2021).

The depth of zero annual ground temperature amplitude

The established decrease in the amplitude of temperature fluctuations causes a decrease in the depth of the bottom of the layer of annual heat exchanges. It is

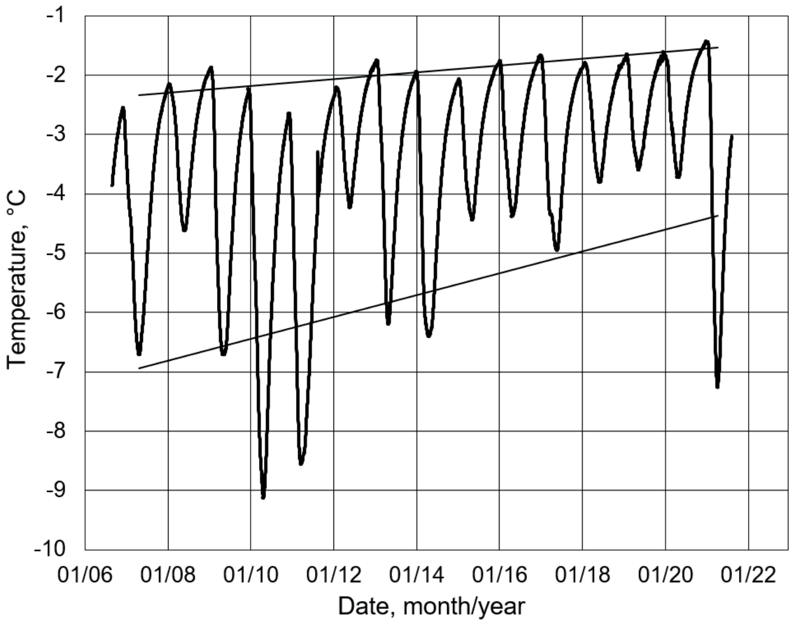

Fig. 4. Time course of permafrost temperature at the depth of 5 m in borehole 1 (wet tundra)

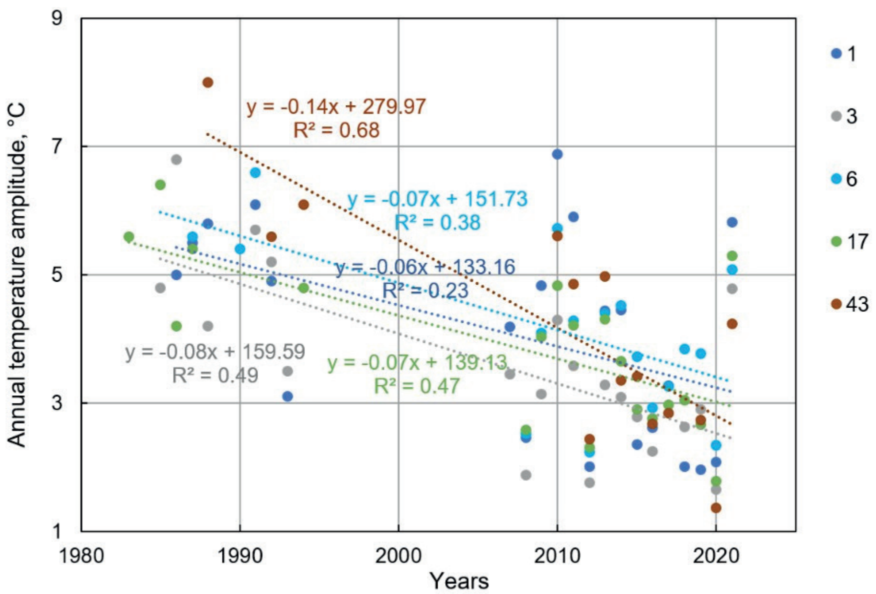

Fig. 5. Change in the annual ground temperature amplitude at a depth of 5 m in time. The legend contains the site ID (borehole). Dotted lines show linear trends

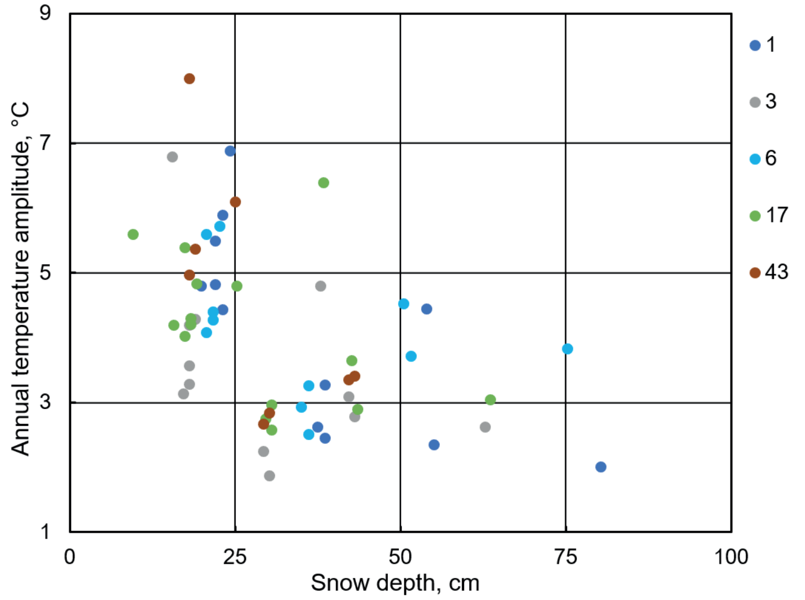

Fig. 6. Dependence of the annual ground temperature amplitude at the 5 m depth on the snow cover thickness. The legend contains the site ID (borehole)

determined by the boundary below which the difference in annual temperature fluctuations does not exceed 0.2°C. Given that the depth of the layer of annual heat transfers exceeds the depth of the boreholes, the level of zero annual amplitude is obtained by extrapolating the temperature curves down the section. The depth of zero annual amplitude decreased in all landscapes (Fig. 7). The most intense decrease is characteristic of the polygonal tundra (borehole 3), the least – for flat-topped peatlands (borehole 17).

DISCUSSION

Direct monitoring measurements of frozen ground temperature in 10 to 12-m deep boreholes conducted in Western Yamal since 1978 showed how the thermal state of permafrost is changing in various landscapes under the conditions of climate warming.

The mean annual permafrost temperature increased both in the initially "cold" landscapes located on positive landforms and in "warm" landscapes located in topographic lows and characterized by higher ground temperatures due to the influence of increased snow accumulation. Due to the increase in winter air temperatures, the amplitude of annual temperature fluctuations in permafrost, primarily in drained landscapes, also decreased. This led to a general decrease in the depth of zero annual temperature amplitude.

A pronounced reduction in the depth of zero annual amplitude over the past 40 years is observed all around the western Russian Arctic both in discontinuous and continuous permafrost zones (Malkova et al., 2022). The studied key site is northernmost in Western Russian Arctic among the areas with long-term permafrost monitoring. It is characterized by lower temperatures compared to the sites in discontinuous permafrost zone (Vasiliev et al., 2020). On the contrary, the rates of permafrost temperature rise here are higher compared to more southern regions, where permafrost temperatures are close to zero and latent heat effects related to melting ground ice becomes important (Romanovsky et al., 2018; Vasiliev et al., 2020).

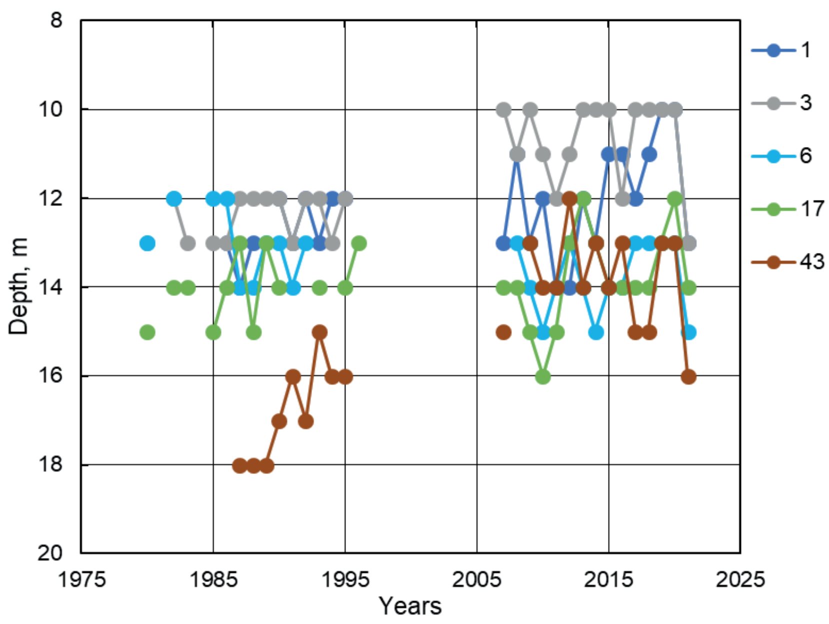

Fig. 7. Change in the depth of zero annual amplitude in time. The legend contains the site ID (borehole)

Currently, the permafrost of the Marre-Sale area is at the initial stage of degradation (Vasiliev, 2020) and is characterized by relatively low ground temperatures and increasing ALT. Further air temperature rise will lead to the next, metastable stage of permafrost degradation when thawing of the transient layer at the permafrost top occurs and the depth of permafrost table increases. Such a situation is observed now at monitoring sites situated more than 150 km south mostly in sporadic, discontinuous and continuous permafrost zones – Kumja, Kape Bolvanskiy, Vorkuta and north of Novy Urengoy (Vasiliev et al., 2020; Malkova et al., 2022). This transition to the next permafrost degradation stage will not occur simultaneously within different landscapes of the Marre-Sale area.

CONCLUSIONS

1. Climate warming in Western Yamal began in the 1970s and continues now. The mean annual air temperature has increased by 6.9°C (from -9.4°C in 1970 to -2.5°C in 2020), while the mean winter temperature is rising faster than the summer temperature. An increase in the mean annual air temperature is accompanied by an increase in the annual precipitation by 100 mm, the height of the snow cover has increased from 16 to 49 cm.

2. For 40 years of observations, the mean annual temperature of the permafrost increased by 1.5-2.2°C. At the same time, the maximum increase in the mean annual temperature is observed in the landscapes of flat and polygonal tundra associated with positive landforms.

3. Climate warming leads to a decrease in the amplitude of annual permafrost temperature fluctuations. The reduction in amplitude at a depth of 5 m was by 0.5-3.6°C in 1983-2021. The main reasons for this are the faster increase in air temperature in the cold period compared to the warm period, an increase in the height of the snow cover, and an increase in soil moisture in the active layer.

4. There is a tendency to reduction of the depth of the zero annual temperature amplitude from 12-18 m (1980) to 13-16 m (2021).

Thus, climate warming in the last 50 years has led to a significant change in the thermal regime of the permafrost – an increase in the mean annual temperature of the permafrost, a reduction in the amplitude of annual ground temperature fluctuations, and a decrease of the depth of zero annual amplitude. At the same time, despite noticeable climatic changes, the permafrost generally retains a stable state.

REFERENCES

AMAP (2011). Snow, Water, Ice and Permafrost in the Arctic (SWIPA). Arctic Monitoring and Assessment Programme (AMAP), Oslo.

AMAP (2021). AMAP Arctic Climate Change Update 2021: Key Trends and Impacts. Arctic Monitoring and Assessment Programme (AMAP), Tromsø, Norway. viii+148pp.

Anthropogenic changes in the ecosystems of the West Siberian gas-bearing province (2006). Ed. Moskalenko N.G. Tyumen: ECI SB RAS, 357 p. (in Russian)

Berner L.T., Massey R., Jantz P., Forbes B.C., Macias-Fauria M., Myers-Smith I., et al. (2020). Summer warming explains widespread but not uniform greening in the Arctic tundra biome. Nat Commun.; 11: 1–12. Pmid:32963240.

Biskaborn B.K., Smith S.L., Noetzl J. et al. (2019). Permafrost is warming at a global scale. Nature communications, 10; 264.

Brown J., Hinkel K.M., Nelson F.E. (2000). The circumpolar active layer monitoring (CALM) program: research designs and initial results. Polar Geogr. 24 (3), 166-258.

Drozdov D.S., Ukraintseva N.G., Tsarev A.M., Chekrygina S.N. (2010). Changes of permafrost temperature field and geosystem state on the Urengoy oil-gas-field territory during the last 35 years (1974–2008). Earth's Cryosphere, 14(1), 22-31 (in Russian with English summary). Available at: http://earthcryosphere.ru/arch/eng2010-1/drozdov_eng2010-1/

Dubrovin V.A. and Kritsuk L.N. (2011). Evaluation of the permafrost dynamics and temperature regime in the Marre-Sale area according to monitoring observations. Proceedings of the Fourth Conference of Geocryologists of Russia. Moscow: MSU. Vol. 2. 236-243 (in Russian).

Farquharson L.M., Romanovsky V.E., Cable W.L., Walker D.A., Kokelj S.V., Nicolsky D. (2019). Climate change drives widespread and rapid thermokarst development in very cold permafrost in the Canadian High Arctic. Geophysical Research Letters, 46, 6681-6689. DOI: 10.1029/2019GL082187.

Jespersen R.G., Anderson-Smith M., Sullivan P.F., Dial R.J., Welker J.M. (2023) NDVI changes in the Arctic: Functional significance in the moist acidic tundra of Northern Alaska. PLoS ONE 18(4): e0285030. DOI: 10.1371/journal.pone.0285030.

Kanevskiy M.Z., Streletskaya I.D., Vasiliev A.A. (2005). Formation of cryogenic structure of Quaternary sediments in Western Yamal (by the example of Marre-Sale area). Earth's Cryosphere, 9(3), 16-27 (in Russian with English abstract).
Available at: http://earthcryosphere.ru//archive/2005_3/2005_3_16-27.pdf

Kaverin D.A., Pastukhov A.V., Novakovskiy A.B. (2017). Active layer thickness dynamics in the tundra permafrost-affected soils: a calm site study, the European North of Russia. Earth's Cryosphere, 21(6), 30-38. Available at: http://earthcryosphere.ru/arch/eng2017-6/

Khrustalev L.N., Klimenko V.V., Emelyanova L.V., Ershov E.D., Parmuzin S.Yu., Mikushina O.V., Tereshion A.G. (2008). Dynamics of permafrost temperature in southern regions of cryolithozone under different scenarios of climate change. Earth's Cryosphere, 12(1), 3-11 (in Russian with English abstract). Available at: http://earthcryosphere.ru//archive/2008_1/01.Khrustalev_1_2008.pdf

Konstantinov P.Ya., Fedorov A.N., Ugarov I.S., Argunov R.N., Susdalov D.A., Iijima Y. (2014). Results of investigations on interannual variability of seasonal thaw depth in the vicinity of Yakutsk. Earth's Cryosphere, 18(4), 20-28. Available at: http://earthcryosphere.ru/arch/eng2014-4/

Kotov P.I., Khilimonyuk V.Z. (2021). Building stability on permafrost in Vorkuta, Russia. Geography, Environment, Sustainability, 14(4), 67-74. DOI: 10.24057/2071-9388-2021-043.

Landscapes of the permafrost zone of the West Siberian gas-bearing province (1983). Ed. Melnikova E.S. Novosibirsk: Nauka, 164 p. (in Russian).

Malkova G., Drozdov D., Vasiliev A., Gravis A., Kraev G., Korostelev Y., Nikitin K., Orekhov P., Ponomareva O., Romanovsky V. et al. (2022). Spatial and Temporal Variability of Permafrost in the Western Part of the Russian Arctic. Energies, 15, 2311. DOI: 10.3390/en15072311.

Melnikov V.P., Skvortsov A.G., Malkova G.V. et al. (2010). Seismic studies of frozen ground in Arctic areas. Russian Geology and Geophysics, 51(1), 136-142. DOI: 10.1016/j.rgg.2009.12.011.

Moskalenko N.G. (2009). Permafrost and vegetation changes in the Nadym region of West Siberian northern taiga due to the climate change and technogenesis. Earth's Cryosphere, 13(4), 18-23 (in Russian with English abstract).
Available at: http://earthcryosphere.ru//archive/2009_4/02.Moskalenko_4_2009.pdf

Noetzli, J., Christiansen, H.H., Hrbacek, F., Isaksen, K., Smith, S.L., Zhao, L., and Streletskiy D.A. (2021). Cryosphere – 1) Permafrost thermal state [in «State of the Climate in 2020»]. Bulletin of the American Meteorological Society 102(8): 42-45. DOI: 10.1175/BAMS-D-21-0086.1.

Oblogov G.E., Vasiliev A.A., Streletskaya I.D., Zadorozhnaya N.A., Kuznetsova A.O., Kanevskiy M.Z., Semenov P.B. (2020). Methane content and emission in the permafrost landscapes of Western Yamal, Russian Arctic. Geosciences, 10, 412. DOI: 10.3390/geosciences10100412.

Pavlov A.V. (1997). Permafrost-climatic monitoring of Russia: methodology, results of observation and forecast. Earth's Cryosphere, 1(1), 47-58 (in Russian with English abstract). Available at: http://earthcryosphere.ru//archive/1997_1/47-58.pdf.

Pavlov A.V., Malkova G.V., Skachkov Yu.B. (2007). Modern tendencies in the evolution of thermal state of cryolithozone under the climate changes. Proceedings of the International Conference «Cryogenic Resources of Polar Regions», Salekhard, v. 1, 34-38 (in Russian with English summary).

Romanovsky V.E. (2006). Thermal state of permafrost in Alaska during the past 20 years. Proceedings of the International Conference «Earth's cryosphere assessment: theory, applications and prognosis of alterations», Tyumen, v.1, 96-101 (in English and Russian).

Romanovsky V., Drozdov D., Oberman N., Malkova G., Kholodov A., Marchenko S., Moskalenko N., Sergeev D., Ukraintseva N., Abramov A., Vasiliev A. (2010). Thermal state of permafrost in Russia. Permafrost Periglacial Process. 21(2), 136-155.

Romanovsky V., Smith S., Isaksen K., Shiklomanov N., Streletskiy D., Kholodov A., Christiansen H., Drozdov D., Malkova G. and Marchenko S. (2018) Terrestrial Permafrost. In: 'State of the Climate in 2017', Bull. Am. Meteorol. Soc. 99 S161–5.

Sergeev D.O., Stanilovskaya J.V., Perlshtein G.Z., Romanovsky V.E., Bezdelova A.P., Alexutina D.M., Bolotyuk M.M., Khimenkov A.N., Kapralova V.N., Motenko R.G., Maleeva A.N. (2016). Background geocryological monitoring in Northern Transbaikalia region. Earth's Cryosphere, 20(3), p. 24-32.

Stocker T.F., Qin D., Plattner G.-K., Tignor M., Allen S.K., Boschung J., Nauels A., Xia Y., Bex V. and Midgley P.M. (eds.). IPCC, 2013: Climate Change 2013: The Physical Science Basis. Contribution of Working Group I to the Fifth Assessment Report of the Intergovernmental Panel on Climate Change. Cambridge University Press, Cambridge, United Kingdom and New York, NY, USA, 1535 pp.

Streletskaya I.D., Pismeniuk A.A., Vasiliev A.A., Gusev E.A., Oblogov G.E. and Zadorozhnaya N.A. (2021) The Ice-Rich Permafrost Sequences as a Paleoenvironmental Archive for the Kara Sea Region (Western Arctic). Front. Earth Sci. 9:723382. DOI: 10.3389/feart.2021.723382

Streletskiy D.A., Sherstiukov A.B., Frauenfeld O.W., Nelson F.E. (2015). Changes in the 1963-2013 shallow ground thermal regime in Russian permafrost regions. Environ. Res. Lett., 10, 125005.

Streletskiy D.A., Maslakov A.A., Streletskaya I.D., Nelson F.E. (2021). Permafrost Regions In Transition: Introduction. Geography, Environment, Sustainability, 14(4):6-8. DOI: 10.24057/2071-9388-2021-081.

Tregubov O.D., Glotov V.E., Konstantinov P.Y., Shamov V.V. (2021). Hydrological conditions of drained lake basins of the Anadyr Lowland under changing climatic conditions. Geography, Environment, Sustainability, 14(4), 41-54, DOI: 10.24057/2071-9388-2021-030.

Vasilchuk A.C. and Vasilchuk Yu.K. (2015a). Engineering-geological and geochemical conditions of polygonal landscapes on the Bely Island (the Kara Sea). Engineering Geology, 1, 50-72 (in Russian with English summary).

Vasilchuk A.C. and Vasilchuk Yu.K. (2015b). Engineering-geological and geochemical conditions of polygonal landscapes in the area of the Tambey River mouth (the north of the Yamal Peninsula). Engineering Geology, 4, 36-54; 82-83 (in Russian with English summary).

Vasilchuk Yu.K., Budantseva N.A., Chizhova Yu.N. (2017). Rapid degradation of palsa near the Abez settlement, north-east of the European Russia. Arctic and Antarctica, 3, 30-51 (in Russian). DOI: 10.7256/2453-8922.2017.3.24432.

Vasiliev A., Drozdov D., Gravis A., Malkova G., Nyland K. and Streletskiy D. (2020). Permafrost degradation in the Western Russian Arctic. Environmental Research Letters, 15(4): 045001. DOI: 10.1088/1748-9326/ab6f12.

Vasiliev A.A., Gravis A.G., Gubarkov A.A., Drozdov D.S., Korostelev Yu.V., Malkova G.V., Oblogov G.E., Ponomareva O.E., Sadurtdinov M.R., Streletskaya I.D., Streletskiy D.A., Ustinova E.V., Shirokov R.S. (2020). Permafrost degradation: results of the long-term geocryological monitoring in the Western sector of Russian Arctic. Earth's Cryosphere, 24 (2), 15–30. Available at: http://earthcryosphere.ru/arch/eng2020-2/Vasiliev_2020_2_eng/

Vasiliev A.A., Streletskaya I.D., Shirokov R.S., Oblogov G.E. (2011). Coastal permafrost evolution of Western Yamal in context of climate change. Earth's Cryosphere, 15 (2), 56-64 (in Russian with English summary). Available at: http://earthcryosphere.ru/arch/eng2011-2/

von Fischer J.C., Rhew R.C., Ames G.M., Fosdick B.K., von Fischer P.E. (2010). Vegetation height and other controls of spatial variability in methane emissions from the Arctic coastal tundra at Barrow, Alaska. J. Geophys. Res., 115, G00I03.

Walker D.A., Raynolds M.K., Daniëls F.J.A., Einarsson E., Elvebakk A., Gould W.A., Katenin A.E., Kholod S.S., Markon C.J., Melnikov E.S., Moskalenko N.G., Talbot S.S., Yurtsev B.A. (2005). The Circumpolar Arctic Vegetation Map. J. Veg. Sci., 16 (3), 267-282.

Walker D.A., Epstein H.E., Raynolds M.K., Kuss P., Kopecky M.A., Frost G.V., Daniëls F.J.A., Leibman M.O., Moskalenko N.G., Matyshak G.V. (2012). Environment, vegetation and greenness (NDVI) along the North America and Eurasia Arctic transects. Environ. Res. Lett. 7 015504. DOI: 10.1088/1748-9326/7/1/015504.

RESEARCH PAPER

MONITORING OF ANTHROPOGENIC IMPACT ON THE BAIKAL NATURAL TERRITORY: MUNISIPAL LEVEL

Evgenii V. Antonov[1], Yuri R. Belyaev[1], Viktoria R. Bityukova[1], Andrei V. Bredikhin[1], Vladimir S. Dehnich[2], Ekaterina A. Eryomenko[1], Natalia A. Koldobskaya[1], Oleg E. Prusikhin[1], Sergei G. Safronov[1], Nikolay S. Kasimov[1]

[1]Lomonosov Moscow State University, Faculty of Geography, Moscow, 119991, Russia

[2]Department of Ecology and Nature Management, Lomonosov Moscow State University, 010010, Republic of Kazakhstan, Astana, Kazhymukana str., 11, Kazakhstan branch

*Corresponding author: v.r.bityukova@geogr.msu.ru

Received: February 27th, 2023 / Accepted: September 4th, 2023 / Published: October 10th, 2023

https://DOI-10.24057/2071-9388-2023-2779

ABSTRACT. The purpose of the presented study is to develop a methodology for assessing the anthropogenic impact on the environment in the municipalities of the Baikal Natural Territory (BNT) and applying the obtained methodology to the studied territory. The article analyzes the existing methodological approaches to the assessment of anthropogenic impact on the environment. To carry out a comprehensive integrated assessment, the authors proposed an algorithm for calculating the anthropogenic impact index based on 22 indicators integrated into 7 subindexes (impact on the atmosphere, water and forest resources, agricultural impact, solid waste, disturbed lands and objects of accumulated harm, as well as background impact).

The weight of the indicators was determined by interviewing experts representing the scientific community (leading experts in the field of integrated assessments of certain types of impacts or specialists in the field of environmental problems of the BNT), the expert community (leading analytical agencies developing environmental ratings), as well as the environmental management system of the regions included in the BNT. The inertial nature of the anthropogenic impact characteristic of municipalities within the boundaries of the BNT, as well as the general tendency to reduce the impact, has been revealed. At the same time, the absence of positive changes in the environmental state was noted, especially characteristic of the largest impact centers with their inherent unfavorable environment, which suggests the need to take measures to reduce the impact. The advantage of the methodology proposed by the authors can be considered the possibility of extending monitoring in the future, which opens up the possibility of using this algorithm to assess the environmental situation and form environmental policy priorities. The analysis of the results confirmed the quality of the integrated assessment methodology and showed that the districts, cities and towns of the BNT are highly polarized in terms of the level of anthropogenic impact concentrated in certain areas, primarily in the zone of atmospheric influence. The main strengthening of the AI is characteristic of municipalities located along transport corridors, the axis of which is the Trans-Siberian Railway, The Baikal–Amur Mainline and the «Power of Siberia» gas pipeline.

KEYWORDS: municipalities, municipal level, environmental policy, spatial development, integral index, dynamics of a comprehensive assessment of anthropogenic impact

CITATION: Antonov E. V., Belyaev Y. R., Bityukova V. R., Bredikhin A. V., Dehnich V. S., Eryomenko E. A., Koldobskaya N. A., Prusikhin O. E., Safronov S. G., Kasimov N. S. (2023). Monitoring Of Anthropogenic Impact On The Baikal Natural Territory: munisipal Level. Geography, Environment, Sustainability, 3(16), 83-91
https://DOI-10.24057/2071-9388-2023-2779

ACKNOWLEDGEMENTS: This research was performed within the framework of project No. 8/D-2021 «Development of an integrated assessment of anthropogenic impact and the state of the environment of Lake Baikal», the topic of the state assignment of the Department of Economic and Social Geography of Russia «Modern dynamics and factors of socio-economic development of regions and cities of Russia and neighboring countries» (No.21051100161-9), topic of the state assignment of the Department of Geomorphology and Paleogeography «Evolution of the natural environment in the Cenozoic, relief dynamics, geomorphological hazards and risks of nature management» (No. 121040100323-5).

Conflict of interests: The authors reported no potential conflict of interest.

INTRODUCTION

One of the actual tasks of forming public guidelines for spatial environmental policy that investors and other interested parties can use for responsible investment or following the sustainable development agenda is the introduction of a permanent system for monitoring the environmental situation, which requires both a component-by-component assessment of individual indicators and a comprehensive anthropogenic impact (index AI). Differentiation of spatial characteristics of AI is characteristic of all levels of the administrative-territorial hierarchy, but the municipal level is of fundamental importance, since the scenarios of spatial development and closely related changes in anthropogenic impact (AI) are best displayed if municipalities are used as basic municipal «territorial cells».

Existing approaches to the assessment of regions or cities can theoretically be applied to the assessment of municipalities (at least at the level of municipal districts and urban/municipal districts) (Bityukova 2020; Kasimov 2017). For municipalities indicators of emission from stationary sources, water consumption, wastewater, household and industrial waste are important. However, the municipal level also has a number of limitations: financial weakness of local budgets, statistical support. The methodology for assessing the territorial differentiation of AI for municipal levels should be different: a fundamentally different level of detail is needed, a special method for calculating emission from mobile sources, the area of disturbed land, accounting for emission from furnace fuel in individual residential buildings, etc.

It is important that the municipal level allows to carry out assessments, ignoring the borders of regions, since the same type of municipalities from different regions have much more in common with each other than different types of territories within the same region. The Baikal Natural Territory includes the municipalities of three regions, on the territory of which the lake water protection zone is located. Baikal, the catchment area within the territory of the Russian Federation, as well as specially protected natural territories, which is regulated by a separate federal law (Federal Law No. 94-FZ of 01.05.1999).

BNT is a unique natural and economic system, which, despite the enormous value of a unique natural object, is characterized first by a resource, and then (during the years of Soviet Union) and an industrial type of development. Along the Angara River, the Angara-Yenisei territorial production complex was formed, specializing in non-ferrous metallurgy, forestry and woodworking industry, hydropower. In the coastal zone of the lake there are a number of large cities, such as Irkutsk, Angarsk, Ulan-Ude, in which more than 1.3 million people live in total, there are a number of large industrial centers. Currently, the tourist and recreational resources of the region are becoming relevant. All this creates the need to monitor the anthropogenic impact on this territory in order to take effective measures to reduce it.

CURRENT STUDIES OF THE TOPIC

Studies devoted to the typologization of municipalities, as a rule, reveal contrasts and asymmetry in the development of socio-economic processes at the municipal level (Voroshilov 2019; Romashina 2019). O.V. Kuznetsova notes (Kuznetsova 2021) that the existing typologies of municipalities are actually the result of development of municipalities monitoring and not the basis for such monitoring, since they are based on an assessment of the current socio-economic situation of municipalities. This observation is also true in relation to environmental assessments at the municipal level. They are aimed at finding municipal differences for one region and differ in the goals and breadth of the indicators. Statistically available demographic indicators, volumes of emission, wastewater, agricultural development, as well as phenomena caused not only by anthropogenic, but by natural causes (in particular, the level of forest cover, the development of erosion processes) are most often used. The use of demographic indicators brings some simplification and modeling of specific impacts from the population on the natural environment. In the absence of detailed data for the level of municipalities, this is especially in demand for conducting integral and partial AI assessments (Igenbayeva 2006; Kropyanko 2014; Saprin 2017). Indicators of the natural components state (acidification and salinization of soils, biological and chemical contamination of drinking water sources (Barnaeva 2011; Ovchinnikova 2012), population health (Kuprienko 2006), the degree of anthropogenic transformation of the landscape (Ulengov 2008), the coefficients of population and production concentration or AI correlated with the potential of environmental sustainability (Ugarova 2005; Rybkina 2005) are used less often.

Researches devoted to integral environmental assessments abroad began to develop earlier than in the USSR on the way from social to ecological, combining the ecological situation with economic development and social progress. The municipal level is represented by estimates of cities (The Urban Sustainability 2012; City Prosperity 2017; Sustainable Cities... 2015; The Green City 2012). In Soviet and Russian practice, environmental indexes appeared earlier, leading positions among them were taken by AI Indexes based on statistical indicators (Kasimov et al. 2014).

Long-term foreign experience reflects the methodological incompatibility of the indexes, the lists of evaluation factors differ, which range from a bias towards documentation of mechanisms to the assessment of quantitative variables such as polluting emissions. Thus, a study in the discrepancy of ESG ratings according to different methods of Kinder, Lydenberg and Domini, Sustainalytics, Moody's ESG, S&P Global, Refinitiv, MSCI, conducted in 2022, revealed the reasons for the discrepancy of ratings assigned to the same object. At the first stage of any assessment, the coverage of the initial elements is determined – it accounts for 38% of the divergence, the discrepancy in the assessment of the initial elements (variables) accounts for 56%, and the differences in the weights of the elements account for the remaining 6% of the divergence (Berg et al. 2002).

In addition, the evaluation criteria for the same element may differ. The most popular approach in building an assessment scale based on the intensity of private impacts on the environment is the method of rationing, mainly using the linear scaling procedure, the second most popular method is ranking, i.e. ranking territorial cells from the minimum value to the maximum. Less numerous are works where a different system of ordering particular indicators is used: a binary system (Kadashova 2011), a point or categorical system (Kalikhman 2010; Barneva 2011; Saprin 2017).

A review of an extensive set of publications in recent years devoted to the widest range of BNT problems allows us to conclude that integrated assessments of various types of anthropogenic impact for this territory have not yet been carried out, but at the same time numerous problems of the territory have been deeply investigated (Vladimirov et al. 2016; Ecological Atlas 2015).

MATERIALS AND METHODS

The methodology of integral indicators proceeds from the general principles that determine the effectiveness of an integral indicator for monitoring purposes: managerial targeting, multilevel targeting, theoretical validity, reliability and sensitivity, single-criteria and decomposability, informativeness, conciseness (Ayvazyan 2012). The municipal level of assessment most fully meets these principles.

The problem of the harmonized AI assessment is that there is no a posteriori set of indicators, unification of measurement scales and a mechanism for interpreting the parameter assessment itself. Based on these principles and taking into account the significance for the BNT, the following were selected as initial elements (subindexes) and variables for their evaluation.

For the subindex of AI on the atmosphere, quantitative variables were calculated on the basis of official statistics (the density of pollutant emission from stationary sources based on the area of built-up land, from motor transport and small vessels, thousand tons/km of the route network, the toxicity coefficient of emissions), and emissions from autonomous heating systems calculated on the basis of statistical data were also used about the number of households, decryption of satellite images, survey of the population and heads of settlements.

The subindex of anthropogenic impact on water resources integrates indicators of water intake, wastewater discharge, and polluted wastewater discharge per capita of the permanent population. The need to use two indicators of wastewater discharge is due to the fact that wastewater discharge mainly includes warm wastewater from fuel energy facilities, while polluted wastewater comes from industry and housing and communal services, their share varies from 10 to 100% for municipalities of the BNT.

The "Waste" subindex includes the density of solid municipal waste generated and the reduced volume of industrial waste, taking into account hazard class I-V.

Agriculture is a specific area type of load, which is described by the share of farmland in the area of the municipalities, the share of acreage in the total area of farmland, the density of cattle per pasture area.

Taking into account the specifics of the BNT, the subindex "Disturbed lands and objects of accumulated harm" was included in the methodology. The area of the disturbed lands was calculated by the method of visual decoding of high-resolution satellite images Sentinel-2, Landsat-8, WorldView-1, WorldView-2 with further verification of key areas during the expedition research. Information about the localization of deposits of various types of minerals was obtained using an interactive electronic map of subsoil use of the Russian Federation (openmap.mineral.ru), which is accessed through the Internet portal of the Federal Agency for Subsoil Use (rosnedra.gov.ru). By means of GIS, the areas of all contours of disturbed lands were obtained for each time slice, and their dynamics for the period from 2014 were estimated by 2020 in the context of municipalities of the BNT and in the context of settlements of the Central Ecological Zone (CEZ) (Environmental monitoring ... 2009). The objects of accumulated harm include non-recultivated production zones, storage sites of accumulated waste of hazard class I-II, sludge accumulators of waste of hazard class 3, but located near Lake Baikal or rivers flowing into the lake.

The subindex "Background impact" is designed to reflect those types of loads that are not reflected in statistical indicators. The density of the permanent population allows to simulate the intensity of the impact on the environment from everyday (non-productive) life. The density of roads characterizes the degree of transformation of the natural landscape, creates opportunities for the use of resources, pollution of land resources, penetration of the population into the territory, etc. The density of persons (tourists) staying in collective accommodation facilities for the period of rest has a comparable effect with the permanent population on AI. The level of motorization indirectly reflects the intensity of traffic for a territory with an average type of settlement over long distances between settlements.

The most important element for BNT is the impact on forest resources. This is the most unstable type of load, which is determined by both natural and socio-economic factors. It is described by indicators of the proportion of forests that died under the influence of adverse factors, passed by fires and the ratio of the actual volume of wood harvesting to the maximum allowed.

The method of constructing the integral index of AI provides for the possibility of not only its territorial, but also temporal comparison. The key point for the possibility of dynamic use of the integral index is the choice of normalization using stable reference points. The normalization of the indicators included in the index is carried out according to the linear method according to the data for 2014-2020, therefore, the determination of the value of each indicator takes into account the values for the entire period under consideration. At the same time, limitations in the availability of data on some indicators in the context of municipalities in different years lead to the fact that the number of indicators taken into account varies in different years. For this reason, it is necessary to take into account that the dynamics of the index may be due not only to objective reasons for changes in anthropogenic impact, but also to subjective reasons for differences in the completeness of statistical data.

In order to neutralize the influence of statistical outliers, the so-called interquartile interval method was used to determine the rationing boundaries. Its essence consists in allocating a rationing interval cleared of emissions and assigning a minimum or maximum value to emissions (0 or 1 if the rationing interval is taken as [0;1]). The value of the interquartile interval is calculated as the difference between 75 and 25 percentile elements. After determining the interquartile distance, the normalization boundaries [a;b] are determined by formula 1.

$$\left[x_{25}-1.5\times\left(x_{75}-x_{25}\right);x_{75}+1.5\times\left(x_{75}-x_{25}\right)\right] \quad (1)$$

where x_{25} and x_{75} 25 and 75 percentiles of the indicator distribution,

$$a=x_{25}-1.5\times\left(x_{75}-x_{25}\right),b=x_{75}+1.5\times\left(x_{75}-x_{25}\right)$$

The final normalization of all observations is made according to the formula 2:

for $x_i\varepsilon$ $$x_i\varepsilon[a;b]-x_i^n=\frac{x_i-a}{b-a} \quad (2)$$

where x_i^n – normalized observation value, a and b are defined in formula 1;

for $$x_i>b=1;\, for\; x_i<a=0$$

To assess the significance of various indicators, 47 experts from different fields of science, different scientific schools, academic institutes and universities, experts in the field of environmental ratings and representatives of the environmental management system in the territory of the BNT were interviewed. The weight of each indicator was determined as the average value of the scores set by experts in the range 1-9.

The integral index of anthropogenic impact (IAI) is calculated as the sum of the average values of the sub-indices and theoretically can vary in the range [0:1]. In order to exclude the influence of a subjective factor in assessing the integral index of anthropogenic impact, when considering its dynamics for 2014-2020, the «Waste» block was excluded from its composition due to the lack of basic statistical data for the period 2014-2018. The choice of the period for assessing the dynamics is due to minimal changes both in the methodology of environmental indicators and in the economy of the regions. It is especially important for the BNT that the largest source of pollution, the pulp and paper mill in Baikalsk, was closed before this period, further development of the territory will take place while preserving the remaining sources.

DISCUSSION AND RESULTS

The dynamics of the AI index for the period 2014-2020 for all 41 municipalities included in the BNT shows a wave dynamic: from 2014 to 2016, there is an increase in the average and median value of the index – from 0.283 to 0.308 (+7.2%), since 2017 - its gradual decrease – to the level of 0.269 (-12.8% of the local maximum). Such dynamics may indicate a reduction in the level of anthropogenic impact in municipalities in recent years.

The municipalities included to the BNT demonstrate a relatively stable level of the IAI, the leaders and outsiders retain their positions, which indicates that the results obtained are not accidental (Fig. 1).

The cores of environmental tension localized in the Irkutsk-Angara agglomeration with an equal contribution of all subindexes, as well as the districts … (Selenginsky, Petrovsk-Zabaikalsky, Mukhorshibirsky municipal districts) are among the leaders.

The group of areas with an increased level of anthropogenic impact has expanded during the period under review. There are urban municipalities that have an increased level of background impact due to the population, the average value of the AI subindex on the atmosphere and water resources (urban districts of Ulan-Ude, Severobaikalsk, Petrovsk-Zabaikalsky, Svirsk and Shelekhovskoye municipality). The impact increased in suburban and coastal areas (Tarbagataysky, Irkutsk, Slyudyansky), in areas with developed mining (Bichursky, Cheremkhovsky, Krasnochikoysky), as well as in the peripheral Kazachinsko-Lena district, where the main impact on water and forest resources is formed as a result of the implementation of the «Power of Siberia» gas pipeline project.

The medium level of AI remained in a small number of rural areas and small towns with an average level of impact of agriculture and forestry (Usolsky and semi-peripheral Kyakhtinsky districts, as well as districts of Ust-Ordynsky district) due to the fact that this group left areas in which the impact increased.

The reduced level of AI is formed mainly in semi-peripheral municipalities. Due to the absence of large sources, the level of impact is quite stable, but the ratio of

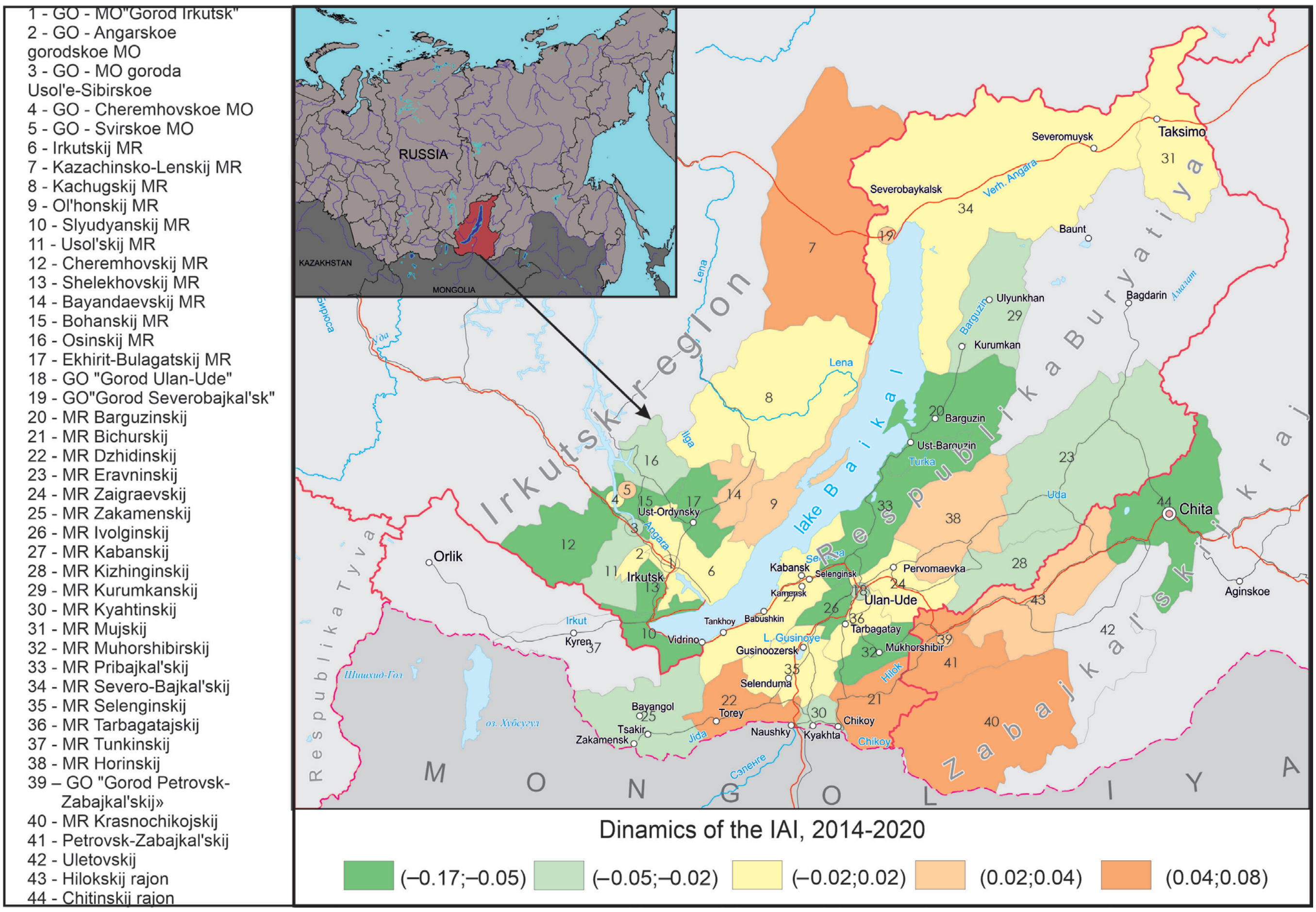

Fig. 1. Dynamics of the AI index in 2014-2020 in the municipalities of the BNT

Source: authors' calculations

subindixes is constantly changing, since the main role is played by unstable impacts on forest resources. In some suburban areas with developed agriculture and relatively high development density (Baikal, Ivolginsky and Chita in the part included in the BNT districts), the level of motorization and development is changing. In Khiloksky, Dzhidinsky and Zaigraevsky districts, the damage caused to forest resources is reduced in the index structure. In Kabansky district, atmospheric pollution has decreased as a result of the introduction of new cleaning systems at the pulp and cardboard mill, but the background impact has increased as a result of the life of the population and recreation.

Districts with low AI levels are the most stable group. The index of anthropogenic impact is characterized by moderate but increasing values of the background and agricultural sub-indices. Stability is also promoted by a relatively high proportion of atmospheric pollution from heating oil.

Among the municipalities included in the BNT, for the period 2014-2020, 14 demonstrated significant dynamics (deviation by 20% or more from the values of 2014): in 5 of them, the IAI significantly increased. Among the municipalities included in the BNT, for the period 2014-2020, 14 demonstrated significant dynamics (deviation by 20% or more from the values of 2014): in 5 of them, the AI index significantly increased (Krasnochikoysky district +37.5%, Bichursky district +26.6%, Olkhonsky district +24.8%, Djidinsky district +24.3%, Petrovsk-Zabaikalsky district + 20.6%), decreased significantly in 9 (Chitinsky D district -47.1%, Bokhansky district -32.7%, Mukhoshibirsky district -29.5%, Ivolginsky district -26.9%, Shelekhovsky district -25.7%, Pribaikalsky district -24.8%, Barguzinsky district -24.3%, Slyudyansky district -23.4%, Cheremkhovsky district -22.5%).

The high relative increase in the index of anthropogenic impact in 2014-2020 in 5 municipalities is associated with various reasons. In the Olkhonsky district, a small absolute increase due to the effect of a low base led to a relatively high increase in the integral indicator. At the same time, the main contribution to the increase in the index was made by the block "Background impact" due to intensive motorization of the population. In the Krasnochikoysky district, the impact on the block of indicators "Water resources" increased significantly, to a lesser extent, the increase was associated with an increase in the area of disturbed land. All this is connected with the development of the gold mining industry in the municipality. Mining (coal mining) is also associated with growth in the Petrovsk-Zabaikalsky district due to an increase in production at the Tigninsky field (Fig. 2).

In the group of municipalities with the maximum relative decrease, the key reason for the decrease in the integral IAI is the reduction of the component of the impact on forest resources (Fig. 3) in all municipalities, and in the Barguzinsky and Ivolginsky districts – also the impact on water resources.

A component-by-component analysis of the integral index of anthropogenic impact (based on median values for all municipalities) allows us to identify the causes of dynamics for 2014-2020. (Fig. 4). A steady upward trend is characteristic of the block of indicators "Background impact", which is associated with the trend of increasing motorization of the population and an increase in the density of highways on the territory of the BNT. The territorial mobility of the population is steadily increasing, which causes, on the one hand, an increase in the consumption of motor fuel, and on the other hand leads to an increase in the degree of "penetration" of the population into the territory – the frequency and mass of visits to the landscapes surrounding settlements.

The impact on the block of indicators "Agriculture" is relatively stable (a decrease of 7.3% for 2014-2020). This is due to the relatively conservative situation in the area of agricultural land, as well as the downward dynamics in the intensity of land plowing and cattle breeding on the territory of the BNT. The latter trend is largely due to the processes of depopulation of the rural population and the refusal to keep pets in private subsidiary farms of the population.

The subindex characterizing the impact on the atmosphere demonstrates low volatility: the median value for all municipalities decreased by 6.6% in 2014-2020. The highest relative level of reduction (more than 20%) was recorded in Zaigraevsky (-39.3%), North Baikal (-31.2%) districts, as well as a group of municipalities of the Irkutsk region located in the zone of atmospheric influence of the BNT: Bayandaevsky (-55.2%), Ehirit-Bulagatsky (-57.3%), Bokhansky (-32.4%), Osinsky (-36.1%) municipal districts. The growth of AI in the block of indicators "Atmosphere" by 20% or more is noted in three municipalities – Djidinsky district (+20%) of the Republic of Buryatia, Irkutsk (+60.6%), Olkhonsky districts (+59.1% but from a low base level) Irkutsk region and in the town of Petrovsk-Zabaikalsky (+40.9%) of the Zabaikalsky krai.

The upward dynamics in these municipalities is associated with an increase in the emission of pollutants into the atmosphere from stationary sources and vehicles, the number of which is constantly increasing.

A small dynamism is characteristic of the block of indicators characterizing disturbed lands and the presence of objects of accumulated harm. The development of new mineral deposits leads to an increase in the area of disturbed lands, while the reclamation process does not compensate for their new areas. Noticeable dynamics is typical for a small number of municipalities in the Irkutsk region, Shelekhovsky (+42%) and Usolsky districts (+120%), as well as Krasnochikoysky district (+30%) and Bichursky district (+73%) stand out against the general background.

The greatest changes in the subindex and, as a result, the maximum contribution to the dynamics of the entire index of anthropogenic impact is made by a block of indicators of impact on forest resources. This is due to a set of indicators in the block, the volatility of which is very high from year to year and is associated with the death of forests, the scale of which, due to natural and anthropogenic reasons, can vary many times from year to year (fires, forest diseases). During the period 2014-2020, the median value of the subindex was reduced by almost two times, and from the peaks reached in 2015-2016 – by more than 4 times. The main reason for the reduction is the reduction of the area of forests that died from adverse factors and the area of forests covered by fires. According to statistics, in 2015, 1.18 million hectares were affected by fires on the territory of the BNT, and in 2020 it was 9 times less – only 0.14 million hectares; the difference in the area of dead forests from unfavorable factors in 2015 (taken into account according to 2016 statistics) and in 2020 also reduced by 8 times.

The key impact on forests within the BNT, where industrial exploitation of forest resources is limited (and actually prohibited within the Central Ecological zone (CEZ), are fires and diseases, the spread of which is facilitated by human activity or, conversely, inaction associated with improper care of forest resources.

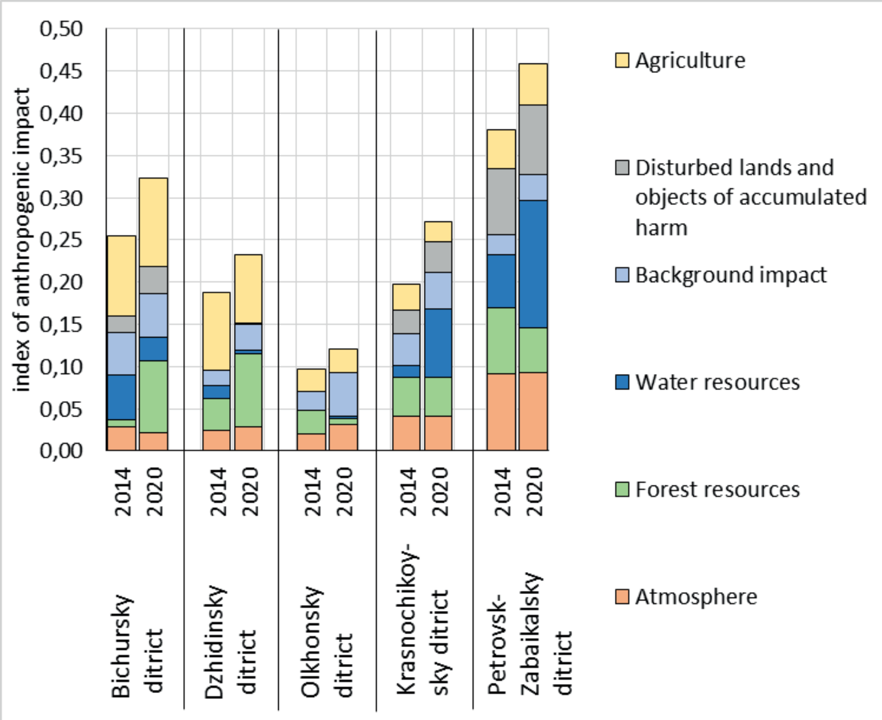

Fig. 2. The structure of the AI index for the municipalities of the BNT, which showed the maximum relative increase in 2014-2020

Source: calculated by the authors

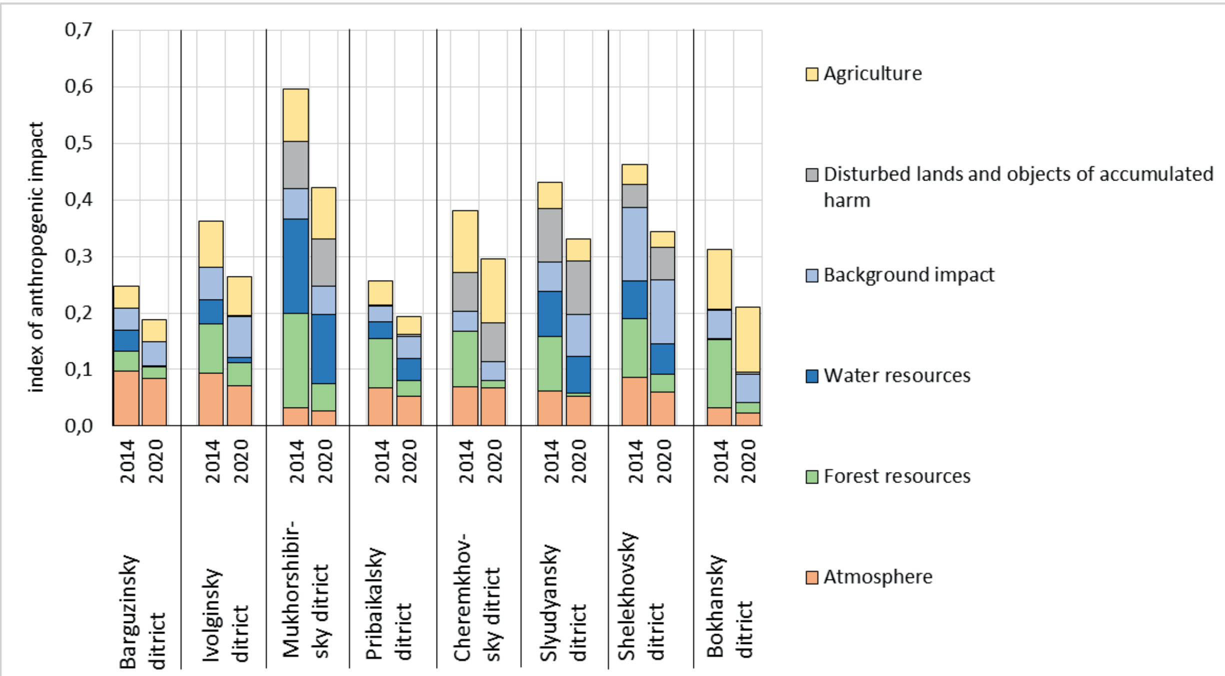

Fig. 3. The structure of the AI index for the municipalities of the BNT, which showed the maximum relative reduction in 2014-2020

Source: calculated by the authors

Most of the fires in the Baikal forests are associated with anthropogenic factors (Evdokimenko 2013), and shortcomings in the organization of work and financing of forestry enterprises, lack of technical capability and inaccessibility of forests within the BNT, create favorable conditions for the development of wildfires and the death of forests from diseases (for example, from bacterial dropsy that affected the forests of the southern Baikal region). There are legal conflicts: for example, the actual impossibility to organize the arrangement of mineral strips around settlements in the CEZ or to organize continuous sanitary logging of affected areas of protective forests. This does not allow solving the pressing problems of forest management. In this regard, the reduction of the subindex of the impact on forest resources should not be misleading. It was achieved rather not by reducing the impact or more rational use of forest resources, but due to the high base of previous years – large-scale forest loss (2015-2016) at the beginning of the study period, against which the current values due to more favorable weather conditions are lower.

The relative increment of the IAI index is important for tracking the dynamics of anthropogenic impact, however, without taking into account the base position of the municipality in 2014, it is difficult to draw conclusions about the absolute scale of the impact transformation. To do this, it is necessary to consider the increment of the IAI by its absolute value (Fig. 5).

The maximum increase in absolute terms among the municipalities of the BNT occurred in three municipalities in the south-east of Lake Baikal: Petrovsk-Zabaikalsky and Krasnochikoysky districts of the Zabaikalsky krai and Bichursky district of the Republic of Buryatia. We can say that a fairly large area of increased anthropogenic impact on the environment has been formed. The main reasons for the increased impact are the development of the mining industry in these municipalities, primarily the development of coal and placer gold deposits. Despite the sufficient distance from the lake, the reasons for the increase in the impact and the nature of the spread of possible consequences (through runoff through the hydrographic network) suggest an increase in the potential danger of anthropogenic activity for Lake Baikal.

In the Kazachinsko-Lensky district of the Irkutsk region, the increase in anthropogenic load is also associated with the extractive industry (development of gas fields and construction of gas transportation infrastructure), and in the Dzhidinsky district of the Republic of Buryatia – with an increase in the impact on forest resources.

The second group of municipalities that showed a weak growth in the IAI (about 0.02 units) is represented by seven territories scattered across various parts of the BNT. It is impossible to single out a single reason for increasing the IAI for them, it is individual for each municipality. 12 municipalities demonstrate insignificant dynamics of IAI, 8 municipalities show a slight decrease (in the range of 0.02-0.05 units), 10 municipalities show a significant decrease (more than 0.05) (Figure 5). The decrease in IAI in 18 municipalities is primarily due to the contribution of a block of indicators of impact on forest resources.

The observed dynamics of the IAI in 2014-2020 and its subindexes allows us to make some assumptions about the nature of its changes in the near future. First of all, it is worth considering that the background impact on the environment from daily human activities will, most likely, increase. This is due to the increase in spatial mobility of the population – the growth of motorization, construction and modernization of highways in the BNT zone. Despite the fact that the rural population density in the absolute majority of municipalities will continue to decline for natural reasons, in large cities it will decrease much more slowly in the near future. The temporary population, especially in the context of the development of domestic tourism, which has been experiencing an upswing in recent years against the background of a decrease in outbound tourist traffic, on the contrary, will increase. At the same time, the existing infrastructure (communal, household, recreational) is clearly insufficient to meet all current needs. Of particular importance in this case is the high degree of concentration of exposure from the temporary population, which is localized in a small number of tourist destinations directly on the lake shore.

There are also few prerequisites for reducing IAI by decreasing the impact on the atmosphere, water resources, and reducing the areas of disturbed land. The industrial profile of the municipalities' economy will remain in view of the high inertia of the economy of the Baikal regions focused on the exploitation of natural resources. Some prospects for reducing the impact are possible if a large-scale program of gasification of the territory is implemented, which will allow the energy and utility sector to switch from coal to natural gas. However, given the current pace of construction of gas transportation infrastructure, this is possible only in the medium and long term.

The impact from agriculture, due to the inertia of the branch, has few prospects for a significant reduction. The crop industry plays a vital role for the local population, and abandoning it does not meet the interests of food security in the region. Reducing the impact of the livestock industry is possible in the case of the development of intensive industrial enterprises that operate taking into account all modern requirements for environmental protection, but this will require large-scale investments. The impact from private households in the foreseeable future will decrease due to the natural causes of a decrease in the density of the rural population.

The greatest concerns about the reversal of the dynamics of the IAI are caused by the impact on forest resources. The accumulated problems in the industry after the adoption of the Forest Code are increasing every year, creating prerequisites for the death of forests from anthropogenic and natural causes. The question of when

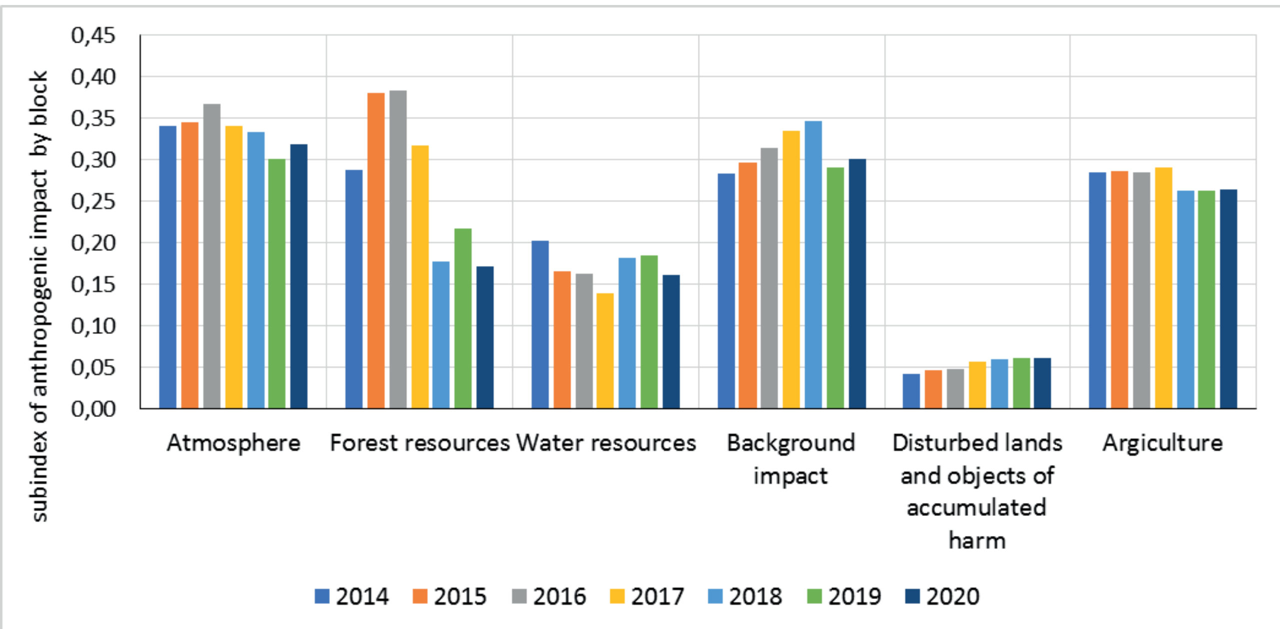

Fig. 4. Median values of private indexes of anthropogenic impact by indicator blocks, 2014-2020

Source: authors' calculations

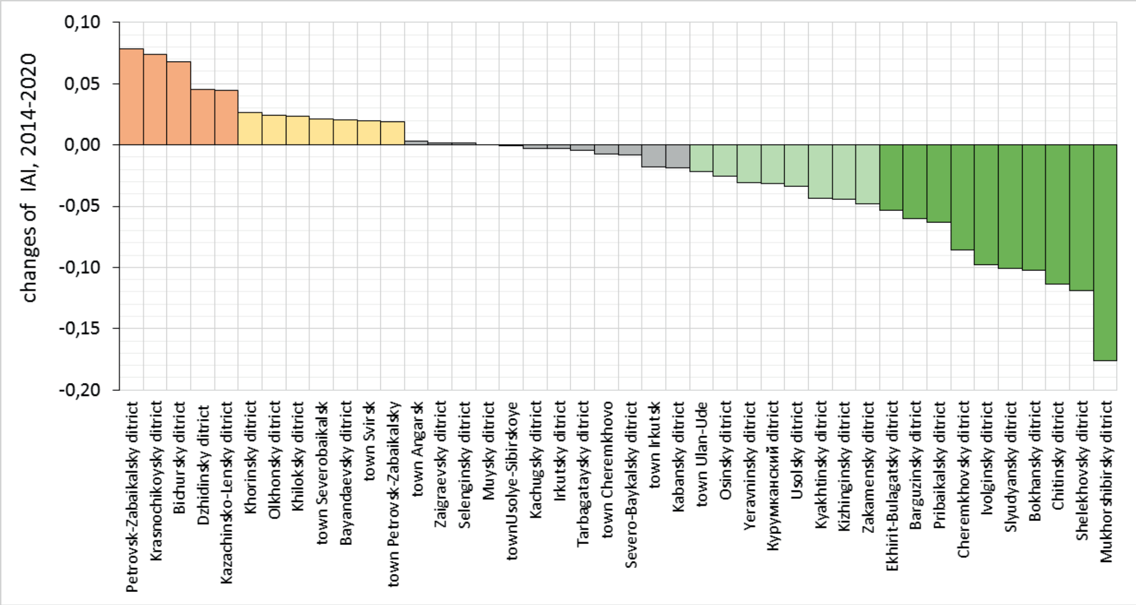

Fig. 5. Dynamics of changes in the absolute value of AI in the municipalities of BNT for 2014-2020

Source: calculated by the authors

they are realized in the form of the loss of these resources is only a matter of time and weather fluctuations. Unlike all other areas of influence, in this direction it can be realized in the shortest possible time.

CONCLUSIONS

The elaborated method of integral assessment of anthropogenic impact made it possible to trace the change in the load in retrospect. The analysis of the results confirmed the quality of the integrated assessment methodology and showed that the districts, cities and towns of the BNT are highly polarized in terms of the level of anthropogenic impact concentrated in certain areas, primarily in the zone of atmospheric influence. The main strengthening of the AI is characteristic of municipalities located along transport corridors, the axis of which is the Trans-Siberian Railway, The Baikal–Amur Mainline and the «Power of Siberia» gas pipeline.

1. The average (median) values of the integral index of anthropogenic impact on municipalities for the period 2014-2020 has a general downward trend, in 2015-2016 its local increase was observed;

2. Municipalities included in the Baikal Natural Territory demonstrate a high level of stability IAI, which indicates the inertial nature of the anthropogenic impact associated with the accumulated impact actors on their territory. Low volatility indicates the adequacy of the methods used to assess AI;

3. The contribution of the assessment indicator blocks to the overall dynamics is different: the upward trend is realized through an increase in background exposure from the population and an increase in the area of disturbed land; the decrease in the IAI is associated with a reduction in the impact of agricultural activities, partly due to a reduction in the impact on the atmosphere, but especially large due to a reduction in the impact on forest resources. The latter trend, however, is also related to natural causes and should not be misleading when assessing the real causes of changes in IAI.

4. The differences between the buffer zone and the atmospheric pollution zone are gradually decreasing, since the impact of the largest sources is decreasing on the west bank, accumulated damage objects are being eliminated, in the buffer zone the impact on forests, disturbed lands and even emissions are slightly increasing.

The absence of positive changes in the ecological state indicates the need to take measures to reduce the level of impact, primarily in the largest centers, the environmental situation in which remains unfavorable. An important advantage of the presented algorithm is the possibility of its extension in the future to track trends and form priorities of intraregional environmental policy.

REFERENCES

Ajvazyan S. (2012) Analysis of the quality and lifestyle of the population. Econometric approach. Moscow, Nauka, 426. (in Russian).

Barneva T. (2011). Monitoring and integrated assessment of changes in the state of the lands of oil and gas fields of the Middle Ob region (Candidate dissertation). St. Petersburg State University. St. Petersburg. (in Russian).

Basic Indicators of Environmental Protection. (2017). Federal State Statistics Service. Available at: http://www.gks.ru/bgd/regl/b_oxr17/Main.htm [Accessed 02 December 2018].

Berg F., Kölbel J., Rigobon R. (2022). Aggregate Confusion: The Divergence of ESG Ratings. Review of Finance. Available at: https://ssrn.com/abstract=3438533 [Accessed 10 April 2022].

Bobylev S., Minakov V., Solovyova S. and Tretyakov V. Ecological and economic index of the regions of the Russian Federation. (2012). Moscow: WWF of Russia, RIA Novosti. Available at: https://wwf.ru/upload/iblock/dc8/index.pdf [Accessed 10 April 2022].

City Prosperity Initiative Index: Using AHP Method to Recalculate the Weights of Dimensions and Sub–Dimensions in Reference to Tehran Metropolis. (2017). By Parsa Arbab. European Journal of Sustainable Development, 6(4), 289–301.

Database of indicators of Municipalities (2022). Environmental protection is carried out by the Federal State Statistics Service (Rosstat). Available at: http://www.gks.ru [Accessed 08 July 2022].

Database of Rosprirodnadzor (2022) (Federal Service for Supervision of Natural Resources). Available at: http://rpn.gov.ru/opendata [Accessed 08 July 2022].

Ecological Atlas of the Baikal Lake Basin. (2015). Irkutsk. Publishing House of IG SB RAS.

Ecological monitoring of the Baikal Lake. (2022). Information resource. Available at: http://www.baikalake.ru/about/uvpn/ [Accessed 26 February 2022].

Ecological rating of the cities of the world. (2015). The Blacksmith Institute. Available at: http://www.blacksmithinstitute.org [Accessed 21 January 2022].

EMISS State Statistics. (2022). Available at: https://www.fedstat.ru/indicator/36702 [Accessed 15 June 2022].

Federal Law No. 94-FZ of 01.05.1999 (as amended on 30.12.2021) «On the Protection of Lake Baikal». (1999). (in Russian).

Igenbayeva N. (2006). Anthropogenic transformation of forest-steppe landscapes of the Omsk Irtysh region (Candidate dissertation). Altai State University. Barnaul. (in Russian).

Improvement of the housing stock in the subjects of the Russian Federation. Rosstat. Available at: https://rosstat.gov.ru/storage/mediabank/Jil_bl.xls [Accessed 10 July 2022].

Kalikhman T. (2010). Geoecological structure and ways of development of protected natural territories of the Baikal region (Candidate dissertation). V.B. Sochava Institute of Geography of the Russian Academy of Sciences. Irkutsk. (in Russian).

Kasimov N., Bityukova V., Malkhazova S., Kosheleva N., Nikiforova E., Shartova N., Vlasov D., Timonin S. and Krajnov V. (2014). Regions and cities of Russia: integral assessment of the ecological state. Ed. Academician of the Russian Academy of Sciences N.S.Kasimov. Moscow. IP Filimonov M.V. 560. (in Russian).

Kropyanko L. (2014). Geoecological assessment and zoning of the Azov-Black Sea coast of Russia (Candidate dissertation). Southern Federal University. Rostov-on-Don. (in Russian).

Kuprienko V. (2006). Integrated assessment and mapping of the geoecological situation of the region of intensive industrial and agricultural development (on the example of the Voronezh region) (Candidate dissertation). Voronezh State University. Voronezh. (in Russian).

Kuznetsova O.and Babkin R. (2021). Typology of municipalities for monitoring their socio-economic development. Federalism. 26.4 (104). 35–53. DOI: 10.21686/2073-1051-2021-4-35-53. (in Russian).

Ovchinnikova T. (2012). Land management in regions with intensive manifestation of natural and man-made emergencies (Doctoral dissertation). Voronezh State Technical University. Voronezh. (in Russian).

Romashina A. (2019). Typology of Russian municipalities by specialization of economy and position in the settlement system. Regional study, 3, 42–52. (in Russian with English summary).

Rybkina I. (2005) Assessment of environmental hazards in the settlement systems of the Altai Krai (Candidate dissertation). Institute of Water and Environmental Problems SB RAS. Barnaul. (in Russian).

Saprin S. (2017) Assessment of ecological sustainability of agricultural landscapes of the Voronezhskaya oblast (Candidate dissertation). Voronezh State Agrarian University Voronezh. (in Russian).

State report «On the state of Lake Baikal and measures for its protection in 2020». (2021). Irkutsk. V.B. Sochava Institute of Geography SB RAS.

Sustainable Cities Index (2015). Balancing the economic, social and environmental needs of the world's leading cities. Arcadis. Available at: https://sustainablestalbans.org/wp-content/uploads/2015/05/arcadis-sustainable-cities-index-report.pdf [Accessed 19 February 2022].

The Green City Index (2012). A research project conducted by the Economist Intelligence Unit, sponsored by Siemens. Munich: Siemens AG Corporate Communications and Government Affairs. Available at: https://assets.new.siemens.com/siemens/assets/api/uuid:cf26889b-3254-4dcb-bc50-fef7e99cb3c7/gci-report-summary.pdf [Accessed 19 February 2022].

The population of the Russian Federation by municipalities. (2022). Rosstat. Available at: https://rosstat.gov.ru/compendium/document/13282 [Accessed 25 March 2022].

The Urban Sustainability Index: A New Tool for Measuring China's Cities. (2012). The Urban China Initiative. Available at: http://www.urbanchinainitiative.org/research/usi–urban–sustainability–index/ [Accessed 15 February 2022].

Ugarova N. (2011). Ecological and economic optimization of the territorial planning structure of large cities (Candidate dissertation). Moscos State University. Moscow. (in Russian).

Ulengov R. (2008) Anthropogenic transformation of geosystems of the Republic of Tatarstan and current geoecological situation (Candidate dissertation). Tatar State Humanitarian and Pedagogical University. Kazan. (in Russian).

Vladimirov I., Korytnyj L., Plyusnin V. and Sorokovoj A. (2016). Studies of the V. B. Sochava Institute of Geography SB RAS on the Baikal Natural Territory. Geography and natural resources, S5, 6-14. (in Russian).

Vorobyov A. (2020). Big data in the study of localization and mobility of the population. Geography and natural resources, 5, 203–207. DOI: 10.21782/GiPR0206–1619–2020–5(203–207). (in Russian with English summary).

Voroshilov N. (2019). On the issue of typologization of municipalities. Development of territories. 3, 28–34. (in Russian with English summary).

RESEARCH PAPER

SEASONAL CHARACTERISTICS OF LONG-RANGE TRANSPORT AND POTENTIAL ASSOCIATED SOURCES OF PARTICULATE MATTER (PM_{10}) POLLUTION AT THE STATION ELK, POLAND, ON 2021-2022 DATA

Sheyar Abdo[1,2]*, **Yulia Koroleva**[1]

[1]Immanuel Kant Baltic Federal University, Institute of Living Systems, Universitetskaya 2, Kaliningrad, 236041, Russia

[2]Tishreen University, Faculty of Literature and Humanities, Geography Department, Latakia, Syria

*Corresponding author: abdosheyar@gmail.com

Received: May 26th, 2022 / Accepted: September 4th, 2023 / Published: October 10th, 2023

https://DOI-10.24057/2071-9388-2022-2461

ABSTRACT. The current study aimed to determine the potential sources of distant emissions of PM_{10} particles that significantly affect PM_{10} levels at a given site in southeastern Baltic. The EEA Air Quality Monitoring Station in Elk City, northeastern Poland, was selected for this study. This station is located approximately 50 km from the border of the Russian exclave (Kaliningrad Region). In this study, the NOAA HYSPLIT_4 trajectory model, potential source contribution function (PSCF), and concentration-weight trajectory (CWT) were employed to investigate the origin of the measured PM_{10} mass at a receptor site. PSCF and CWT utilize back-trajectory analysis and Lagrangian particle dispersion simulations to reconstruct the advection pathways of air masses arriving at the site. These reconstructed retroplumes provide detailed information regarding the geographic locations traversed by polluted air masses on their way to the receptor. By integrating trajectory information with concurrent pollutant concentration data, the PSCF and CWT enable the identification of potential source regions and quantification of their impact on the observed atmospheric levels. From January 1, 2021, to December 31, 2022, at 200 m the 72h backward trajectories of air masses entering the receptor point were calculated and categorized by clustering them into 5-4-4-5 clusters. Subsequently, the PM_{10} levels at the Elk site associated with each air mass cluster were examined during the observation period. The seasonal variation in PM_{10} was generally characterized by a peak in winter and minimum values in summer. PM_{10} was lower during warmer periods, particularly during summer, and significantly, higher concentrations were observed during colder periods. Cluster analyses showed that airflow followed a seasonal pattern, with different results obtained in different seasons. According to the PSCF and CWT results, in winter and spring, the receptor site was influenced more by long-range PM_{10} pollution, particularly from heavily industrialized areas in Central-Eastern Europe. In contrast, in summer and autumn, the receptor site was less influenced by long-range pollution. The findings demonstrate that the seasonal distributions of PM_{10} source areas obtained using these two methods generally share similar characteristics, suggesting the credibility and accuracy of the analytical results.

KEYWORDS: pollution sources; PM_{10}; HYSPLIT; backward trajectory; potential source contribution function; concentration-weighted trajectory

CITATION: Abdo S., Koroleva Y. (2023). Seasonal Characteristics Of Long-Range Transport And Potential Associated Sources Of Particulate Matter (Pm_{10}) Pollution At The Station Elk, Poland, On 2021-2022 Data. Geography, Environment, Sustainability, 3(16), 92-101

https://DOI-10.24057/2071-9388-2022-2461

ACKNOWLEDGEMENTS: The authors express their gratitude to the Elk station team and European Union (EU) Environment Agency for providing air pollution data without charge. The authors also thank NOAA's Air Resources Laboratory (ARL) for providing the HYSPLIT transport and dispersion model used in this paper. We also gratefully thank the reviewers for their constructive comments.

Conflict of interests: The authors reported no potential conflict of interest.

INTRODUCTION

Today's atmosphere differs significantly in terms of its chemical composition from the natural atmosphere that existed before the Industrial Revolution. If the natural atmosphere is considered clean, it means that in today's atmosphere, clean air is never found (Daly and Zanetty, 2007). The history of air pollution dates back centuries, when the industrial revolution (circa 1760) was a major contributor to the issue, as the widespread use of fossil fuels has led to the release of large quantities of pollutants, such as sulfur dioxide, nitrogen oxides, and particulate matter into the atmosphere (Kim, 2013; Yang and Smintek, 2014). In the twenty-first century, one of the biggest challenges was air pollution, not only at the global scale but also at the local and regional levels. Particulate matter (PM) is one of the main pollutants of concern because of its negative impacts on ecosystems and human health, as exposure to PM can cause a range of health problems, including premature death, cardiovascular and respiratory diseases, and reduced lung function (Manisalidis et al., 2020).

The southern Baltic is a geographically diverse region with a various disparities in areas such as economic development, climate type, landform, and resource endowment. These disparities have resulted in large differences in pollutant and PM levels in the region. While the Baltic States and Kaliningrad region have relatively low levels of PM, Poland frequently experiences PM pollution levels that exceed the limits recommended by the WHO. According to a report by the European Environment Agency (EEA) published in 2021, Poland had the highest average annual concentration of PM2.5, with levels exceeding the EU's recommended limit of 10 µg/m^3 and the second-highest average annual concentration of PM_{10} in Europe, with levels exceeding the EU's recommended limit of 20 µg/m^3.

The main sources of PM in Poland can be attributed primarily to coal-fired power plants, industrial emissions, and residential heating using solid fuels such as coal and wood. Open burning of agricultural waste is also a common practice in Poland, which releases large amounts of PM into the air that can also be transported over long distances (Jasiński et al., 2021; Kobza et al., 2018). In addition to this local sources, Long-range transport is another major source of PM pollution in Poland due to its geographical location in the center of Europe and its proximity to industrialized countries such as Germany, the Czech Republic, and Ukraine, which contribute to the high levels of PM pollution due to the prevailing westerly winds that carry pollutants from these countries to Poland (Nazar and Niedoszitko, 2022; Zareba and Danek, 2022).

Various computational approaches have been used to solve long-range pollutant transport. Air mass back-trajectory analysis is frequently used to determine the direction and sources of air pollution at a receptor site. The basic idea behind air mass back-trajectory analysis is that the air masses that reach a receptor site have traveled through the atmosphere and may have picked up pollutants along the way. By analyzing back trajectories, scientists can gain insights into the sources of air pollution, the transport of pollutants across different regions, and the potential impacts of pollution on human health and the environment. Back trajectories are often used in conjunction with other atmospheric modeling tools, such as receptor models, to provide a more complete understanding of air pollution dynamics (Bodor et al., 2020; Pouyaei et al., 2020; Stein et al., 2015).

Several studies have used back trajectory analysis to investigate the long-range transport of air pollution; However, there is a lack of studies of air mass back-trajectories for south eastern Baltic region. In scarce previous studies performed for this region, potential sources of particulate matter (PM_{10}) were identified using cluster trajectory analysis and the concentration-weighted trajectory (CWT) approach at a rural background site in northeastern Poland (Diabla Góra) (Reiser and Orza, 2018). Backward trajectory analysis was also performed to identify the main atmospheric pathways affecting PM_{10} concentrations at urban background sites in Warsaw, Poland (Majewski et al., 2018). Another study by Bihałowicz et al., (2021) used backward trajectory analysis to study the dispersion of selected air pollutants and greenhouse gases from landfill fires and their impact on air quality in Poland. At the regional level, several studies have been conducted, the most important of which was a study conducted by Byčenkiene et al., (2014) to investigate the transport pathways and potential sources of Black Carbon (BC) and aerosol particle number concentration (PNC) observed in Lithuania.

The objective of this study is to investigate the potential source region of air pollution contributing to PM_{10} levels in an urban background location in northeastern Poland (Elk) based on back-trajectories and PM_{10} observations for 2021-2022. Elk station is located approximately 50 km away from the border of the Russian enclave (Kaliningrad Region). Therefore, this study can also provide an overview of the characteristics of PM_{10} pollution in the region, as no such observations have been carried out in the Kaliningrad region. Cluster analysis of back trajectories was used to assess the main transport pathways of air masses, whereas a hybrid receptor model as a function of the potential source contribution function (PSCF) and concentration-weighted trajectory (CWT) was used to identify potential PM_{10} source areas.

MATERIALS AND METHODS

Study Area and Data Sources

In this study, air mass back-trajectories arriving at a monitoring site in Elk, Poland were investigated. Elk is an urban background monitoring site operated within the EEA air quality network (European Environment Agency). This site is located in the north-eastern part of Poland, in the Warmian-Masurian Voivodeship (53°49'17"N 22°21'44"E, 133 m.a.s.l.).

Regional or mesoscale transport distances are consistently within 1000 km for about 2 to 3 days in the boundary layer (Li et al., 2012). As a result, we chose a 72-hour backward trajectory with 72 latitude-longitude data pairs per trajectory. Eight back trajectories were calculated at an altitude of 200 m above the ground starting point at 02:00, 05:00, 08:00, 11:00, 14:00, 17:00, 20:00, and 23:00 LT. The following are the reasons for selecting 200 m agl as the receptor height: First, PM_{10} concentrations are often measured below the surface layer, typically at a height of 200 m agl, where pollutants are well mixed. Second, when computing the backward trajectory, both the horizontal and vertical advections were considered. Air masses from higher or lower altitudes can reach a receiving height of 200 m agl (Bari et al., 2003; Zhu et al., 2011). The NCEP Global Forecast System (GFS) with a resolution (0.25x0.25 degree) offered daily meteorological data, which could be downloaded from the HYSPLIT website (https://www.ready.noaa.gov/archives.php). Hourly PM_{10} concentrations for receptor site during the period from January 1, 2021, to December 31, 2022, were obtained from the European Environment Agency Platform. Data are available at (https://discomap.eea.europa.eu/map/fme/AirQualityExport.htm/).

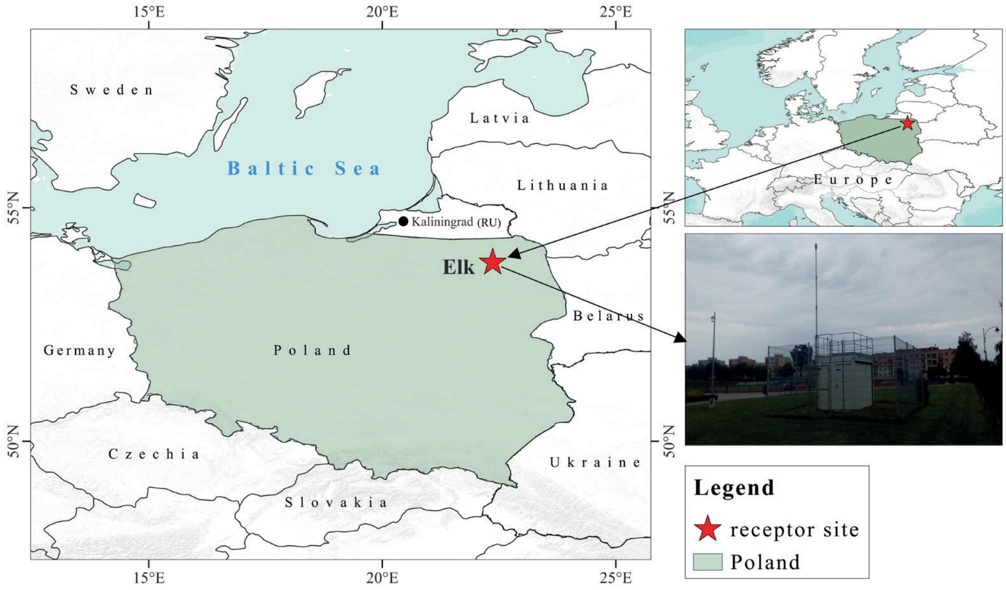

Fig. 1. The location of the study area. The red star represents the receptor point, i.e., the arrival point for air masses

Trajectory Models

To determine the potential impact of cross-region wind transport on air pollutants' concentrations, Trajectory Models were used. In the 1940s, the first Trajectory Models were developed (Draxler and Hess, 1998; Stein et al., 2015). They can help identify areas with transboundary air pollution sources by using regional weather data and Lagrangian functions to reconstruct air parcel routes at specific locations and over selected time periods (Draxler and Hess, 1998). To analyze atmospheric transport, several trajectory models have been constructed. They can be used to investigate how the movement of the atmosphere forward or backward in time. Flexible Trajectory Model (FLEXTRA; Fleming et al., 2012) and the HYSPLIT trajectory model (Draxler and Hess, 1998) are two examples. They have been used for retrospective analyses or prediction of possible pollution sources or pollution points. These models are considered relatively efficient and effective tools for atmospheric transport and dispersion modeling, as they require less computational effort than more complex and computationally demanding models.

The HYSPLIT model is one of the most widely used models for trajectory analysis. It is a comprehensive system that can calculate everything from simple air packet trajectories to complicated propagation and deposition simulations (Yerramilli et al., 2012a). The National Oceanic and Atmospheric Administration's (NOAA) Air Resources Laboratory used HYSPLIT model to investigate the sources and pathways of air pollution (Heffter et al., 1975). The model provides high-precision and time-continuous simulation results and has been widely used in the study of migration and diffusion of various pollutants in different fields. The HYSPLIT model is divided into two parts: the backward transport model and the forward diffusion model, which address the source- and sink-related problems, respectively (Draxler and Hess, 1998; Li et al., 2020; Sahu et al., 2019).

Trajectory clustering analysis

Cluster analysis is a multivariate statistical technique that has become more popular in studies of air pollution. Clustering means that, according to the similarity principle, data objects with higher similarity can be divided into the same cluster, and data objects with higher heterogeneity can be divided into different clusters (Moody and Galloway, 2017; S. Wang et al., 2017). The trajectory data was divided into many classes or clusters using trajectory clustering analysis, a multivariate statistical analytic technique. Data in the same class or cluster share a higher degree of similarity, whereas those in different classes or clusters vary more significantly (Xin et al., 2016). This study uses TrajStat, a plugin of MeteoInfo (Wang et al., 2009); this plugin can view, query, and cluster trajectories and includes two clustering methods: Euclidean distance and angle distance. The angle distance clustering approach is utilized to cluster airflow trajectories since this study determines the direction from which air masses arrive at the site. The angle distance, which varies between 0 and π, is often used to define the mean angle between the two trajectories (Sirois and Bottenheim, 1995). The PM_{10} concentrations associated with backward trajectories were then compared in each cluster.

$$d_{12} = \frac{1}{n}\sum_{i=1}^{n}\cos^{-1}\left(0.5\frac{\left(A_i + B_i - C_i\right)}{\sqrt{A_i B_i}}\right) \tag{1}$$

$$A_i = \left(X_1(i) - X_o\right)^2 + \left(Y_1(i) - Y_o\right)^2 \tag{2}$$

$$B_i = \left(X_2(i) - X_o\right)^2 + \left(Y_2(i) - Y_o\right)^2 \tag{3}$$

$$C_i = \left(X_2(i) - X_1(i)\right)^2 + \left(Y_2(i) - Y_1(i)\right)^2 \tag{4}$$

where n is total duration of a trajectory, "d_{12} is the mean angle between the two backward trajectories, as seen from the trajectory origin point and the variables X_0 and Y_0 define as the position of the receptor site (backward trajectory origin point). X_1 (Y_1) and X_2 (Y_2) reference backward trajectories 1 and 2, respectively".

Potential source contribution function (PSCF)

The PSCF (Hopke et al., 1995) is a commonly used method for identifying regional sources that is based on the HYSPLIT model, which uses meteorological data in its analytic scheme to generate a probability field that may be used to determine source emission potential (C. Y. Hsu et al., 2019). PSCF is a conditional probability function that estimates the likelihood of a pollutant-laden air parcel arriving at a receptor site after passing through a specified upwind source area. A gridded i by j array is used to split the possible source region (Hopke et al., 1995). PSCF is often applied to selecting concentrations exceeding a certain level to pinpoint sources having the potential to induce high concentrations at the site, and many criteria are suggested in the literature to choose such 'cut-off' values. In this study, the PSCF threshold for PM_{10} concentrations was set at the 90th percentile.

The PSCF value for the ijth cell is then defined as the following:

$$PSCF_{ij} = n_{ij}/N_{ij} \tag{5}$$

where N_{ij} is the number of trajectories that crossed in the ij^{th} grid during the study period and n_{ij} is the number of trajectories that arrived at a receptor site with pollutant concentrations exceeding a predefined criteria value (Hopke et al., 1995).

The PSCF value can be considered the conditional probability that analyte concentrations above the threshold level are related to air parcel passage through the ij^{th} cell during transport to the receptor location. That is, cells with high PSCF values are linked to the arrival of air parcels with analyte concentrations higher than the threshold value at the receptor location. These cells represent regions where the constituent has a 'high potential' contribution (Wang et al., 2006). Studies have demonstrated that great uncertainty exists in the calculated result when N_{ij} is extremely small (Dimitriou et al., 2021). To eliminate this uncertainty, an arbitrary weight function, W_{ij}, was applied when the number of endpoints in a particular cell was less than three times the average number of endpoints for each cell (Hopke et al., 1995).

$$WPSCF_{ij} = W_{ij} \times PSCF_{ij} \tag{6}$$

$$W_{ij} = \begin{cases} 1.00 & N_{ij} > 80 \\ 0.70 & 20 < N_{ij} \le 80 \\ 0.42 & 10 < N_{ij} \le 20 \\ 0.05 & 0 < N_{ij} \le 10 \end{cases} \tag{7}$$

Concentration weighted trajectory (CWT)

Because the PSCF method has difficulty distinguishing between strong and moderate pollution sources, the CWT method was used to estimate the relative importance of probable sources (Hsu et al., 2003). As previously stated, one shortcoming of the PSCF approach is that grid cells with sample concentrations that were either slightly higher or significantly higher than the threshold could have the same PSCF result. As a result, distinguishing between moderate and powerful sources may be challenging (Ma et al., 2019). To identify the sources in each grid, the concentration-weighted trajectory method (CWT) was applied with the aim of producing a geographical overview of possible emission areas within the study region (Hsu et al., 2003). CWT method is allow to reconstruct "potential sources" or more precisely spatial distribution of mean contribution of potential sources to content of admixture in a receptor point (Shukurov and Shukurova, 2017). The calculation formula of the CWT method is given as follows (Hsu et al., 2003):

$$CWT_{ij} = \frac{\sum_{K=1}^{N} C_k \tau_{ijk}}{\sum_{K=1}^{N} \tau_{ijk}} \tag{8}$$

where CWT_{ij} is mean contribution of potential sources located in ij-cell into concentration in receptor point; N is the total number of trajectories; k denotes a trajectory; Ck is the PM_{10} concentration of trajectory k when it passes through ij-cell, which can be calculated using the HYSPLIT model; and τ_{ijk} is the duration in which trajectory k stays in ij-cell. In addition, the CWT method causes great uncertainties, thus the weight coefficient W_{ij} is needed to reduce these uncertainties (Y. K. Hsu et al., 2003; Stohl, 1998). Similarly, W_{ij} is determined using Equation (7), and the introduction of the coefficient is as follows:

$$WCWT_{ij} = W_{ij} \times CWT_{ij} \tag{9}$$

In this study, the domain for the PSCF grid covers the longitudes of about 30°W-60°E and the latitudes of 30°–75°N and contained 16,200 grid cells of 0.5° × 0.5°.

RESULTS AND DISCUSSION

PM_{10} Pollution Characteristics

The average hourly variations in PM_{10} concentrations from January 2021 to December 2022 are shown in Figure 2, and the monthly and seasonal variations are shown in Figure 3. The PM_{10} annual average concentrations for 2021 and 2022 are 20.6 μg/m³ and 19.6 μg/m³, respectively, which is less than twice the EU standard (40 μg/m³). In addition, the number of days the EU air quality standard was exceeded was 38 between January 1, 2021, and December 30, 2022 (the 24-hour standard was 50 μg/m³). The particulate matter (PM_{10}) concentrations measured in Elk showed clear seasonal variations, with the highest average PM_{10} concentrations observed in the winter months. For the period January 1, 2021 to December 30, 2022, the highest PM_{10} concentrations of approximately 23.34 μg/m³ are found in winter (December, January and February), followed by spring (March to May) with 22.31 μg/m³. In contrast, the lowest concentrations were recorded in summer (June to August) and autumn (September to November) with only 17.68 μg/m³ and 17.44 μg/m³, respectively. This suggests that the higher PM_{10} concentrations in winter were due to increased PM_{10} emissions from human activities, such as burning fossil or renewable fuel during the heating season. The highest monthly concentration was in March (33 μg/m³) and the lowest was in September (13.7 μg/m³).

Transport Pathways

This section discusses potential pollutant transport pathways to the Elk Site based on the results of the clustering analysis of backward trajectories calculated at 02:00, 05:00, 08:00, 11:00, 14:00, 17:00, 20:00, and 23:00 (LT) every day from January 2021 to December 2022 (Fig. 4).

TrajStat was used to process the airflow data to obtain seasonal transport trajectories. However, it was impossible to determine the exact number of trajectories in different directions using these airflow trajectories. Therefore, the trajectories in winter, spring, summer, and autumn were integrated into 5-4-4-5 clusters according to the consistency of the temporal and spatial distribution of backward trajectories (Fig. 5). Backward clustering trajectories that exceed the 90th percentile threshold for PM_{10} concentrations are presented and defined as "high-polluted" trajectories, while backward clustering trajectories corresponding to concentrations below the 90th percentile threshold are defined as "low-polluted" low-polluting trajectories.

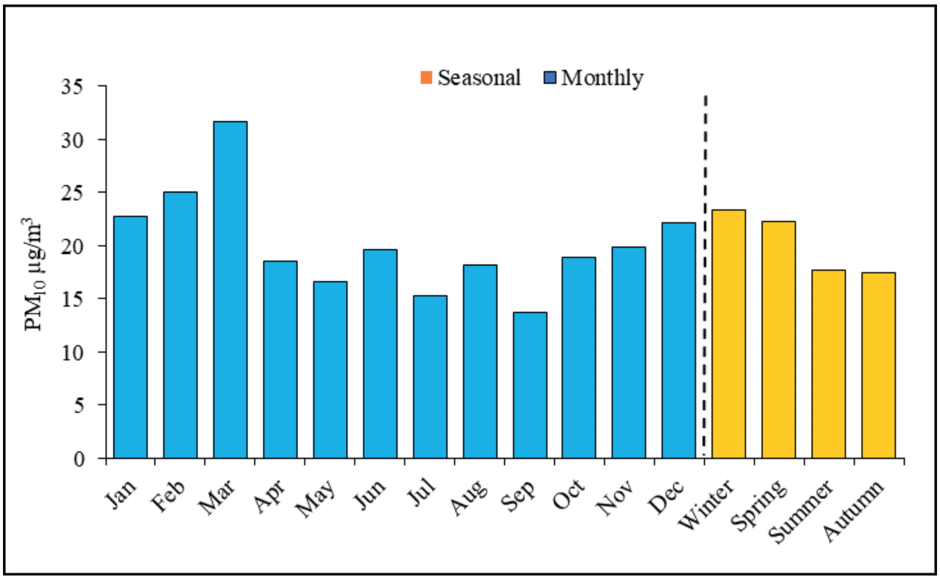

Fig. 2. Monthly and seasonal average PM_{10} variation at EEA station in the Elk city (Poland) from January 2021 to December 2022

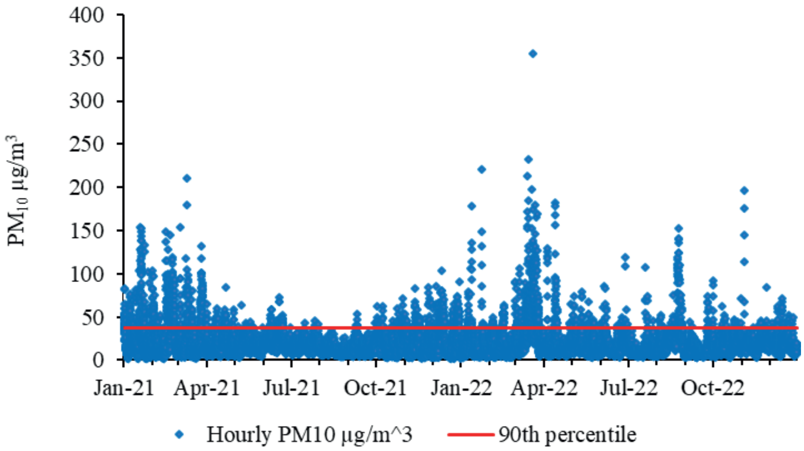

Fig. 3. Hourly average PM_{10} variation at EEA station in the Elk city (Poland) from 1 January 2021 to 31 December 2022

In winter, five clusters of backward trajectories were identified. The winter air flows were mainly from the west (cluster 4), accounting for 48.7% of the winter airflow. In spring, the backward trajectories were grouped into four clusters. Airflows from the northwest (cluster 4) accounted for the largest portion of airflows in spring at 33%, followed by the north (cluster 3) with 23.6% of airflows in spring. The airflows in summer were divided into four clusters. In summer, the airflows arriving at Elk have a divergent distribution. The western (cluster 4) and eastern airflows (cluster 3) had the largest shares of 43.8% and 28.9%, respectively. In autumn, there are five clusters of backward trajectories, the airflows are mostly western (cluster 3, accounts for 31% of the airflows in autumn), with longer transmission distances and faster speeds.

Based on the results of the clustering analysis of seasonal airflow backward, combined with the PM_{10} concentration data of Elk (Table 1), the potential impacts of various trajectories on PM_{10} levels in Elk were quantified. Consistent with the results discussed above, the PM_{10} concentration and number of polluted trajectories in winter and spring is higher than that in summer and autumn.

In winter, the airflows associated with clusters 3 and 5 are identified as the most polluted, with high levels of PM_{10} of 71.9 µg/m^3 and 59.4 µg/m^3, respectively. However, when considering the number of polluted trajectories, cluster 4, which is associated with the west airflow originating from the UK through the northern Netherlands and from Germany to western Poland, shows greater significance. Despite having a low PM_{10} concentration (approximately 51 µg/m^3), cluster 4 had the highest number of pollution trajectories, which exceeded the threshold of 37.5 µg/m^3. Specifically, it contributed to over 46% of the total winter-pollution trajectories. The high concentrations of PM_{10} may be related to the fact that these areas are in heating season, leading to increased anthropogenic emissions of pollutants, e.g., from the use of solid fuels for heating.

For spring, the highest average PM_{10} concentration for the polluted trajectories observed at the Elk site (74.9 µg/m^3) was associated with the easterly airflow of cluster 2, which contributed 13.2% of the polluted trajectories in spring (Fig. 5b). High PM_{10} concentrations were also associated with northwesterly airflows (cluster 3), which contributed 41.9% of the pollution trajectories, with an average PM_{10} concentration of 66 µg/m^3.

In summer, the average PM_{10} concentrations and the number of pollution trajectories associated with clusters were the least significant compared to the other seasons. In summer, many plants flourish, and the total leaf area of the surface vegetation significantly increases, which is conducive to the adsorption of atmospheric particulates (Indumali and Appuhamillage, 2018). The eastern airflow (cluster 2) was the most important in this season, as it accounted for more than 80% of the summer pollution trajectories, with an average PM_{10} concentration of 61.9 µg/m^3.

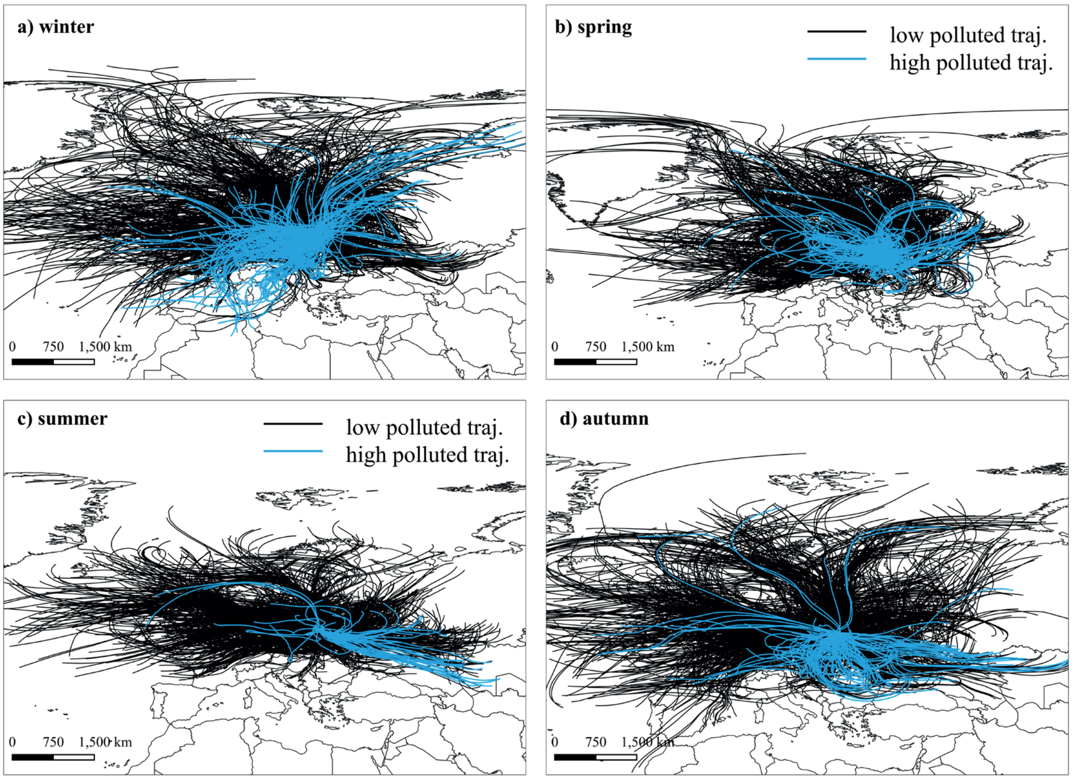

Fig. 4. 72-h backward trajectories for the four seasons (from January 2021 to December 2022); bold blue trajectories were identified as pollution trajectories (PM10 concentration >37.5 μg/m³).

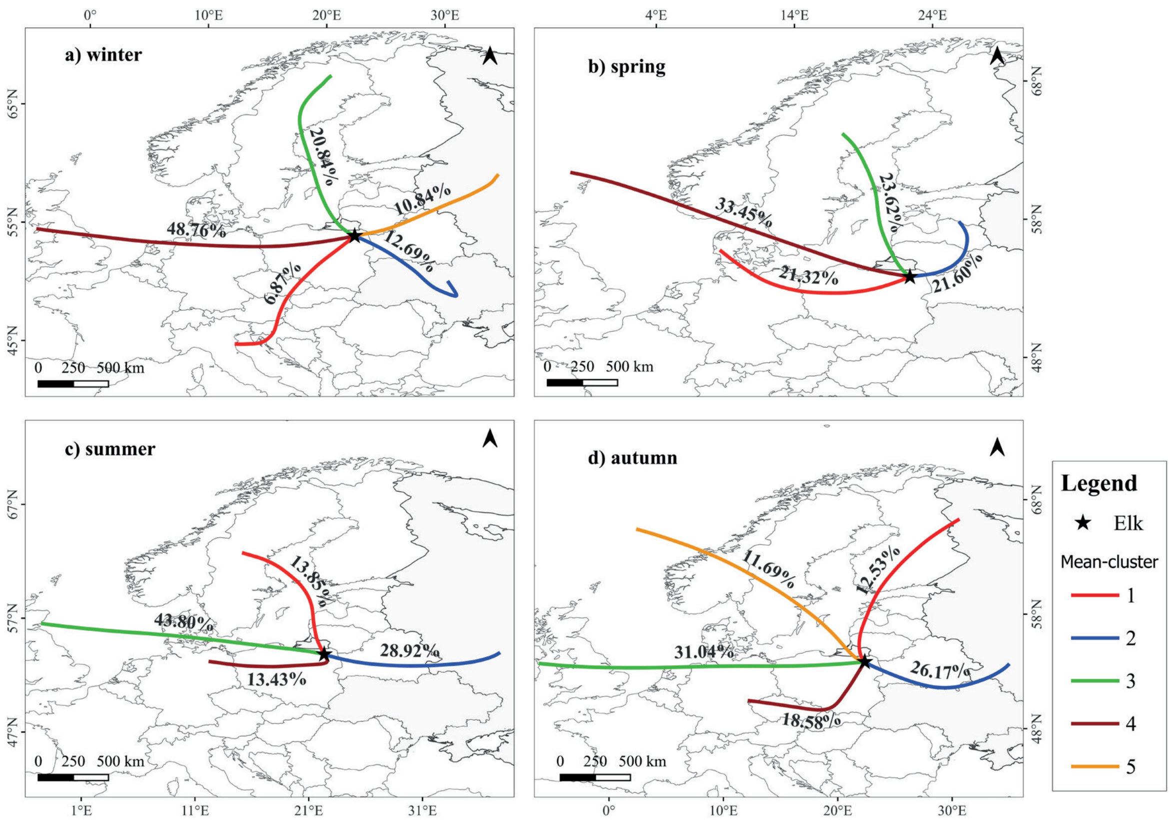

Fig. 5. Mean-Cluster backward trajectories at Elk site for the four seasons from January 2021 to December 2022

Table 1. Summary statistics of the cluster analysis showing the number of trajectories in each cluster and the mean concentration and standard deviation of PM_{10} concentrations.

Season	Cluster	All trajectories		Polluted trajectories	
		Number of traj.	Mean PM_{10} (µg/m^3)	Number of traj.	Mean PM_{10} (µg/m^3)
Winter	1	95	44.63±24.58	52	58.61±25.28
	2	177	28.38±13.85	30	50.85±18.24
	3	294	15.20±19.16	21	70.91±33.79
	4	683	22.12±16.21	114	51.27±12.22
	5	153	27.05±19.86	27	59.45±27.39
	All	1402	23.52±19.03	244	55.38±21.28
Spring	1	495	15.92±12.45	28	56.01±15.47
	2	336	17±19.05	23	74.92±33.94
	3	310	30.54±26.58	73	66.07±33.51
	4	317	25.11±21.36	50	59.60±33.51
	All	1458	21.28±20.50	174	63.76±31.67
Summer	1	204	12.13±8.10	4	48.11±14
	2	394	25.83±16.86	41	61.90±27.64
	3	630	11.95±5.65	2	56.80±17.49
	4	189	18.58±8.44	4	54.04±20.84
	All	1417	16.72±12.19	51	60.01±25.94
Autumn	1	180	10.02±7.58	2	54.40±6.92
	2	372	23.53±14.56	46	51.48±17.83
	3	443	16.77±13.75	16	60.60±42.98
	4	267	26.03±10.48	32	46.97±7.97
	5	162	12.10±10.24	3	64.39±20.81
	All	1424	18.89±13.62	99	51.95±21.99

In autumn, PM_{10} concentrations associated with western and northwestern airflows (clusters 3 and 5) were the highest (60.6 µg/m^3, 64.4 µg/m^3, respectively), but less significant in terms of the number of polluted trajectories. In contrast, eastern airflows were more significant (cluster 2), accounting for 46% of the total number of pollution trajectories in autumn, with an average PM_{10} concentration of 51.4 µg/m^3.

Source analysis of PM10 based on PSCF and CWT methods

In order to fully reflect the long-range impact characteristics and contributions of potential source areas to PM_{10} mass concentrations in Elk, we conducted a potential source contribution function (WPSCF) analysis and a concentration-weighted trajectory (WCWT) analysis based on the backward trajectory of each season from 2021 to 2022.

Trajectory clustering analysis can be utilized to determine the main migration path of pollutants in the receptor station; however, the relative contribution level of the potential source area cannot be identified and simulated (Wang et al., 2017; Yerramilli et al., 2012). Further research is required to investigate the potential sources of PSCF and CWT methods, to obtain a better understanding of the long-range transport of pollutants to the Elk site, and to find potential source areas. Figure 6 and 7 show the calculation results of the WPSCF and WCWT of PM_{10} across the four seasons in Elk, respectively. WPSCF values of 0.1 – 0.3, 0.3 – 0.5, 0.5 – 0.7 and ≥ 0.7 were divided into very light, light, moderate, and severe pollution grids, respectively, to identify potential source grid attributes. The colors represent the contribution levels of the potential source area, and the red color could be associated with high concentrations (i.e., where the main potential sources were concentrated), whereas the blue color represents low concentrations (i.e., secondary potential sources).

In general, the spatial distributions of PM_{10} potential source areas and WPSCF and WCWT values were large in winter and spring, and lowest in summer and autumn. In winter, the main potential source areas contributing to high PM_{10} concentrations in Elk, with WPSCF values (≥ 0.7), were located in southwestern Poland, eastern Czech Republic, large areas of Slovakia, and north of Hungary. In these regions, the WCWT values were (≥ 50 µg/m^3) (Fig. 6a and

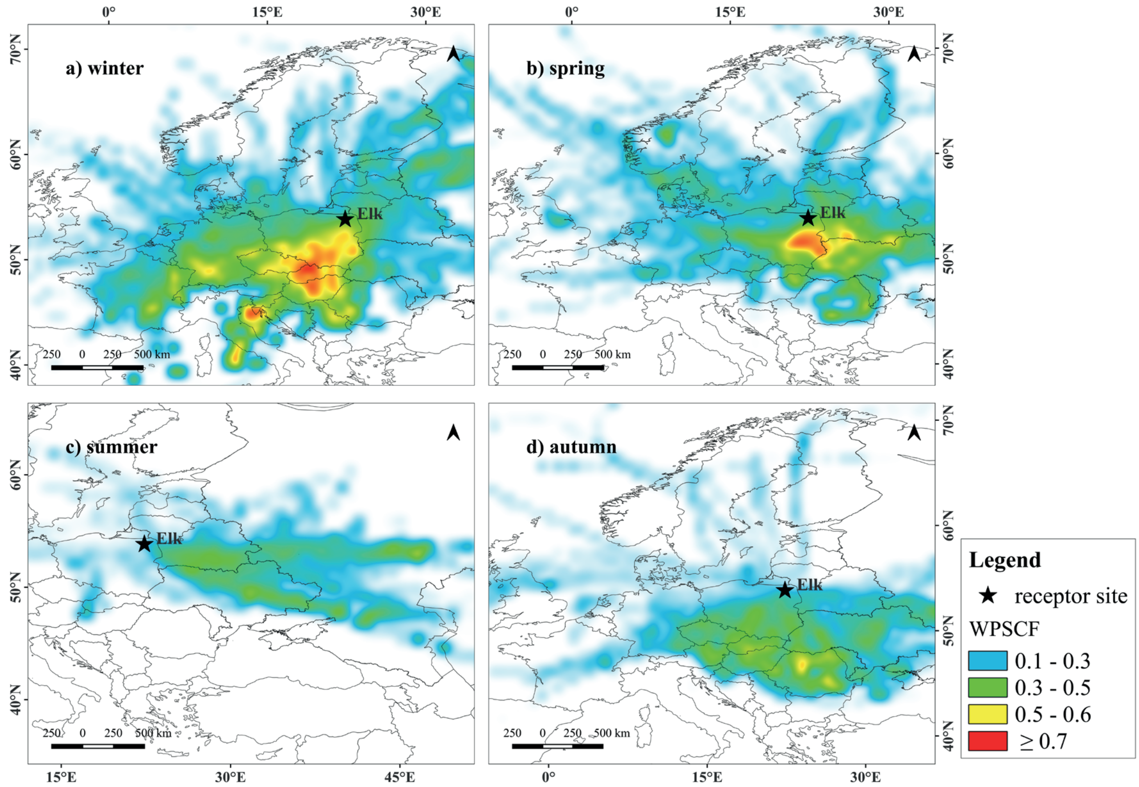

Fig. 6. Weighted Potential Source Contribution Function (WPSCF) map for PM_{10} from January 2021 to December 2022. The red color represents the high probable potential sources of extreme PM_{10} (over 90th percentile) while the blue color represents the low probable

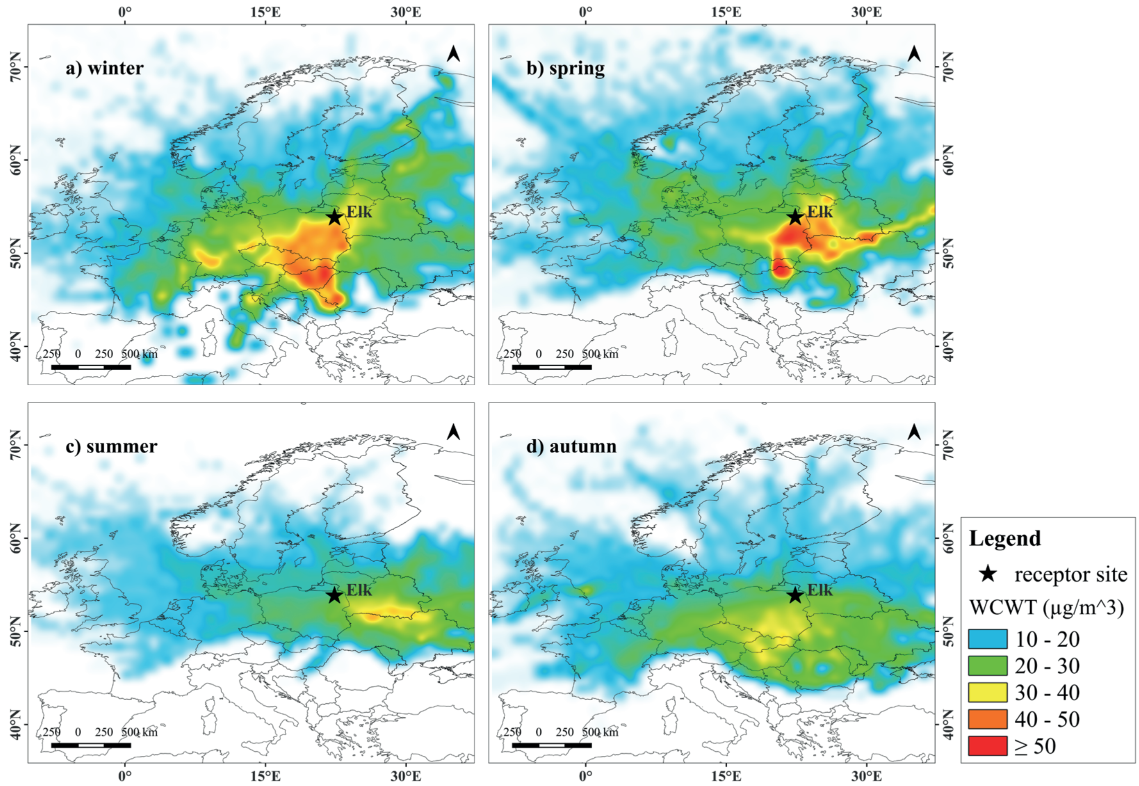

Fig. 7. Weighted Concentration-weighted Trajectories (WCWT) map for PM_{10} from January 2021to December 2022

7a). According to the European Environment Agency (EEA), the air quality in these regions has been found to exceed the limit values for PM_{10} concentrations in the air, as this region is highly industrialized, with a high concentration of coal-fired power plants and other sources of air pollution.

In spring, compared with winter, the main potential source areas of PM_{10} moved eastward, and the severe pollution source areas with high WPSCF values (≥ 0.7) were more concentrated in local areas south of the Elk site in east-central Poland (Mazovia Province). High WCWT values were mainly observed at ≥ 50 μg/m^3 in local areas south of the Elk site and the west of Belarus and northwest Ukraine, and some distributions in eastern Slovakia and northern Hungary. In summer, the spatial distributions of PM_{10} were mainly light polluted grids, with low WPSCF values of 0.1–0.5, and corresponding WCWT values (30–40 μg/m^3), associated with south-eastern air masses, were mainly concentrated in the south of Belarus, southeast of Ukraine and small distributions in southern Russia in the North Caucasus (Fig. 6c and 7c). In autumn, the light and moderate pollution source areas of PM_{10} were concentrated in southeastern Poland and some individual distributions over Slovakia and Hungary (Central Transdanubia and Southern Transdanubia provinces) with WCWT values between (30 and 40 μg/m^3) (Fig. 7d).

CONCLUSIONS

In this study, cluster trajectory, Potential Source Contribution Function (PSCF), and Concentration-Weighted Trajectory (CWT) methods were used to identify potential source regions that could potentially affect a given PM_{10} measurement site in southeastern Baltic (Elk site).

The annual average of PM_{10} at the Elk site for the years 2021 and 2022 was 20.6 μg/m^3 and 19.6 μg/m^3, respectively, which are less than twice the EU standard. The PM_{10} mass showed seasonal variation, with a peak in winter and trough in summer. The high PM_{10} monthly mean values were related to heating in winter and peaked in March (31.7 μg/m^3). Conversely, the minimum monthly mean value of PM_{10} was observed in September at 13.7 μg/m^3.

Cluster analysis showed that the Elk atmosphere was mainly influenced by air masses from the western and southwestern directions. In addition, it was found that the main potential source regions contributing to high PM_{10} in winter are located in southwestern Poland and large areas of the Czech Republic and Slovakia, with WPSCF values ≥ 0.7, and corresponding WCWT values ≥ 50 μg/m^3. In spring, the main potential source areas of PM_{10} moved eastward, and high WPSCF and WCWT values were observed mainly in localized areas south of Elk in east-central Poland and northwestern Ukraine, with WPSCF values of ≥ 0.5 and WCWT values of 50 μg/m^3. In contrast, The WPSCF and WCWT values were low in summer and autumn, and the Elk site was less affected by the long-range transport.

In the future, we will conduct a case study and focus specifically on a high PM event in the southeastern Baltic region. In-depth research will also be conducted on how meteorological factors, such as temperature, wind speed, and relative humidity, affect PM concentrations.

REFERENCES

Bari A., Dutkiewicz V.A., Judd C.D., Wilson L.R., Luttinger D. and Husain L. (2003). Regional sources of particulate sulfate, SO2, PM2.5, HCl, and HNO3, in New York, NY. Atmospheric Environment, 37(20), 2837–2844. doi: 10.1016/S1352-2310(03)00200-0

Bihałowicz J.S., Rogula-Kozłowska W. and Krasuski A. (2021). Contribution of landfill fires to air pollution – An assessment methodology. Waste Management, 125, 182–191. doi: 10.1016/J.WASMAN.2021.02.046

Bodor Z., Bodor K., Keresztesi Á. and Szép R. (2020). Major air pollutants seasonal variation analysis and long-range transport of PM10 in an urban environment with specific climate condition in Transylvania (Romania). Environmental Science and Pollution Research International, 27(30), 38181. doi: 10.1007/S11356-020-09838-2

Byčenkiene S., Dudoitis V. and Ulevicius V. (2014). The Use of Trajectory Cluster Analysis to Evaluate the Long-Range Transport of Black Carbon Aerosol in the South-Eastern Baltic Region. Advances in Meteorology, 2014. doi: 10.1155/2014/137694

Draxler R.R. and Hess G.D. (1998). OverviewHYSPLIT4. Aust. Meteor. Mag., 47, 295–308.

Daly A. and Zannetti P. (2007). An Introduction to Air Pollution-Definitions, Classifications, and History. Retrieved from http://www.arabschool.org.sy

Dimitriou K., Grivas G., Liakakou E., Gerasopoulos E. and Mihalopoulos N. (2021). Assessing the contribution of regional sources to urban air pollution by applying 3D-PSCF modeling. Atmospheric Research, 248, 105187. doi: 10.1016/J.ATMOSRES.2020.105187

Fleming Z.L., Monks P.S. and Manning A.J. (2012). Review: Untangling the influence of air-mass history in interpreting observed atmospheric composition. Atmospheric Research, 104–105, 1–39. doi: 10.1016/J.ATMOSRES.2011.09.009

Heffter J.L., Taylor A.D. and Ferber G. (1975). A regional-continental scale transport, diffusion, and deposition model. Retrieved from https://repository.library.noaa.gov/view/noaa/14895

Hopke P.K., Barrie L.A., Li S.M., Cheng M.D., Li C. and Xie Y. (1995). Possible sources and preferred pathways for biogenic and non-sea- salt sulfur for the high Arctic. Journal of Geophysical Research, 100(D8). doi: 10.1029/95JD01712

Hsu, C. Y., Chiang, H. C., Chen, M. J., Yang, T. T., Wu, Y. S., & Chen, Y. C. (2019). Impacts of hazardous metals and PAHs in fine and coarse particles with long-range transports in Taipei City. Environmental Pollution, 250, 934–943. doi: 10.1016/J.ENVPOL.2019.04.038

Hsu Y.K., Holsen T.M. and Hopke P. K. (2003). Comparison of hybrid receptor models to locate PCB sources in Chicago. Atmospheric Environment, 37(4), 545–562. doi: 10.1016/S1352-2310(02)00886-5

Indumali U. and Appuhamillage W. (2018). THE IMPACT OF LIVING WALLS IN THE REDUCTION OF ATMOSPHERIC PARTICULATE MATTER POLLUTION.

Jasiński R., Galant-Gołębiewska M., Nowak M., Kurtyka K., Kurzawska P., Maciejewska M. and Ginter M. (2021). Emissions and Concentrations of Particulate Matter in Poznan Compared with Other Polish and European Cities. Atmosphere 2021, Vol. 12, Page 533, 12(5), 533. doi: 10.3390/ATMOS12050533

Kim D.S. (2013). Air Pollution History, Regulatory Changes, and Remedial Measures of the Current Regulatory Regimes in Korea. Journal of Korean Society for Atmospheric Environment, 29(4), 353–368. doi: 10.5572/KOSAE.2013.29.4.353

Kobza J., Geremek M. and Dul L. (2018). Characteristics of air quality and sources affecting high levels of PM10 and PM2.5 in Poland, Upper Silesia urban area. Environmental Monitoring and Assessment, 190(9), 1–13. doi: 10.1007/S10661-018-6797-X/TABLES/5

Li C., Dai Z., Liu X. and Wu P. (2020). Transport Pathways and Potential Source Region Contributions of PM2.5 in Weifang: Seasonal Variations. Applied Sciences 2020, Vol. 10, Page 2835, 10(8), 2835. doi: 10.3390/APP10082835

Li M., Huang X., Zhu L., Li J., Song Y., Cai X. and Xie S. (2012). Analysis of the transport pathways and potential sources of PM10 in Shanghai based on three methods. Science of The Total Environment, 414, 525–534. doi: 10.1016/J.SCITOTENV.2011.10.054

Ma Y.F., Du B.Y., Wang Q., Hu Q.Q., Bian Y.S., Wang M.B. and Jin S.Y. (2019). Analysis of the atmospheric pollution transport pathways and sources in Shenyang, based on the HYSPLIT model. IOP Conference Series: Earth and Environmental Science, 351(1), 012030. doi: 10.1088/1755-1315/351/1/012030

Majewski G., Rogula-Kozłowska W., Rozbicka K., Rogula-Kopie, P., Mathew, B. and Brandyk A. (2018). Concentration, Chemical Composition and Origin of PM1: Results from the First Long-term Measurement Campaign in Warsaw (Poland). Aerosol and Air Quality Research, 18(3), 636–654. doi: 10.4209/AAQR.2017.06.0221

Manisalidis I., Stavropoulou E., Stavropoulos A. and Bezirtzoglou E. (2020). Environmental and Health Impacts of Air Pollution: A Review. Frontiers in Public Health, 8, 505570. doi: 10.3389/FPUBH.2020.00014/BIBTEX

Moody J.L. and Galloway J.N. (2017). Quantifying the relationship between atmospheric transport and the chemical composition of precipitation on Bermuda. Tellus B: Chemical and Physical Meteorology, 40(5), 463–479. doi: 10.3402/tellusb.v40i5.16014

Nazar, W., Niedoszytko, M. (2022). Air Pollution in Poland: A 2022 Narrative Review with Focus on Respiratory Diseases. International Journal of Environmental Research and Public Health, 19(2), 895. doi: 10.3390/IJERPH19020895

Pouyaei A., Choi Y., Jung J., Sadeghi B. and Han Song C. (2020). Concentration Trajectory Route of Air pollution with an Integrated Lagrangian model (C-TRAIL Model v1.0) derived from the Community Multiscale Air Quality Model (CMAQ Model v5.2). Geoscientific Model Development, 13(8), 3489–3505. doi: 10.5194/GMD-13-3489-2020

Reizer M. and Orza J.A.G. (2018). Identification of PM10 air pollution origins at a rural background site. E3S Web of Conferences 28, Air Protection in Theory and Practice. doi: 10.1051/e3sconf/20182801031

Sahu S.K., Zhang H., Guo H., Hu J., Ying Q. and Kota S.H. (2019). Health risk associated with potential source regions of PM 2.5 in Indian cities. Air Quality, Atmosphere and Health, 12(3), 327–340. doi: 10.1007/S11869-019-00661-4/FIGURES/7

Shukurov K. and Shukurova L.M. (2017). Potential sources of Southern Siberia aerosols by data of AERONET site in Tomsk, Russia. 208. doi: 10.1117/12.2287936

Sirois A. and Bottenheim J.W. (1995). Use of backward trajectories to interpret the 5-year record of PAN and O3 ambient air concentrations at Kejimkujik National Park, Nova Scotia. Journal of Geophysical Research: Atmospheres, 100(D2), 2867–2881. doi: 10.1029/94JD02951

Stein A.F., Draxler R.R., Rolph G.D., Stunder B.J.B., Cohen M.D. and Ngan F. (2015a). Noaa's hysplit atmospheric transport and dispersion modeling system. Bulletin of the American Meteorological Society, 96(12), 2059–2077. doi: 10.1175/BAMS-D-14-00110.1

Stohl A. (1998). Computation, accuracy and applications of trajectories—A review and bibliography. Atmospheric Environment, 32(6), 947–966. doi: 10.1016/S1352-2310(97)00457-3

Wang S., Yu S., Li P., Wang L., Mehmood K., Liu W., Yan R. and Zheng X. (2017). A Study of Characteristics and Origins of Haze Pollution in Zhengzhou, China, Based on Observations and Hybrid Receptor Models. Aerosol and Air Quality Research, 17, 513–528. doi: 10.4209/aaqr.2016.06.0238

Wang S., Yu S., Yan R., Zhang Q., Li P., Wang L., Liu W. and Zheng X. (2017). Characteristics and origins of air pollutants in Wuhan, China, based on observations and hybrid receptor models. Http://Dx.Doi.Org/10.1080/10962247.2016.1240724, 67(7), 739–753. doi: 10.1080/10962247.2016.1240724

Wang Y.Q., Zhang X.Y. and Arimoto R. (2006). The contribution from distant dust sources to the atmospheric particulate matter loadings at Xian, China during spring. The Science of the Total Environment, 368(2–3), 875–883. doi: 10.1016/J.SCITOTENV.2006.03.040

Wang Y., Zhang X. and Draxler R.R. (2009). TrajStat: GIS-based software that uses various trajectory statistical analysis methods to identify potential sources from long-term air pollution measurement data. Environmental Modelling & Software, 24, 938–939. doi: 10.1016/j.envsoft.2009.01.004

Xin Y., Wang G. and Chen L. (2016). Identification of Long-Range Transport Pathways and Potential Sources of PM10 in Tibetan Plateau Uplift Area: Case Study of Xining, China in 2014. Aerosol and Air Quality Research, 16, 1044–1054. doi: 10.4209/aaqr.2015.05.0296

Yang H. and Smyntek P. (2014). Use of the mercury record in Red Tarn sediments to reveal air pollution history and the implications of catchment erosion. Environmental Science. Processes & Impacts, 16(11), 2554–2563. doi: 10.1039/C4EM00334A

Yerramilli A., Dodla V.B.R., Challa V.S., Myles L.T., Pendergrass W.R., Vogel C.A., Dasari H.P., Tuluri F., Baham J.M., Hughes R.L., Patrick C., Young J.H., Swanier S.J. and Hardy M.G. (2012). An integrated WRF/HYSPLIT modeling approach for the assessment of PM2.5 source regions over the Mississippi Gulf Coast region. Air Quality, Atmosphere and Health, 5(4), 401–412. doi: 10.1007/S11869-010-0132-1/TABLES/6

Zaręba M. and Danek T. (2022). Analysis of Air Pollution Migration during COVID-19 Lockdown in Krakow, Poland. Aerosol and Air Quality Research, 22(3), 210275. doi: 10.4209/AAQR.210275

Zhu L., Huang X., Shi H., Cai X. and Song Y. (2011). Transport pathways and potential sources of PM_{10} in Beijing. Atmospheric Environment, 45, 594–604. doi: 10.1016/j.atmosenv.2010.10.040

RESEARCH PAPER

ANALYSIS OF THE BOTTOM TOPOGRAPHY OF THE RESERVOIR DUE TO SEDIMENT TRAPPING (ACCORDING TO THE KRASNODAR RESERVOIR, RUSSIA)

Anatoly V. Pogorelov[1], Andrey A. Laguta[1], Petr B. Netrebin[1], Dmitry A. Lipilin[1, 2*]
[1]Kuban State University, Stavropolskaya street, 149, Krasnodar, 350040, Russia
[2]Kuban State Agrarian University named after I.T. Trubilin, Kalinina street, 13, Krasnodar, 350044, Russia
*Corresponding author: LipiLin_dmitrii@mail.ru
Received: May 24th, 2023 / Accepted: September 4th, 2023 / Published: October 10th, 2023
https://DOI-10.24057/2071-9388-2023-2907

ABSTRACT. Morphometric descriptions of reservoirs are usually limited to the type, shape, altitude position, bed size and volume of water in them. The article presents the results of the analysis of the bottom topography of the Krasnodar reservoir and the transformations of this for 2005-2021. The analysis was carried out based on the materials of bathymetric surveys for the usable volume of the reservoir on an area of 224 km^2 with the creation of digital elevation models. The topography of the reservoir bottom is represented by flat sections of flooded accumulative plain with prevailing slopes of about 0.2–0.4°, dissected by riverbeds of lower-order tributaries. The transformation of the topography is caused by gradual silting. The total volume of sediments for this area in 2005-2021 amounted to 127 million m^3 with an average siltation layer of 0.4 m. To describe the morphological properties of the bottom topography, we used geomorphometry techniques with the calculation of the BPI index (Bathymetric Position Index) and the classification of mesoscale topography forms based on it. For the riverbed, there are topography forms related to three types of surfaces: flat (Lower Bank Shelves), concave (Depressions, Deep Depressions) and convex (Reef Crests, Back Reefs, Mid-Slope Ridges). The constructed maps reflect the differentiated morphology of the bed surface, the evolution of topography forms and the change in roughness under conditions of continuous transformation of the basin and allow judging the prevailing morphogenetic processes. Morphologically, the coastal zone and the shallow part of the riverbed are the most difficult to construct. Here, along with long-shore reef crests of different genesis, deep depressions and simple depressions in the form of underwater channels on the deltas of extension can form on the accumulative shoal.

KEYWORDS: valley reservoir, sediment trapping, transformation, bottom topography, morphometric analysis, topography forms, Bathymetric Position Index (BPI), GIS, Krasnodar Reservoir

CITATION: Pogorelov A. V., Laguta A. A., Netrebin P. B., Lipilin D. A. (2023). Analysis Of The Bottom Topography Of The Reservoir Due To Sediment Trapping (According To The Krasnodar Reservoir, Russia). Geography, Environment, Sustainability, 3(16), 102-112
https://DOI-10.24057/2071-9388-2023-2907

ACKNOWLEDGEMENTS: The research was carried out with the financial support of the Russian Science Foundation and Kuban Science Foundation in the framework of the scientific project No. 22-27-20008.

Conflict of interests: The authors reported no potential conflict of interest.

INTRODUCTION

The Krasnodar Reservoir on Kuban River (Russia) was put into operation in 1973, and according to the classification is a large reservoir (Avakyan et al., 1987). The reservoir located in the south of Russia near Krasnodar on the border of two regions – Krasnodar Territory and the Republic of Adygea, has two key functions – flood control and irrigation. When filled to the design level in 1975, the area of the reservoir reached 400 km^2, and the total volume was about 3 km^3. The reservoir belongs to the valley type, has an elongated shape. It had a length of 46 km, a maximum width of 11 km with an average depth of 5.9 m and a maximum depth of 24.7 m at the initial stage of operation (Lurie et al., 2005).

The reservoir serves as a reference object of the entire irrigation system of Krasnodar Territory and the main source of water for rice crops in the lower reaches of Kuban River with an annual intake of water in about 3.3 km^3 for irrigation. In this sense, an important characteristic is the useful volume of the reservoir – 2.2 km^3 according to the design parameters. The peculiarity of the water regime is seasonal volume regulation with relatively large intra–annual amplitudes of the water level reaching 7 m in some years. This amplitude acts as a factor in the formation of the bed surface, contributes to the formation of significant areas of variable flooding, constant movement of the contact zone "water – land", and also affects the circulation of water masses.

Among the rivers of Russia, on which large reservoirs have been created, Kuban River has the highest turbidity – 0.68 kg/m^3. According to (Rules..., 2008; Alekseevsky et al., 2012), up to 95-98% of sediments brought by the river are deposited in the reservoir. According to our calculations, during 1973-2021, as a result of sediment trapping, the useful volume of the reservoir decreased from 2,160 to 1,270 million m^3, and the mirror area – from 400 to 224 km^2 (Pogorelov et al., 2022). Sediment trapping is accompanied by a continuous restructuring of the underwater topography due to interrelated geomorphological and hydrological processes – sediment deposition, changes in the local structure of currents, etc. (Litovka et al., 2019; Pogorelov, Laguta, 2020; Pogorelov et al., 2021, 2022). Note that the above processes are typical for a number of similar hydraulic structures (Zhang Wei et al., 2015; Andjelkovic et al., 2017; Honek et al., 2020; Shiferaw, Abebe, 2021; Li Xin et al., 2023). Of particular interest are studies related to the use of remote sensing (Dalu et al., 2013; Abaev et al., 2022) and having a long follow-up period (Peng, Chen, 2010; Liu, Lv, Li, 2021).

In the formation of the topography of the reservoir bed and its transformation, the leading role belongs to fluvial processes, of which delta formation processes are the most active. During the period of the reservoir's existence, the evolution of Kuban and Belaya river deltas significantly affected its morphometric characteristics (Laguta, Pogorelov, 2019; Pogorelov et al., 2021). Immediately after the filling of the Krasnodar Reservoir, the alienation of its north-eastern part – the former Tshchik Reservoir - started (Kurbatova, 2014), which was facilitated by the development of the delta of Belaya River, the preservation of the old dam and the collapse of the Tshchik Reservoir. At certain elevations, the section of the former Tshchik Reservoir lying above did not become riverbed, which is usually characteristic of valley reservoirs. At present, the estranged Tshchik Reservoir has its own circulation conditions and sediment deposits.

According to our calculations for the period 2005-2021 (Fig. 1) the volume of sediment accumulation in the main reservoir without taking into account the separated Tshchik Reservoir and deltaic sediments of the dividing bridge amounted to 127 million m^3 (Pogorelov et al., 2022). The maximum volumes of sediments and sedimentation rates during the removal of suspensions were recorded in the deltas of Kuban and Belaya, the smallest – in the dead volume area, i.e. in the western (deepest) part of the basin. As we can see (Fig. 1), the underwater topography near the shore is most susceptible to transformations, where in the process of active long-shore and transverse sediment transport, the continuous formation and transformation of accumulative and abrasive forms occurs. The activity of topography formation in valley reservoirs in the zone of long-range transport with the formation of mesoscale forms is confirmed (Finarov, 1986; Nazarov et al., 2011; 2013). The presence of local negative landforms (pits) is the result of limited technogenic removal of bottom sediments in 2005-2021. The total area of such forms is 13 km^2.

Standard morphometric characteristics of reservoirs adopted in hydrometry reflect the type, shape, altitude position, size of the bed of reservoirs and the volume of water in them. However, little attention is paid to the study of bottom morphology, despite its role in the formation of integral morphometric parameters. The reason is the difficulty of obtaining the source data. In this regard, we note a number of works (Van Maren et al., 2013; Su Teng et al., 2015; Mahfouz, Dekhkanova, 2019; Liu et al., 2020; Wang Yanjun et al., 2020). At the same time, the geomorphological features of the reservoir bottom topography, as well as the dynamics of the topography, are key ones to understanding the processes of reservoir transformation and forecasting its morphometric characteristics (area, depth, volume of water at different levels, bathygraphic and volumetric curves of the reservoir, etc.). With the development of spatial analysis tools using DEM (Zemlyanov et al., 2011; Kalinin et al., 2018; Akylbekov et al., 2022), including geomorphometry tools (Geomorphometry..., 2009; Florinsky, 2021), the analysis of the bottom topography of reservoirs has reached a new technical level. Studies have appeared related to the modeling of sediment trapping of reservoirs based on channel, erosion and related processes (Suresh Babu et al., 2000; Yutsis et al., 2014; Zhou Yongqiang et al., 2015; Alahiane et al., 2016; Rakhuba and Shmakova, 2022).

The morphological properties of the bottom topography of the Krasnodar reservoir have not been studied and are of particular interest from the perspective of its long-term evolutionary transformations. The article reveals the main tasks:

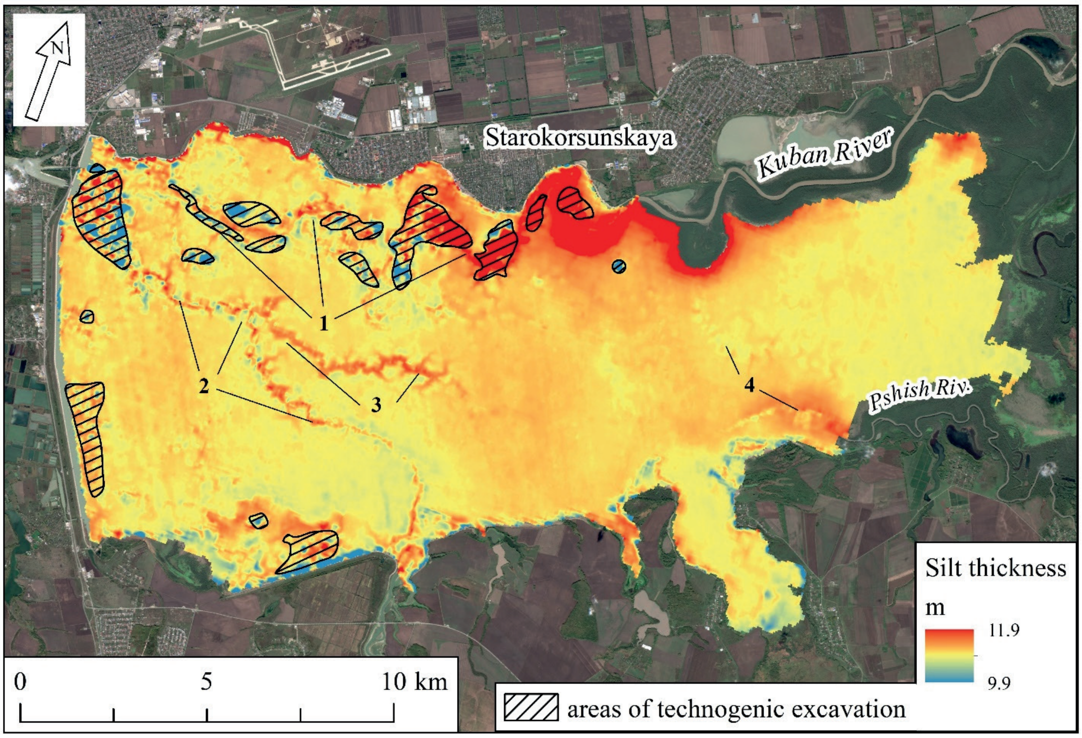

Fig. 1. Increment of the sediment trapping layer of the Krasnodar Reservoir over the period 2005–2021. Flooded riverbeds of Kuban (1), Psekups (2), Tuapcha (3) and Pshish (4) river

1) to describe the morphological properties of the underwater topography of the Krasnodar reservoir using geomorphometry techniques, to determine the main topography forms of the reservoir basin and build appropriate maps;

2) to establish long-term morphometric changes caused by the restructuring of underwater and surface (shallow water, shore) topography, to assess the intensity of deformations of the reservoir bottom.

3) to identify the dominant morphogenetic processes to establish the regularities of sedimentation, the nature of its manifestation in the topography of the bed and the coastal zone.

MATERIALS AND METHODS

The analysis was carried out according to bathymetric surveys of the Krasnodar Reservoir made with the participation of the authors in 2005 and 2021. Bathymetric surveys were carried out in accordance with (Guidance Document ..., 2012); the methodology of field research and processing of raw materials is described (Laguta, Pogorelov, 2018). Bathymetric surveys 2005 and 2021 are of the same type in terms of technical support, tacking and density of sounding points. The surveying conditions of different years did not affect the final DEM and the correctness of the comparative analysis. Morphometric analysis and calculations were performed using pre-constructed digital models of the reservoir bottom topography with a spatial resolution of 50 m (Fig. 2). The features of the operation of the reservoir in the period 2005–2021 generally should be considered ordinary: the fully supply level was reached annually with significant seasonal level variability. During this period, the reservoir provided anti-flood and irrigation functions against the background of a permanent decrease in its useful capacity. Since in the process of transformation of the reservoir, its north-eastern part (the former Tshchik Reservoir) separated from the main basin of the reservoir, the main calculations were performed for the regulated section of the Krasnodar Reservoir with an area of 224 km^2 (Fig. 1).

Morphometric analysis included the recognition of surface elements and assessment of the roughness of the bottom of the Krasnodar Reservoir by DEM. The classification of morphometric surface elements by DEM is based on the method of calculating the BPI (Bathymetric Position Index) and classification of morphological elements based on it (Guisan et al., 1999; Weiss, 2001). This index, being a modification of the TPI index (Topographical Positions Index) (Jenness, 2006), is focused on working with bathymetric survey materials. Until now, it has been used mainly to study the topography of the seabed (Wilson et al., 2007). The BPI index is multiscale and involves the construction of "rough" (Broad-BPI) and detailed (Fine-BPI) bitmaps. The calculation of the BPI was preceded by the conversion of the original DEM into a bathymetric model; at the same time, we selected the forced level of 35.23 m as zero, and assigned negative values to the heights.

BPI is the difference between the absolute height of a given point (in the raster layer – cells) and the average height of points in a given buffer around the source point. Positive index values correspond to surface bulges; negative values correspond to concave shapes; values near 0 indicate that the surface is close to flat. To reduce the effect of autocorrelation of the initial data on the results of morphometric classification, we use the normalized index value (Weiss, 2001). Normalization is carried out according to the formula:

$$BPI = int\left(\left(\left(\frac{BPI - mean_{BPI}}{\sigma_{BPI}}\right)\times 100\right)+0.5\right) \qquad (1)$$

where BPI_{sd} – normalized value of BPI, int – conversion to an integer, meanBPI – average value of the BPI index (across the entire dataset), – the mean square deviation of the BPI index values (across the entire dataset).

In addition to the raster layers of the Fine-BRIL and Broad-*BPI* indexes, a slope map and a bathymetric map are needed to recognize (classify) elementary landforms. The number of classes, their name and morphometric parameters are set by the user in CSV format. The procedure for isolating morphometric elements of the

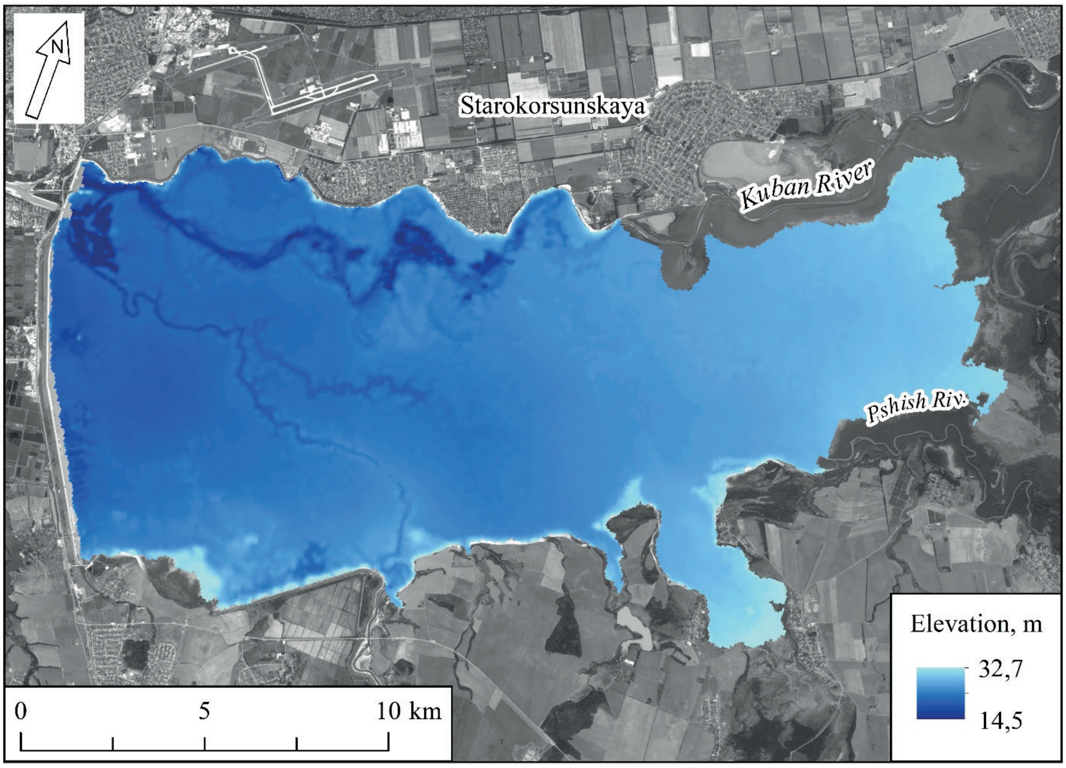

Fig. 2. Digital elevation model of the bottom of the Krasnodar Reservoir, built according to the 2005 survey data

bottom surface is described (Verfaillie et al., 2007). We have experimentally established the parameters for calculating the BPI index, which provide an optimal level of detail of the bottom topography forms in relation to the spatial resolution of DEM. A search box in the form of a ring with specified internal and external radii was used (Table 1). When choosing the parameters, we were guided by the sizes of recognized positive and negative forms of the bottom topography of the reservoir under study, which we refer to mesoscale, namely, long-bank shafts with their ridges and slopes, depressions and deep depressions.

The reconstruction of the bottom topography under the influence of silting was analyzed using roughness parameters. From the point of view of morphology, the ruggedness index can be interpreted as a measure of the complexity (heterogeneity, variability) of the topography. There is no generally accepted method for calculating ruggedness: we have applied the index of Terrain Ruggedness Index (TRI) (Riley, 1999) and Vector Measure of Ruggedness (VRM) (Sappington, 2007; Hobson (1972). Ruggedness parameters were calculated according to DEM data in a sliding window of 3×3 cells.

RESULTS AND DISCUSSION

Features of the bottom topography

Among the morphometric features of the Krasnodar valley reservoir that determine the restructuring of the topography, we highlight the following: the topography of the reservoir bottom inherited both elements of river valleys with cut-in channels (Kuban, Pshish, Psekups) and extensive fragments of a flat plain that existed before flooding in 1973-1976. The Kuban riverbed, flooded near the right bank, is particularly well traced (Fig.. 2). The Kuban valley on the reservoir site is characterized by transverse asymmetry, namely, a high steep right bank descending into the old Kuban riverbed, and a gentle sloping left bank with a weakly pronounced terrace. Between the banks there is a plateau-shaped slightly dissected surface. Currently, there is an increased accumulation of sediment in flooded riverbeds in comparison with the background (Fig. 1). In the flooded riverbed of Kuban, which has maximum depths, the turbid flow is localized. Hydrodynamic activity here manifests itself in a special way: the jet in the flooded channel of Kuban is pressed against the right bank, which contributes to intensive erosion of the shore until an accumulative body is formed in the form of a retractable delta.

The predominant process in the topography formation of the bed during the study period is the gradual leveling of its surface, leveling from above in the process of continuous sediment trapping. The average thickness of silt layer in the studied water area for 2005-2021 was 0.40 m; the variability of the sediment trapping layer thickness over an area of 224 km^2 is characterized by a standard deviation of 0.81 m. The average slope of the bed surface in 2005 was 0.20°, in 2021 – 0.18°. A decrease in the average slope is an obvious sign of gradual leveling of the bed during silting. Elevated slopes on the accumulative plain, as a rule, mark the flooded coastal slopes of river valleys.

Elementary forms of topography: selection and analysis

Against the background of these geomorphological features, it is of interest to reveal the elementary topography forms of the accepted methodology (Fig. 3), as well as the dynamics of the transformation of these forms for 2005-2021. (Fig. 3, Table 2). Examples of terrain profiles divided into morphological types of landform elements are shown in Fig. 4.

In the process of classifying the surface of the reservoir bed, six morphological elements were identified (Table 2, Fig. 3, 4), belonging to three categories of surfaces: flat (plateaus), concave (depressions) and convex (shafts and their slopes). Let us consider the origin and dynamics of each one and the selected elementary forms of the reservoir basin.

According to the survey data of 2021, 89.2% of the reservoir area is occupied by an accumulative plateau-type plain, which before flooding was the Kuban floodplain, dissected by riverbeds. The prevailing slopes within the plain are 0.1–0.4°. The concept of a plateau reflects to the greatest extent the basic properties of this form of topography – plane, flatness.

Negative forms – hollow-shaped depressions and more pronounced elongated depressions – occupy 2% and 4.1% of the area, respectively. Genetically, the depressions have different origins: some belong to flooded riverbeds, some to the concave foothills of long–bank accumulative form – ridges. At the same time, old channels in the process of silting and reduction of the inclined surface as a result of the action of denudation demolition evolve in the sequence "depression – deep depression – lower bank shelf", and newly formed channels (for example, in the delta of Pshish River) form depressions during embedding. The most difficult in the morphological sense is the coastal area and the shallow part of the bed (littoral), where, along with positive topography forms (long-shore shafts), negative forms (depressions) can form on the accumulative part on the abrasive part of the shoal.

The flooded valleys of Kuban, Psekups and Tuapcha rivers (the former right tributary of Psekups) are well expressed in topography. During the study period, the valleys of the last two were divided into separate sections and are currently evolving towards the plateau. In general, the share of depressions in the total area of the reservoir bed is decreasing, which cannot be said about the depressions (Table. 2), some of which are formed in the areas of newly formed banks of fluvial origin – deltas of extension.

The positive elements of the morphology of the bed are represented by a group of wave-like forms, within which we distinguish three elementary forms: reef crests, back reefs, mid-slope ridges, frontal (distal) slopes and rear (proximal) slopes. As in the case of the group of negative landforms, the origin of the ridges is different. And is genetically determined by the contribution of accumulative (alluvial) and abrasive processes (see below). The location of the characteristic genetically homogeneous elementary forms is illustrated in Figure 5. We reveal the following genetically homogeneous topography forms.

Table 1. Accepted parameters for calculating the BPI index

Index	Form of the search box	Inner radius		Outer radius	
		number of cells	m	number of cells	m
Fine-BPI	Ring	3	150	5	250
Broad-BPI	Ring	5	250	30	1500

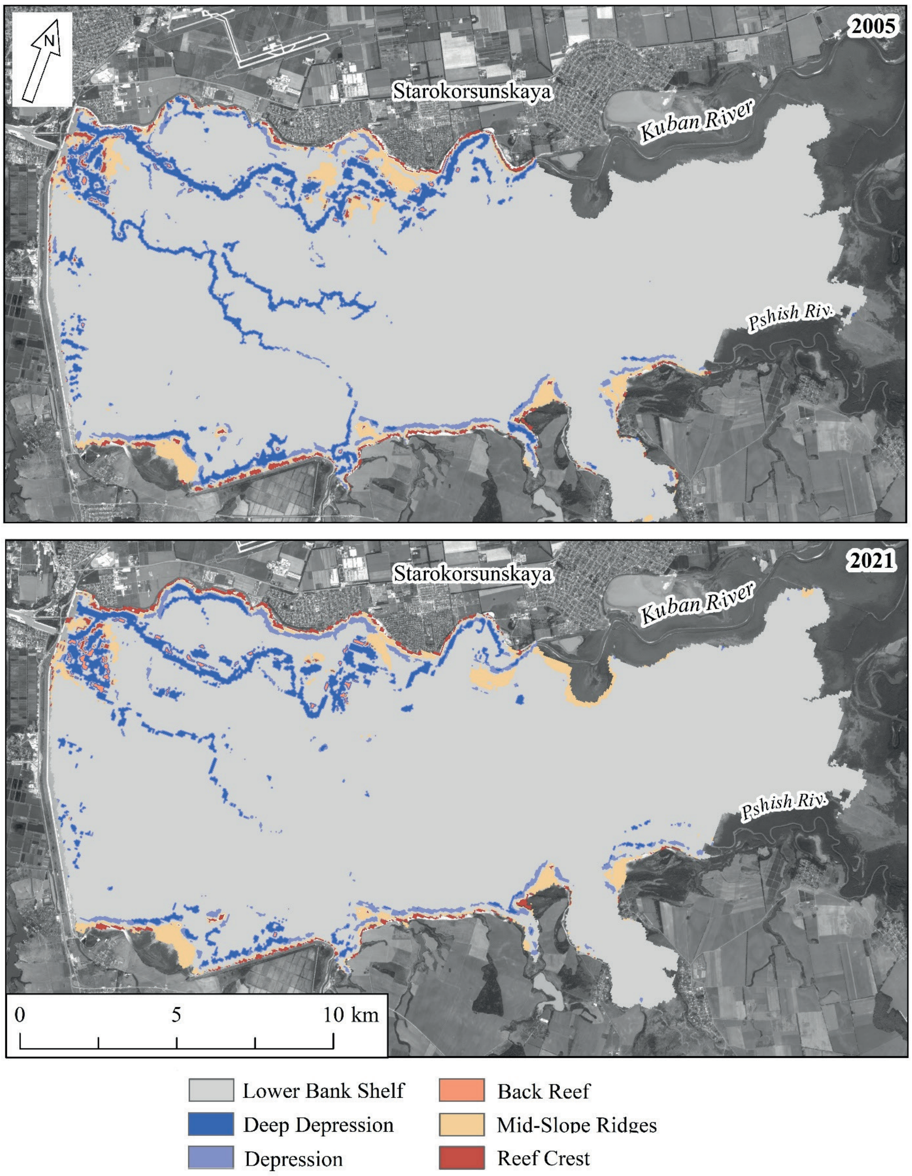

Fig. 3. Reservoir bed topography forms identified based on survey data from 2005 and 2021

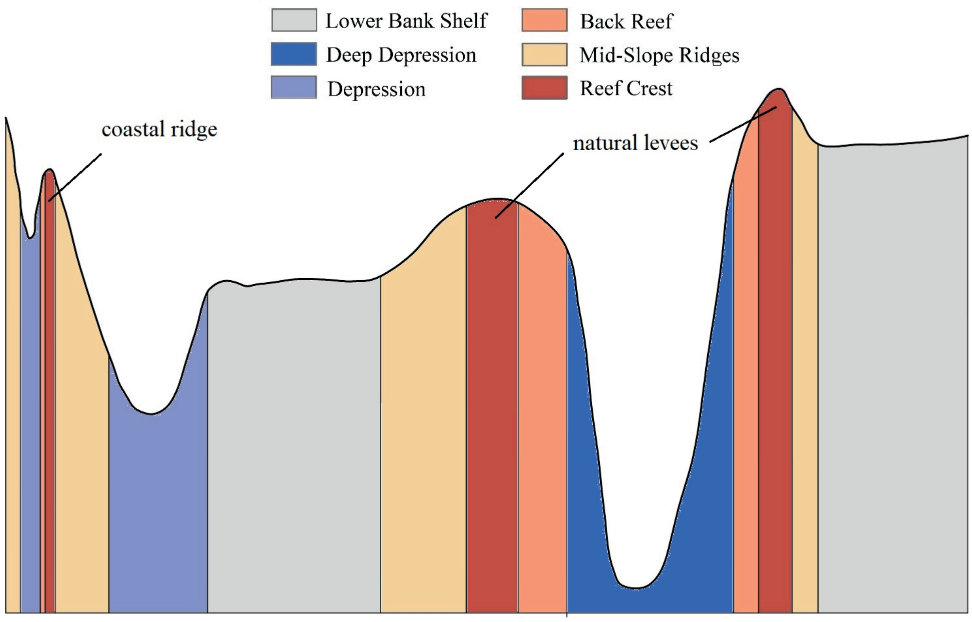

Fig. 4. Examples of terrain profiles divided into morphological types of landform elements

Table 2. Morphological elements of the bottom surface of the Krasnodar reservoir and their change in 2005–2021

Form of topography	2005			2021		
	Number of fragments	Area		Number of fragments	Area	
		ha	%		ha	%
Plateau (Lower Bank Shelf)	280	19787	88,3	222	19984	89,2
Depression	258	387	1,7	257	438	2,0
Deep Depression	172	1172	5,2	184	919	4,1
Mid-Slope Ridges	197	640	2,9	212	666	3,0
Reef Crest	208	317	1,4	166	295	1,3
Back Reef	144	98	0,4	92	98	0,4

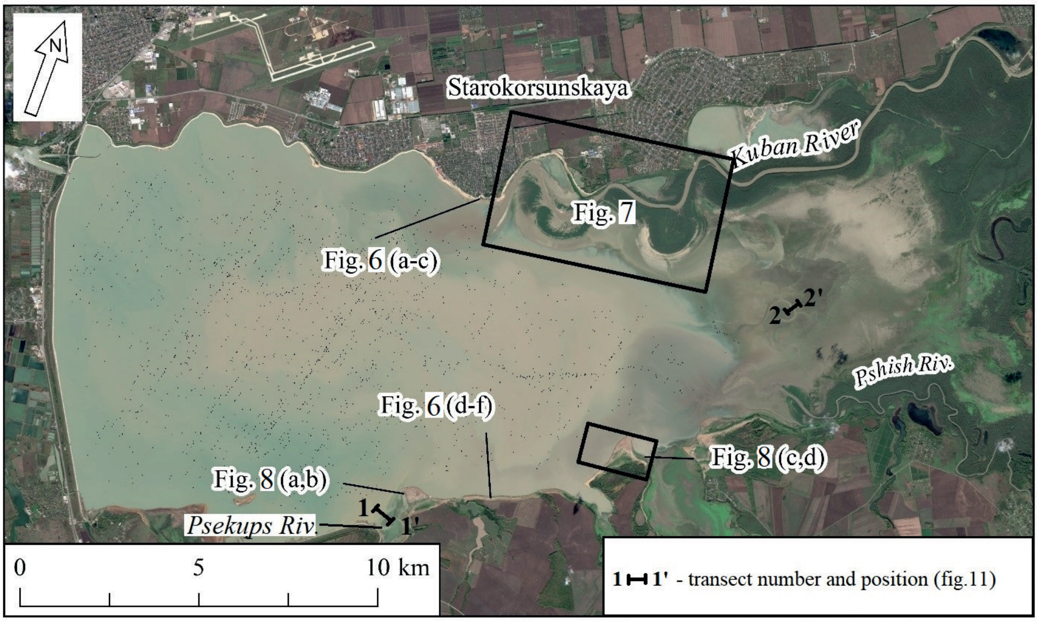

Fig. 5. Location of typical genetically homogeneous topography elements

1. In the littoral zone of the reservoir (coastal shoal) as a result of the transverse movement of sediments under the influence of the surf, accumulative forms – coastal ridges - have been formed both at abrasive and non-abrasive shores. Morphologically, the crests and mid-slopes of the ridges are expressed here, as well as the depressions separating the coastal ridge from the underlying lower bank shelf. The rear (shore-facing) slopes are not detected at the scale determined by the spatial resolution of the survey. The images (Fig. 6 a-e) accurately illustrate the series of coastal ridges, which has two main reasons – variable reservoir backwater and different intensity of waves. These two circumstances determine the limits of localization of the considered topography form. Long-shore ridges are also formed under the influence of the fluvial factor of morpholithogenesis - solid river runoff with a volume in the total material balance exceeding the contribution of the surf. The natural movement of the mouth as a source of sediment in the process of delta growth causes a constant change in the conditions of the formation of coastal ridges, giving rise to their new generations with the release of old ridges from wave surf effects (Fig. 7 a-b).

2. In the deep part of the reservoir bed, the natural levees of flooded riverbeds have been preserved. This form is found fragmentally along the flooded channel of Kuban River (Fig. 3). The presence of rudiments of the rear slopes of the ridges (here – facing inward to the channel), despite the loss of integrity as a result of long-term anthropogenic impact, indicates their former massiveness.

3. In addition to the above, reef-like forms are formed in the form of a naes or a tombolo connecting the uplands that existed before the flooding with the shore in the presence of a wave shadow (tombolo effect) (Fig. 8 a-d).

Consider the evolution of this topography. During the analyzed period, the coastal areas of the bottom, as well as flooded riverbeds (Fig. 9) and, accordingly, elementary landforms located in these areas were most subjected to morphological transformations. The transformations affected 34.1 km^2 or about 15% of the analyzed reservoir area. The differentiated nature of morphological transformations is reflected in Table 3.

When analyzing the transformation of convex forms, the following should be taken into account. Due to the almost complete overgrowing of the littoral of the reservoir in the zone of delta formation, most of the coastal ridges that have left and are leaving the zone of wave action by 2021 turned out to be inaccessible for bathymetric survey. Comparison of two different-temporal DEMs does not fully cover the boundary of the 2005 survey. Within the comparison boundaries, among the convex landforms (Reef Crests, Back Reefs and Mid-Slope Ridges) identified in the 2005 survey, there are still no coastal ridges formed with the participation of the fluvial process, although in the 2021 survey their participation in this category reaches up to 30%. With comparable areas of convex landforms in 2005 and 2021 (Table 2), their significant differences in genesis should be noted. The differences are due, on the one hand, to the appearance and development

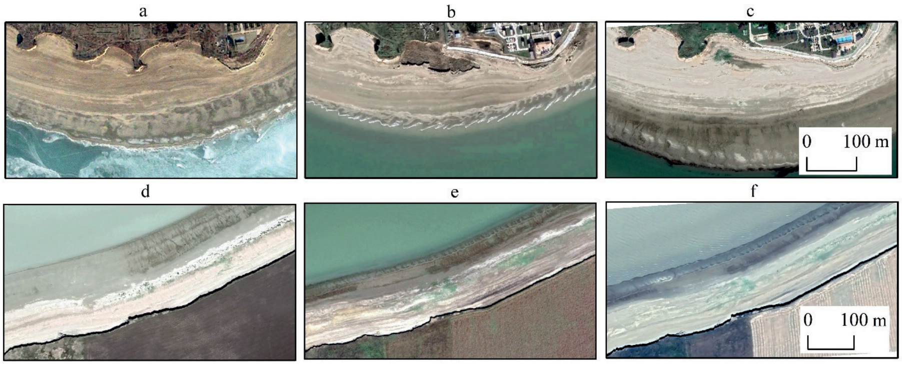

Fig. 6. Formation of characteristic convex topography forms – coastal ridges and their slopes. Imagery data: 30.12.2012 (a), 24.11.2016 (b), 18.10.2018 (c), 09.09.2014 (d), 24.09.2014 (e), 28.09.2017 (f). Maxar Technologies

Fig. 7. Generations of coastal ridges of the growing advanced delta of the Kuban River. Imagery data: 23.09.2014 (a), 18.10.2018 (b), 18.12.2022 (c). Maxar Technologies

Fig. 8. Formation of reef-like forms of topography in the form of a naes or a tombolo. Imagery data: 17.08.2005 (a), 28.09.2017 (b), 30.05.2013 (c), 30.12.2012 (d). Maxar Technologies – a, d; CNES / Airbus – b, c

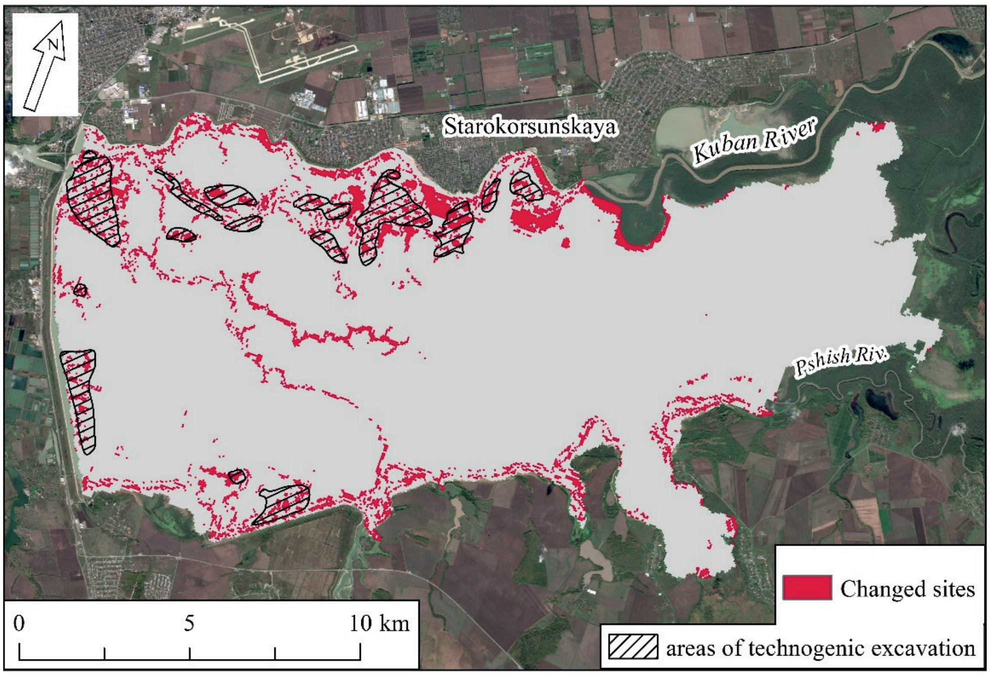

Fig. 9. Bottom areas subjected to morphological changes in 2005–2021

Table 3. Morphological transformation of the identified elementary landforms during 2005–2021

Topography forms		Area, ha
2005	2021	
Lower Bank Shelf	Back Reef	52
	Deep Depression	303
	Depression	179,25
	Mid-slope Ridges	232
	Reef Crest	31,5
Depression	Depression	29
	Lower Bank Shelf	165,75
	Mid-slope Ridges	11,75
	Reef Crest	0,75
	Back Reef	0
Deep depression	Reef Crest	6,5
	Deep depression	39,25
	Lower Bank Shelf	525
	Mid-slope Ridges	6,75
	Reef Crest	5,75
Mid-slope ridge	Back Reef	2
	Deep depression	5,75
	Depression	36
	Lower Bank Shelf	225,75
	Reef Crest	41,25
Back Reef	Depression	7,5
	Deep depression	0,75
	Plateau	53
	Mid-slope Ridges	0,5
	Reef Crest	9,5
Reef Crest	Back Reef	9,75
	Depression	3,75
	Deep Depression	4,75
	Lower Bank Shelf	78,75
	Mid-slope Ridges	76,75

of swells on potamogenic (deltaic) shores and, on the other hand, to the reduction in the area of ridges near the abrasion-type shores. A significant part of the Back Reefs and Mid-Slope Ridges are new forms formed on the former plateau, which reflects the intensity of the formation of new banks in the reservoir.

Negative surface shapes have also undergone transformations. The area of depressions tends to decrease, the area of hollows tend to increase (Tables 2, 3). At the same time, the number of detected depressions has increased slightly with a general reduction in their area, which indicates their fragmentation into separate fragments. A striking example of the "self-destruction" of depressions under the action of silting is the former channel of Tuapcha River, traces of which are practically not detected in 2021 (Fig. 3). The part of the depressions has been transformed into depressions. Along with this, as it turned out, new concave forms are formed within the former plateau (about 40% of their total area), which is caused by the embedding of the forming channels with the formation of depressions in the accumulative part of the shoal and underwater slopes of deltas. Thus, a section of a new underwater channel for 2005-2021 was formed near Pshish River in the form of a depression on the delta of the extension. The total area of concave forms during the study period as a whole decreased from 1559 ha to 1357 ha due mainly to their silting.

Let us single out the dominant geomorphological process of the evolution of the reservoir bed – the steady leveling of its surface, which was actually expressed in the growth of the plateau area by 2 km^2 over 16 years. The main "donors" of the process were Depressions and Mid-slope Ridges (Tables 2, 3).

Changing the ruggedness of the bottom topography

Similar trends were found in the changes in the ruggedness of the studied surface over the period 2005-2021, regardless of the parameters used (VRM, TRI). In general, in the process of silting up the reservoir, judging by the spatial statistical characteristics of VRM and TRI (Table 4), there is a decrease in the complexity, variability of the bottom topography. Thus, the CPI index for 16 years decreased from 0.32 to 0.29 m. In most of the plateau-type sections of the reservoir bed, the ruggedness parameters have not changed. Significant changes in ruggedness were noted in the areas of active topography transformation: in the places of emerging deltas of extension (Fig. 9), as well as in flooded channels due to leveling of the surface (Fig. 11) and fragmentation of channels (Fig. 3, 10).

Table 4. Statistical characteristics of ruggedness

Statistical characteristics	VRM		TRI	
	2005	2021	2005	2021
Average	2,3×10^{-5}	2×10^{-5}	0,32 m	0,29 m
Median	6,5×10^{-7}	6×10^{-5}	0,10 m	0,10 m
Standard deviation	7×10^{-5}	8×10^{-5}	0,51 m	0,51 m
Minimum	1,7×10^{-9}	2,7×10^{-10}	0 m	0 m
Maximum	0,0018	0,0017	7,40 m	7,90 m

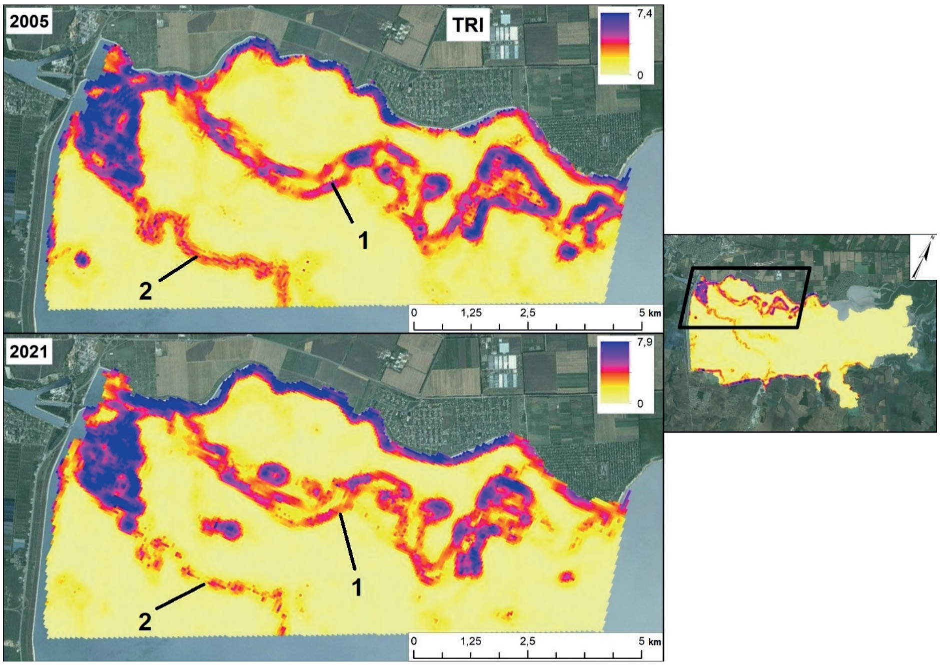

Fig. 10. Changes in the surface ruggedness index TRI for 2005-2021. Flooded riverbeds of the rivers Kuban (1) and Psekups (2)

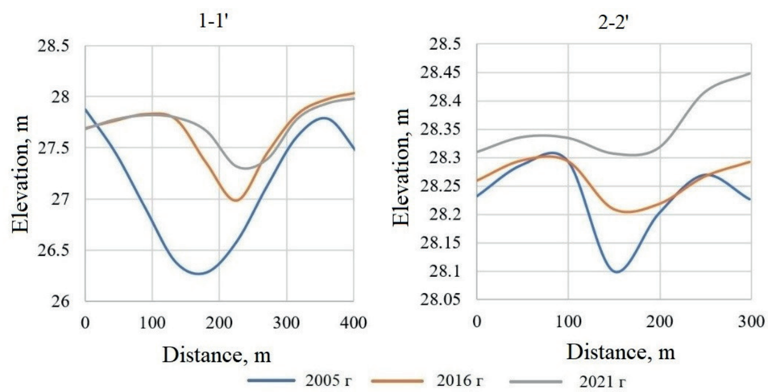

Fig. 11. Characteristic changes in the transverse profiles of flooded riverbeds of Psekups (left) and Pshish (right) rivers for 2005-2021

CONCLUSIONS

1. Standard morphometric characteristics of reservoirs adopted in hydrometry are limited by the type, shape, altitude position, bed size and volume of water in the reservoir, as well as bathygraphic curves. Morphometric analysis techniques using digital modeling bring the analysis of the bottom topography of reservoirs to a new level, contributing to the understanding of the processes of morphogenesis and the direction of transformation of reservoirs. One of the effective tools of geomorphometry is the multiscale BPI index (Bathymetric Position Index), followed by the allocation of elementary forms of bottom topography.

2. The key geomorphological process of the Krasnodar Reservoir is the accumulation of sediments, which generally leads to leveling of the bed surface. The average silt layer in the studied water area for 2005-2021 was 0.40 m, however, the thickness of the sediment trapping layer with average slopes of the bed surface of about 0.20 is very uneven. In the topography of the valley basin of the Krasnodar Reservoir, despite almost half a century of operation, the flooded valleys of Kuban, Psekups and Tuapcha rivers (the former right tributary of Psekups) have been well preserved.

3. As a result of morphometric analysis of the surface of the bed of the Krasnodar reservoir within a regulated volume on an area of 224 km^2, according to bathymetric surveys of 2005 and 2021, characteristic topography forms belonging to three categories of surfaces were determined by BPI: Lower Bank Shelf, Depression, Deep Depression, Reef Crest, Back Reef, Mid-Slope Ridges. In 2021, 89.2% of the reservoir bed area was occupied by Lower Bank Shelf, 4.1% – Depressions, 2% – Deep Depressions, 1.3% – coastal Reef Crests, 3% - Mid-Slope Ridges, 0.4% of the area – Back Reefs. The established topography forms, despite the morphological similarity, may have different genesis. Thus, some of the depressions are formed by flooded riverbeds, some by concave foothills of long–bank accumulative form – crests. The origin of the crests is also different and is determined by the synergy of fluvial (delta coast crests) and abrasive-accumulative processes (coastal crests).

4. In 2005-2021, morphological transformations affected 34.1 km^2 or 15% of the analyzed reservoir area. The coastal areas of the bottom, as well as flooded riverbeds, underwent the greatest restructuring. Some of the flooded valleys (Psekups, Tuapcha, etc.) turned out to be divided into separate fragments and in the process of sediment trapping evolve through the "depression – deep depression – lower bank shelf" stages. The evolution of the lower bank shelves, on the contrary, is characterized by defragmentation – a decrease in the number of fragments from 280 to 222 during the study period with an increase in the area of plateau-type surfaces by 2 km^2. The total area of deep depressions tends to decrease, and depressions – to increase. The formation of depressions, as topography forms, is noted on the accumulative shoal and underwater slopes of the emerging deltas of the extension (Kuban, Pshish). Positive topography forms are also subject to continuous transformation. A significant part of the Back Reefs and Mid-Slope Ridges are new formations formed on the former Lower Bank Shelf.

REFERENCES

Abayev N.N., Sagatdinova G.N., Maglinets Yu.A., Terekhov A.G., 2022. Assessment of Shardara Reservoir siltation during 1999–2021 using satellite data (Syrdarya River, Kazakhstan). Modern problems of remote sensing of the Earth from space. 19 (5): 210-221. DOI: 10.21046/2070-7401-2022-19-5-210-221.

Akylbekov O., Said N.A., Martínez-García R., Gura D., 2022. ML models and neural networks for analyzing 3D data spatial planning tasks: Example of Khasansky urban district of the Russian Federation. Advances in Engineering Software. 173. 103251. DOI: 10.1016/j.advengsoft.2022.103251

Alahiane N., Elmouden A., Aitlhaj A., Boutaleb S., 2016. Small dam reservoir siltation in the Atlas Mountains of Central Morocco: analysis of factors impacting sediment yield. Environmental Earth Sciences. 75 (12): 1-11. DOI 10.1007/s12665-016-5795-y.

Alekseevsky N.I., Berkovich K.M., Chalov R.S., Chalov S.R., 2012. Spatial temporal variability of channel deformations on the rivers of Russia. Geography and natural resources, 3: 13–21 (in Russian).

Andjelkovic A., Ristic R., Janic M. [et al.], 2017. Genesis of sediments and siltation of the accumulation duboki potok of the barajevska river basin, Serbia. Journal of Environmental Protection and Ecology. 18(4): 1735-1745.

Avakyan A.B., Saltankin V.P., Sharapov V.A., 1987. Reservoirs. Moscow: Mysl'. 331 (in Russian).

Dalu T., Tambara E. M., Clegg B. [et al.], 2013. Modeling sedimentation rates of Malilangwe reservoir in the south-eastern lowveld of Zimbabwe. Applied Water Science. 3 (1): 133-144. DOI: 10.1007/s13201-012-0067-9.

Finarov D.P., 1986. Geomorphological analysis and forecasting of the reformation of the coastal zone and the bottom of reservoirs. Leningrad: Nauka. 227 (in Russian).

Florinsky I.V., 2021. Geomorphometry today. Proceedings of the International Conference «InterCarto. InterGIS». Moscow: MSU, Faculty of Geography. 27(2): 394–448 (in Russian). DOI: 10.35595/2414-9179-2021-2-27-394-448.

Guidance document 52.08.767-2012. Water consumption on watercourses. Measurement methods by acoustic Doppler profilers «Stream Pro» and «Rio Grande». FSBI «GGI» of Roshydromet. 2012.

Guisan A., Weiss S.B., Weiss A.D., 1999. GLM versus CCA spatial modeling of plant species distribution. Plant Ecology. 143: 107–122. DOI:10.1023/A:1009841519580.

Hengl T., Reuter H.I., 2009. Geomorphometry: Concepts, Software, Applications. Oxford: Elsevier. 765.

Hobson R. D., 1972. Chapter 8 - surface roughness in topography: quantitative approach. Spatial analysis in geomorphology. Harper & Row, New York, New York, USA. 221-245.

Honek D., Michalková M. Š., Smetanová A. [et al.], 2020. Estimating sedimentation rates in small reservoirs - Suitable approaches for local municipalities in central Europe. Journal of Environmental Management. 261: 109958. DOI: 10.1016/j.jenvman.2019.109958.

Jenness J., 2006. Topographic Position Index (TPI) v. 1.2. 46.

Kalinin V.G., Pyankov S.V., Perevoshchikova O.A., 2018.On the formation of the underwater topography of valley reservoirs (by the example of the Kama Reservoir). Geographical bulletin. 1(44): 128–137 (in Russian). DOI: 10.17072/2079-7877-2018-1-128-137.

Kurbatova I.E., 2014. Monitoring of the transformation of the Krasnodar Reservoir using high resolution satellite data. Actual problems of remote sensing of the Earth from space. 11 (3): 42–53 (in Russian).

Laguta A.A., Pogorelov A.V., 2018. Peculiarities of Krasnodar water reservoir silting. Evaluation based on the data of bathymetric surveys. Geographical bulletin. 47: 54–66 (in Russian). DOI:10.17072/2079-7877-2018-4- 54-66.

Laguta A.A., Pogorelov A.V., 2019. Peculiarites of delta formation in rivers flowing into the valley reservoir (a case study of Krasnodar reservoir). Geographical bulletin. 50: 119–134 (in Russian). DOI: 10.17072/2079-7877-2019-3-119-134.

Li Xin, Ren Jinqiu, Xu Quanxi, Yuan Jing, Zhang Wei, 2023. Impact of cascade reservoirs on the delayed response behaviour of sedimentation in the Three Gorges Reservoir Journal of Geographical Sciences. 33(3): 576-598. DOI: 10.1007/s11442-023-2097-7.

Litovka F.S., Bandurin M.A., Vanzha V.V, 2019. The solutions the problem of silting of the Krasnodar reservoir for the rational use of resources of floodplain territories Electronic scientific journal «Engineering Bulletin of the Don». No. 7 (in Russian).

Liu D., Lv S., Li C., 2021. Silt formation and thickness of shuidonggou reservoir since its operation. Journal of Environmental Protection and Ecology. 22 (5): 1981-1991.

Liu Y., Xu S., Wang T., Zhu T., 2020. Application of multi-source data fusion method in updating topography and estimating sedimentation of the reservoir. Water.12(11): 1-19. DOI: 10.3390/w12113057.

Lurie P M, Panov V D, Tkachenko Ju Ju, 2005 Kuban river: hydrography and flow regime. St. Petersburg: Gidrometeoizdat, 498.

Makhfuz A., Dekhkanova N. T. k., Urazmukhammedova Z. V., 2019. Reformation of the bottom during the operation of reservoirs in Uzbekistan. Eurasian Union of Scientists. 9-2 (66): 27-31.

Nazarov N.N., Tyunyatkin D.G., Frolova I.V., Cherepanov A.V., 2011. Factors and conditions of sediment differentiation in the coastal zone of the Kama reservoirs. Geographical bulletin. 4: 4–10 (in Russian).

Nazarov N.N., Tyunyatkin D.G., Frolova I.V., Cherepanov A.V., 2013. Morpholithogenesis in the zone of alongshore sediment transport in the Kama reservoir (St. 1. Accumulative forms). Geographical bulletin. 1(24): 33–39 (in Russian).

Peng J., Chen S., 2010. Response of delta sedimentary system to variation of water and sediment in the Yellow River over past six decades. Journal of Geographical Sciences. 20(4): 613-627. DOI: 10.1007/s11442-010-0613-z.

Pogorelov A V, Laguta A A, 2020. On the circulation of waters in the valley reservoir (Krasnodar reservoir). Bulletin of higher education institutes North Caucasus region. Natural Sciences, 4: 87–97. (in Russian)

Pogorelov Anatoly, Laguta Andrey, Kiselev Evgeny, Lipilin Dmitry, 2021. Features of the long-term transformation of the Krasnodar reservoir, near the mouth of the Kuban river, Russia. Journal of Geographical Sciences. 31(12): 1895–1904. DOI: 10.1007/s11442-021-1928-7.

Pogorelov, A.V., Laguta, A.A., Kiselev, E.N., 2022. New data on silting of the Krasnodar Reservoir. Geographical Bulletin. 2(61): 166–179 (in Russian). DOI: 10.17072/2079-7877-2022-2- 166-179.

Pogorelov A.V., Lipilin D.A., Kiselev E.N Changes in the hydrographic characteristics of rivers in steppe agrolandscapes over the past decades (on the example of the Beysug river, Krasnodar territory). InterCarto, InterGIS. 2021, 27 (4), 19–32. (In Russian). DOI: 10.35595/2414-9179-2021-4-27-19-32.

Pogorelov A.V., Lipilin D.A., Dudkina A.A., Kopaneva O.V. About technogenic transformations of the river network on the Azov-Kuban plain (Chelbas, Albashi rivers). InterCarto, InterGIS. 2022, 28 (2), 567–582. (In Russian). DOI: 10.35595/2414-9179-2022-2-28-567-582.

Rakhuba A.V., Shmakova M.V., 2022. Regime of Reservoir: Experience in Modeling Riverbed Processes with a Movable Bed. Fundamental and Applied Hydrophysics. 15(2):138-149. (In Russian). DOI: 10.48612/fpg/peru-3z3h-gazh.

Riley, S. J., S. D. DeGloria and R. Elliot, 1999. A terrain ruggedness index that quantifies topographic heterogeneity. Intermountain Journal of Sciences. 5 (1-4): 23-27

Rules for the use of water resources of the Krasnodar reservoir, 2008. Krasnodar: Kubanvodproekt, 158.

Sappington, J.M., Longshore, K.M., Thompson, D.B., 2007. Quantifying Landscape Ruggedness for Animal Habitat Analysis: A Case Study Using Bighorn Sheep in the Mojave Desert. The Journal of Wildlife Management. 71: 1419–1426. DOI: 10.2193/2005-723.

Shiferaw M., Abebe R., 2021.Reservoir sedimentation and estimating dam storage capacity using bathymetry survey: a case study of Abrajit Dam, Upper Blue Nile basin, Ethiopia. Applied Geomatics. 13 (3): 277-286. DOI: 10.1007/s12518-020-00348-x.

Su Teng, Wang Suiji, Mei Yanguo, Shao Wenwei, 2015. Comparison of channel geometry changes in Inner Mongolian reach of the Yellow River before and after joint operation of large upstream reservoirs. Journal of Geographical Sciences. 25 (8): 930-942. DOI: 10.1007/s11442-015-1211-x

Suresh Babu D. S., Nandakumar V., John B. [et al.], 2000. Siltation analysis in the Neyyar reservoir and forest degradation in its catchment: a study from Kerala state, India Environmental Geology. 39 (3-4): 0390-0397.

Van Maren D. S., Yang Sh. L., He Q., 2013. The impact of silt trapping in large reservoirs on downstream morphology: the Yangtze River. Ocean Dynamics. 63 (6): 691-707. DOI 10.1007/s10236-013-0622-4.

Verfaillie E., Doornenbal P., Mitchell A.J., White J., Van Lancker V., 2007. The bathymetric position index (BPI) as a support tool for habitat mapping. Web resource: https://www.researchgate.net/publication/242082725_ Title_The_bathymetric_position_index_BPI_as_a_support_ tool_for_habitat_mapping [Accessed 01.03.2023].

Wang Yanjun, Wu Baosheng, Zhong Deyu, 2020. Adjustment in the main-channel geometry of the lower Yellow River before and after the operation of the Xiaolangdi Reservoir from 1986 to 2015. Journal of Geographical Sciences. 30 (3): 468-486.DOI: 10.1007/s11442-020-1738-3.

Weiss A.D., 2001. Topographic Positions and Landforms Analysis (Conference Poster). Proceedings of the 21st Annual ESRI User Conference. San Diego, CA. July 9–13.

Wilson M.F.J., O'Connell B., Brown C., Guinan J.C., Grehan A.J., 2007. Multiscale terrain analysis of multibeam bathymetry data for habitat mapping on the continental slope. Marine Geodesy. 30 (1–2): 3–35. DOI: 10.1080/01490410701295962.

Yutsis V., Krivosheya K., Levchenko O. [et al.], 2014. Bottom topography, recent sedimentation and water volume of the Cerro Prieto dam, NE Mexico. Geofisica International. 53 (1): 27-38. DOI: 10.1016/S0016-7169(14)71488-6.

Zemlyanov I.V., Shikunova E.Yu., Gorelits O.V., Pavlovsky A.E., 2011. Using digital elevation models to refine modern morphometric characteristics of reservoirs. Scientific-practical conf. Modern problems of reservoirs and their watersheds. Perm, May 17–20. 189–193. (in Russian).

Zhang Wei, Yang Yunping, Zhang Mingjin, Li Yitian, Zhu Lingling, You Xingying, Wang Dong, Xu Junfeng, 2017. Mechanisms of suspended sediment restoration and bed level compensation in downstream reaches of the Three Gorges Projects (TGP). Journal of Geographical Sciences. 27 (4): 463-480. DOI: 10.1007/s11442-017-1387-3.

Zhou Yongqiang, Li Jingbao, Zhang Yunlin, Zhang Xinping, Li Xichun, 2015. Enhanced lakebed sediment erosion in Dongting Lake induced by the operation of the Three Gorges Reservoir. Journal of Geographical Sciences. 25 (8): 917-929. DOI: 10.1007/s11442-015-1210-y.

Disclaimer:

The information and opinions presented in the Journal reflect the views of the authors and not of the Journal or its Editorial Board or the Publisher. The GES Journal has used its best endeavors to ensure that the information is correct and current at the time of publication.

ges.rgo.ru/jour/

ISSN 2542-1565 (Online)